# APPLICATION OF DIGITAL FILTERING TECHNIQUES FOR REDUCING AND ANALYZING IN-SITU SEISMIC TIME SERIES

by

Erick J. Baziw

B.A.Sc., The University of British Columbia, 1986

A THESIS SUBMITTED IN PARTIAL FULFILLMENT OF
THE REQUIREMENTS FOR THE DEGREE OF
MASTERS OF APPLIED SCIENCE

in

THE FACULTY OF GRADUATE STUDIES

Department of Civil Engineering

We accept this thesis as confirming
to the required standard

.....
Dr. R. G. Campanella, Civil Engineering Dept.

.....
Dr. K. Whittall, Geophysics & Astronomy Dept.

THE UNIVERSITY OF BRITISH COLUMBIA

August, 1988

In presenting this thesis in partial fulfilment of the requirements for an advanced degree at the University of British Columbia, I agree that the Library shall make it freely available for reference and study. I further agree that permission for extensive copying of this thesis for scholarly purposes may be granted by the head of my department or by his or her representatives. It is understood that copying or publication of this thesis for financial gain shall not be allowed without my written permission.

Department of Civil Engineering

The University of British Columbia
1956 Main Mall
Vancouver, Canada
V6T 1Y3

Date Sept 12/88

## ABSTRACT

The introduction of digital filtering is a new and exciting approach in analyzing in-situ seismic data. Digital filters are also in the same spirit as the electric cone which replaced the mechanical cone in CPT* testing. That is, it is desirable to automate CPT testing in order to make it less operator dependent and increase the reliability and accuracy.

In CPT seismic cone testing seismic waves are generated at the surface and recorded downhole with velocity or acceleration transducers. The seismic receivers record the different seismic wavelets (e.g., SV-waves, P-waves) allowing one to determine shear and compression wave velocities. In order to distinguish the different seismic events, an instrument with fast response time is desired (i.e., high natural frequency and low damping). This type of instrument is characteristic of an accelerometer. The fast response time (small time constant) of an accelerometer results in a very sensitive instrument with corresponding noisy time domain characteristics. One way to separate events is to characterize the signal frequencies and remove unwanted frequencies. Digital filtering is ideal for this application.

The techniques of digital filtering introduced in this research are based on frequency domain filtering, where Fast Fourier, Butterworth Filter, and crosscorrelation algorithms are implemented. One based on time domain techniques, where a Kalman Filter is designed to model the instrument and the physical environment. The crosscorrelation method allows one to focus on a specific wavelet and use all the information of the wavelets present averaging out any noises or irregularities and relying upon dominant responses. The Kalman Filter was applied in a manner in which it modelled the sensors used and the physical environment of the body waves and noise generation. The KF was investigated for its possible application to obtaining accurate estimates on the P-wave and S-wave amplitudes and arrival times. The KF is a very flexible tool which allows one to model the problem considered accurately. In addition, the KF works in the time domain which removes many of the limitations of the frequency domain techniques.


---

* Cone Penetration Test

The crosscorrelation filter concepts are applied by a program referred to as CROSSCOR. CROSSCOR is a graphics interactive program which displays the frequency spectrums, unfiltered and filtered time series and crosscorrelations on a mainframe graphics terminal which has been adapted to run on the IBM P.C. CROSSCOR was tested for performance by analyzing synthetic and real data. The results from the analysis on both synthetic and real data indicate that CROSSCOR is an accurate and user friendly tool which greatly assists one in obtaining seismic velocities.

The performance of the Kalman Filter was analyzed by generating a source wavelet and passing it through the second order instrumentation. The second order response is then fed into the KF with the arrival time and maximum amplitude being determined. The filter was found to perform well and it has much promise in respect that if it is finely turned, it would be possible to obtain arrival times and amplitudes on line resulting in velocities and damping characteristics, respectively.

TABLE OF CONTENTS

TABLE OF CONTENTS (Cont'd)

LIST OF TABLES

LIST OF TABLES (Cont'd)

LIST OF FIGURES

LIST OF FIGURES (Cont'd)

LIST OF FIGURES (Cont'd)

LIST OF FIGURES (Cont'd)

LIST OF FIGURES (Cont'd)

LIST OF FIGURES (Cont'd)

LIST OF FIGURES (Cont'd)

ACKNOWLEDGEMENTS

The work outlined in this thesis would not have been possible without the funding and guidance of Dr. Campanella. Dr. Ken Whittall from the Geophysics Department was fundamental in helping me with the geophysical aspects of this thesis. In addition, Drs. Robertson, Dunbar and Slauson provided considerable advice in preparing this thesis.

The rest of the in-situ group's help was invaluable. Don Gillespie and John Sully were always available for assistance in formulating my ideas.

I would also like to thank Jim Greig and Michael Ehling for their help with the interactive graphics.

I would like to express my thanks to my buddies at the Savage Mansion, Damon, Steve and Bear for keeping my spirits up at all times.

Lastly, my parents were invaluable in helping me prepare my research and typing it up (Thanks, Mom!).

# I. INTRODUCTION

The objective of this research is to apply digital filtering techniques, in in-situ seismic cone penetration testing, inorder to determine S (Shear) and P (Pressure) wave velocities. There is considerable interest in these soil characteristics because they provide insight into the response of soil to imposed loads such as buildings, heavy equipment, and dynamic loads from earthquakes and explosions. Richart et al. (1970), Mooeny (1974) and Borm (1977) have written extensive literature on the relation of seismic wave velocities to dynamic elastic moduli.

The seismic cone penetration test was first investigated at UBC by Rice (1984) where he found the application of the technique could provide a rapid and accurate method for carrying out a downhole shear wave velocity survey. In his work, Rice determined that a uniaxial geophone was sufficient for identifying shear waves, if the instrument was orientated properly. Rice also investigated several different types of sources and the dominant waves they generated. Rice worked predominantly with geophones which have slower response time compared to an accelerometer. From his work with geophones, which were not amplified at the pick-up, Rice stated "Below 30 metres the strength of individual energy impulses was attenuated such that clear individual shear wave excursions were not always identifiable."

The next to investigate the application of the seismic cone in in-situ testing was Laing (1985). Laing focused her attention on sources and receivers with the seismic cone for both on-shore and off-shore applications. Laing came up with the same conclusion as Rice with respect to the use of the geophone as a seismic receiver, she states, "accelerometers tend to show a response which more closely represents the response of the soil. Thus, damping characteristics of soil should theoretically be attainable from accelerometer responses."

Ideally one would like an instrument to tell the whole seismic story. Figure 1.1 illustrates a typical acceleration and/or velocity measuring device. The dynamics behind the velocity and acceleration measurements can be expressed by the following two second order equations:

acceleration:

$$x_o(s)/s^2x_i = x_o(s)/\ddot{x}_i = k/((s^2/\omega_n^2)+2\zeta s/\omega_n+1) \qquad (1.1)$$

velocity:

$$x_o(s)/sx_i = x_o(s)/\dot{x}_i = s/(s^2+2\zeta\omega_n s+\omega_n^2) \qquad (1.2)$$

$x_o$ = relative displacement of mass M
$x_i$ = absolute displacement of mass M
$\omega_n$ = natural frequency
$\zeta$ = damping
k = proportionality constant
s = Laplace transform variable

The response of the instrument is described by $\omega_n$ and $\zeta$. In general, the higher the value of $\zeta$ and smaller value of $\omega_n$ the greater the reduction in the sensitivity of the instrument. This corresponds to an instrument with a large time constant resulting in slower transient response specifications, this is illustrated in Figure 1.2. In this figure, an instrument with a large time constant associated with it would have comparatively longer response time specifications. Figure 1.3 shows typical frequency response curves for geophones and accelerometers. As is illustrated, an accelerometer has flatter response curves than a geophone for lower frequency inputs, and becomes unstable for higher frequency inputs near its natural frequency. Since P waves typically consists of frequencies between 200 to 2000 Hz, and S waves are typically between 50 to 300 Hz, it is desirable to have an instrument which has a flat response curve below 2000 Hz and is light in mass, due to lack of room in the seismic cone. The above conditions would be met with a light weight accelerometer with natural frequency at approximately 4000 Hz.

The desire of using sensitive accelerometers in in-situ testing calls for the necessity of using digital filters in order to separate out noise and different seismic events. The technique of data reduction used by Rice and Laing relied upon the polarity of shear body waves and the application of analogue filters. In Section II, this technique is outlined with some of its limitations.

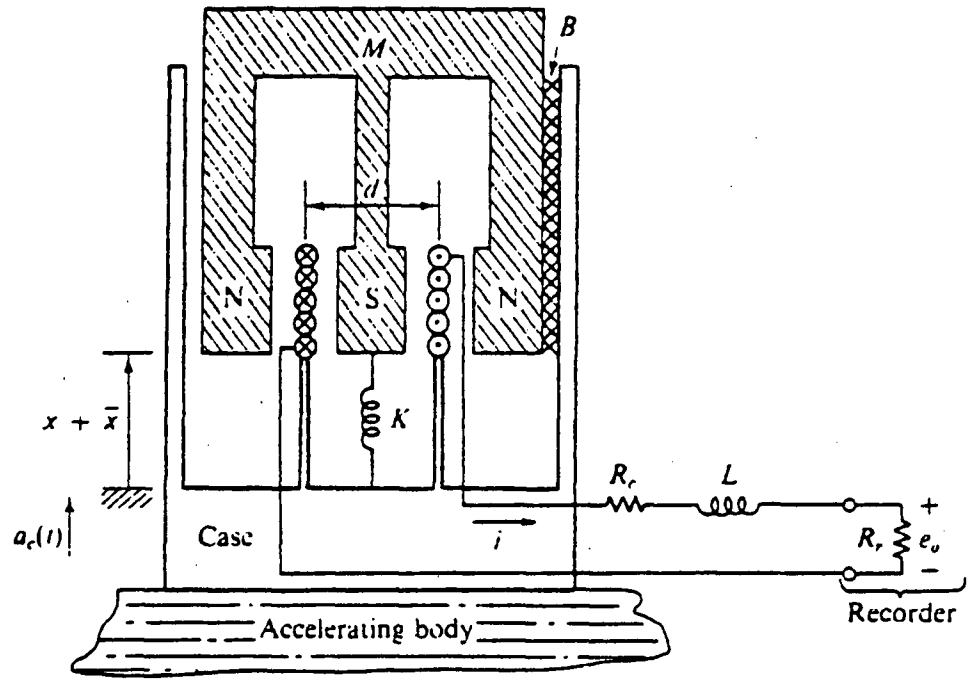


Figure 1.1: Schematic of an Acceleration Measuring Device (Close & Fredrick, 1978)

In Figure 1.1, the following parametres are defined:

M - mass of suspended magnet

B - flux density between magnets

K - stiffness of spring which supports the magnet

D - viscous damping between magnet and the case

N - number of turns in coil

d - diameter of coil

$\ell$ - length of coil, $\pi \cdot d \cdot N$

$R_c$ - resistance of coil

$L_c$ - inductance of coil

$R_r$ - resistance of recorder

$a_c(t)$ - acceleration of case relative to a fixed reference

$x_0$ - equilibrium position of M relative to the case

x - dynamic displacement of M relative to the case

TRANSIENT RESPONSE SPECIFICATIONS

1. Delay time $t_d$
2. Rise time $t_r$
3. Peak time $t_p$
4. Maximum overshoot $M_p$
5. Settling time $t_s$

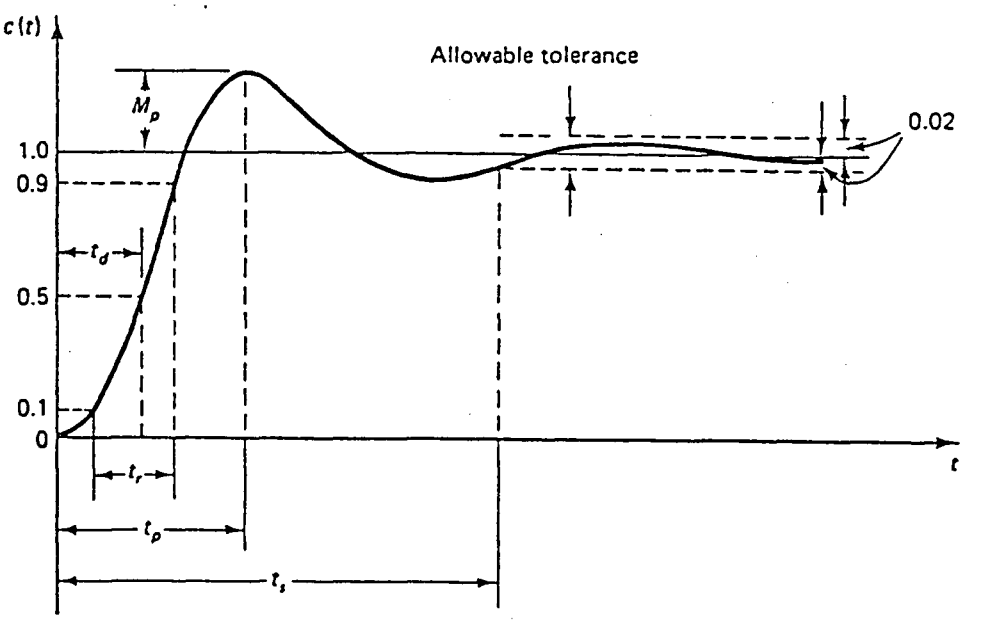


Figure 1.2. Unit Step Response Curve Showing Transient Response Specifications $t_d$, $t_r$, $t_p$, $M_p$, and $t_s$ (Ogata, 1987)

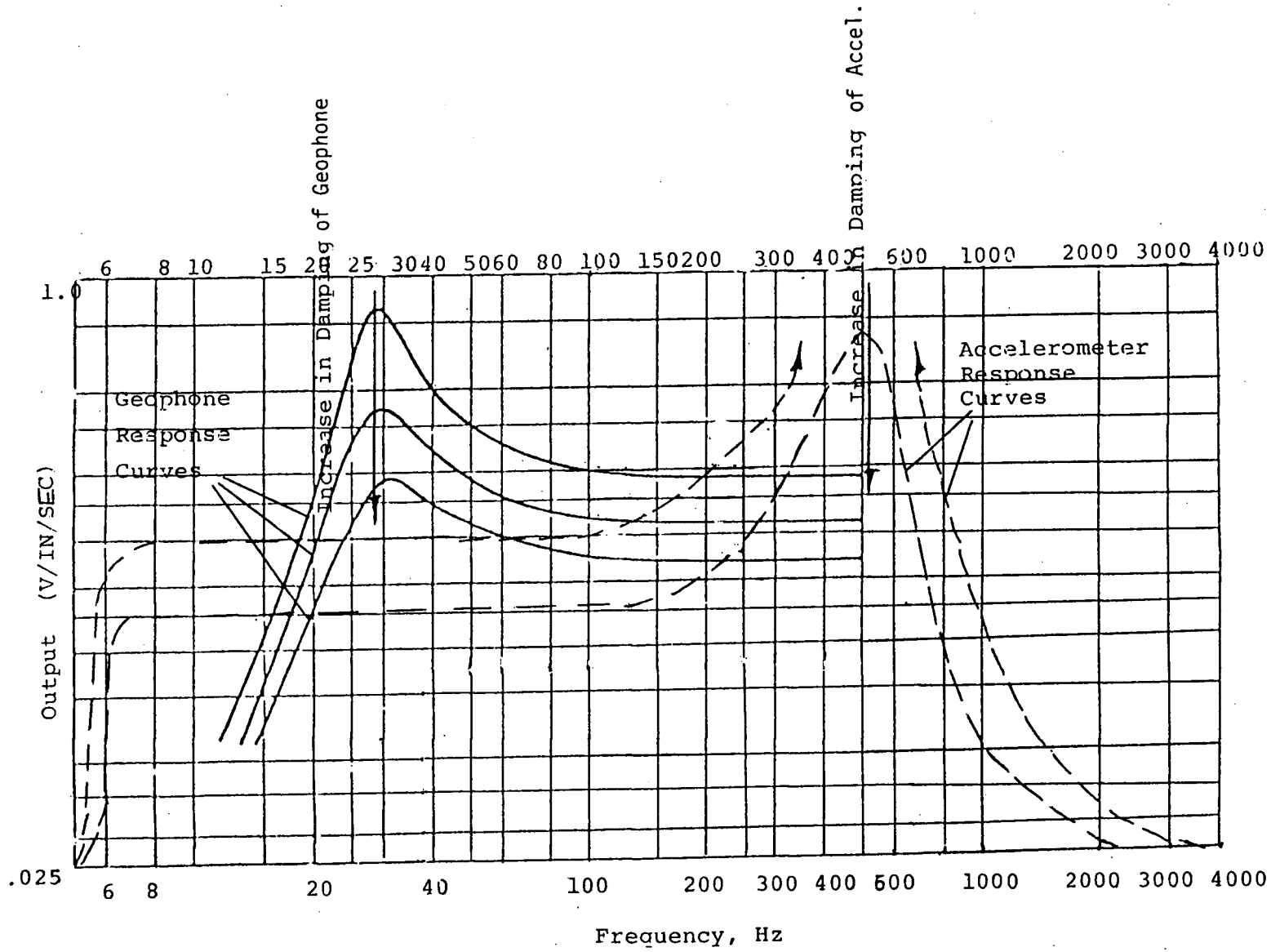


Figure 1.3. Accelerometer and Geophone Frequency Response Curves. The Geophone Illustrated has a Natural Frequency of 28 Hz, and the Accelerometer has a Natural Frequency of 500 Hz.

The dynamic behind source wavelet generation and final velocity determination is as follows. A source, such as a hammer blow or seismic cap, generates potentials at the surface which correspond to SV*, SH**, and P*** waves. These initial potentials can be considered to be Dirac delta functions (i.e., impulses) having a broad frequency spectrum. As these potentials propagate through the earth as seismic waves, their frequency spectra are bandlimited (i.e., higher frequencies are attenuated). This is due to the earth acting as a low-pass analogue filter. At a certain depth, the generated signals are recorded with the three waves (i.e., SV, SH, and P) and noise being superimposed.

The recorded signals are difficult to analyze due to the superposition of many signals. Therefore, a digital filter is applied so one can focus on a specific wavelet (e.g., SH). Once filtering is applied, the time offset between two similar waves (e.g., SH) recorded at successive depths is determined and interval velocities are calculated. The following diagram (Figure 1.4) illustrates the essential relation between source, earth, recorder, filter, and interval velocity calculation.

Referring to Figure 1.4, the major goal was to develop digital filters. These filters should give clear signals without distorting the original signal in terms of time shifts and amplitudes.

The two filtering methods considered in this thesis are the one based on the frequency domain filtering (Section III), where Fast Fourier, Butterworth, and crosscorrelation algorithms are implemented, and one based on the time domain techniques (Section IV), where a Kalman Filter is designed to model both the instrument and the physical environment.

---

* A horizontally traveling shear wave so polarized that the particle motion is all vertical.

** A horizontally traveling shear wave so polarized that the particle motion is all horizontal.

*** Compression wave consisting of particle motion with alternating condensations and rarefactions during which adjacent particles of the solid are closer together and farther apart during successive half cycles. The motion of the particles are always in the direction of wave propagation.

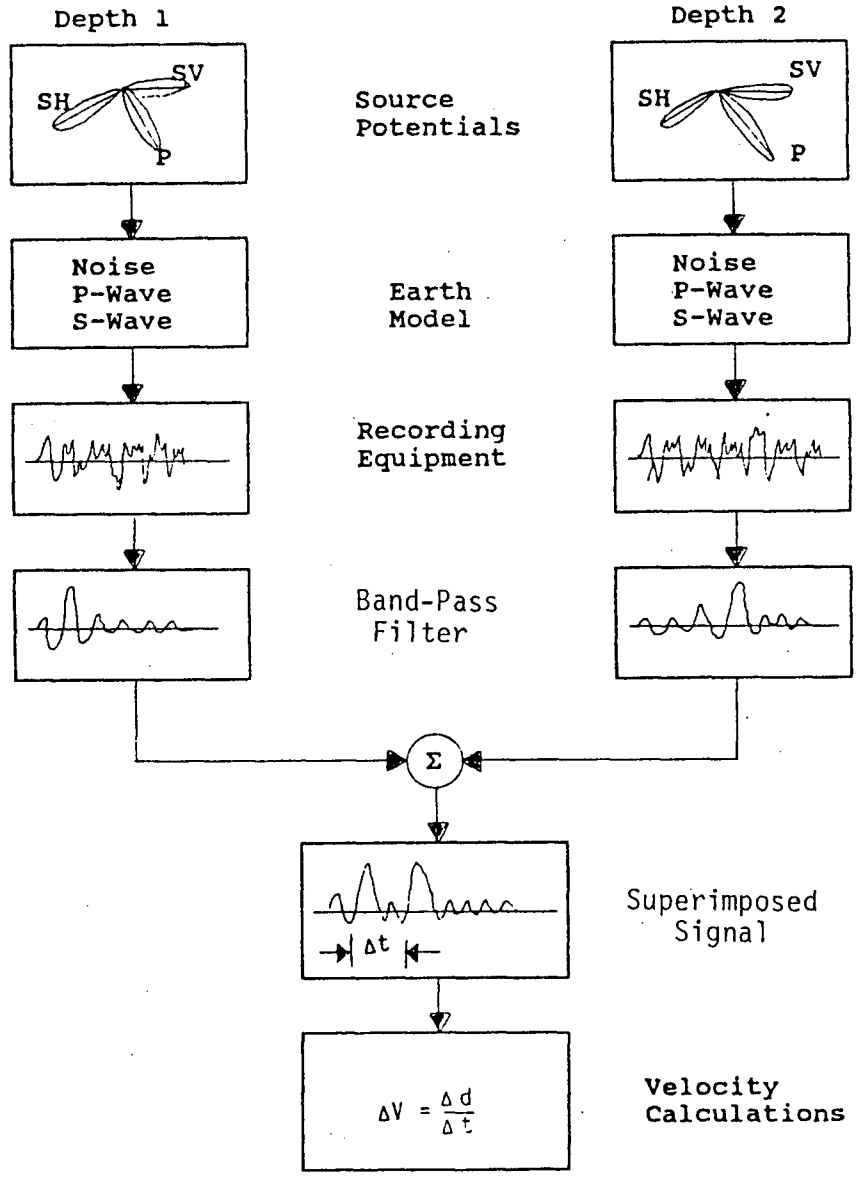


Figure 1.4. Block Diagram of Source, Earth, Recorder, Filter and Velocity Calculation.

## II. DESCRIPTION OF PHYSICAL PROBLEM

A seismic cone investigation is conducted in order to obtain in-situ values of shear wave velocities of a stratigraphic section. The shear wave velocities are directly related to the maximum shear modulus (Rice 1984) of the soil by the following mathematical expression.

$$G_{max} = \rho \cdot V_s^2$$

where

$\rho$ - is the mass density of the soil

$V_s$ - is the shear wave velocity

$G_{max}$ - is the maximum shear modulus at strains less than $10^{-4}$ percent.

The significance of the above strain level is that at strains of $10^{-4}$ percent and less, the shear modulus is maximum and little effected by strain amplitude. The maximum shear parameter is an important soil parameter; shear modulus reduction curves can be generated from it. The shear modulus reduction curves are very important in dynamic soil analysis,because they relate the change in the shear modulus with induced strains.

In seismic cone testing a response signal is recorded at one metre interval depths. The wavelet is generated at the surface by a sledge hammer blow or a seismic cap and received at the cone with either a geophone or an accelerometer. The following diagram illustrates the seismic cone transmission profile.

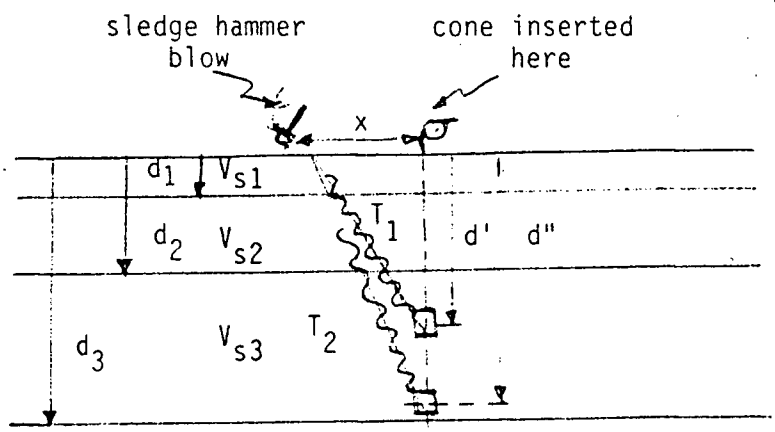


d' - depth to first seismic recording

d" - depth to second seismic recording

$T_1$ - time for shear wave to arrive to first seismic receiver

$T_2$ - time for shear to arrive to second seismic receiver

Figure 2.1. Schematic of Seismic Transmission Profile

The geophone and accelerometer responses were recorded on a Nicolet 4094 digital oscilloscope with a CRT screen and a floppy disk storage capability. A complete description of this oscilloscope is given by Rice (1984).

The seismic cone is pushed into the soil using the U.B.C. In-situ Testing vehicle. The truck illustrated in Figure 2.2 weighs approximately 11 tons and has two hydraulic cylinders with which the cone is pushed into the soil. To provide the reaction force needed to push the cone, the truck is raised on two hydraulic pads as shown in Figure 2.2. The hydraulic pads also act as SH-Wave sources. SH-Wave sources are desired because it is easy to reverse the polarity of the SH-Wave. This energy reversal results in two oppositely polarized wavelets which are recorded on the Nicolet oscilloscope as is shown in Figure 2.3. The first major crossover times illustrated in Figure 2.3 allow the calculation of the relative travel time difference of shear waves between successive depths which allows the calculation of shear wave velocities. The above technique is thoroughly discussed by Rice (1984) and Laing (1985), and will be referred to as the reverse polarity method and/or crossover method.

The crossover times discussed above are related to the velocity profile by the following equations:

$$V_{s3} = \frac{d''_{corr} - d'_{corr}}{T_2 - T_1} \tag{2.2a}$$

where

$$d''_{corr} = \sqrt{x^2 + d''^2} \tag{2.2b}$$

$$d'_{corr} = \sqrt{x^2 + d'^2} \tag{2.2c}$$

and d', d", $T_1$, and $T_2$ are defined in Figure 2.1.

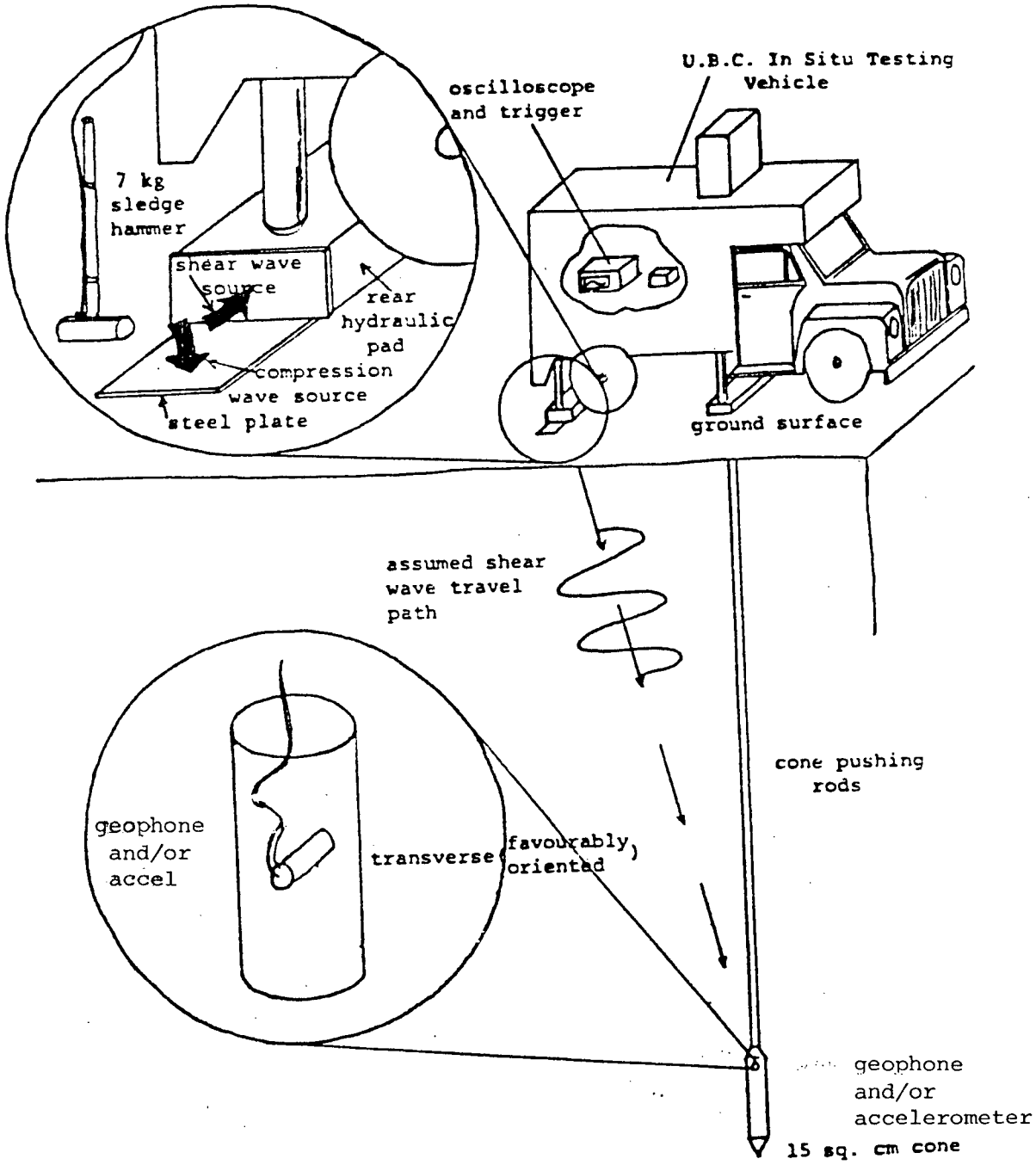


Figure 2.2 CPT Seismic Equipment Layout for Mechanical Source, (after Rice, 1984)

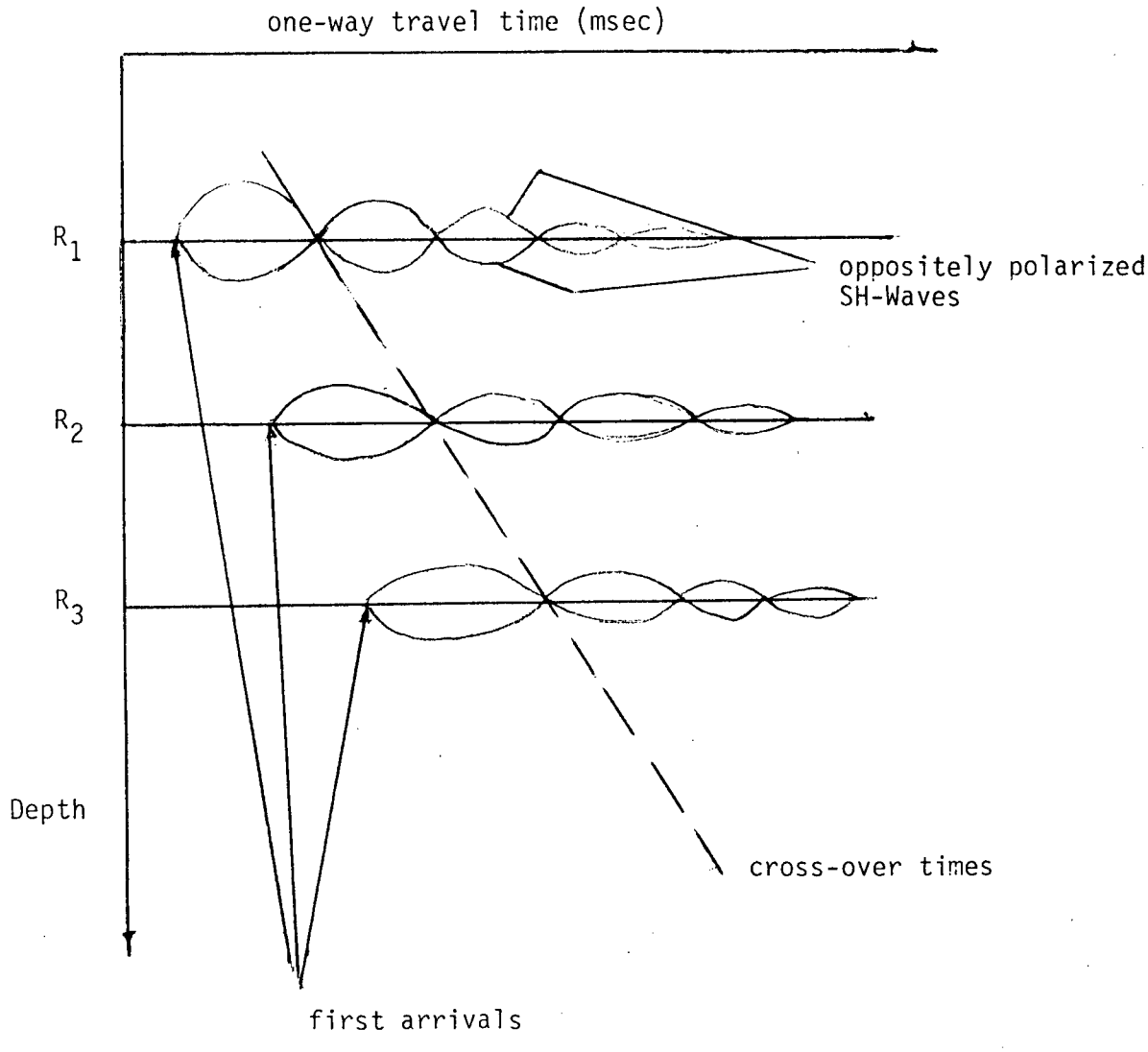


Figure 2.3. Schematic of Recorded Data

These equations and Figure 2.1 apply only if it is assumed that the angle of incidence approaches zero, and the ratio of the interval shear velocities is of the order of unity. These conditions will generally hold for in-situ testing, because velocities for ajacently stratified soils do not differ (Reference 4) significantly (i.e., generally less than 1.5), and the source is not separated much from the receiver, such that we have near normal incidence.

Referring to Figures 2.4 and 2.5, it is seen that for these conditions an incident SV-Wave will have a negligible amount of energy converted to a P-Wave as reflection or transmission (Figures 2.5b and d). The majority of the incident SV energy will be converted to an SV transmission with the angle of incidence approximately equal to the angle of refraction (Figure 2.4b). The same can be said for the P-Wave. An incident P-Wave subjected to these boundary conditions will transmit most of its energy, at an interface, to a P-Wave in the lower medium with the angle of incidence equal to the angle of refraction. Thus, the assumption of straight ray propagation, with little reflection and energy conversion, holds. The above considerations are more throughly assessed in Rice (1984), where he states, "For most practical purposes a straight line travel path assumption would be quite satisfactory."

As was previously discussed, the interval times, $T_1$ and $T_2$, are determined by taking the difference of the crossover times for the successive wavelets. When only noise free shear waves exist, the above procedure is trouble free. In many cases, one is not dealing with an ideal wavelet, but has a seismogram with corrupting P-Waves and noise. These particular signals make it difficult to pick arrival and crossover times. The method which is currently used to obtain clear shear wave signals applys an analogue low-pass filter to remove the higher frequencies of the recorded signal. Stokoe and Hoar, (1978) raised an important point when considering analogue and/or electrical filters. They suggest that filtering should be minimized because it can significantly distort the signal and erroneously alter arrival times. Stokoe and Hoar also state that electronic filters usually introduce time delays which vary with the frequency of the input signal; hence, unfiltered signals were generally preferred and were used in their study. A numerical example of the possible phase shift or corresponding time delay, for an analogue filter, follows.

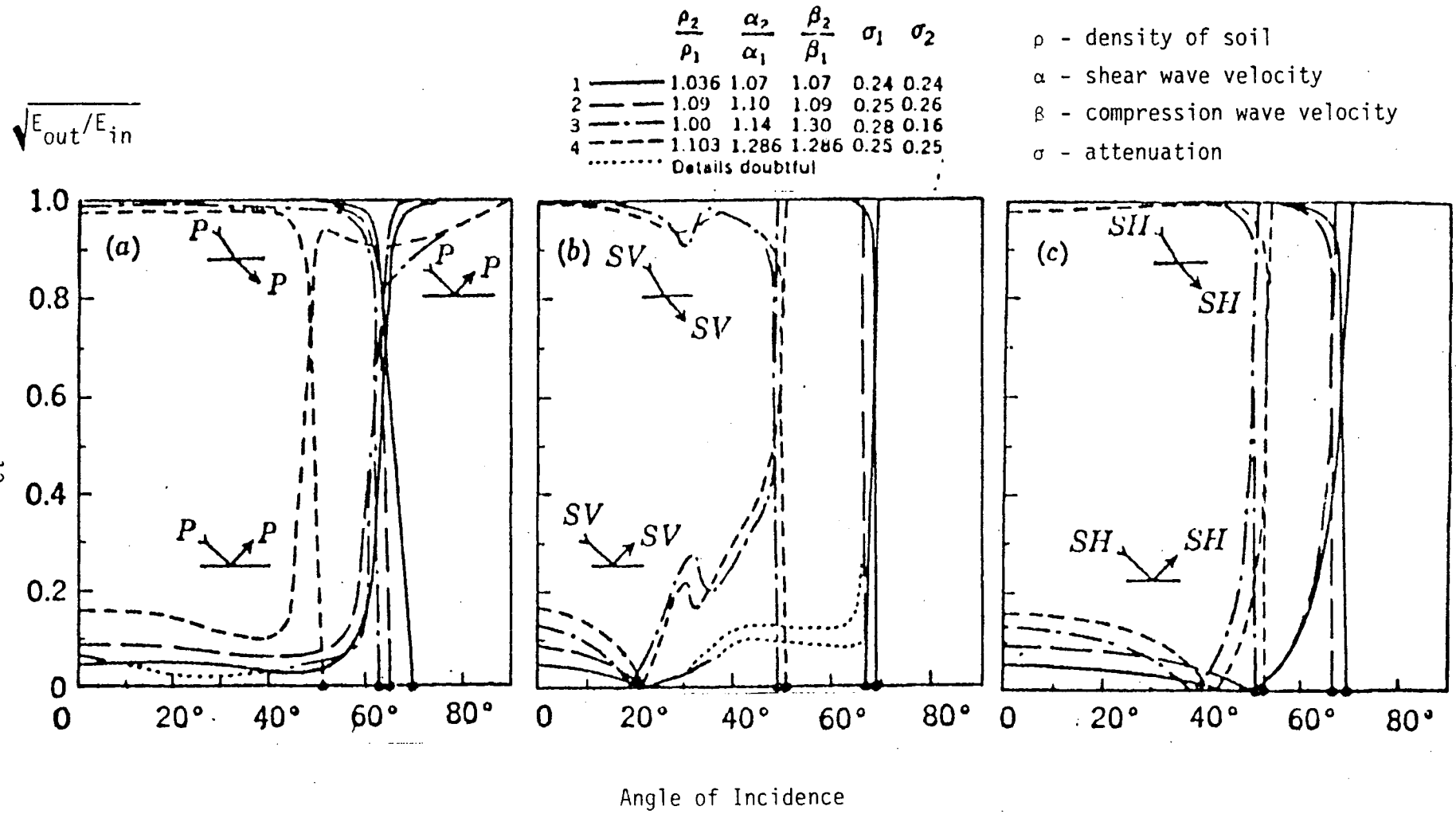


Figure 2.4. Ratio of Reflected or Transmitted Energy to Incident Energy, $\sqrt{E_{out}/E_{in}}$, With No Change in Wave Type Occurring (Ewing, Jardetz, and Press, 1957)

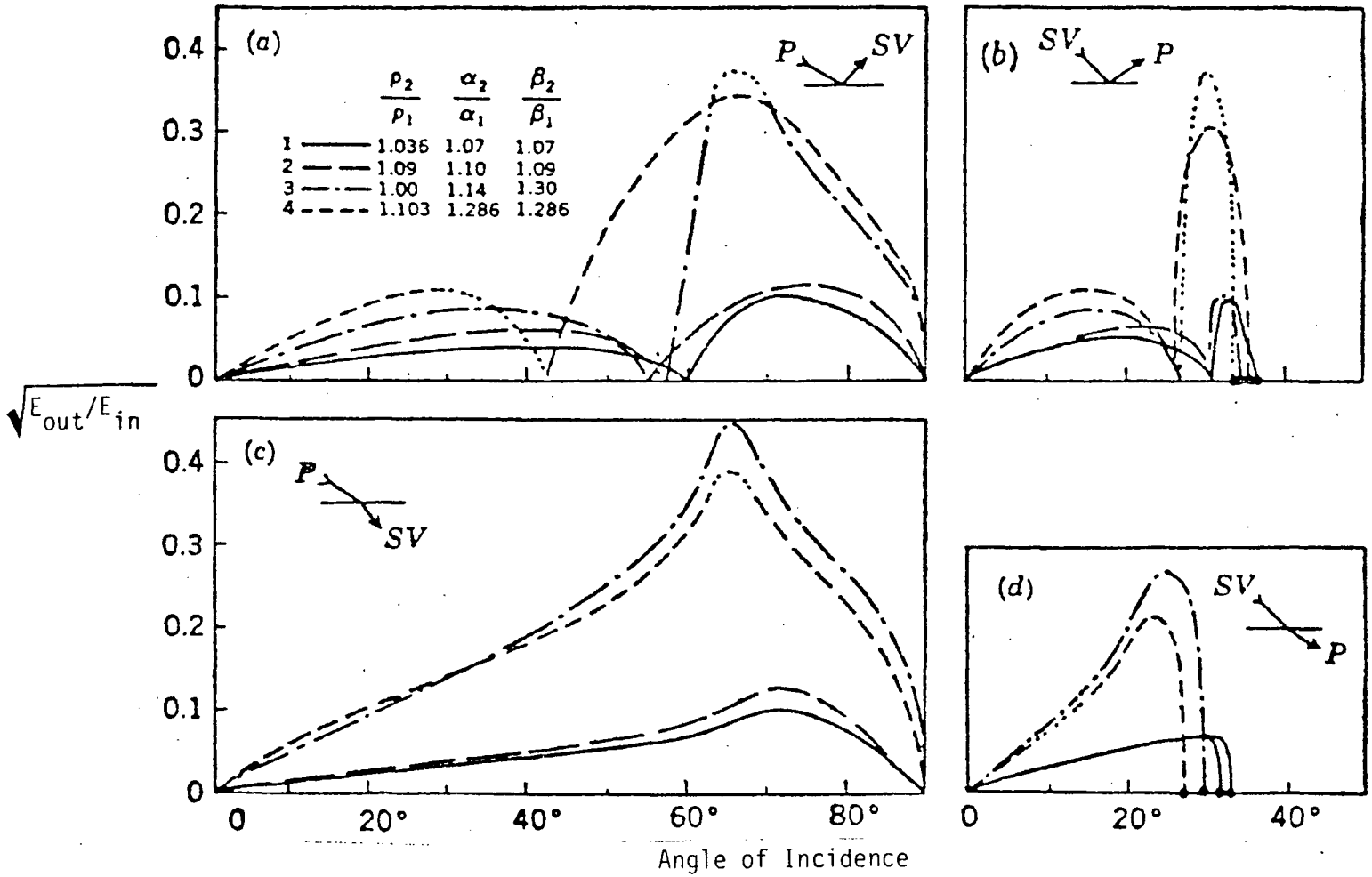


Figure 2.5. Ratio of Reflected or Transmitted Energy to Incident Energy, $\sqrt{E_{out}/E_{in}}$, When Waves Change Type (Ewing, Jardetz, and Press, 1957)

The accelerometers used in this investigation were bimorph transducers, which were 0.5 inches square in dimension and made of G1195 piezoceramic bender material. When mounted, these receivers had a natural frequency of 3 kHz, and underdamped response of 1.3 of critical. More information of this accelerometer can be obtained in technical papers from Piezo Electric Products, Inc., New Jersey. Figure 2.6 illustrates the phase response curve for a typical first-order low-pass analogue filter similar to filters within the Nicolet recorder. Equation (2.3a) illustrates the interaction of the input wavelet, filter, and output wavelet.

$$\underset{\text{input}}{|A(\omega)|e^{j\phi_1}} \rightarrow \underset{\text{filter}}{|Y(\omega)|e^{j\phi_2}} \rightarrow \underset{\text{output}}{|A(\omega)||Y(\omega)|e^{j(\phi_1+\phi_2)}} \tag{2.3a}$$

define

$$A(\omega) = |A(\omega)|e^{j\phi_1} \qquad \text{Input} \tag{2.3b}$$

$$Y(\omega) = |Y(\omega)|e^{j\phi_2} \qquad \text{Filter} \tag{2.3c}$$

$$G(\omega) = |A(\omega)||Y(\omega)|e^{j(\phi_1+\phi_2)} \qquad \text{Output} \tag{2.3d}$$

$\omega$ = angular frequency

If it is assumed that the filter has unity gain, then Equation (2.3d) reduces to,

$$G(\omega) = |A(\omega)|e^{j(\phi_1+\phi_2)} \tag{2.3e}$$

The Fourier transform, for an aperiodic wavelet, of Equation (2.3e) is

$$g(t) = \frac{1}{2\pi}\int_{-\infty}^{\infty} G(\omega)e^{j\omega t}\,d\omega \tag{2.3f}$$

In terms of the frequency, f, we have

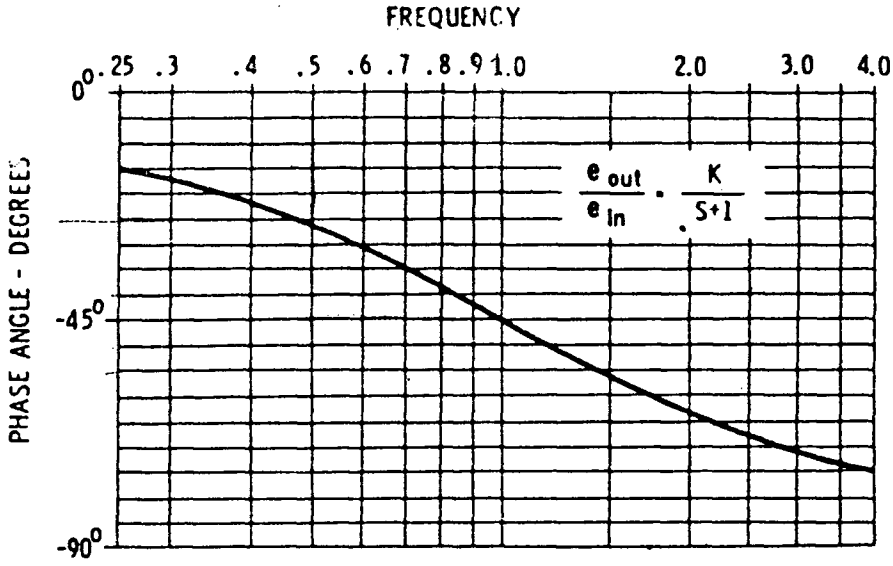


(a) Low-Pass Response

K - Time constant

S - Laplace transform variable

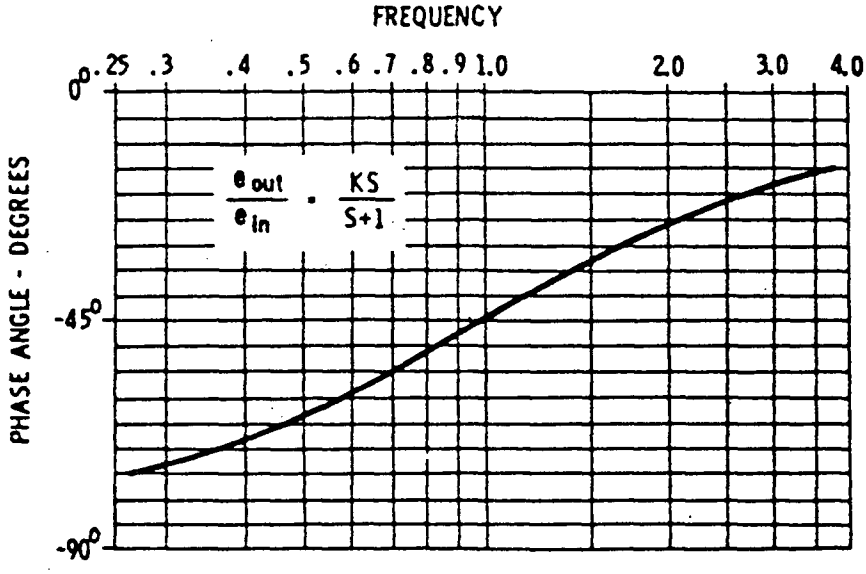


(b) High-Pass Response

Figure 2.6. Phase Response of first Order Low-Pass and High-Pass Filters (Lancaster, 1982)

$$g(t) = \int_{-\infty}^{\infty} G(f)e^{j2\pi ft}\,df \qquad (2.3g)$$

Substituting Equation (2.3e) into Equation (2.3g), gives

$$g(t) = \int_{-\infty}^{\infty} |A(f)|e^{j(2\pi ft+\gamma(f))}\,df \qquad (2.4a)$$

where

$$\gamma(f) = \phi_1(f)+\phi_2(f)$$

For an actual waveform, g(t) is real and hence Equation (2.4a) reduces to

$$g(t) = \int_{-\infty}^{\infty} |A(f)|\cos(2\pi ft + \gamma(f))df \qquad (2.4b)$$

If in Equation (2.3a) it is assumed that $\phi_1=0$ (i.e., there is no phase lag in the input signal), then

$$\gamma(f) = \phi_2 \qquad (2.4c)$$

We next consider varying the frequency of the input wavelets and determine actual time shifts by referring to Figure 2.6, which is normalized to a cutoff frequency of 100 Hz. Since P-Waves are found to lie typically between 200 to 2000 Hz, and S-Waves are typically between 50 to 300 hz in soils, we will work within these ranges.

If our input wavelet has a frequency of 50 hz, then from Figure 2.6, we have $\phi_2=-25^{o}$. From Equation (2.4c), we also have

$$\gamma(f) = -25^{o} = -0.436 \text{ rad}$$

At maximum amplitude, the cosine term in Equation (2.4b) should equal 1.0; thus

$$2\pi ft + \gamma(f) = 0$$

which implies that a time shift of

$$t = \frac{.436}{2\pi(50)} = 1.39 \text{ msec.}$$

If we consider a 150 hz signal, Figure 2.6, indicates that

$$\gamma(f) = \phi_2 = -55^{o} = -.960 \text{ rad}$$

which corresponds to a time shift of

$$t = 0.960/(2\pi(250) = 1.02 \text{ msec}$$

Thus, between 50 and 150 hz, we have a time shift difference of 370 μsec. Figure 2.7 illustrates the delay in the shear wave arrival for different applied cut-off frequencies.

An additional consideration is that the reverse polarity method demands that in picking a crossover, a consistent method must be used. For instance, one may decide that the second crossover will be used throughout the seismic investigation. But it has been found that in numerous cases this may prove to be a difficult criterion to implement due to the signal being masked by low frequency noise as illustrated in Figure 2.8 (where a 300 hz low-pass filter was applied). Ideal wavelets for determining crossovers are illustrated in Figure 2.9. Therefore, since digital filtering allows one to band-pass a desired frequency range (i.e., S or P-Wave) without distortion in and phase shift, and the crosscorrelation function makes use of all the information in the signals (averaging out irregularities and putting significance on dominant responses), this method should provide better and more reliable results than the reverse polarity method. Details of this new approach will be discussed in the next chapter.

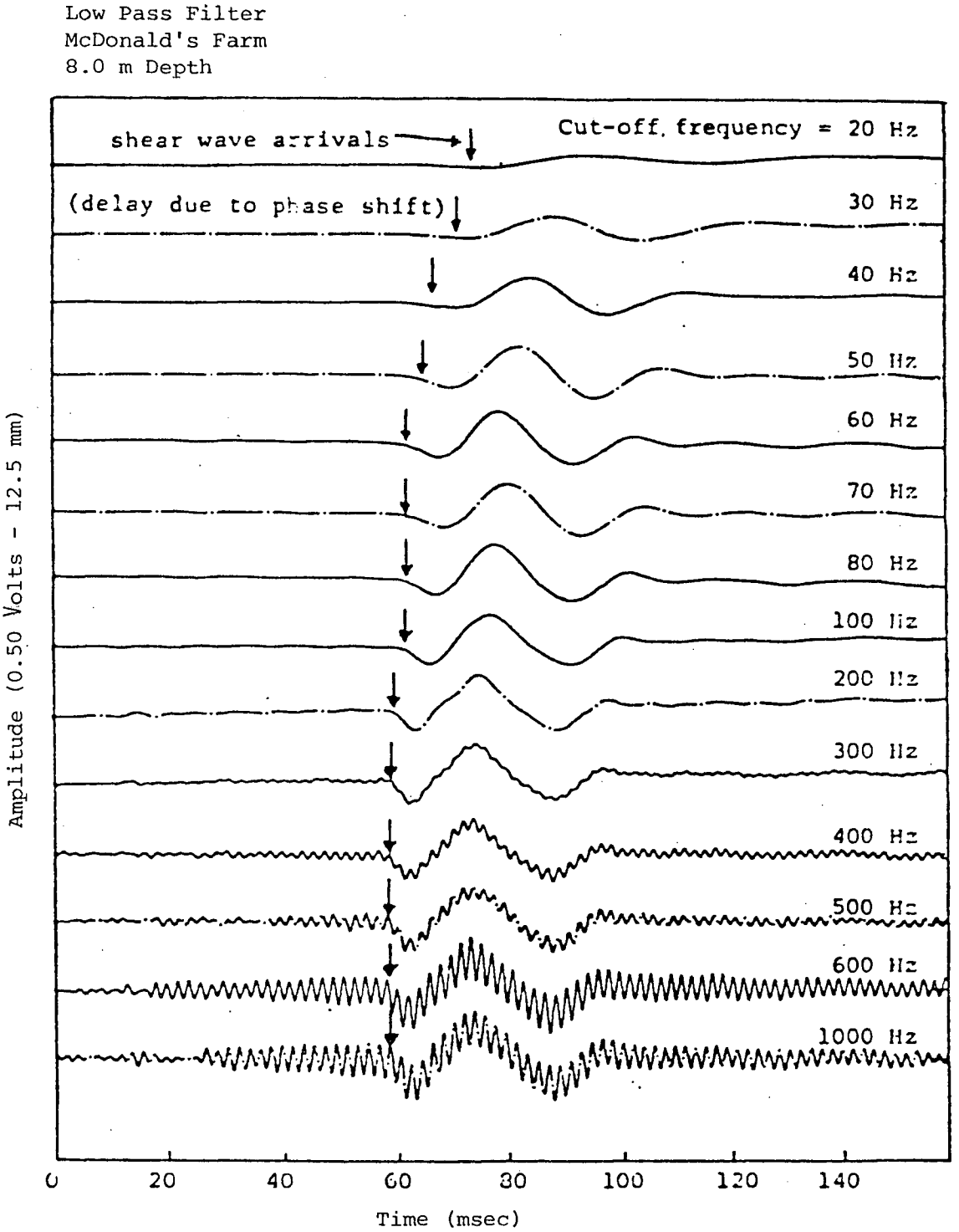


Figure 2.7. Effect of Different Filter Cut-off Frequencies on Accelerometer Responses (Laing, 1985)

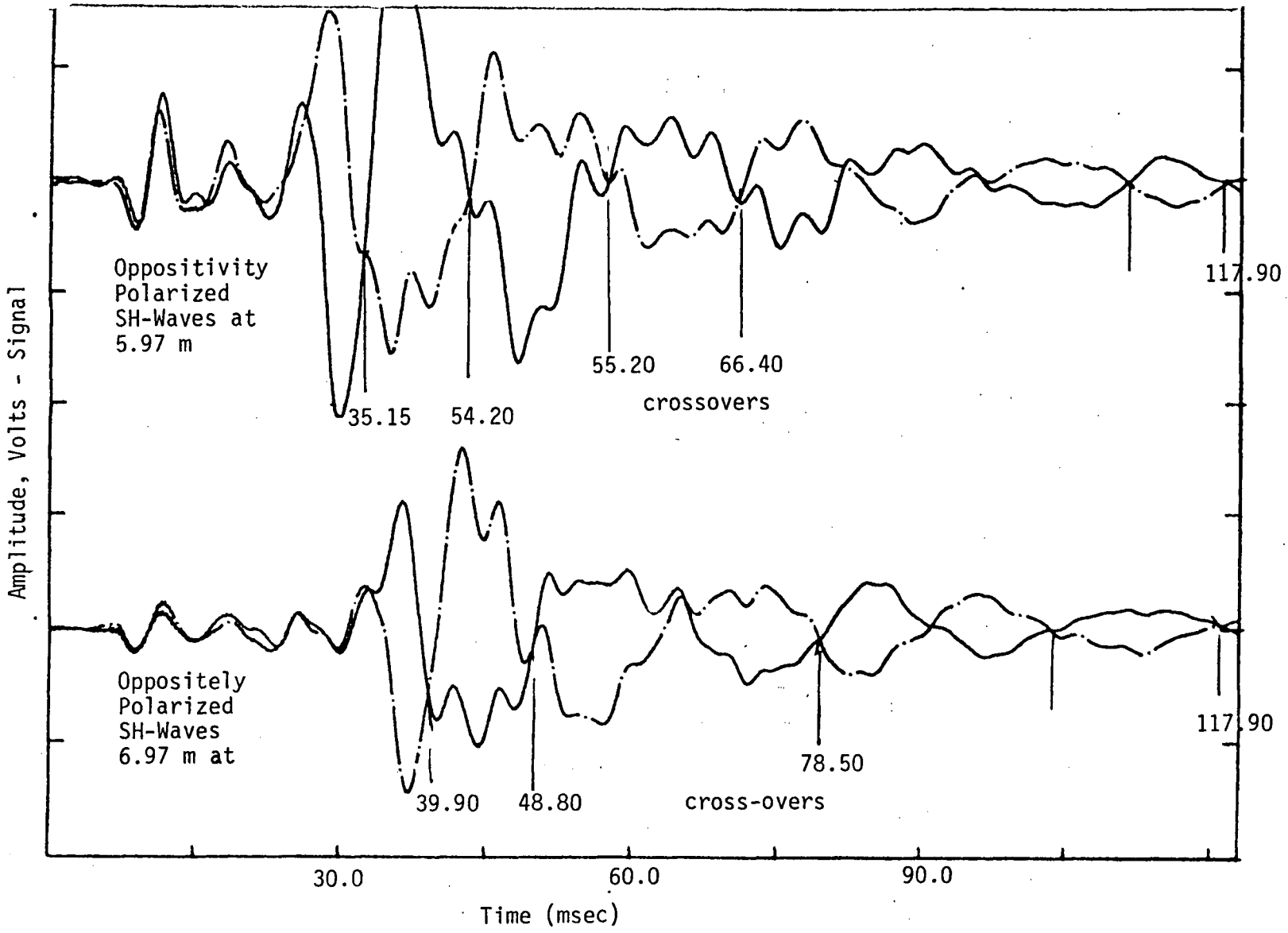


Figure 2.8. Seismic Data Acquired from Annacis Island Vibro-Compaction Site on May 18, 1988. Data Recorded with Accelerometer having a 300 Hz Low Pass Filter Applied. Diagram Illustrates Difficulty in Obtaining Crossovers due to Signal being Masked by Many Dominant Low Frequencies.

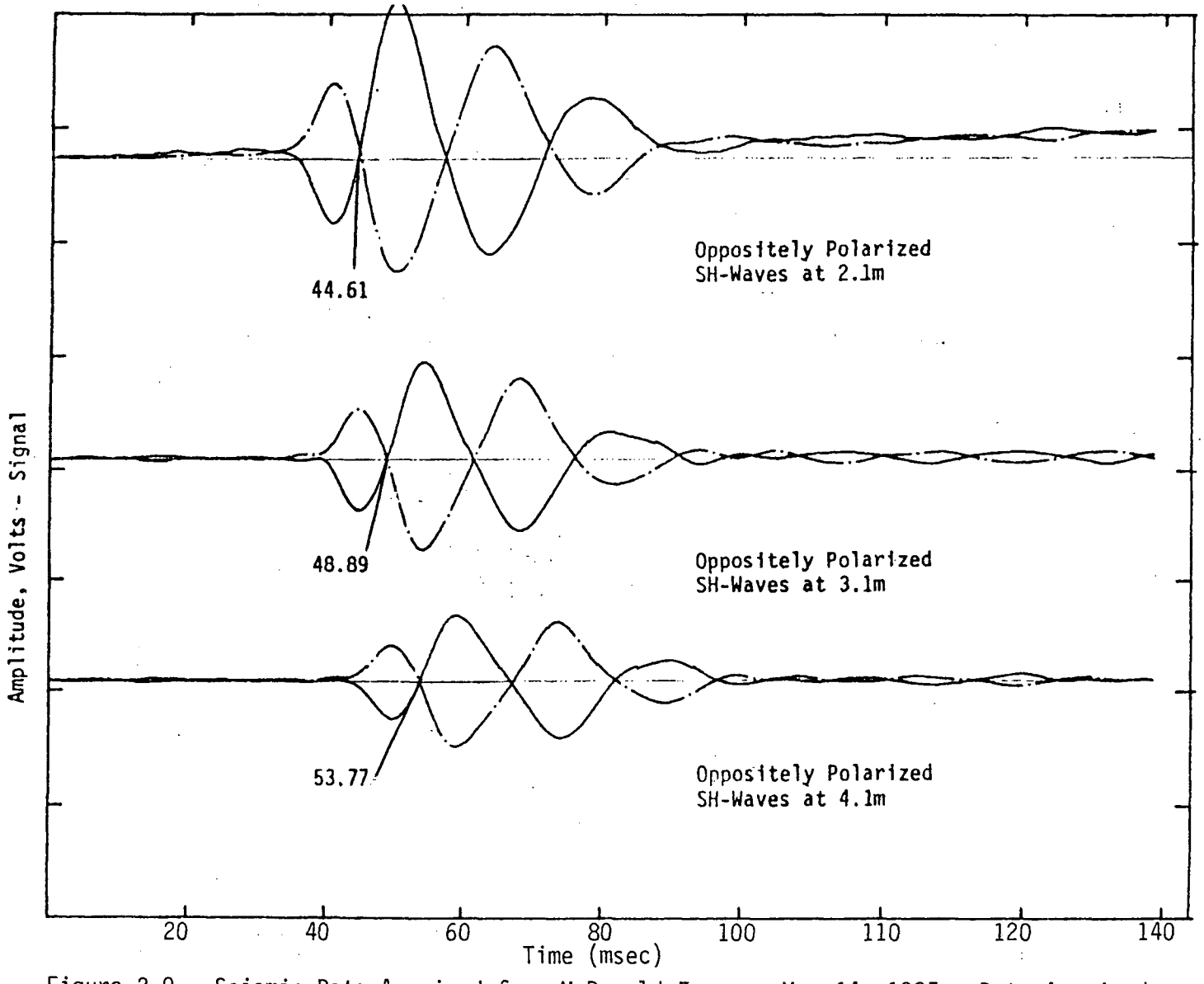


Figure 2.9. Seismic Data Acquired from McDonald Farm on May 14, 1985. Data Acquired with Geophone with Natural Frequency of 28 Hz, and 100 Hz Low Pass Filter Applied. The Diagram Illustrates Ideal Signals for Determining Crossovers.

# III. APPLICATION OF FREQUENCY DOMAIN FILTERING

## A. Discussion of the Crosscorrelation Filter Formulation

In order to obtain an appreciation of the discussed low pass frequency filter, phase lags, and time shifts, one should have a fundamental idea of what is meant by digital signal filtering and the corresponding possible side effects. Frequency filtering refers to obtaining a desired frequency spectrum from a signal which is corrupted with many different components. Most filters permit the selection of the upper and the lower limits of the passband. This concept is illustrated in the following diagram:

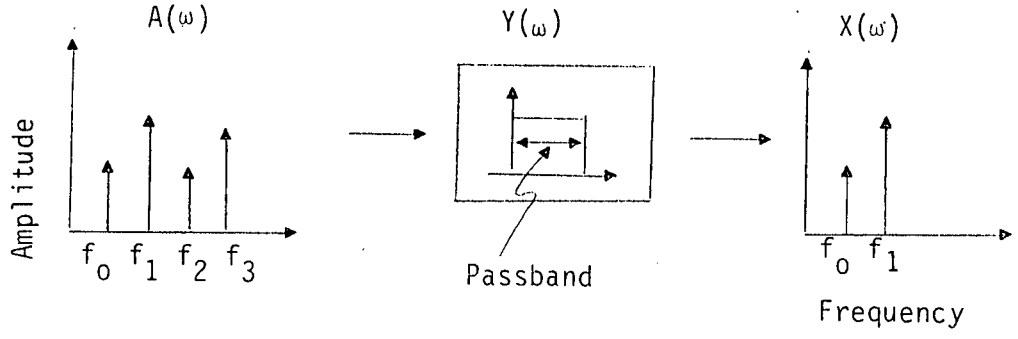


Figure 3.1. Illustration of Filtering Desired Frequencies

It is usually possible to select the sharpness of the cutoff (the rate at which the gain, $|Y(\omega)|^2$, decreases as it leaves the passband). Typical filter response curves are specified by their cutoff frequencies, that is, the frequency at which the gain has dropped by 3 dB (30% of amplitude, 50% of power).

Filter design is critically dependent on the sampling rate of data acquisition. The sampling theorem defines the minimum sampling interval one can apply data acquisition without losing a wavelet's identity (aliasing). In general, no information is lost by regular sampling provided that the sampling frequency is greater than twice the highest frequency component in the waveform being sampled. The above concept is illustrated in Figure 3.2, where we have a 4 ms sampling interval for wavelets of 75 hz, 175 hz and 250 hz frequency components. Note that only (a) in Figure 3.2 gives a true response since the signal of 75 hz is being sampled at 250 hz or about 3 1/2 times faster than the signal.

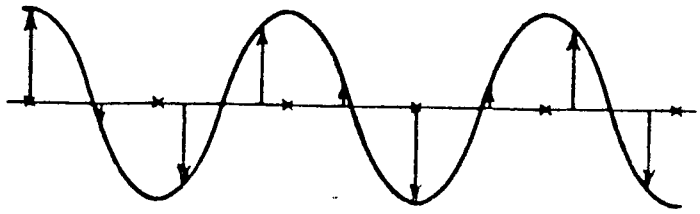

(a)

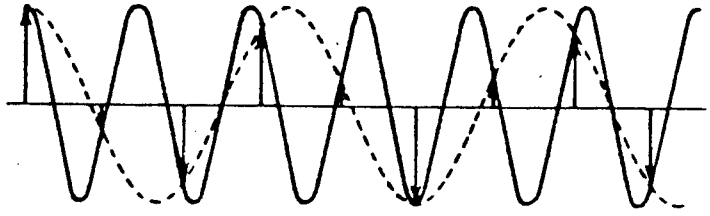

(b)

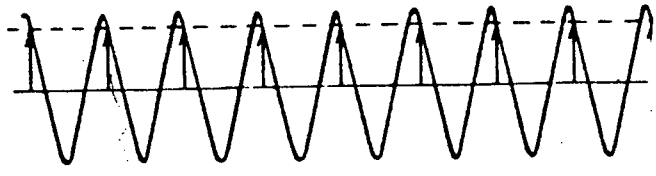

(c)

Figure 3.2. Sampling and Alaising Different Frequencies Sampled at 4 ms Intervals (250 Times Per Second). (a) 75 Hz Signal; (b) 175 Hz Signal Yields Same Sample Values as 75 Hz; (c) 250 Hz Signal Yields Samples of Constant Value (0Hz) (R.E Sheriff and L. P. Geldart, 1983)

Half the sampling frequency is represented by the Nyquist frequency, fN, where $fN=1/(2\Delta t)$, $\Delta t$ being the sampling interval. Frequencies which are greater than fN by the amount $\Delta f$ will be indistinguishable from the lower frequency $fN-\Delta f$. In summary, one can state that wavelet g(t) can be recovered exactly from the sampled values provided g(t) does not contain frequencies higher than the Nyquist frequency. When taking the Fourier transform of g(t), G(f), it will only contain information about g(t) for

frequencies within the interval -fN to fN. The Fourier series will repeat G(f) in each interval of width 2fN.

Having discussed the importance of the sampling rate, it is useful to further expand on filtering concepts. Filters pass the desired information from a source wavelet. Usually filters attempt to remove specified frequency components of a sampled wavelet, which sometimes results in the filter altering the amplitude and/or phase spectra of signals which pass through it. This altering results because a filter is defined by its own amplitude and phase spectra just like a wavelet. When these two interact, they produce an output signal which is a product of the interaction of the wavelet and filter. This output is then defined by its own amplitude and phase spectra. This process is illustrated on page 2-8 and repeated in Figure 3.3 for convenience.

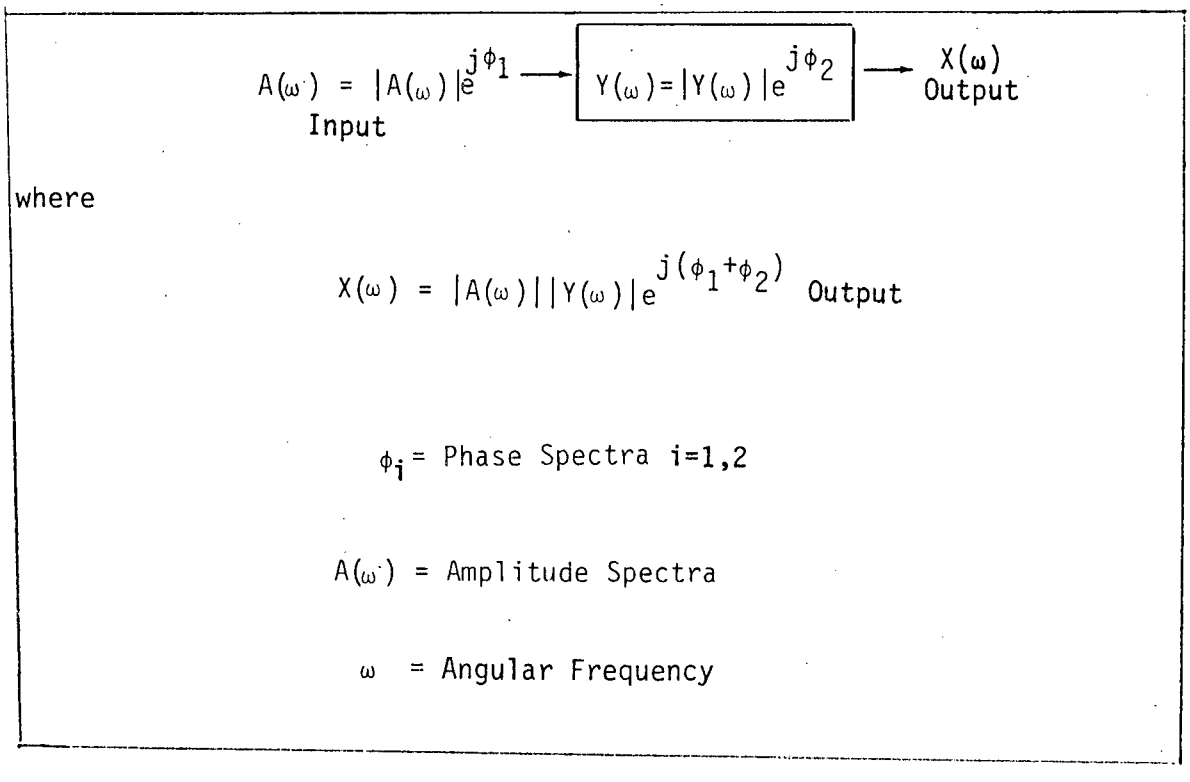


Figure 3.3. Changes in Phase and Amplitude Spectra Resulting from Interaction of Filter and Input

Frequency filters are generally classified as low-pass, high-pass band-pass, respectively, as they discriminate against frequencies above or below a certain limiting frequency or outside of a given band of frequencies. An ideal filter is one which has a gain of unity ($|G(f)|^2=1$) for frequencies within the passband and zero for those within the stopbands. Moreover, it is advantageous that the filter produce zero phase shift, so that the phase spectra, $\phi_2(f)$, is zero for all frequencies. "Ideal" filters of these types are the following

$$\text{Low-pass } G_L(\omega) = \begin{cases} +1, & |\omega| < |\omega_0| \\ 0, & |\omega| < |\omega_0| \end{cases}$$

$$\text{High-pass } G_H(\omega) = \begin{cases} 0, & |\omega| < |\omega_0| \\ +1, & |\omega| > |\omega_0| \end{cases}$$

$$\text{Band-pass } G_B(\omega) = \begin{cases} +1, & |\omega_1| < \omega < |\omega_2| \\ 0, & |\omega_1| > \omega \text{ or } \omega > |\omega_2| \end{cases}$$

$\omega$ = Angular Frequency

These filters are discontinuous at $\omega_0$, $\omega_1$, and $\omega_2$.

The low-pass filter is obtained by applying a box car function with a certain passband $\omega_0$. The box car function is illustrated in Figure 3.4, with its associated transform.

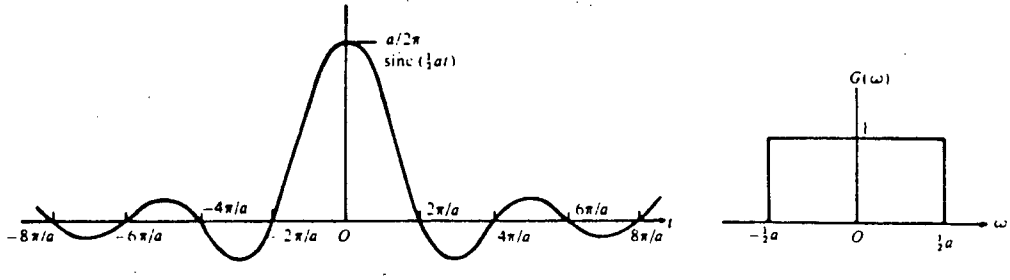


where $\text{sinc}(.5at) = \dfrac{2\sin(.5at)}{at}$

Figure 3.4. Example of a Box Car Function, G(ω), and Its Transform, Sinc (.5at) (R. E. Sheriff & L. P. Geldart, 1983)

The low-pass filter is defined by the following expression:

$$G_L(\omega) = box_{2\omega_0}(\omega) \leftrightarrow (\omega_0/\pi)sinc(\omega_0 t) = g_L(t) \qquad (3.1)$$

where $\leftrightarrow$ denotes the Fourier transform.

For digital functions, provided $|\omega_0| < \omega_N = \pi/\Delta t$, $\omega_N$ = Angular Nyquist frequency

$$g_t^L = (1/\pi) \sum_{n=-L}^{L} \omega_0 \, sinc(n\omega_0 \Delta t) \qquad (3.2)$$

where $L \to \infty$

It can mathematically be proven that the expression of the high-pass filter is essentially the same as that for the low-pass filter, where $g_H(t)=-g_L(t)$, provided both filters have the same cutoff frequency $\omega_0$. In deriving the passband filter one just manipulates the high and low-pass filters to interact where the passband lies within the desired limits.

The result of using a finite series for $g_t^L$ is to introduce ripples, both within and without the passband, the effect is especially noticeable near the cutoff frequency. This is referred to as the Gibbs' Phenomenon. Gibbs' Phenomenon describes the distortions which occur at discontinuities within filtered signals. This phenomenon can be conceptualized in the time domain. A signal truncated due to a short recording time, is analogous to multiplying the signal with a box car function which results in distortions or "ringing" in the frequency domain. As the signal's recording time increases "ringing" becomes less prevalent because more information of the signal is transformed and the finite series expressed in Equation (3.2) is carried out further. These concepts are illustrated in Figure 3.5(b) where a 100 hz cosine signal is being multipled with a box car function. Figure 3.5(a) illustrates the "ringing" effect in the frequency domain.

Figure 3.6 gives an illustration of the harmonic makeup of specific waveforms. In these figures a rectangular wave is constructed by adding a successive number of harmonics to the fundamental frequency. As is illustrated, the more harmonics added, the better is the approximation to a rectangular wave and/or a box car function.

(a)

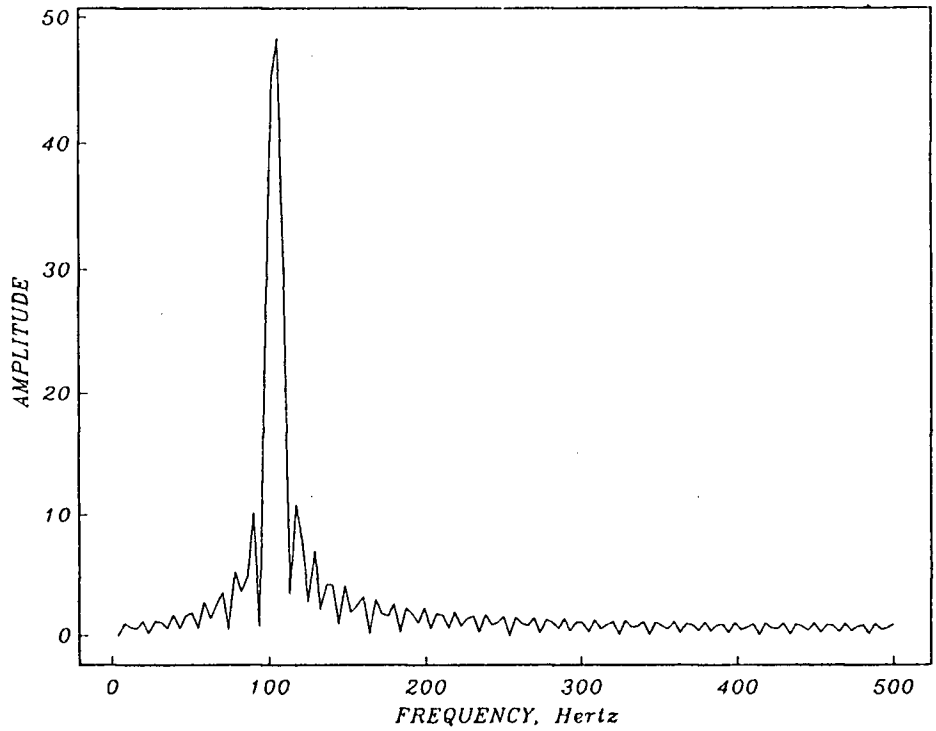


(b)

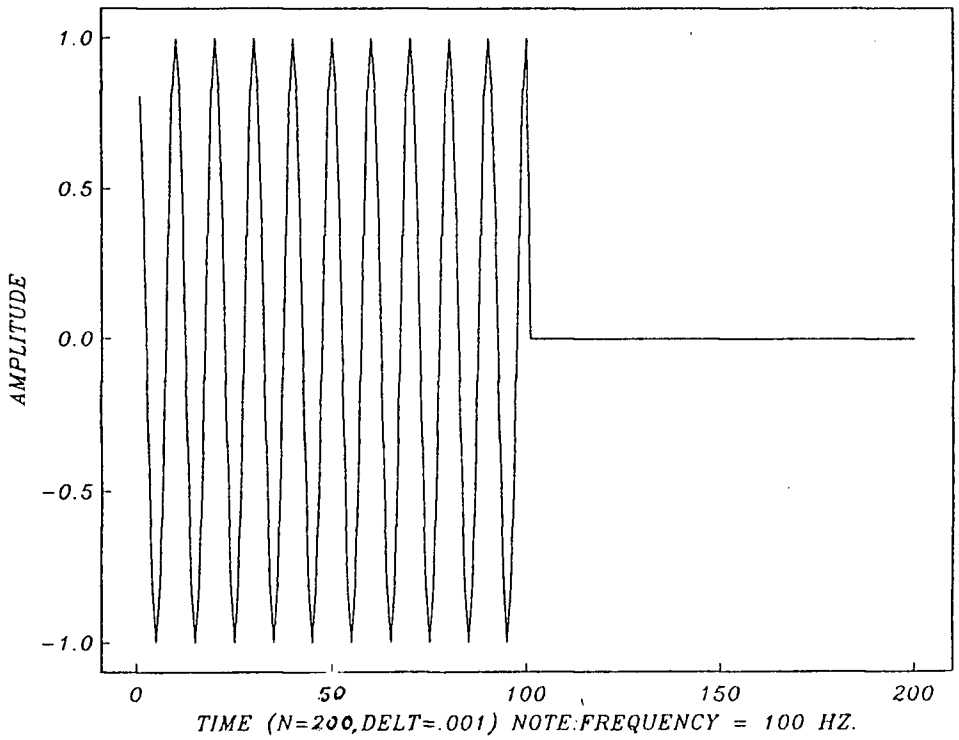


Figure 3.5. Illustrating Gibbs' Phenomenon (a) Frequency Spectrum and (b) Truncated Signal

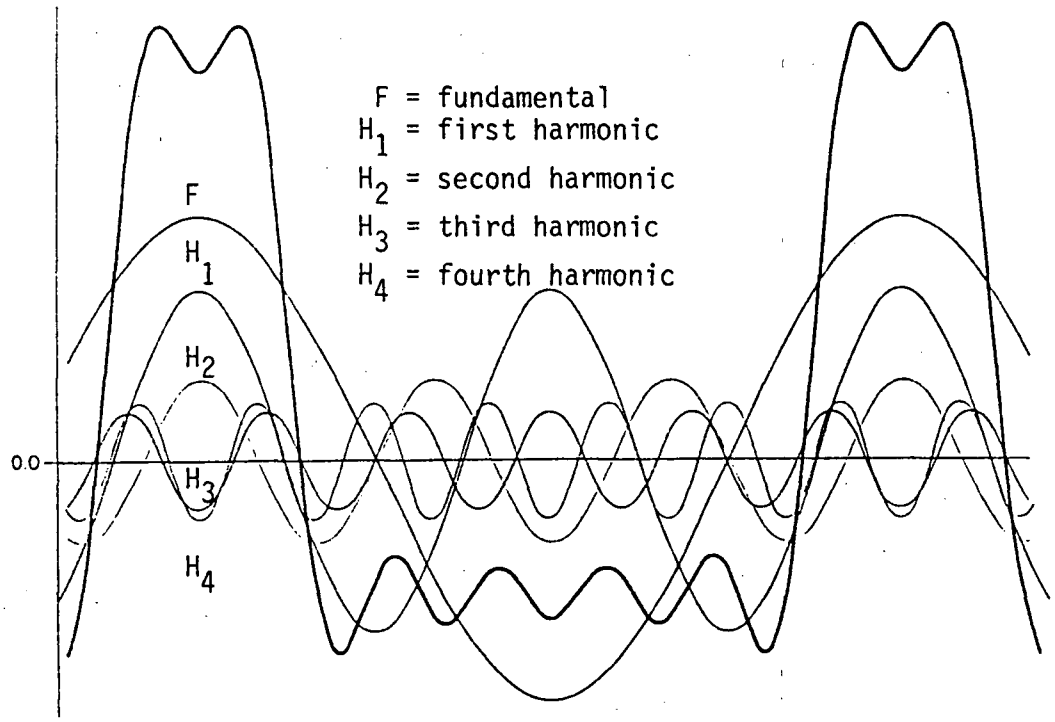


(a) Rectangular Wave Produced by Adding Four Harmonics to the Fundamental. Shape of Composite Wave is Determined by Relative Amplitudes and Phases of Harmonics.

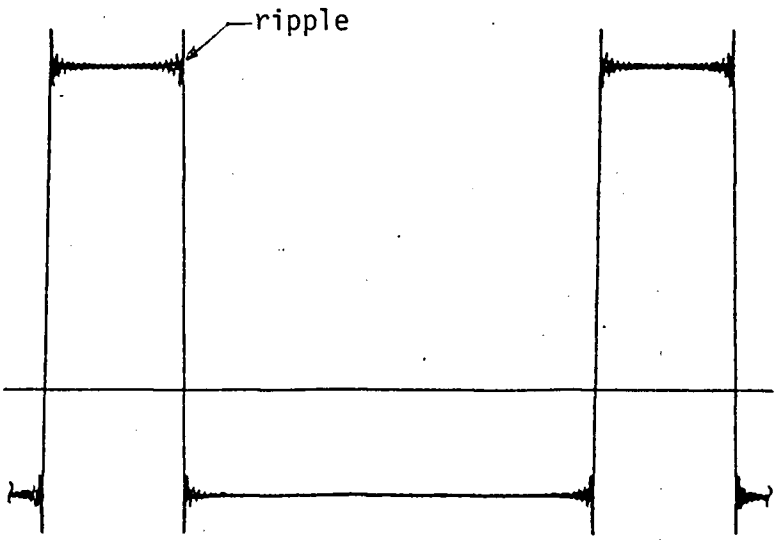


(b) Rectangular Waves Produced by Combining 100 Harmonics. Note Reduction in Ripple.

Figure 3.5. Composition of Rectangular Wave from Harmonics (after, O. W. Stimson, 1983).

Having discussed the problems associated with designing filters, one should now explore existing filters which lessen or remove the severity of undesired filtering effects. A filter which has many advantageous qualities is the Butterworth filter.

## Butterworth Filter

The Butterworth filter is a common form of low-pass filter, and it can be defined by

$$|G(\omega)|^2 = 1/\ \{1+(\omega/\omega_0)^{2N}\} \qquad (3.3)$$

where $\omega_0$ is the "cutoff" frequency and N determines the sharpness of the cutoff. Curves of $|G(\omega)|^2$ for various values of N are shown in Figure 3.7.

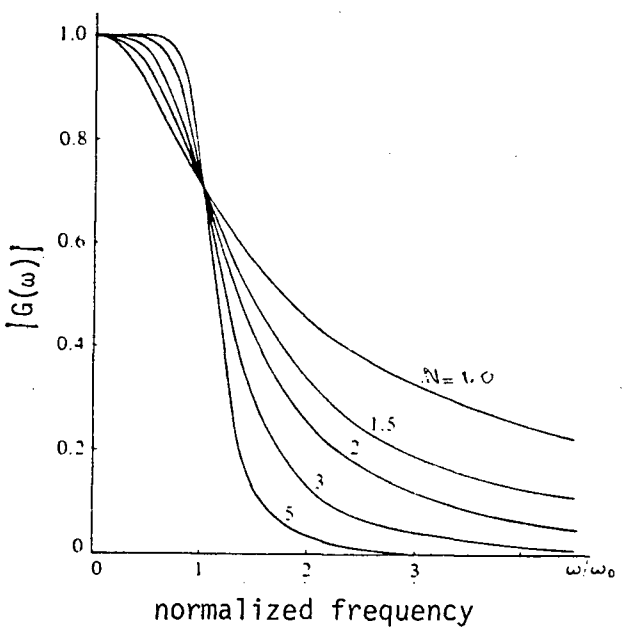


Figure 3.7. Amplitude Response of a Butterworth Filter (R. E. Sheriff & L. P Geldart, 1983)

The advantages associated with the Butterworth filter are as follows:

- o Their transfer functions are smooth and maximally flat both inside and outside the passband.
- o The squared filter (i.e., the input is filtered twice so that the amplitude response is $|G(\omega)|^2$) produced zero phase shift and its power is down by 3 dB (factor of 1/2) at the cutoff frequency. (The cutoff frequency determines the half-power point of the filter).

The value of N specifies the rate of attenuation where a larger value of N gives a greater rate of attenuation and "ringing" effect (i.e., Gibbs' Phenomenon). An example of a calculation to determine the value of N necessary is given below.

If the required attenuation, measured in units of power, at $2\ \omega_o$ is 48 db down from attenuation at $\omega_o=0$, what value of N is necessary for a Butterworth filter? From a definition of the decibel scale (decibel level=10 $\log_{10}$ (power/reference power) and using Equation 3.3, we have

$$\omega/\omega_o \equiv W$$

$$10 \log_{10} (1/(1+W^{2N}))_{W=0}/(1/(1+W^{2N})_{W=2} = 48$$

so that

$$(1/(1+2^{2N})) = 10^{-4.8}$$

Approximately then

$$(1/2^{2N}) = 10^{-4.8}$$

and

$$N = 4.8/2 \log 2 = 4.8/2(.301) = 8$$

Therefore N=8 is required to obtain the required attenuation. In general the power changes by 6 db for a unit change in N.

An important aspect that must be taken into account when applying the Butterworth filter is the aliasing problem. When one approaches the angular Nyquist frequency of the sampled signal, aliasing errors may result when the

transfer function of Equation 3.3 is applied. This is conceptually illustrated in Figure 3.8 where a Fourier transform of a signal with Nyquist of $\omega_N$ is shown. It is noted from Figure 3.8 that the Fourier Transform of this function is periodic with period $2\pi/\omega_N$.

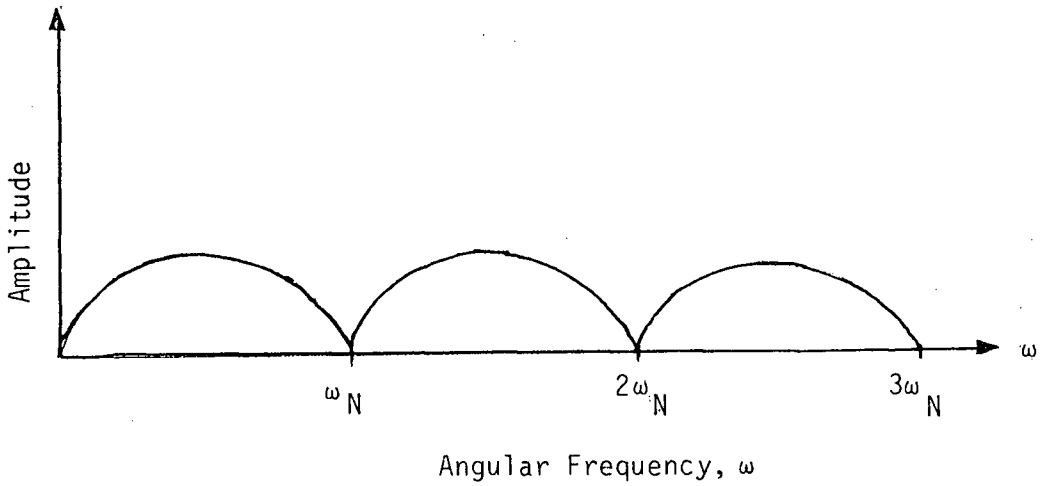


Figure 3.8. Fourier Transform of a Signal with Nyquist $\omega_N$

If we try to filter frequencies higher than the Nyquist (i.e., apply a cut-off frequency higher than the Nyquist), higher frequencies will fold into the filtered signal. This is illustrated in Figure 3.9.

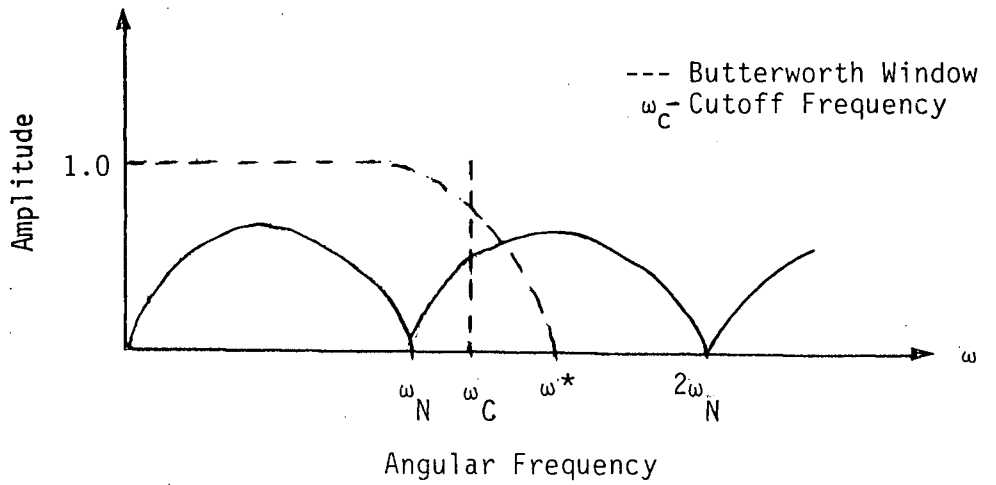


Figure 3.9. Illustration of the Aliasing Problem When Filtering

In Figure 3.9, frequencies within $\omega^*$ are incorporated into the signal. In order to avoid this problem, a bilinear Z transform is applied. The bilinear Z transform converts a continuous transfer function into one which can be used on sampled data. Furthermore it eliminates aliasing errors by applying the following frequency transformation:

$$\omega d = \frac{2}{\Delta t} \tan \frac{\omega \Delta t}{2} \quad -\pi/\Delta t < \omega < \pi/\Delta t \tag{3.4}$$

where

$\omega d$ = transformed or deformed angular frequency used to calculate the bilinear Z transform

$\omega$ = angular frequency in the original transfer function Equation (3.3)

This frequency transformation, $\omega d$, causes warping of the input frequencies when they approach the Nyquist frequency. This warping is illustrated in Figure 3.10.

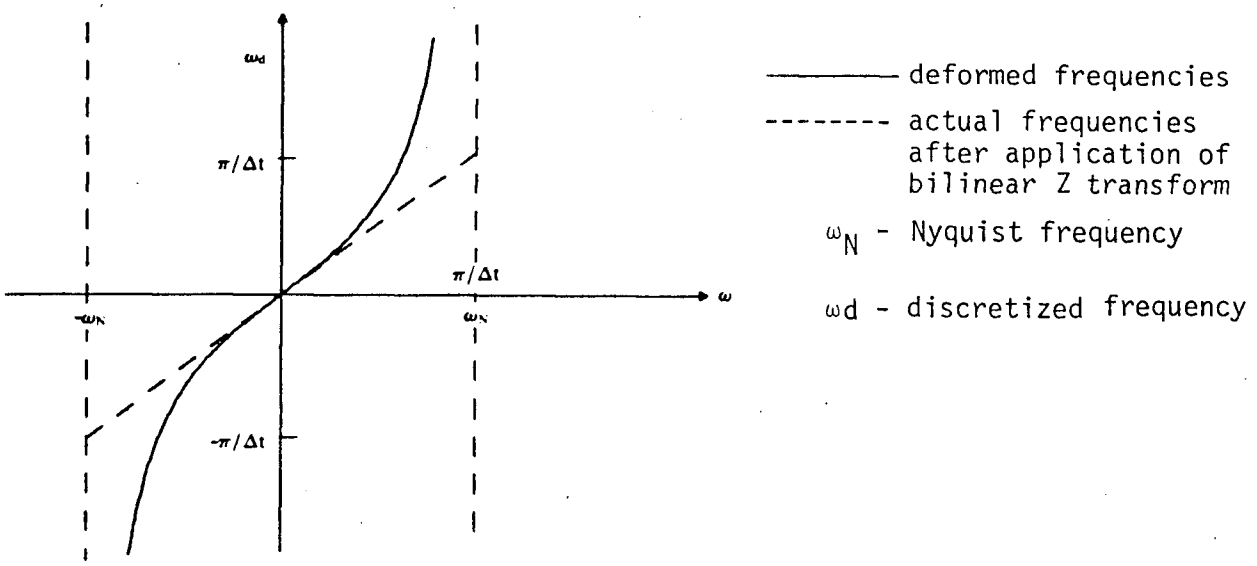


Figure 3.10. Relationship Between the Deformed Angular Frequencies $\omega d$, for the Bilinear Z Transform and the Actual Frequencies, $\omega$, of the Digital Filter (E. R. Kanasevich, 1981).

The Butterworth filter, when constructed in the time domain, is a physically realizable, recursive filter. Physically realizable (causal) filters are those which do not demand future input values to compute output values. A recursive filter is one which feeds back part of the output to compute new output. The Butterworth filter having the transfer function given by Equation 3.3 has the following time-domain relationship

$$Y_n = \sum_{m=0}^{N} C_n X_{n-m} + \sum_{m=1}^{N} B_m Y_{n-m} \qquad (3.5)$$

where the index N determines the order of the Butterworth filter.

The Butterworth transfer function G(f) can be constructed as a product (cascade) of second order (N=2) G2(f) and first order (N=1) G1(f) Butterworth filters. For instance, an eighth order Butterworth filter would be defined by the following expression

$$G(f;8) = G2(f) \times G2(f) \times G2(f) \times G2(f) \qquad (3.6)$$

Use of cascade filtering simplifies the algebra when designing the filter and reduces round-off error relative to a brute force calculation of G(f) for each order (Reference 14). Thomson and Chow (1980) discuss how the Z-domain transfer functions of the first and second order Butterworth filters are obtained, and determine the corresponding time-domain coefficients. The time-domain algorithms for the first order (N=1) and second order (N=2) Butterworth filters are, respectively,

$$Y_n = d_o X_n + d_1 X_{n-1} + e_1 Y_{n-1} \qquad (3.7)$$

$$Y_n = c_o X_n + c_1 X_{n-1} + c_1 X_{n-2} + b_1 Y_{n-1} + b_2 Y_{n-2} \qquad (3.8)$$

where

$X_n$ = input

$Y_n$ = filtered output

The Butterworth filter has zero phase lag because a waveform is front fed and then back fed into the filter. Clearly, if there is a phase shift at a given frequency in the first pass through the filter, there will be an equal phase shift of opposite sign at the frequency in the second pass. By processing the data in reversed chronological order through the filter, the two phase shifts cancel exactly.

Another consideration to take into account when processing the data, is the finite length of the time series. This finite length can be viewed as a truncation, where we multiply an infinite length series by a box car function. This multiplication results in Gibbs' Phenomenon in the frequency domain, as was previously discussed. These concepts are again illustrated in Figures 3.11 and 3.12. In Figure 3.11 we have an ideal infinite length time series with a 60 hz frequency content. The Fourier transform of this signal gives ideal Dirac deltas at -60 and +60 hz in the frequency domain.

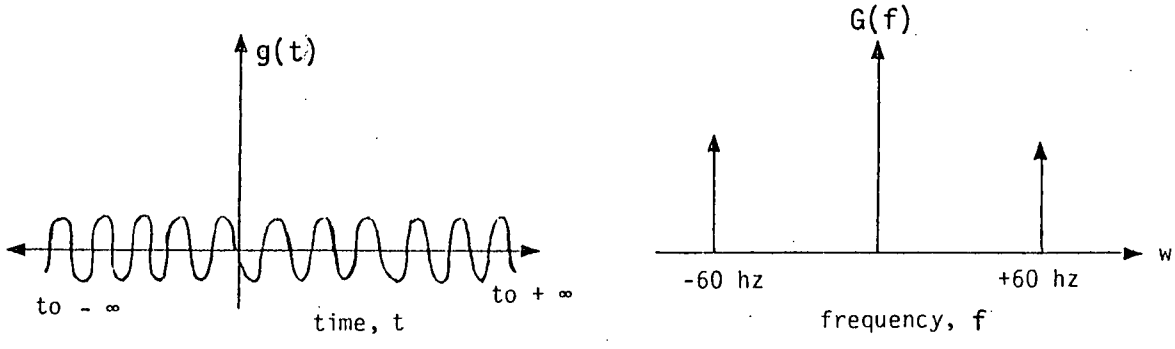


Figure 3.11. An Infinitely Long Sinusoidal and Its' Fourier Transform

Figure 3.12 illustrates the frequency spectrum obtained from a time series truncated by a box car function in the time domain.

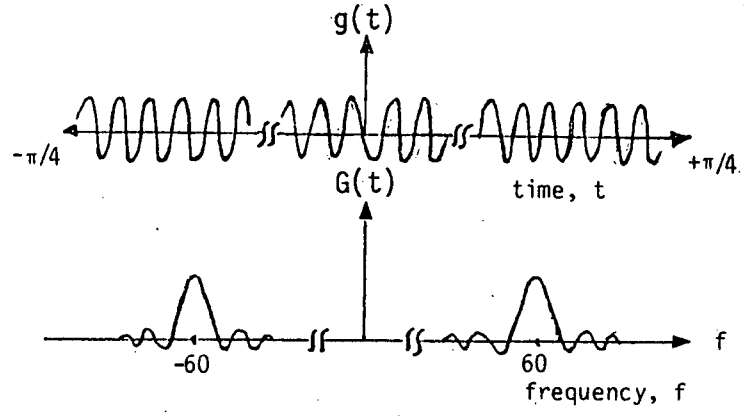


Figure 3.12. A Truncated 60 Cycle Signal and its Fourier Transform. The Signal was Switched on for π/2 Second

In order to remove the "ringing" effect, the data is tapered. The time series can be tapered by a pair of cosine bells, where the first and last points of the trace approach the mean value of the series, which is usually zero. Equation 3.9 gives us the cosine bells, and Figure 3.13 illustrates the tapering window.

$$w_n = \begin{cases} (1 + \cos \frac{\pi(n+L)}{M})/2 & -(L+M) < n < -L \\ 1 & -L \leq n \leq L \\ (1 + \cos \frac{\pi(n-L)}{M})/2 & L < n < L+M \end{cases} \qquad (3.9)$$

where M determines the period of the cosine bell (i.e., the roll-off of the window), and 2L is 80% of the length of the time series. Hamming (1977) recommends that M be about 10% of the existing data with 80% in the flat part of the window. The data can then be padded with zeros. In this way, there are no discontinuities to initiate transients during the Fourier transform.

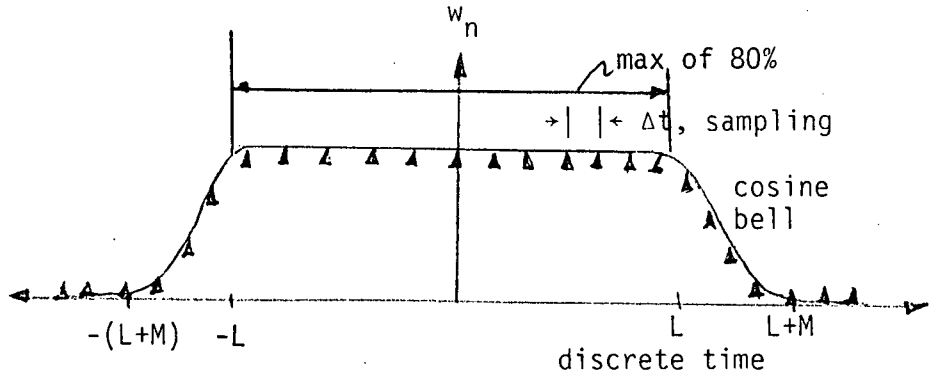


Figure 3.13. A Data Window Used to Taper a Discrete Function

## Crosscorrelation

The first step in determining the interval times, once seismic wavelets are adequately filtered, is to apply crosscorrelations. The crosscorrelation of the successive wavelets is defined as

$$\Phi_{xy}(\tau) = \sum_{K} X_k Y_{k+\tau} \qquad (3.10)$$

where $\tau$ is the time shift between the two time series. The crosscorrelation provides information between the two wavelets. In this case we are looking for the arrival time differences between the dominant responses of the recorded wavelets. With the above consideration, one can postulate that when the value of $\Phi_{xy}(\tau)$ in Equation 3.10 is maximum, we have time shift which is representative of the time interval $\Delta T$ as applied from Equation 2.2a on page 2-2.

As stated previously, $\Phi_{xy}(\tau)$ is the value which represents the difference in the arrival times of the dominant responses of the wavelets. Therefore their crosscorrelation is essentially an autocorrelation if the wavelets are the same with maximum value at $\tau$. This concept is illustrated in Figure 3.14.

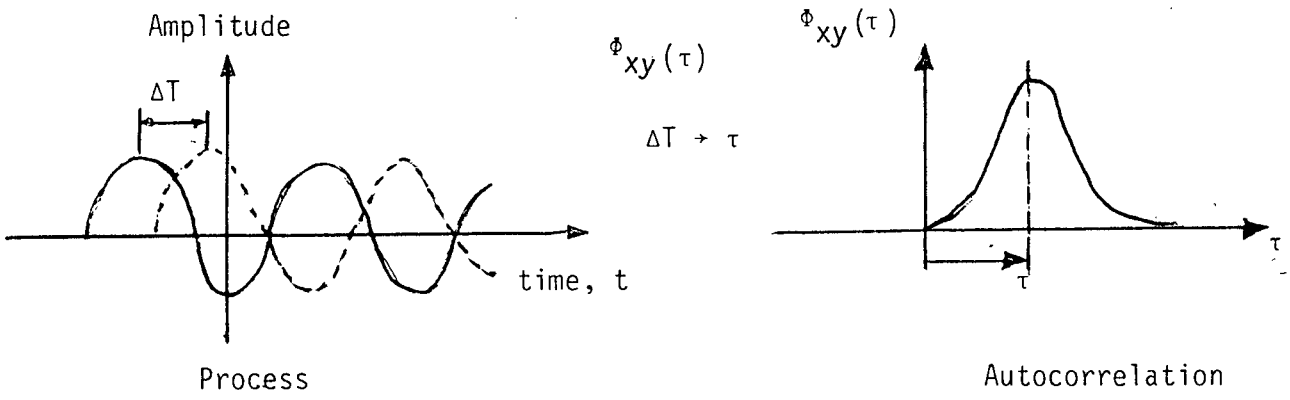


Figure 3.14. Autocorrelation of a Process

An important aspect to consider when applying crosscorrelations to seismic wavelets is D.C. shifts. D.C. shifts occur when the recorded signal is not centred at zero mean. Equation 3.10 defined the crosscorrelation of two data sets $X_t$ and $Y_t$ where $\tau$ is the displacement of $Y_t$ relative to $X_t$. This equation is generally applied to the signals when they have zero mean (which corresponds to zero D.C. offset). A simple example is illustrated by correlating the two functions, $X_t=\{1,-1,-1/2\}$ and $Y_t=\{1,1/2,-1/2\}$, shown in Figure 3.15.

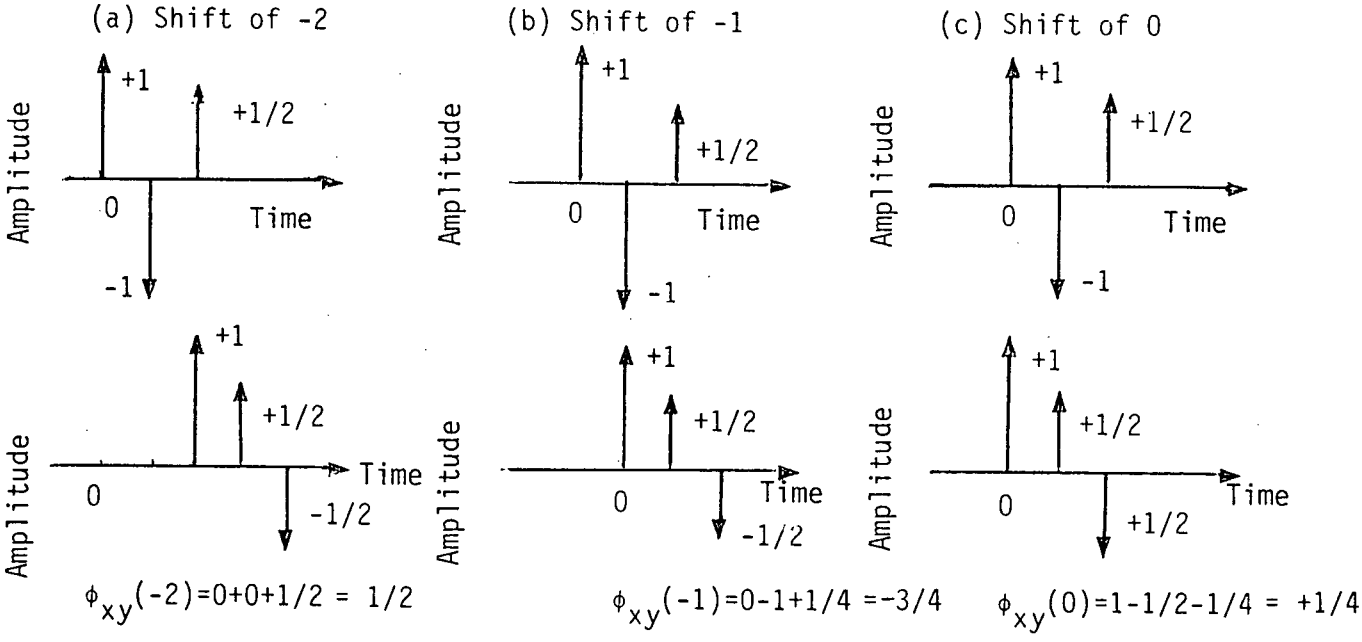


Figure 3.15. Calculating the Crosscorrelation of Two Functions

At the end of the signals the functions are padded with zeros in order that they will provide no contribution to correlation values.

Let us now consider the two signals, shown in Figure 3.16, with negative D.C. offset $d_1$ and $d_2$, respectively.

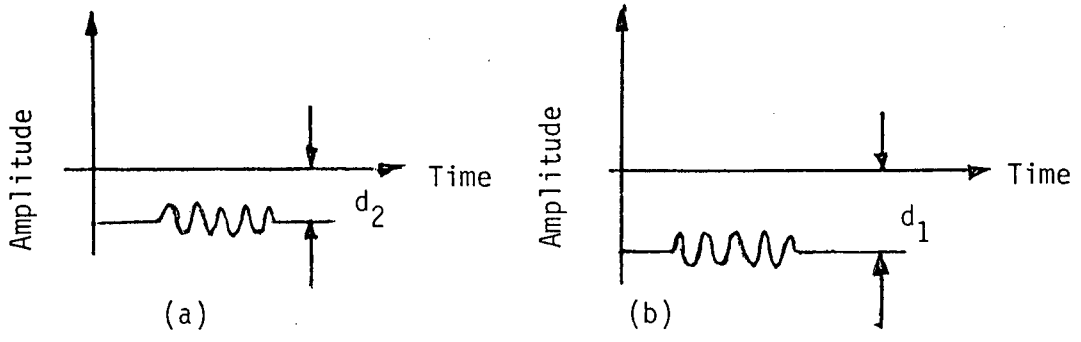


Figure 3.16. Signals with D.C. Shifts $d_1$ and $d_2$

Before taking the crosscorrelation of these signals, they are first padded with zeros, which is illustrated in Figure 3-17.

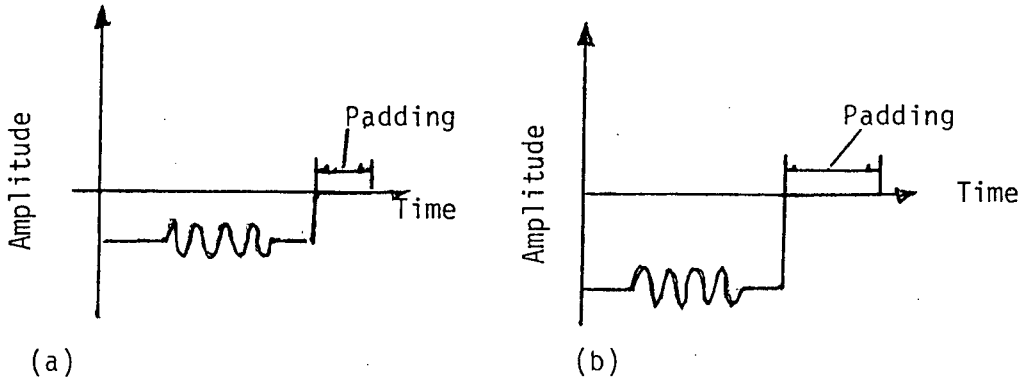


Figure 3.17. Padding Signals with Zeros at the End of Their Time Series

When taking the crosscorrelation of the functions, shown in Figure 3.17, we essentially have the autocorrelation of a box car function, which is illustrated in Figure 3.18.

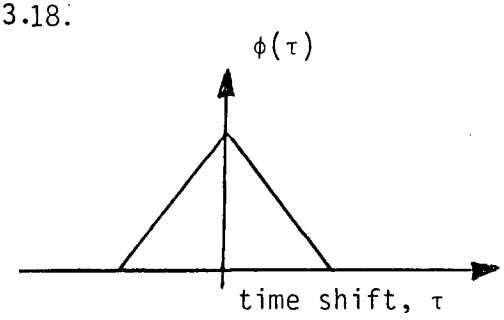


Figure 3.18. Autocorrelation of Box Car Function

Therefore, in order for the signals to give representative crosscorrelation values, they should first be adjusted so that they are centred at zero offset.

Another way of looking at the D.C. shift problem is to consider Equation 3.10. An offset can be represented by shifting one signal relative to the other, that is $X'_k = X_k + C$ where C is a constant. In this case Equation 3.10 becomes

$$\Phi'_{xy}(\tau) = \sum_k X'_k \, Y_{k+\tau} \qquad (3.11a)$$

$$= \sum_k (X_k + C) Y_{k+\tau} \qquad (3.11b)$$

$$\Phi'_{xy}(\tau) = \Phi_{xy}(\tau) + \sum_k C Y_{k+\tau} \qquad (3.11c)$$

Equation (3.11c) clearly shows that the D.C. shift would result in a misrepresentative crosscorrelation value.

For a practical example, consider the two wavelets shown in Figures 3.19 and 3.20 with D.C. shifts of -0.06 and -0.2, respectively.

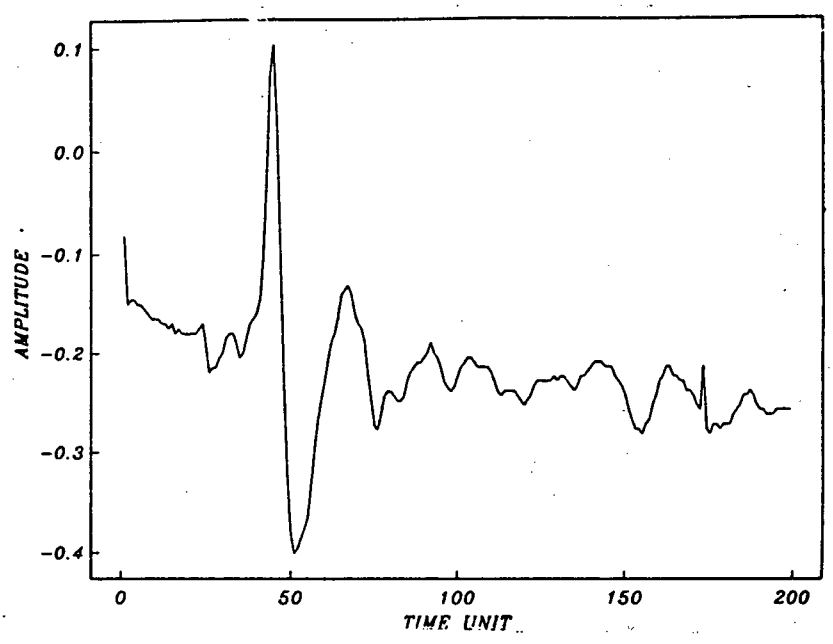


Figure 3.19. Signal with D.C. Offset of -0.20

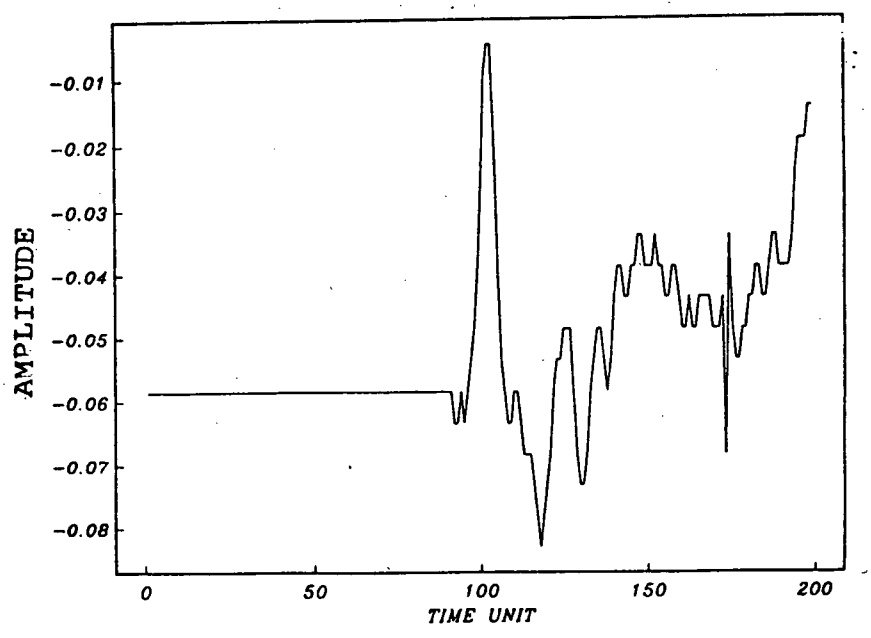


Figure 3.20. Signal with D.C. Offset of -0.06

Taking the crosscorrelation of these two signals, we obtain the triangle function in Figure 3.21 (with positive time shift shown).

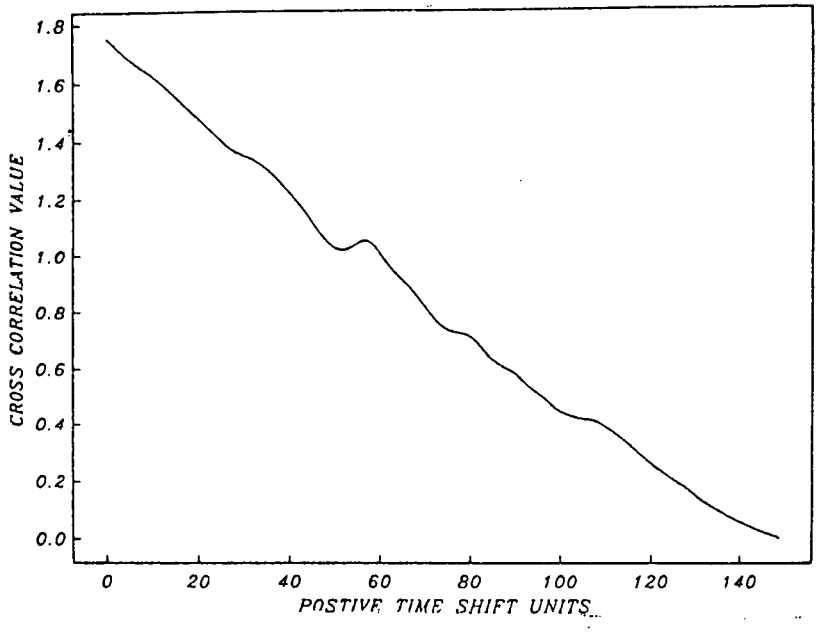


Figure 3.21. Crosscorrelation of Offset Signals

If we correct for D.C. offsets, the signals take the form shown in Figure 3.22 and 3.23, and their crosscorrelation function is shown in Figure 3.24.

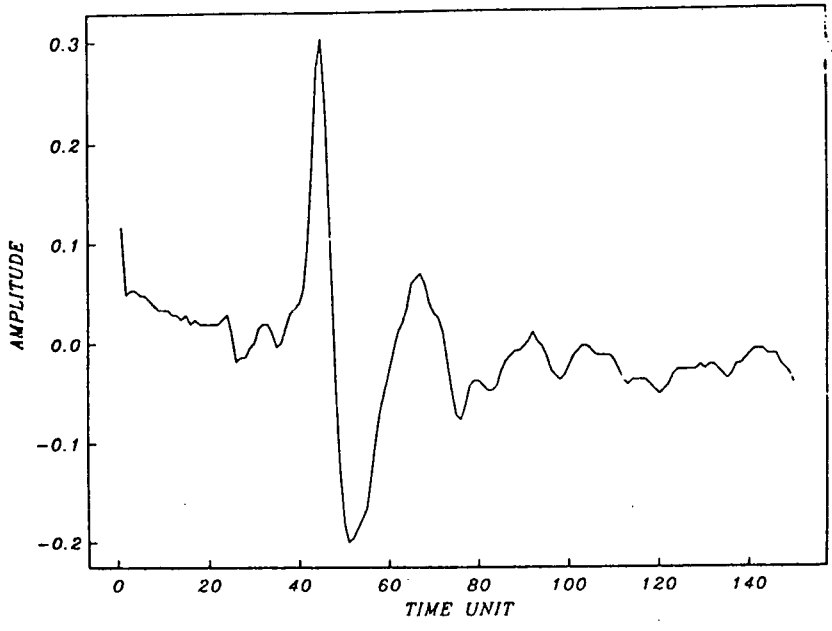


Figure 3.22. Signal 1 Corrected for D.C. Offset with the Number of Points Changed from 200 to 150 Because Dominant Reponse Occurs Between 40 to 60 Time Units

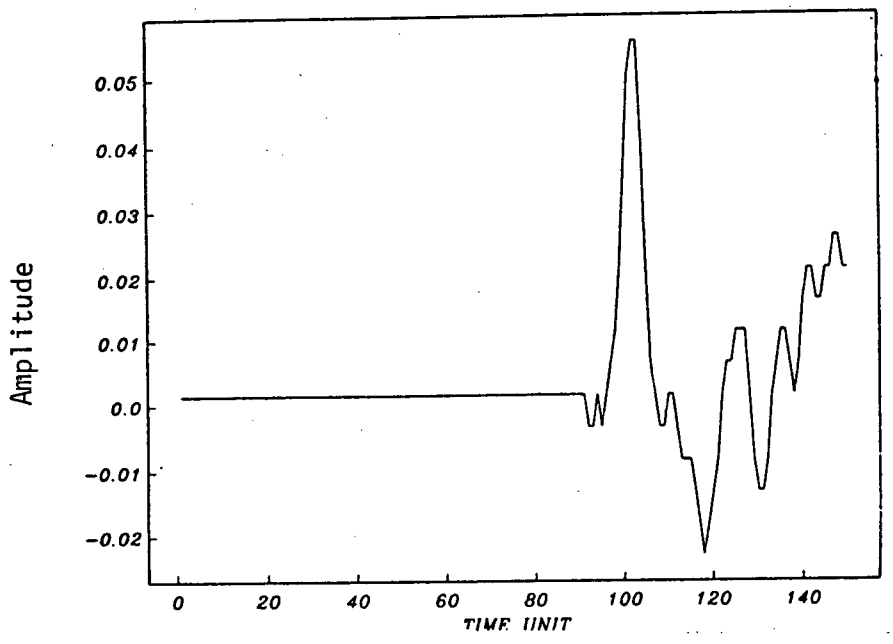


Figure 3.23. Signal 2 Corrected for D.C. Offset

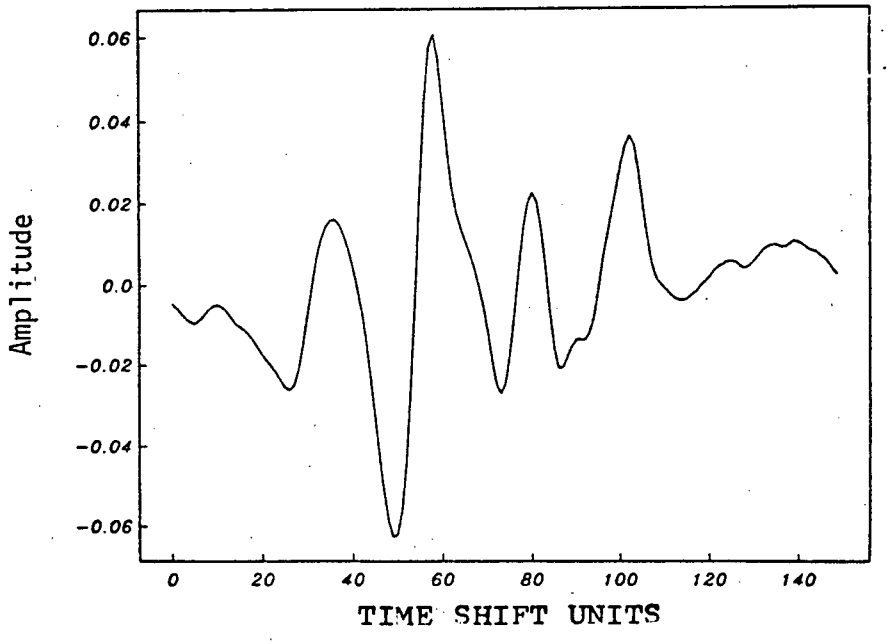


Figure 3.24. Crosscorrelation Value for D.C. Shift Corrected Signals

The maximum of this crosscorrelation occurs at 60 units of time shifts, which is expected by visually picking time shift or lag in Figure 3.25.

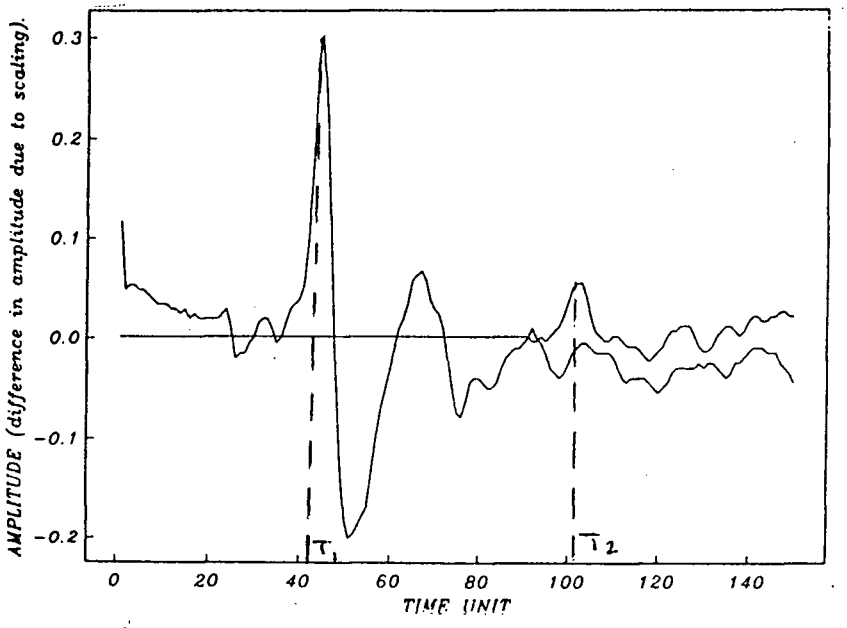


Figure 3.25. Superimposed Signals to give Visual Aid for Estimating Time Lag

The procedure in obtaining the desired velocity profile can thus be summarized as follows:

(1) Record data
(2) Remove D.C. shift
(3) Taper time-domain data with cosine bells
(4) Apply FFT to obtain frequency spectrum
(5) Pick frequencies to be filtered (low & high in the bandpass)
(6) Apply Butterworth filter
(7) Take inverse FFT
(8) Take crosscorrelation of filtered time-domain signals
(9) Determine $\tau$, time offset
(10) Obtain velocities

The program CROSSCOR was developed to apply the above steps. CROSSCOR is a graphics interactive program which displays the frequency spectra, unfiltered and filtered traces, and crosscorrelation plots on a mainframe graphics

terminal and has been implemented on the IBM - P.C. The following subroutines perform Steps 2 through 9.

(2) SUBROUTINE REMAV

(4) & (7) SUBROUTINE FASTF

(3) SUBROUTINE SMOOTH

(5) SUBROUTINE PL AND PLA - MAIN FRAME

(6) SUBROUTINE BNDPAS

(8) SUBROUTINE CROSS

(9) SUBROUTINE MAXSN

Additional subroutines implemented in CROSSCOR are:

(10) SUBROUTINE NORME
NORME normalizes a data series by its RMS energy, in order to bring the contribution of each trace equal in magnitude when crosscorrelating.

(11) SUBROUTINE POW2
POW2 determine M in N=2**M for a specific trace length (i.e., L) and then pads the rest of the trace, L to N, with zeros. The value of N is critical when implementing the FFT, because it requires the length of the trace to be a power of two.

(12) SUBROUTINE FXFFT

This subroutine saves computing time, because it allows for only one call to FASTF. In FASTF one trace is input as a real component and second trace is input as an imaginary components. Reference 5 further expands on this (Chapter 3, Section 3.6)

CROSSCOR was tested for performance by superpositioning several sinusoidal waves and filtering out the desired frequencies. In Figure 3.26 there is an identical traces containing fequencies of 30, 50, and 100 Hertz. The signals are offset from each other by 20 time units. The signals are then bandpassed between 40 and 80 Hertz resulting in only the 50 Hertz signal remaining as illustrated in Figure 3.26(c). The crosscorrelation function is illustrated in Figure 3.26(d) where negative and positive time shifts are illustrated. In determining the arrival time differences between the successive wavelets, it is only necessary to obtain the maximum positive correlation value at a positive time shift. This is due to the fact that the crosscorrelation function is comparing arrival time differences of the dominant responses (i.e., maximum positive correlation value) and the wavelet from the deeper layer will always have a longer arrival time (positive time shift). The crosscorrelation function from the filtered signals in Figure 3.26(c) gave a correct maximum time shift of 20 units.

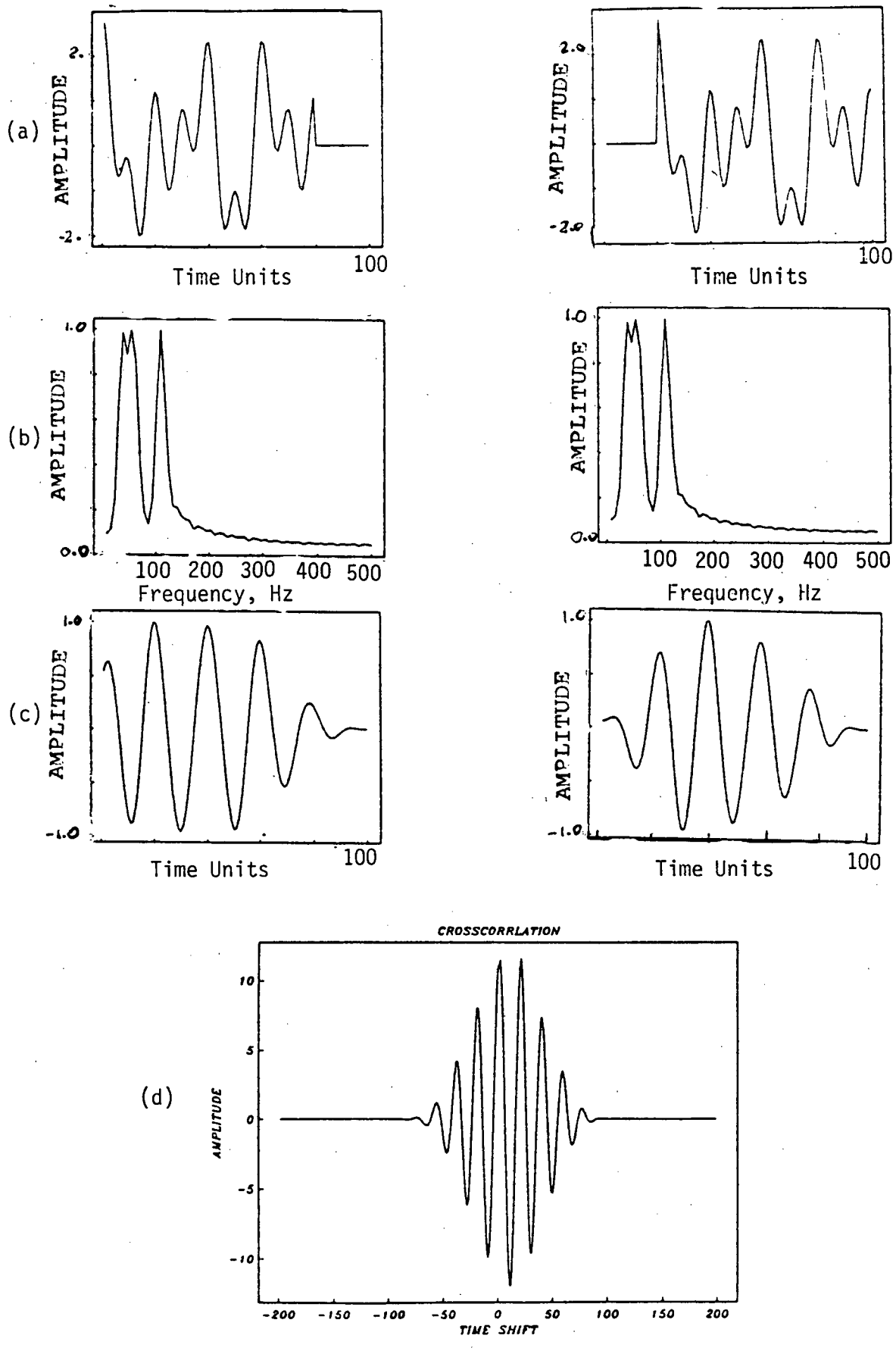


Figure 3.26 Processing Synthetic Data with CROSSCOR. (a) Input Trace (b) Frequency Spectrums (c) Bandpassed Traces (40 to 80 Hz) (d) Crosscorrelation Function of the Filtered Traces.

B. Field Program and Discussion of Results

In this section CROSSCOR is applied to real data to assess its performance and reliability. Results from five research sites are given, and the velocity profiles from different data and methods of data reduction are presented and compared. The research sites are illustrated in Figure B.1 and are as follows:

1) McDonald Farm Site
2) Grant McConachie Way Site at Laing Bridge
3) Tilbury Island Natural Gas Plant Site
4) Annacis Bridge Pile Research Site
5) Lower Langley 232nd St. Site on Trans Canada Highway

The McDonald Farm Site data was acquired on June 25 and July 2, 1987. In this investigation five sets of data were compiled and two different sensors were used. The first sensor was the Hogentogler Super Cone with a Geospace* velocity transducer and the second sensor was the UBC Seismic Cone Pressuremeter, which had two (Piezoelectric bender element) accelerometers installed. The seismic data (i.e., hammer shear source) was reduced by both the reverse polarity method and CROSSCOR. In this research site, CROSSCOR was found to be very helpful in respect to reducing noisy accelerometer data where picking cross-overs was very difficult or impossible.

The Grant McConachie Way Site data was acquired on November 17, 1987, where the UBC #7 Seismic Cone was used with a Piezoelectric bender element accelerometer sensor installed. Two different types of sources were used in this investigation, i.e., the hammer shear source and the P-plate source. From the frequency spectrums obtained there were three distinct responses of the accelerometer observed. The first response was due to the shear wave (S-wave) occurring at 100 Hz, second response was a compression wave, (P-wave), at 900 Hz , the third response resulted from the resonanting accelerometer at 3000 Hz.

The Tilbury Island Natural Gas Plant Site data was acquired on July 16, 1987, where the UBC Seismic Cone Pressuremeter was used with a shear source. In this research site it was not possible to use the reverse polarity method due to the very noisy responses. However, CROSSCOR proved to be extremely helpful in reducing and analyzing the time series.

* See Laing (1985).

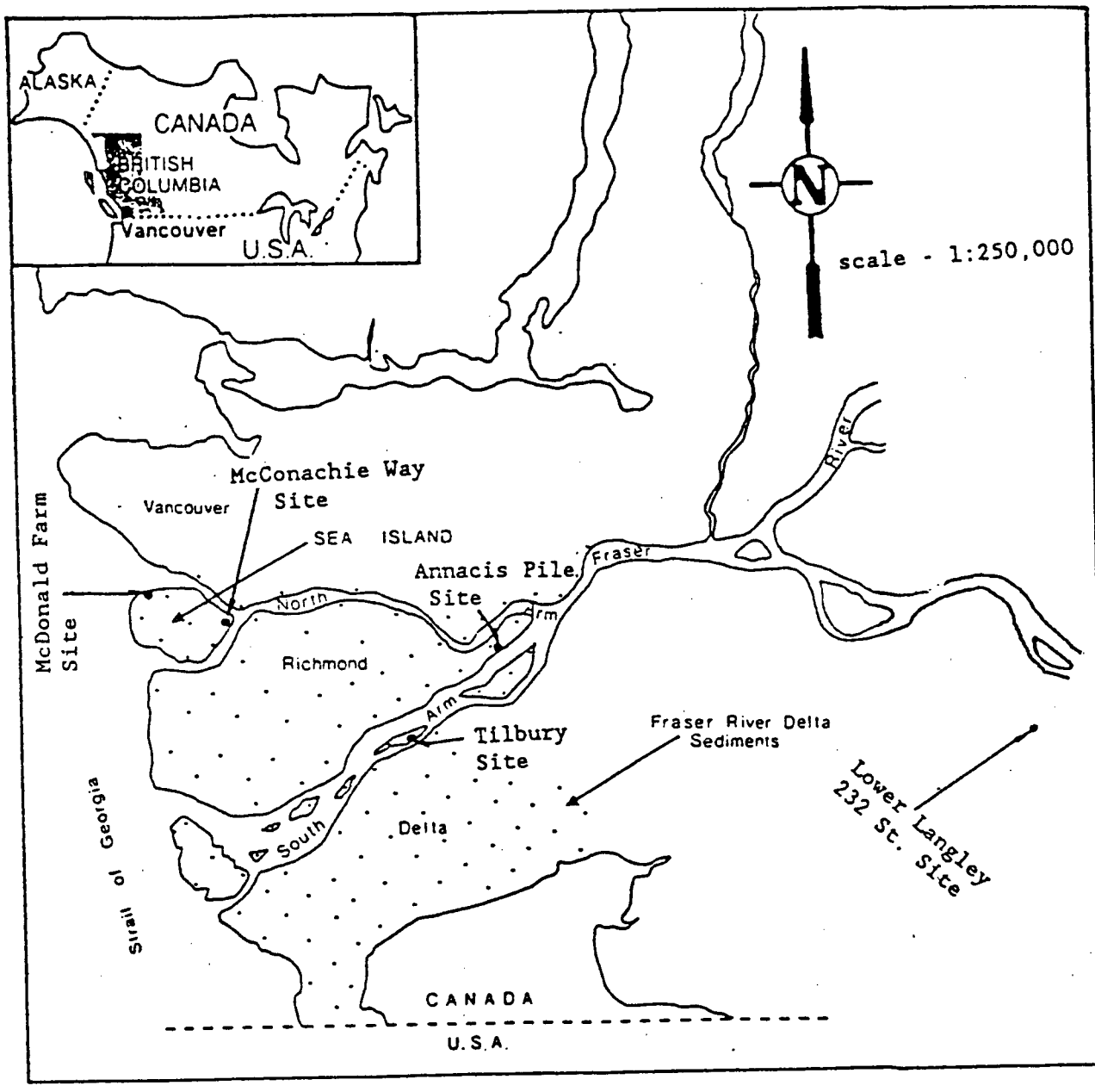


Figure B.1. General Site Location Map

The Annacis Pile Research Site data was acquired on January 8, 1988 and February 10, 1988. On January 8, 1988 the UBC Seismic Cone Pressuremeter was used for data acquisition, and on February 10, 1988 the UBC #8 Seismic Cone was applied. In these investigations shear velocities were obtained using shear sources. Since both sides of the shear source were used, it was possible to obtain two velocity estimates for one depth increment using CROSSCOR as opposed to the reverse polarity and visual pick method which allows for only one velocity estimate.

The Lower Langley 232nd St. data was acquired on November 19, 1987, where the UBC #7 Seismic Cone was used for data acquisition. In this investigation filtered (analogue) and unfiltered reverse polarized hammer shear source data was obtained. In addition, point source Buffalo Gun data was reduced with CROSSCOR which resulted in separating and measuring both shear and compression wave velocities.

The analysis to follow in Section B is as follows:

Section B.1: In this section the research sites investigated are presented along with typical subsurface stratigraphy and cone penetration profiles which give some indication of the geotechnical properties of soils investigated. To obtain a more thorough understanding of the significance of profiles presented, one should refer to the numerous UBC in-situ Group reports.

Section B.2: In this section CROSSCOR is compared to the established reverse polarity method in obtaining velocity estimates with low-pass analogue filtered data and self-filtering geophone data. The purpose of this investigation is to prove that CROSSCOR works as well as the reverse polarity method when reducing clean signals, and CROSSCOR works better than the reverse polarity method with signals containing many dominant low frequencies

Section B.3: In this section CROSSCOR is investigated for its performance in removing P-waves and noise from unfiltered accelerometer data. The velocities obtained from these noisy traces are than compared to velocities obtained from corresponding low-pass analogue filtered data.

Section B.4: In this section CROSSCOR is tested for its performance in obtaining velocity estimates from nonpolarized sources (e.g., the Buffalo Gun Source and comparing one side of the Hammer Shear source to the other). This section illustrates the flexibility of CROSSCOR in working with different types of sources and giving more velocity estimates for a downhole seismic profile as opposed to the reverse polarity method.

Section B.5: In this section CROSSCOR is tested for its ability to extract compression wave events from seismic traces and give corresponding compression wave velocities.

Section B.6: In this section specifying the Bandwidths (i.e., cutoff frequencies) when applying CROSSCOR is addressed.

## B.1 Research Sites

### McDonald Farm Site

McDonald Farm is situated upon Sea Island which is part of the Canadian DOT land at Vancouver International Airport. As was shown in Figure B.1, Sea Island is located between the North Arm and Middile Arm of the Fraser River. Therefore, the McDonald Farm Site is located on a river delta complex with a corresponding subsurface typical of this type of environment.

The general geology consists of deltaic distributary channel fill and marine sediments (Armstrong 1978). A typical CPT* profile from the site is illustrated in Figure B.1.1 and has the corresponding stratigraphy:

| | |
|---|---|
| 0-2m | soft organic silty clay |
| 2-13m | loose to dense coarse sand; some layers of fine sand |
| 13-15m | fine sand, some silt; transition zone |
| 15 > 80m | soft normally consolidated clayey silt |

The groundwater table is generally found to lie 1m below ground surface. Additional information can be obtained from Campanella et al, 1981.

* Cone Penetration Test

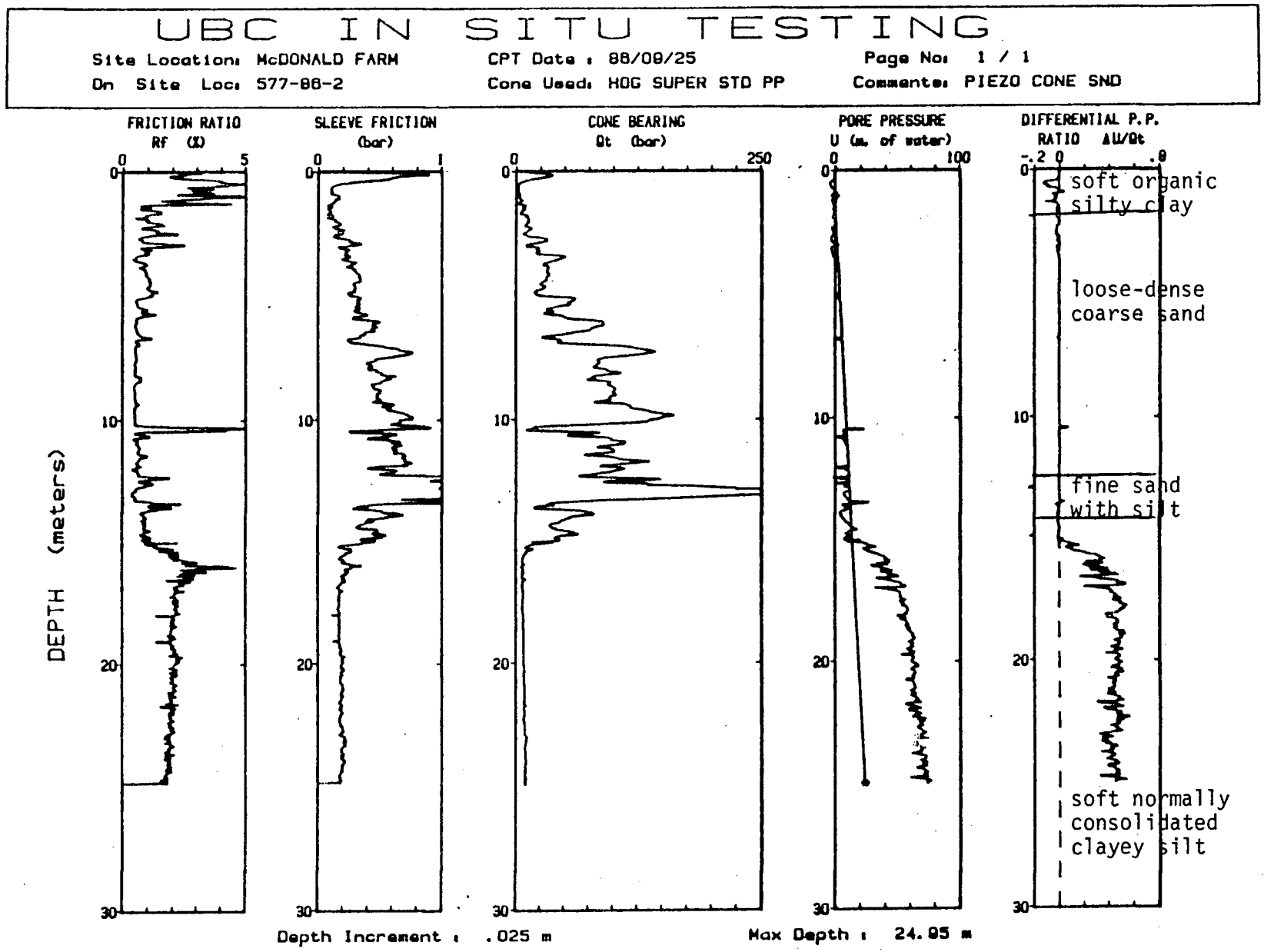


Figure B.1.1. Cone Penetration Profile for McDonald Farm Site

Laing Bridge Site

The Laing Bridge Site is located at the eastern end of Sea Island adjacent to Laing Bridge approach fill at Grant McConachie Way as shown in Figure B.1. The research site is located next to over-pass embankments where extensive research has been conducted by Donna Le Clair (1988) into predicting settlements.

A typical CPT profile from the site is illustrated in Figure B.1.2 and has the corresponding stratigraphy:

| | |
|---|---|
| 0.2m | extraneous soil, top soil, and sandy silty clay |
| 2-20m | medium dense to very dense sands |
| 20-60 to 65m | normally consolidated clayey silt |

The groundwater table is generally found to lie between 1m and 1.5m below ground surface, with fluctuation due to tidal influence.

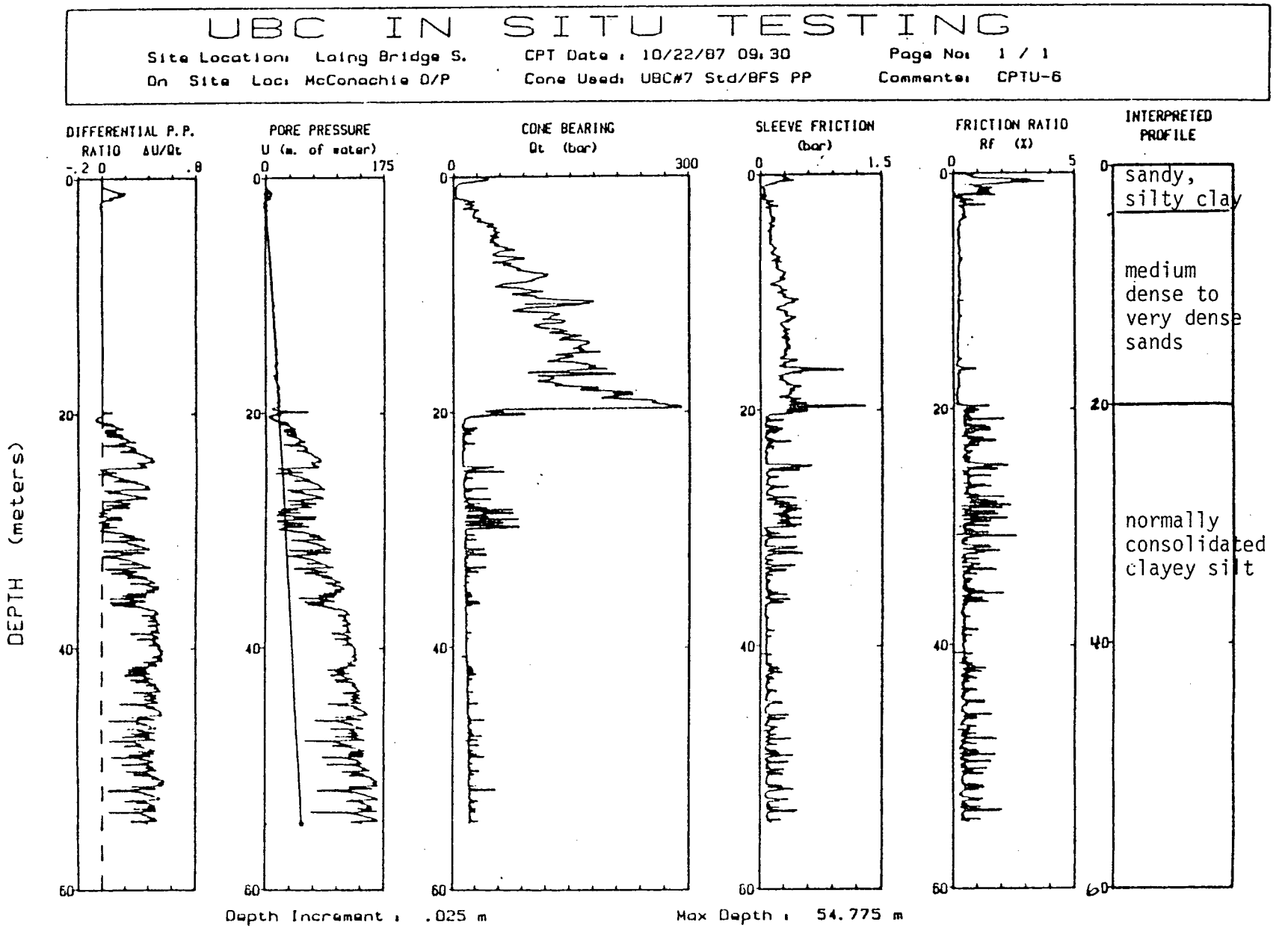


Figure B.1.2. Cone Penetration Profile for Laing Bridge Site

Tilbury Island Natural Gas Plant Site

The Tilbury Island Natural Gas Plant is located on Tilbury Island, as shown in Figure B.1. The research site is located in the South Arm of the Fraser River which has subsurface stratigraphy typical of a river delta complex. John Howie (1987-88) conducted extensive work with the UBC Seismic Cone Pressuremeter at this site.

A typical CPT profile from the site is illustrated in Figure B.1.3 and has the following stratigraphy:

| | |
|---|---|
| 0-2m | Fill |
| 2-25m | Sand |
| 25-45m | Interbedded sand-silt layers |

The groundwater table is generally found to lie 1m below ground surface, with fluctuation due to tidal influence.

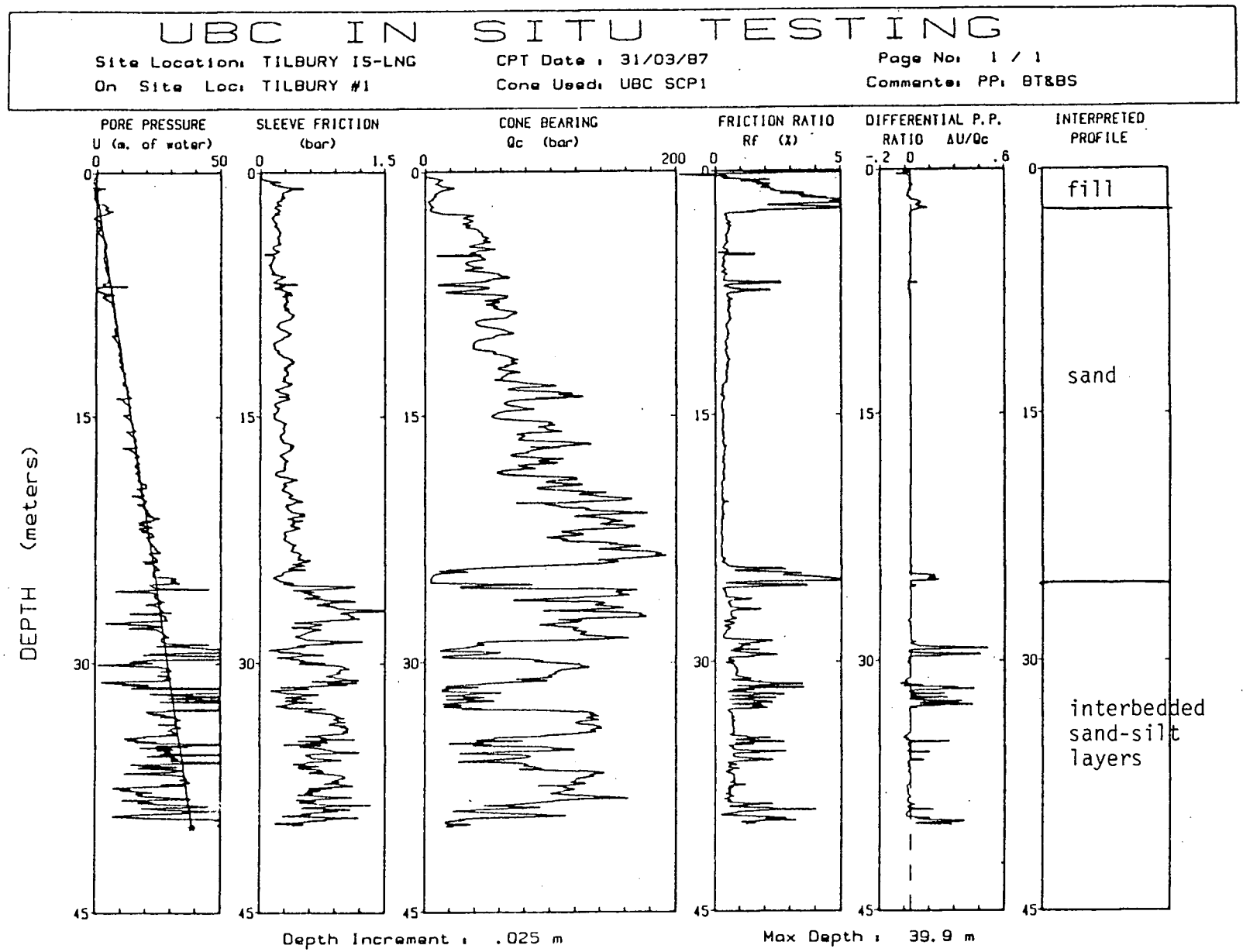


Figure B.1.3. Cone Penetration Profile for Tilbury Island Site

Annacis Pile Research Site

The Annacis Pile Research Site is located on the extreme east end of Lulu Island which is part of the Fraser River delta deposits. This research site, shown in Figure B.1, has been extensively investigated for geotechnical and geological parameters by Michael Davies (1987) and the British Columbia Ministry of Transportation and Highways (1984).

The surficial geology of the Lulu Island region is similar to that of Sea Island and Tilbury Island (i.e., deltaic distributary channel fill and marine sediments). A typical CPT profile from the site is illustrated in Figure B.1.4 and has the corresponding stratigraphy:

| | |
|---|---|
| 0-2m | sand fill |
| 2-15m | soft organic silty clay |
| 15-28m | medium dense sand with minor silty sand lenses |
| 28-60m | normally consolidated clayey silt with thin sand layers |

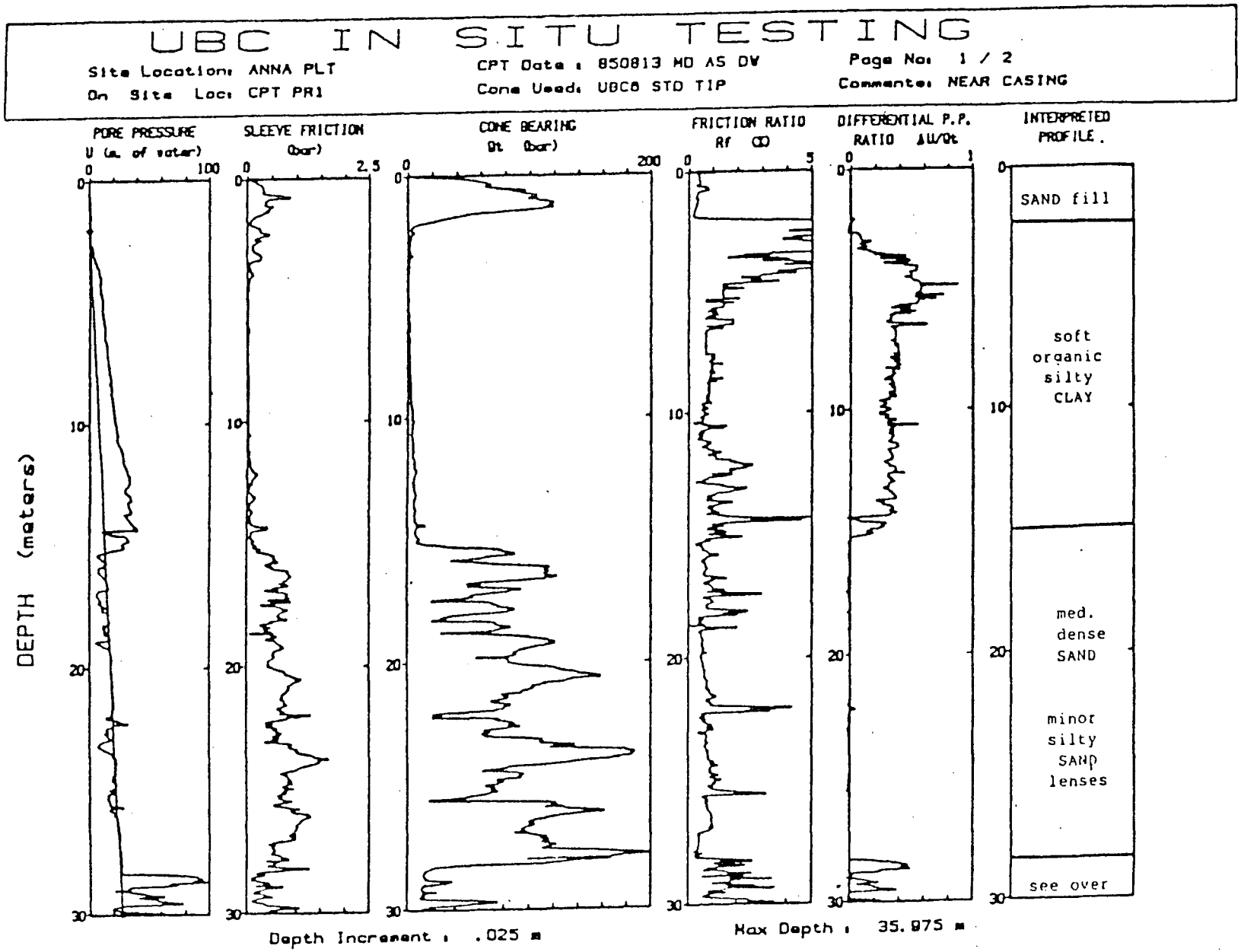


Figure B.1.4. Cone Penetration Profile for Annacis Bridge Pile Research Site

Lower Langley 232nd St.

The Lower Langley 232nd St. Site is located adjacent to the northern exit road on the westbound lane of the main Trans Canada Highway out of Vancouver which follows the Fraser Valley. The exit road is the off ramp to 232nd Street. This site has been investigated for geotechnical and geological parameters by John Sully (1987) and James Greig (1985).

The surficial geology of this site is typical of the Fraser Lowland area. A CPT profile from the Lower Langley 232nd St. Site is illustrated in Figure B.1.5 and consist predominantly of normally consolidated sensitive silty clay with occasional sand lense. The near surface material is overconsolidated due to dessication.

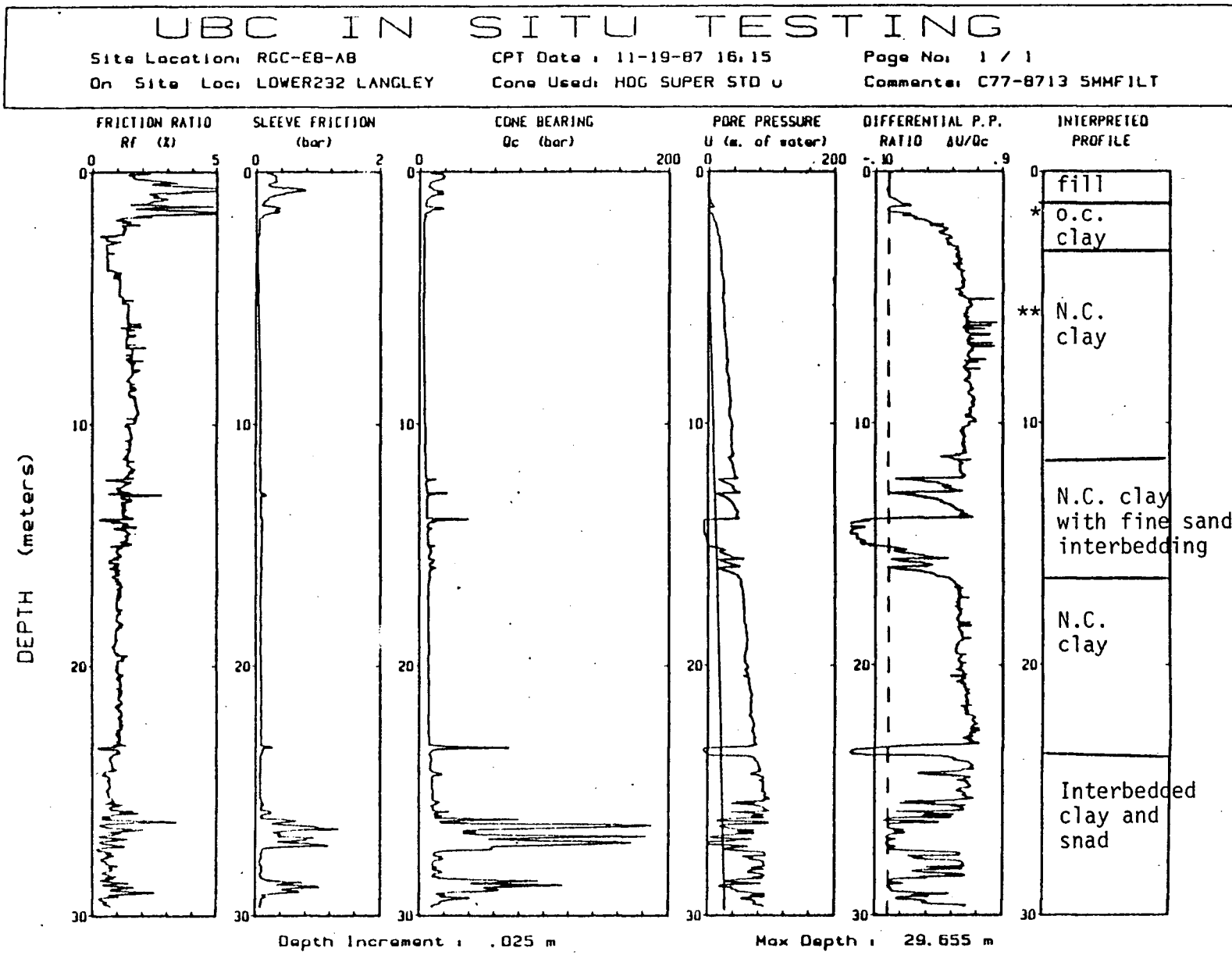


* Overconsolidated

**Normally consolidated

Figure B.1.5. Cone Penetration Profile for Lower Langley 232nd St. Site

## B.2 Cross-Over Method vs. CROSSCOR with Analogue Filtered Applied and Different Seismic Probes Used

In this section the well established reverse polarity or Cross-Over method is compared to the newly developed CROSSCOR in obtaining shear wave velocities. The seismic traces have been recorded with the piezoelectric bender element accelerometers (with a 300 Hz low-pass analogue filter applied) and the self filtering Geospace geophone (Natural Frequency = 28 Hz).

As was previously discussed in Section II, the Cross-Over method demands that in picking a Cross-Over, a consistent method must be used throughout the seismic profile. But it was found that in some cases seismic traces may be masked by several dominant low frequencies making Cross-Over picks difficult or impossible (e.g., Figure 2.8). The above problem is futher illustrated in Figure B.2.1 with data recorded at Annacis Island. In the discussion to follow, it will be illustrated that the Cross-Over method will give identical velocities to that of CROSSCOR with clean signals (i.e., containing one dominant frequency as was illustrated in Figure 2.9) and that CROSSCOR will give more reliable estimates with traces like those of Figure 2.8 and B.2.1.

### McDonald Farm

The first set of data presented in Table B.2.1 is from McDonald Farm, where the Hogentogler Super Cone velocity transducer was used for data acquisition on July 2, 1987. Table B.2.1 illustrates the velocities obtained from the Cross-Over method and CROSSCOR. As is shown, the velocities are very comparable due to the clean signals the slow responding velocity transducer gives. One must keep in mind that since CROSSCOR uses all the information contained in the seismic traces, the velocities obtained from it would be more accurate. The velocities from this set of data is plotted along with the McDonald Farm cone bearing profile in Figure B.2.2. Figure B.2.2 illustrates that the Cross-Over method and CROSSCOR give velocities that are very comparable and vary with the cone bearing profile (i.e., increase in velocity with increase in bearing).

The second set of data presented is also from the McDonald Farm Site, where the UBC Seismic Cone Pressuremeter (SCPM) was used for data acquisition on June 25, 1987. In this investigation the signals recorded had several dominant frequencies present even with the 300 Hz low-pass filter applied. This character-

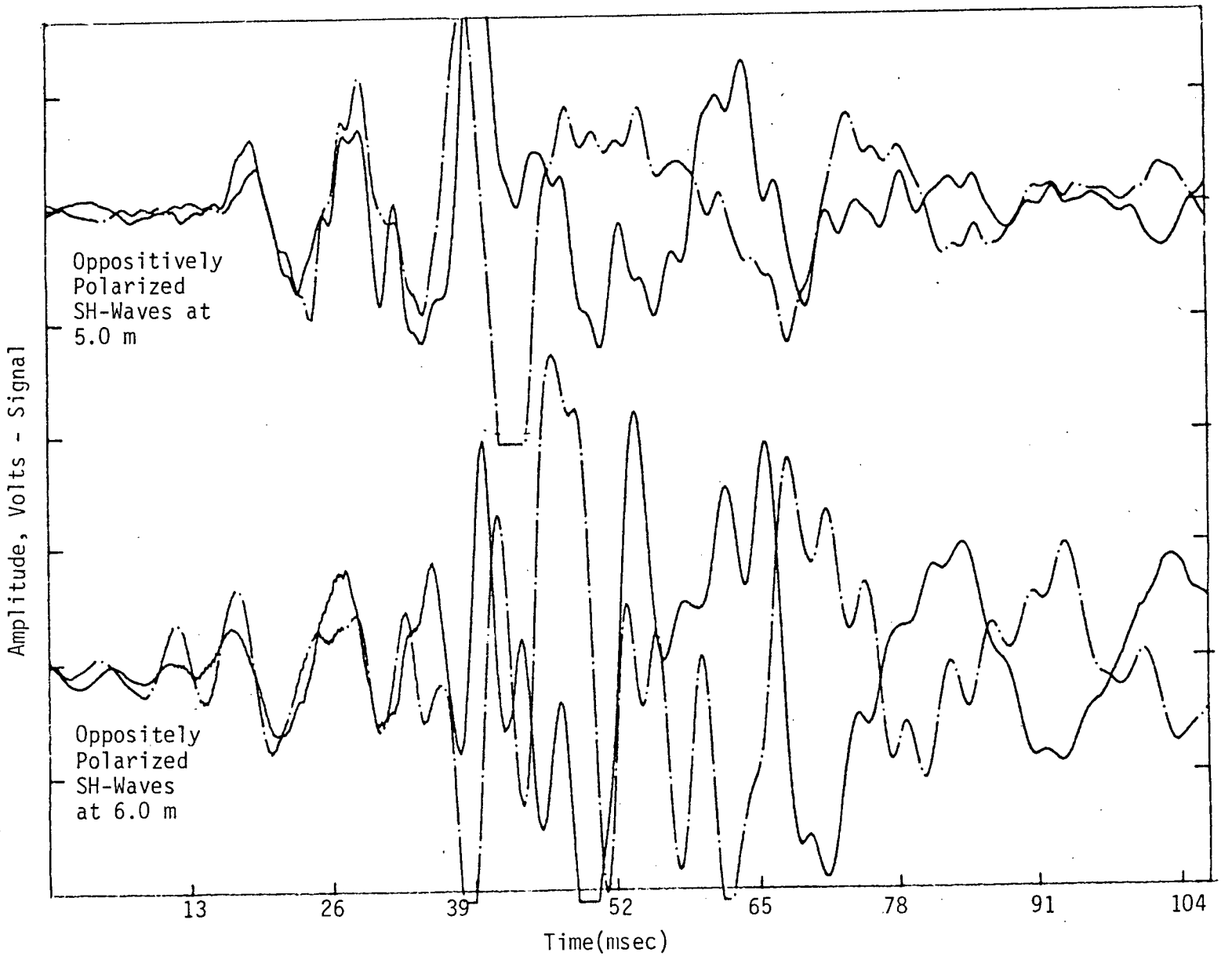


Figure B.2.1. Seismic Data Acquired from Annacis Island Vibro-Compaction Site on May 18, 1988. Data Recorded with Accelerometer having a 300 Hz Low-Pass Filter Applied. Diagram Illustrates Difficulty in Obtaining Cross-Overs Due to Signal Being Masked by Many Dominant Low Frequencies.

Table B.2.1

Calculated Velocity Profiles from McDonald Farm Comparing the Cross-Over Method with CROSSCOR. The Data was Obtained with a Self-Filtering (Natural Frequency = 28 Hz) Geophone.

| Average Depth (m) | Depth (m) Interval | Cross-Over Hammer Source July 2, 1987 Hog-Super Vs (m-sec) | CROSSCOR Hammer Source July 2, 1987 Hog-Super Vs (m/Sec) |
|---|---|---|---|
| 3.2 | 2.7-3.7 | 113 | 115 |
| 4.2 | 3.7-4.7 | 146 | 150 |
| 5.2 | 4.7-5.7 | 137 | 141 |
| 6.2 | 5.7-6.7 | 153 | 155 |
| 7.2 | 6.7-7.7 | 149 | 143 |
| 8.2 | 7.7-8.7 | 189 | 189 |
| 9.2 | 8.7-9.7 | 180 | 174 |
| 10.2 | 9.7-10.7 | 225 | 220 |
| 11.2 | 10.7-11.7 | 200 | 193 |

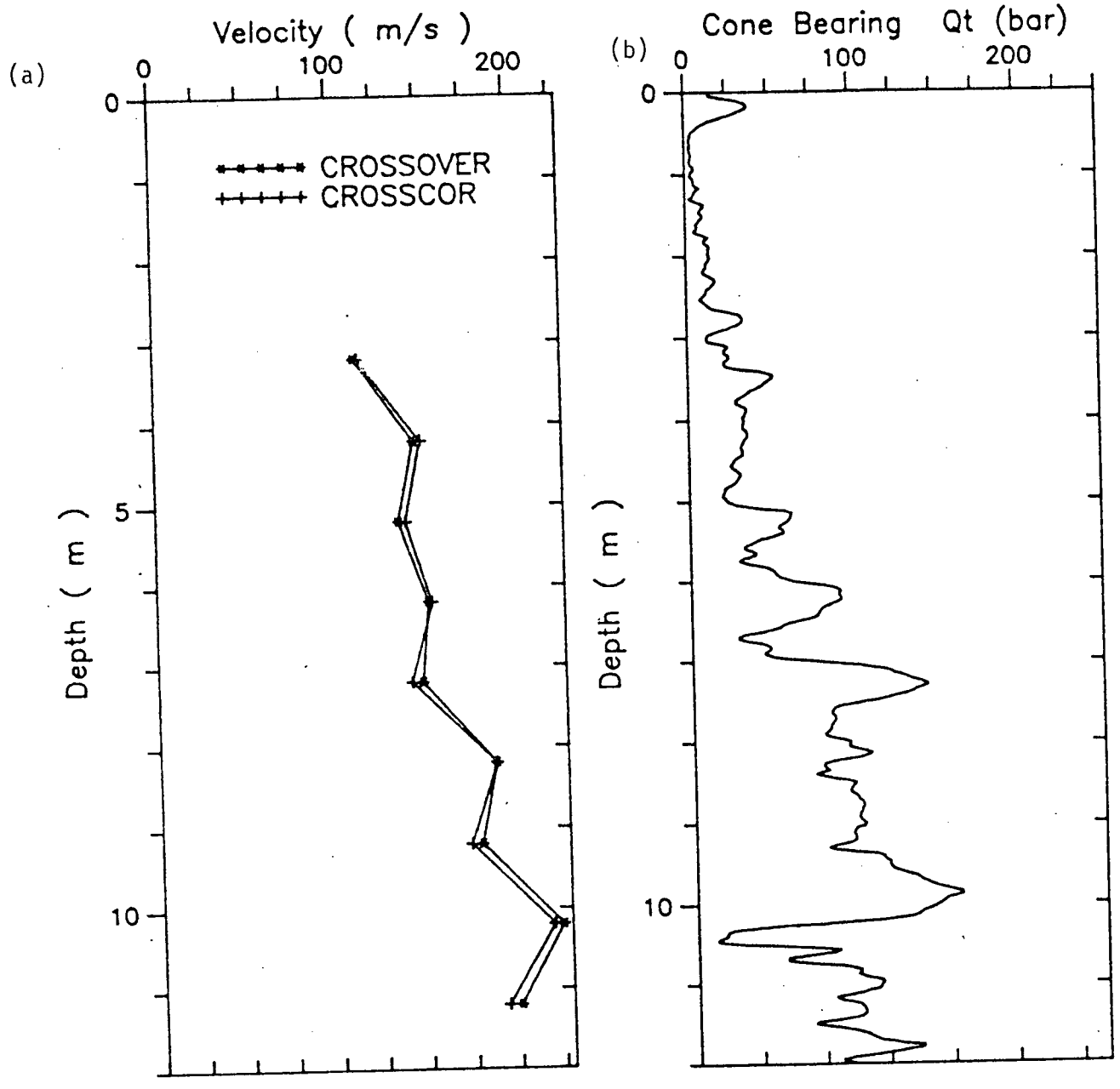


Figure B.2.2. (a) Velocity Profile from McDonald Farm Comparing the Cross-Over Method and CROSSCOR. The Data was Obtained with a Self Filtering (Natural Frequency = 28 Hz) Geophone. (b) Cone Bearing Profile from McDonald Farm.

istic of these seismic traces is typical of the accelerometer transducer due to its high sensitivity. The velocities determined from the Cross-Over method and CROSSCOR are given in Table B.2.2. The SCPM has accelerometers in both the cone portion and the pressuremeter portion of the instrument. The cone accelerometer (SCPM CN) gives noticeable discrepancies between the two methods of velocity calculation. But when these velocities are compared to the SCPM pressuremeter accelerometer (SCPM PM), the velocities obtain from CROSSCOR are more similar. The velocities obtained from this research site are plotted in Figure B.2.3(a). Figure B.2.3(b) illustrates the cone bearing profile for McDonald Farm and as is shown, the velocities in Figure B.2.3(a) vary with the cone bearing profile.

Laing Bridge Site

The third set of data presented is from the Laing Bridge Site, where the data was acquired on November 17, 1987 with the UBC #7 Seismic Cone. For this data it was also not possible to accurately determine consistent Cross-Overs, due to the sensitive nature of the accelerometer (as discussed in Section I). The shear wave velocities obtained from the Cross-Over method and CROSSCOR are illustrated in Table B.2.3. Again we see noticeable discrepancies between the two methods of velocity determination (note depths 6.3, 10.3, 11.3 and 13.3m), but when compared to the velocities obtained from the P-Plate source at 10.3 and 11.3m, CROSSCOR gives the most repeatable values. The velocities obtained from this site are plotted in Figure B.2.4 along with the cone bearing profile.

The last set of data presented in this section was obtained from the Lower Langley 232nd St. on November 19, 1987, where the UBC #8 Seismic Cone was used for data acquisition. In this investigation very clean signals were recorded with predominantly one S-wave frequency of 80 Hz present. The calculated velocities from the Cross-Over method and CROSSCOR are given in Table B.2.4. As is illustrated, the velocities obtained are in very close agreement. The velocities are also plotted in Figure B.2.5 along with the cone bearing profile.

Table B.2.2

Calculated Velocity Profiles from McDonald Farm Comparing the Cross-Over Method and CROSSCOR. The Seismic Traces were Acquired with a 300 Hz Low-Pass Filter Applied and Using SCPM with Piezoelectric Bender Accelerometers.

| Average Depth (m) | Depth (m) Interval | Cross-Over June 25, 1987 SCPM - CN Vs (m/sec) | CROSSCOR June 25, 1987 SCPM - CN Vs (m/sec) | CROSSCOR June 25, 1987 SCMP - PM Vs (m/sec) |
|---|---|---|---|---|
| 3.58 | 3.08-4.08 | 150 | 164 | |
| 4.58 | 4.08-5.08 | 168 | 158 | |
| 5.45 | 4.95-5.95 | | | 154 |
| 6.58 | 6.08-7.08 | 95 | 185 | |
| 7.45 | 6.95-7.95 | | | 214 |
| 7.58 | 7.08-8.08 | 153 | 188 | |
| 8.45 | 7.95-8.95 | | | 189 |
| 8.58 | 8.08-9.08 | 208 | 216 | |
| 9.58 | 9.08-10.08 | 189 | 190 | |
| 10.58 | 10.08-11.08 | 225 | 235 | |
| 11.58 | 11.08-12.08 | 185 | 191 | |

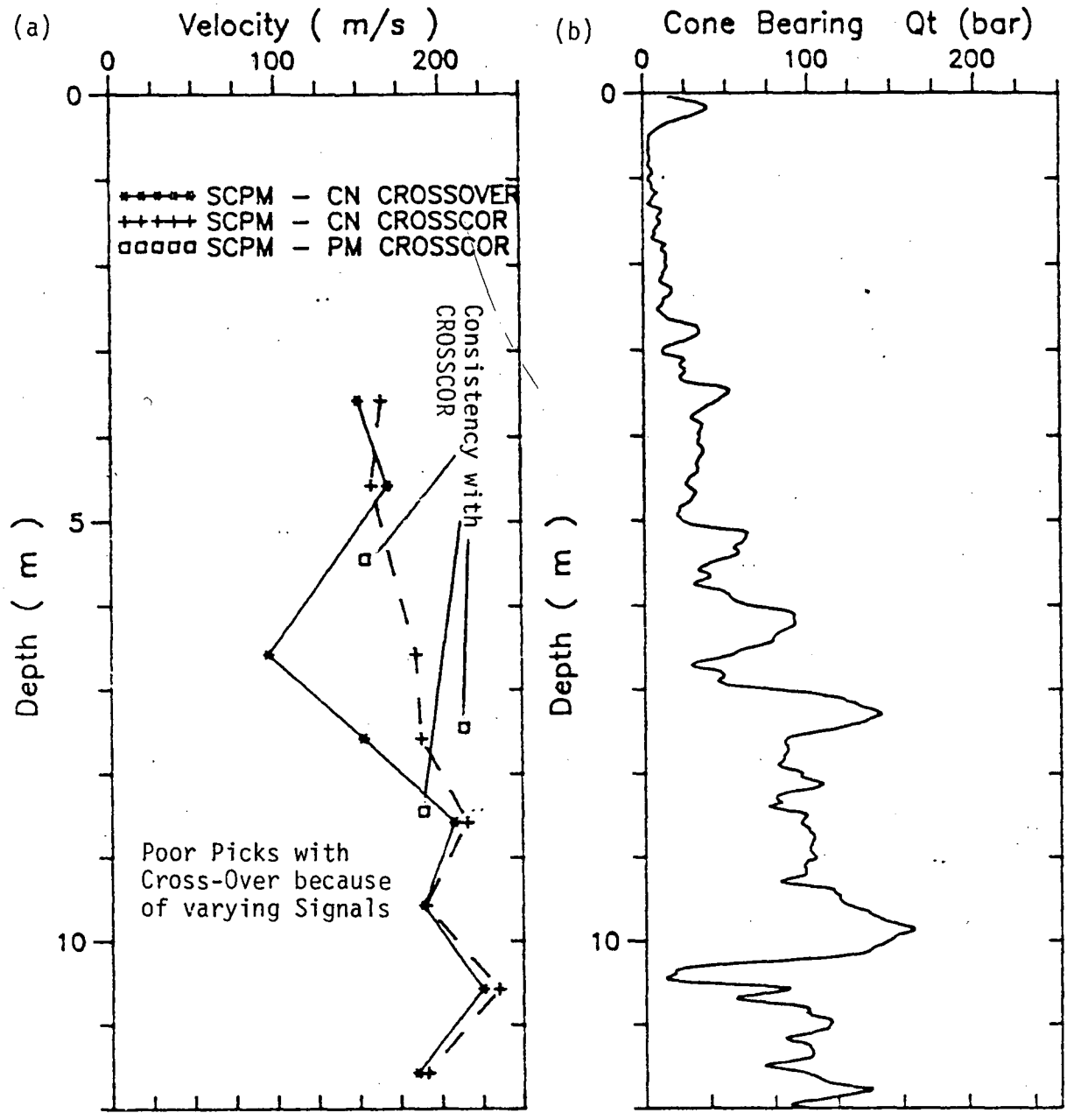


Figure B.2.3. (a) Velocity Profile from McDonald Farm Comparing the Cross-Over Method and CROSSCOR. The Seismic Traces were Acquired from an Accelerometer with a 300 Hz Analogue Filter Applied. (b) Cone Bearing Profile from McDonald Farm.

Table B.2.3

Calculated Velocity Profiles from Laing Bridge, Comparing the Cross-Over Method with CROSSCOR. The Data was Obtained with an Accelerometer with a 300 Hz Low-Pass Filter Applied. In this Set of Data it was not Possible to Obtain Accurate Cross-Over Picks.

| Average Depth (m) | Seismic Cone Shear Wave Source Cross-Over Vs (m/sec) | Seismic Cone Shear Wave Source CROSSCOR Vs (m/sec) | Seismic Cone P-Plate Source CROSSCOR Vs (m/Sec) |
|---|---|---|---|
| 4.3 | 94 | 140 | |
| 5.3 | 144 | 120 | |
| 6.3 | 124 | 171 | |
| 7.3 | 154 | 167 | |
| 8.3 | 143 | 138 | |
| 9.3 | 188 | 187 | |
| 10.3 | 152 | 197 | 189 |
| 11.3 | 210 | 150 | 152 |
| 12.3 | 145 | 144 | |
| 13.3 | 120 | 197 | |
| 14.3 | 193 | 183 | |
| 15.3 | 197 | 224 | |
| 16.3 | 246 | | |

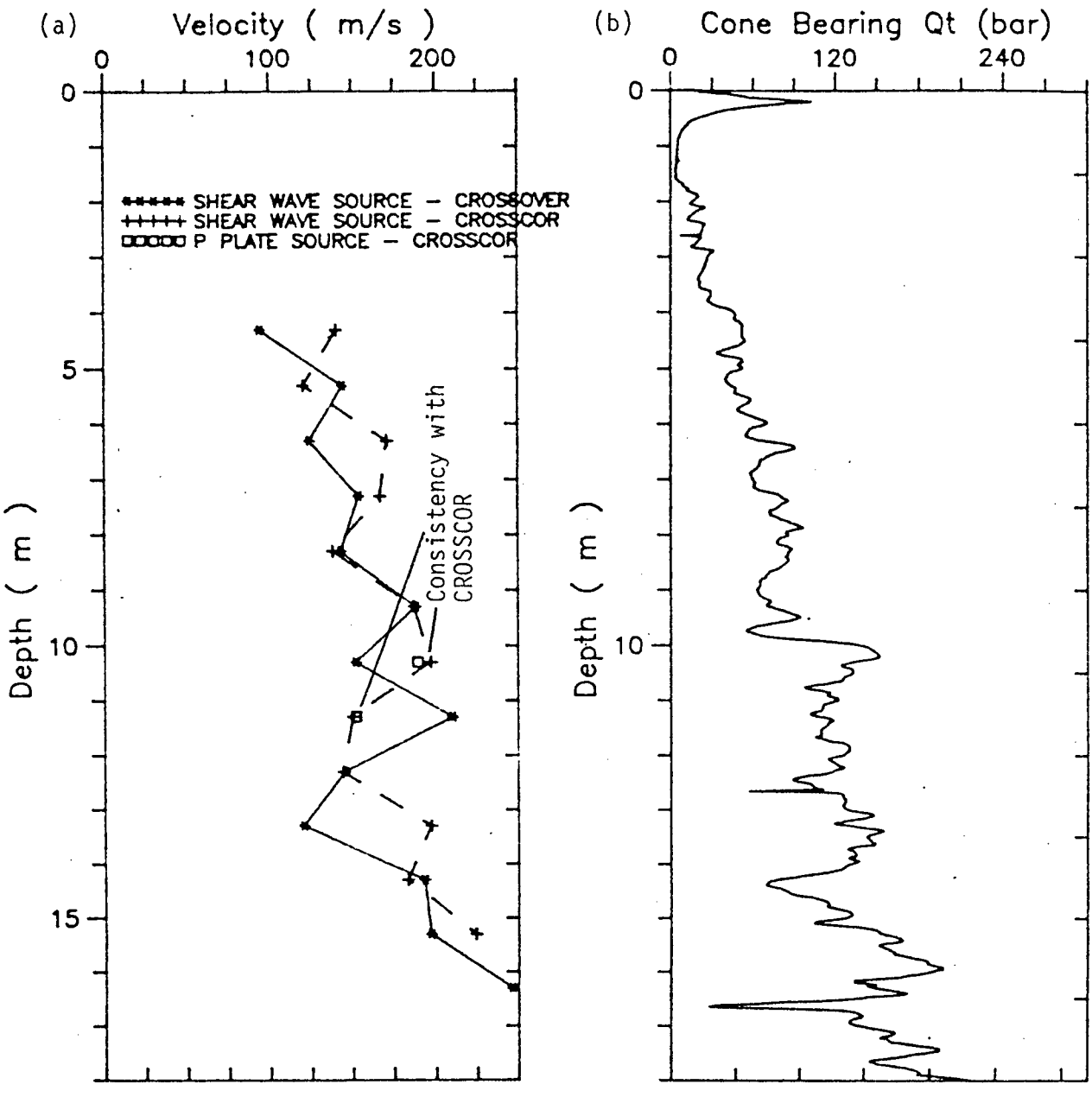


Figure B.2.4. Velocity Profile from Grant McConachie Way Comparing the Cross-Over Method with CROSSCOR. The Data was Obtained with an Accelerometer with a 300 Hz Low-Pass Filter Applied. In this Set of Data it was not Possible to Obtain Accurate Cross-Over Picks. (b) Cone Bearing Profile from the Laing Bridge Site.

Table B.2.4

Calculated Velocity Profiles from Lower Langley (232) Comparing the Cross-Over and CROSSCOR. The Seismic Traces were Acquired with an Accelerometer with a 300 Hz Analogue Filter Applied.

| Average Depth (m) | Depth (m) Interval | Cross-Over Hammer Source Filter On Vs (m/sec) | CROSSCOR Hammer Source Filter On Vs (m/sec) |
|---|---|---|---|
| 2.2 | 1.7-2.7 | 82 | 83 |
| 3.2 | 2.7-3.7 | 92 | 101 |
| 4.2 | 3.7-4.7 | 103 | 104 |
| 5.2 | 4.7-5.7 | 104 | 105 |
| 6.2 | 5.7-6.7 | 96 | 96 |
| 7.2 | 6.7-7.7 | 98 | 99 |
| 8.2 | 7.7-8.7 | 108 | 110 |
| 9.2 | 8.7-9.7 | 104 | 104 |
| 10.2 | 9.7-10.7 | 109 | 103 |
| 11.2 | 10.7-11.7 | 117 | 113 |
| 12.2 | 11.7-12.7 | 119 | 123 |
| 13.2 | 12.7-13.7 | 118 | 123 |
| 14.2 | 13.7-14.7 | 128 | 124 |
| 15.2 | 14.7-15.7 | 128 | 130 |
| 16.2 | 15.7-16.7 | 137 | 134 |
| 17.2 | 16.7-17.7 | 127 | 130 |
| 18.2 | 17.7-18.7 | 134 | 131 |
| 19.2 | 18.7-19.7 | 149 | 138 |
| 20.2 | 19.7-20.7 | 140 | 150 |
| 21.2 | 20.7-21.7 | 139 | 135 |
| 22.2 | 21.7-22.7 | 155 | 160 |
| 23.2 | 22.7-23.7 | 162 | 151 |
| 24.2 | 23.7-24.7 | 177 | 172 |
| 25.2 | 24.7-25.7 | 174 | 184 |
| 26.2 | 25.7-26.7 | 184 | 171 |
| 27.2 | 26.7-27.7 | 213 | 192 |
| 28.2 | 27.7-28.7 | 189 | 191 |

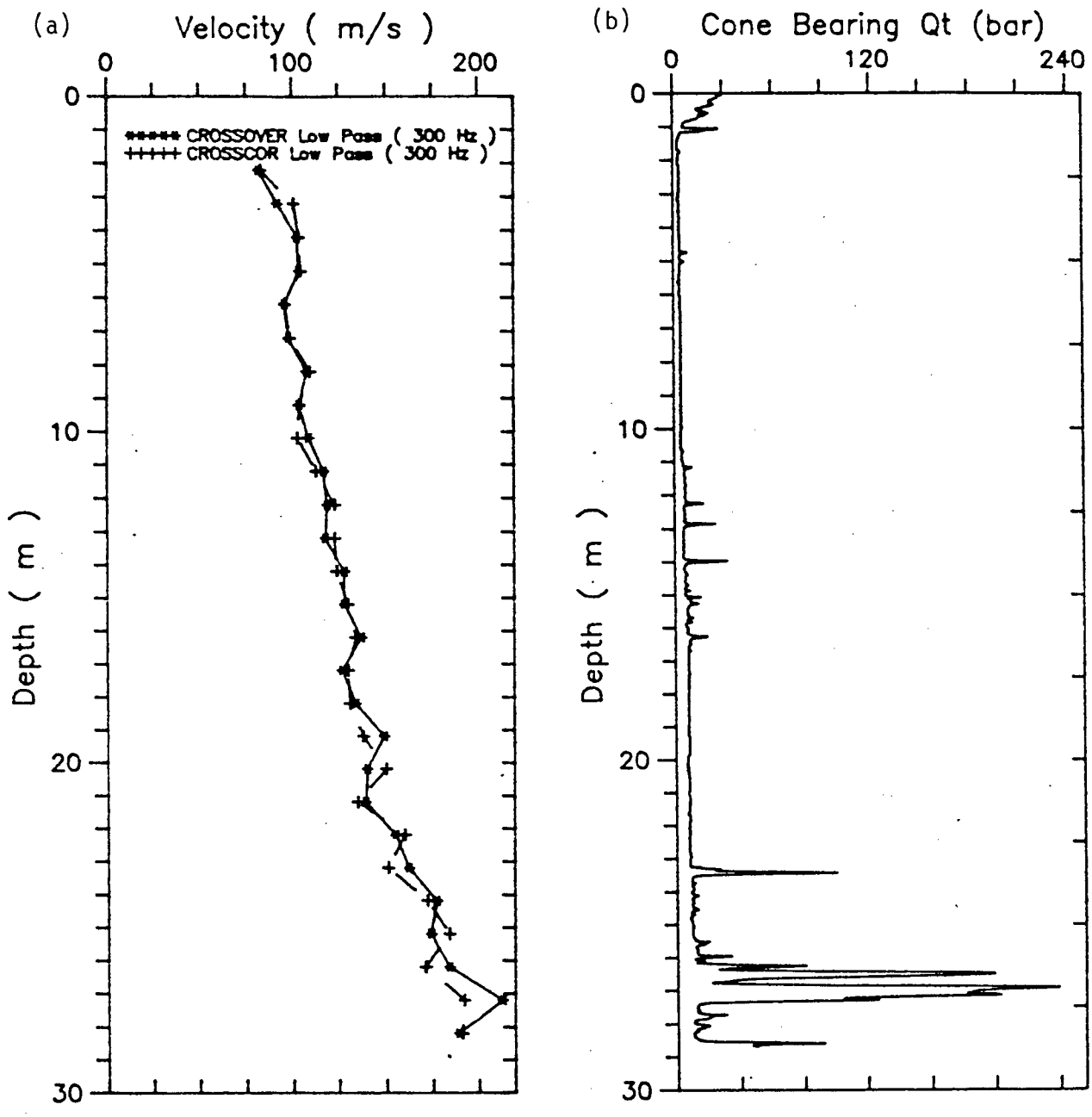


Figure B.2.5. Velocity Profile from Lower Langley Comparing the Cross-Over Method and CROSSCOR. The Seismic Traces were Acquired with an Accelerometer with a 300 Hz Analogue Filter Applied. (b) Cone Bearing Profile from the Lower Langley Site.

## B.3 Comparing CROSSCOR with Filtered (Analogue) and Unfiltered (i.e., Removing P-Waves and Noise With CROSSCOR) Seismic Traces

In this section CROSSCOR is applied to unfiltered seismic traces and compared to traces filtered with a 300 Hz low-pass analogue filter. Figure B.3.1 illustrates a trace recorded at Laing Bridge in which the frequency spectrum clearly illustrates three responses recorded by the accelerometer. The first response is the shear wave located at 100 Hz, the second response is the compression wave at 800 Hz and the third corresponds to the accelerometer resonating at 3000 Hz. From this trace, it was possible to isolate the shear wave by applying a bandpass of 80 to 120 Hz, as is illustrated in Figure B.3.2. The above extraction of the shear wave was possible with most of the unfiltered seismic traces recorded and the selection of the bandwidth was not a critical criterion. The important consideration was to make sure that the bandwidth was consistent throughout the profiling and contained all the frequencies within the shear wave. In most of the data reduced, determination of the velocity was routine, because one only had to specify the same bandwidth throughout the profile.

### Lower Langley 232nd St.

The first set of data is from the Lower Langley Site. In this investigation the shear wave was located at 85 Hz, and the applied bandwidth was 70 to 100 Hz. The effect of time shifts resulting from the 300 Hz low-pass analogue filter was determined by crosscorrelating the filtered and unfiltered traces. From this procedure, it was found that time shifts were negligible. The calculated velocities are illustrated in Table B.3.1. Figure B.3.3(a) is a plot of the velocities calculated from CROSSCOR and the reverse polarity method, and the cone bearing profile is given in Figure B.3.3(b). The Figure illustrates that the unfiltered and filtered results are nearly identical and vary along with the cone bearing profile. Thus, in this set of data CROSSCOR separated out the shear waves from the P-waves and noise, and gave velocities which were repeatable and varied as the cone bearing profile.

### Tilbury Island Natural Gas Plant Site

The second set of data is from the Tilbury Natural Gas Plant Site, where it was not possible to pick Cross-Overs. Therefore, CROSSCOR was found to be a invaluable tool in obtaining the shear velocities. In this case the shear wave

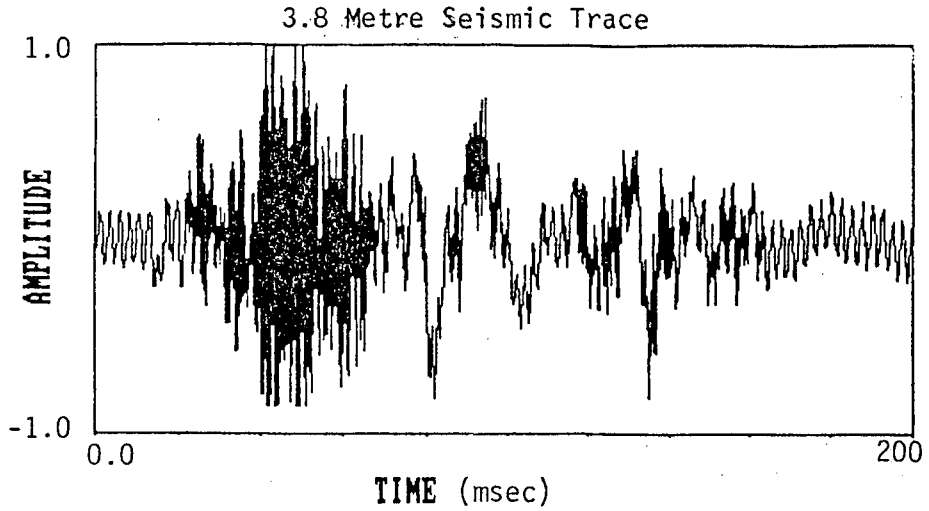


(a) Seismic Trace Recorded at Laing Bridge with the P-Plate Source (Unfiltered).

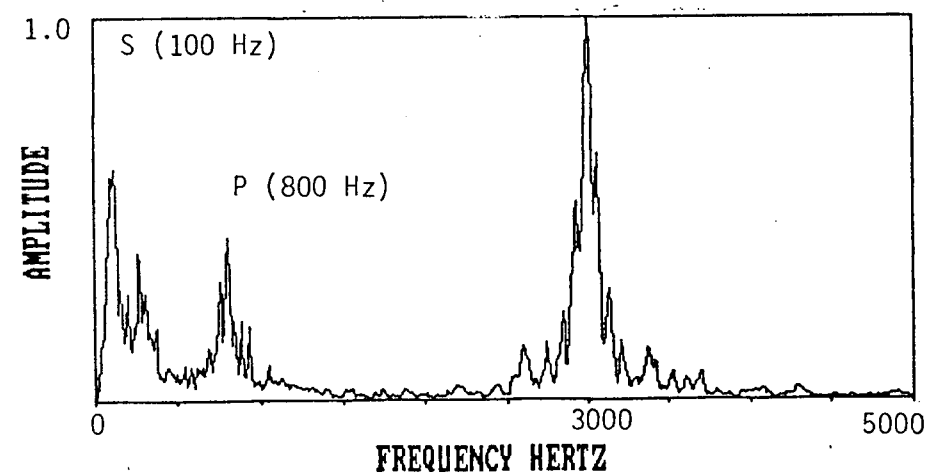


(b) Frequency Spectrum of the Above Trace Illustrating Three Responses Recorded by the Accelerometer: S-Wave at 100 Hz, P-Wave at 800 Hz, and Resonanting Accelerometer at 3000 Hz.

Figure B.3.1. Seismic Trace from Laing Bridge

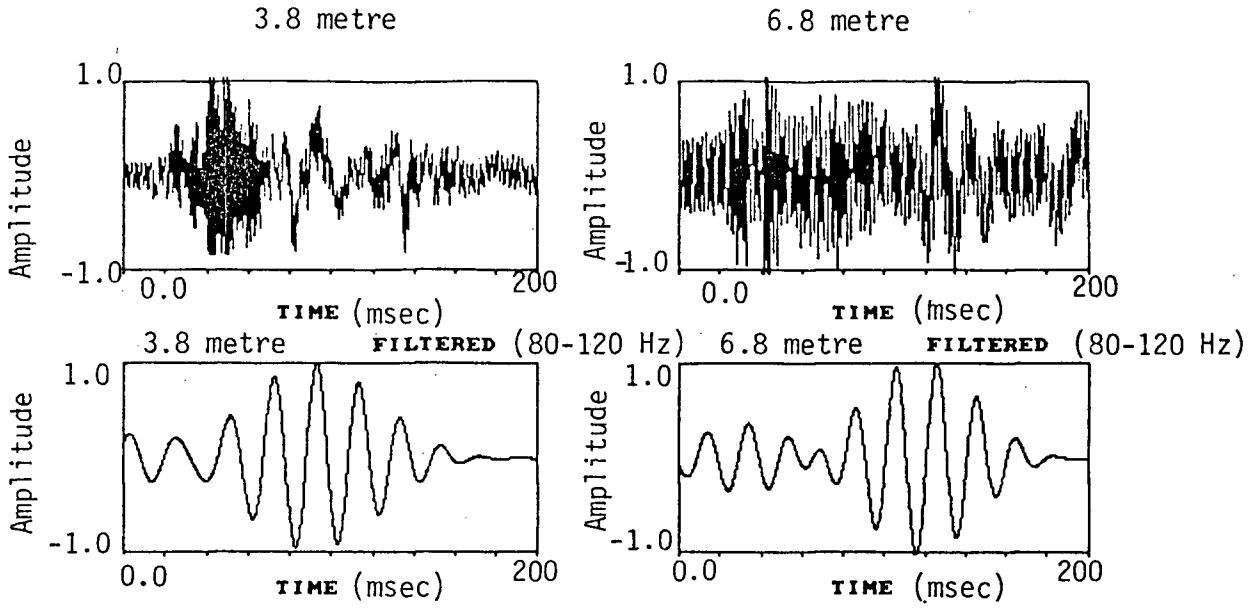


(a) Seismic Traces from Laing Bridge from Depths of 3.8 and 6.8 Metres. These Wavelets are then Filtered with a Bandpass of 80 to 120 Hz Inorder to Extract the Shear Wave.

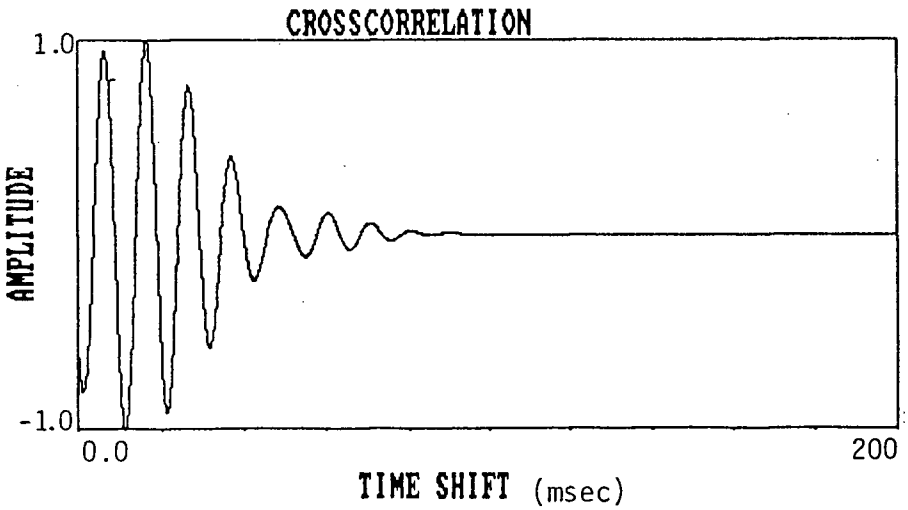


(b) Corresponding Crosscorrelation Function

Figure B.3.2. Seismic Traces from Laing Bridge

Table B.3.1

Calculated Velocity Profiles from Lower Langley (232) Comparing Filtered (300 Hz Low-Pass) and Unfiltered Seismic Data. The Data was Acquired with an Accelerometer.

| Average Depth (m) | Depth (m) Interval | Cross-Over Hammer Source Filter On Vs (m/sec) | Cross-Over Hammer Source Filter Off Vs (m/sec) | CROSSCOR Hammer Source Filter On Vs (m/sec) | CROSSCOR Hammer Source Filter Off Vs (m/sec) |
|---|---|---|---|---|---|
| 2.2 | 1.7-2.7 | 82 | * | 83 | |
| 3.2 | 2.7-3.7 | 92 | * | 101 | 101 |
| 4.2 | 3.7-4.7 | 103 | * | 104 | 109 |
| 5.2 | 4.7-5.7 | 104 | * | 105 | 99 |
| 6.2 | 5.7-6.7 | 96 | * | 96 | 96 |
| 7.2 | 6.7-7.7 | 98 | * | 99 | 100 |
| 8.2 | 7.7-8.7 | 108 | * | 110 | 110 |
| 9.2 | 8.7-9.7 | 104 | * | 104 | 111 |
| 10.2 | 9.7-10.7 | 109 | * | 103 | 104 |
| 11.2 | 10.7-11.7 | 117 | * | 113 | 120 |
| 12.2 | 11.7-12.7 | 119 | * | 123 | 120 |
| 13.2 | 12.7-13.7 | 118 | * | 123 | 120 |
| 14.2 | 13.7-14.7 | 128 | * | 124 | 127 |
| 15.2 | 14.7-15.7 | 128 | * | 130 | 133 |
| 16.2 | 15.7-16.7 | 137 | * | 134 | 138 |
| 17.2 | 16.7-17.7 | 127 | * | 130 | 124 |
| 18.2 | 17.7-18.7 | 134 | * | 131 | 141 |
| 19.2 | 18.7-19.7 | 149 | * | 138 | 134 |
| 20.2 | 19.7-20.7 | 140 | * | 150 | 160 |
| 21.2 | 20.7-21.7 | 139 | * | 135 | 131 |
| 22.2 | 21.7-22.7 | 155 | * | 160 | 160 |
| 23.2 | 22.7-23.7 | 162 | * | 151 | 155 |
| 24.2 | 23.7-24.7 | 177 | * | 172 | 172 |
| 25.2 | 24.7-25.7 | 174 | * | 184 | 185 |
| 26.2 | 25.7-26.7 | 184 | * | 171 | 168 |
| 27.2 | 26.7-27.7 | 213 | * | 192 | 199 |
| 28.2 | 27.7-28.7 | 189 | * | 191 | 198 |

* => not possible to pick Cross-Overs because of varying signals.

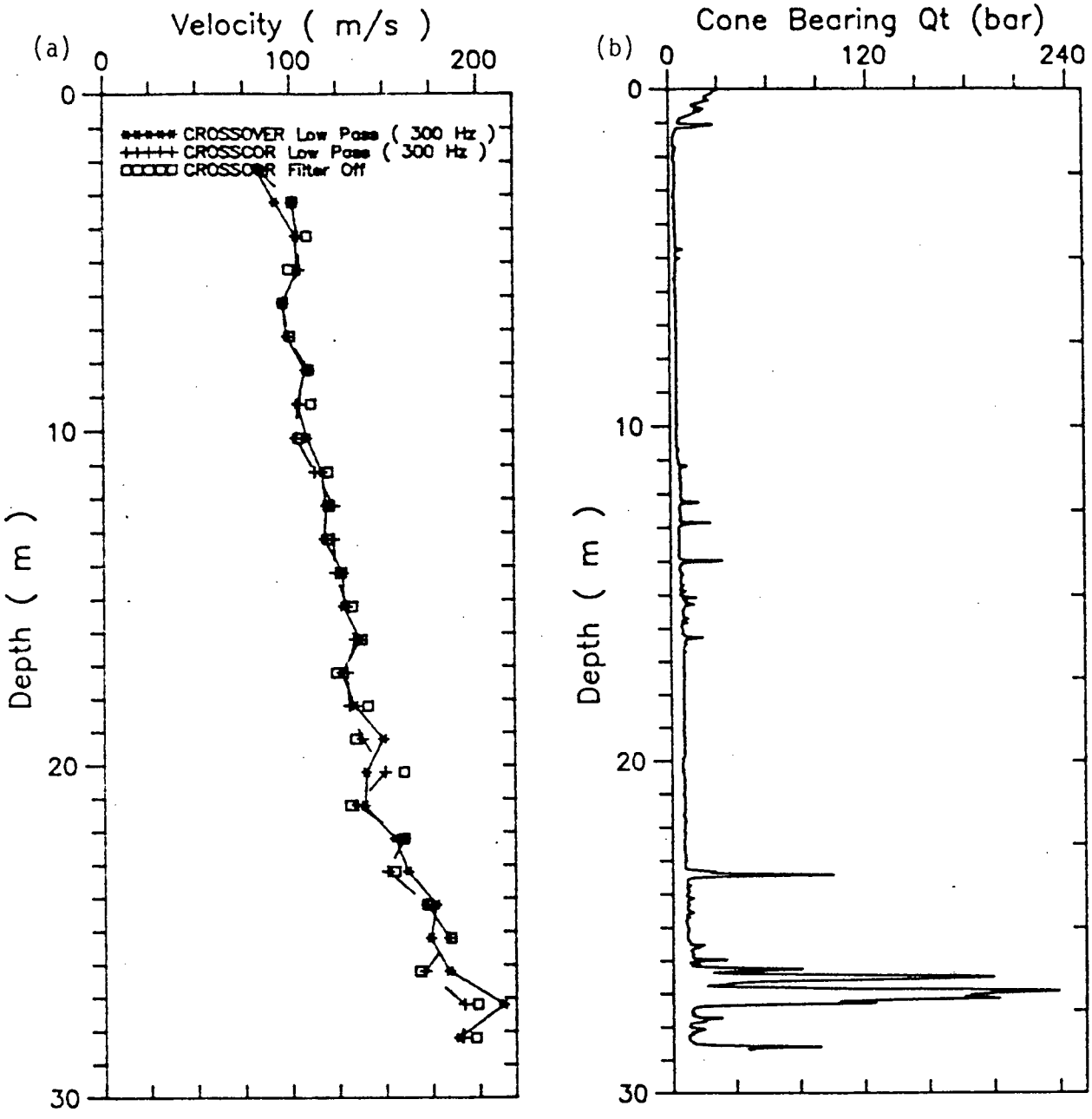


Figure B.3.3. (a) Velocity Profile from Lower Langley Comparing Filtered (300 Hz Low-Pass) and Unfiltered Seismic Data. The Data was Acquired with an Accelerometer. (b) Cone Bearing Profile from Lower Langley.

maximum energies were centered at 100 Hz and the resulting velocities are illustrated in Table B.3.2 and compared in Figure B.3.4 with the cone bearing profile. The calculated velocities vary with the cone bearing profile except for the velocities at 3.66 and 6.64 metres. This maybe due to poor responses being recorded at these depths.

Table B.3.2

Calculated Velocity Profiles from Tilbury Site Comparing Shear Wave Velocities Obtained with CROSSCOR from Seismic Data Acquired by Two Different Accelerometers. In this Set of Data it was not Possible to Obtain Accurate Cross-Over Picks.

| Average Depth (m) | SCPM-CN Seismic Cone Accelerometer Vs (m/sec) | SCPM-PM Pressuremeter Accelerometer Vs (m/sec) |
|---|---|---|
| 2.37 | | 57 |
| 2.91 | | 126 |
| 3.22 | 113 | |
| 3.66 | 91 | |
| 4.72 | 61 | |
| 4.94 | | 131 |
| 5.39 | | 93 |
| 5.45 | 134 | |
| 6.11 | | 121 |
| 6.12 | 123 | |
| 6.64 | 88 | |
| 7.11 | | 146 |
| 8.11 | | 172 |

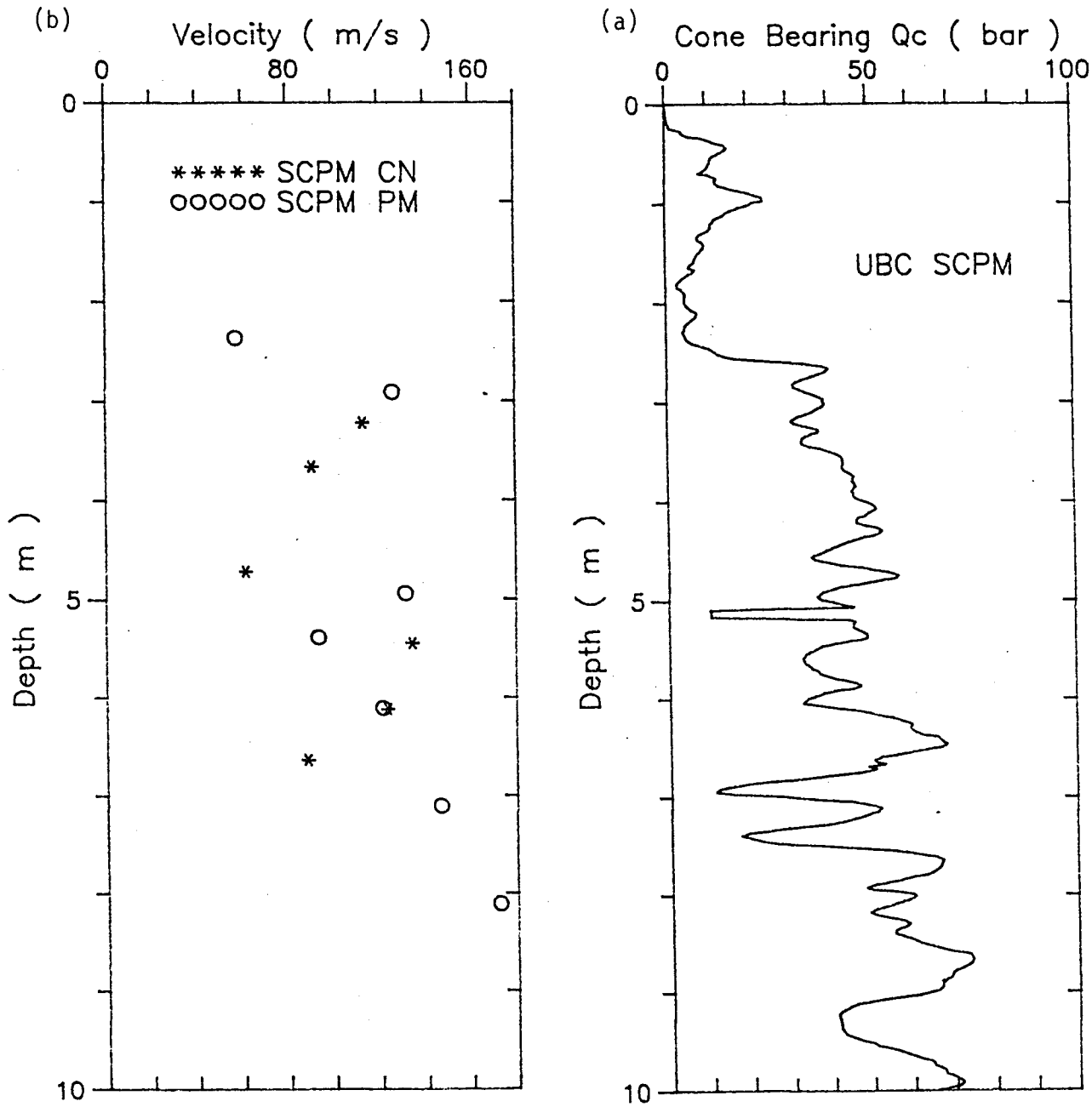


Figure B.3.4. Calculated Velocity Profiles from Tilbury Site Comparing Shear Wave Velocities Obtained with CROSSCOR from Seismic Data Acquired by Two Different Accelerometers. The Velocity Profiles are also Illustrated with the Cone Bearing Profile. In this Seismic Data it was not Possible to Obtain Accurate Cross-Over Picks. (b) Cone Bearing Profile from the Tilbury Island Site.

## B.4 CROSSCOR with Nonpolarized Sources

In this section the application of CROSSCOR to nonpolarized shear sources is addressed. The two sources discussed are the Buffalo Gun and comparing one side of the Hammer Shear Source to the other side (i.e., right and left). The Buffalo Gun source is thoroughly discussed in Reference 2 by Laing (1985) with regard to design and use. The Buffalo Gun is desirable because it can be used both on and off shore to obtain both shear and compression wave velocities without the problems associated with a seismic cap or explosive source. CROSSCOR is applied to data obtained from striking each Hammer Shear Source in one direction, therefore, it allows one to obtain two velocity estimates for one depth increment (one for hitting the left side and one for hitting the right side). This is opposed to the reverse polarity method which allows for only one velocity estimate for each depth increment.

### Lower Langley 232nd St.

The first set of data discussed is from the Lower Langley Site, where an extensive Buffalo Gun profile was obtained. This seismic section is illustrated in Figure B.4.1. From this figure, one can clearly distinguish the compression and shear waves. The shear waves were obtained by bandpassing the data from 90 to 150 Hz. The resulting shear wave velocities are given in Table B.4.1 where they are compared to the Hammer Shear Source velocities. Some of these values are comparable, while others deviate considerably. This deviation was found to result from triggering problems with the Buffalo Gun. The Buffalo Gun source is triggered with a geophone which may result in inconsistency. This is illustrated in Figure B.4.2, where two seismic traces from the same depth (13 metres) were crosscorrelated and a resulting 2.71 msec shift was recorded. For a Vs of 100 m/sec the interval time is 10 msec over a 1 metre distance and 2.71 msec error represents $\pm$27% error on measured Vs. If the trigger error were a constant 2.72 msec then the potential maximum error increases as Vs increases. The measured trigger error of 2.72 msec appears to be a maximum when compared to the percent differences between Hammer and Buffalo Gun data in Table B.4.1. This triggering problem will be resolved by using an accelerometer (having a fast response time) instead of the geophone as well as gounding the Buffalo Gun firing pin to create a contact closure (similar to the shear plate).

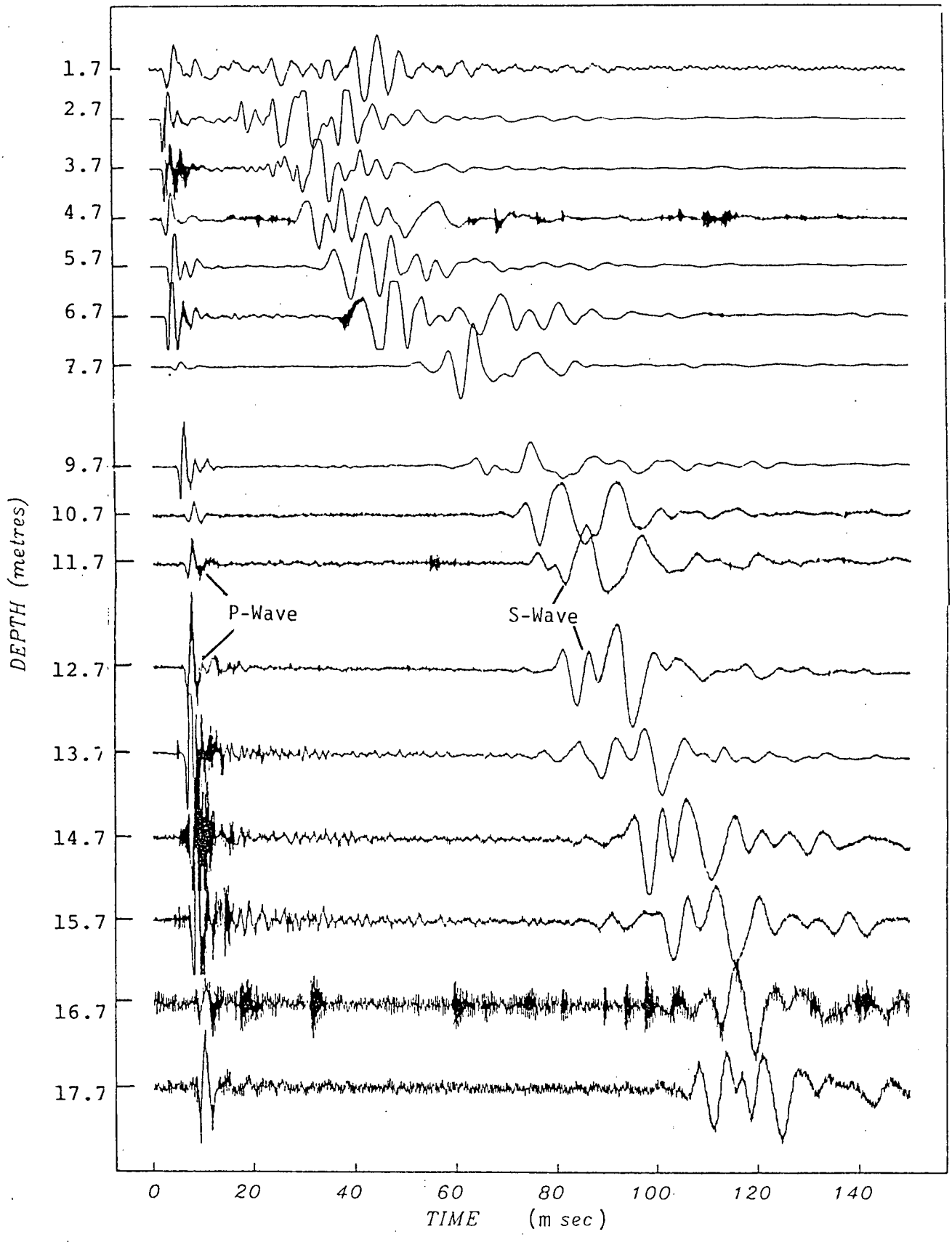


Figure B.4.1. Seismic Section from Lower Langley Where a Buffalo Gun was Used as the Source and An Unfiltered Accelerometer Recorded the Data.

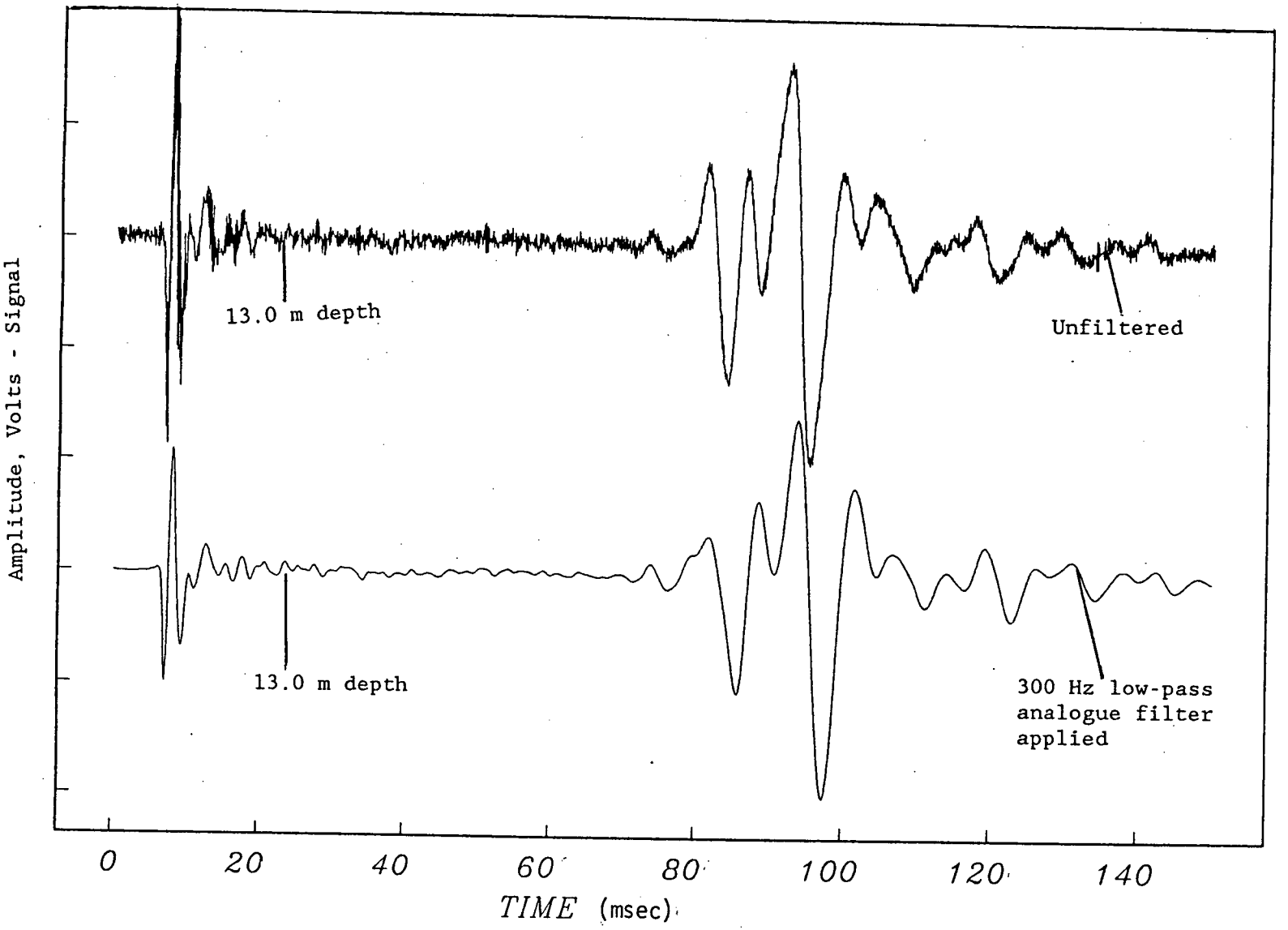


Figure B.4.2. Two Buffalo Gun Seismic Traces from Lower Langley Illustrating triggering Problems with the Buffalo Gun Source. The Data was Acquired with an Accelerometer at a Depth of 13 Metres. The Resulting Time Difference was 2.72 msec.

Table B.4.1

Calculated Velocity Profiles of Lower Langley (232) Comparing Shear Wave Velocities Obtained from the Hammer Shear Source and the Buffalo Gun Source. The Data was Acquired with an Accelerometer (Unfiltered).

| Depth (m) Interval | CROSSCOR Hammer Source Filter Off Vs (m/sec) | CROSSCOR Buffalo Gun Filter Off Vs (m/sec) | % Difference (Hammer Reference) |
|---|---|---|---|
| 2.7-3.7 | 101 | 106 | +5 |
| 3.7-4.7 | 109 | 94 | -14 |
| 4.7-5.7 | 99 | 90 | -9 |
| 5.7-6.7 | 96 | 96 | 0 |
| 10.7-11.7 | 120 | 114 | -5 |
| 11.7-12.7 | 120 | 120 | -0 |
| 12.7-13.7 | 120 | 101-low | -16 |
| 13.7-14.7 | 127 | 108-low | -15 |
| 14.7-15.7 | 133 | 155-high | +17 |
| 15.7-16.7 | 138 | 133-low | -18 |
| 16.7-17.7 | 124 | 122 | - 2 |
| 17.7-18.7 | 141 | 165-high | +17 |
| 18.7-19.7 | 134 | 114-low | +15 |

Note: One trigger error creates two incorrect successive measurements of Vs.

Annacis Bridge Pile Research Site

The second set of data is from the Annacis Pile Research site, where velocities obtained from striking each side of the pads for the Hammer Shear Source are compared. The velocities from the SPCM-CN are given in Table B.4.2 and plotted along with the cone bearing profile in Figure B.4.3. The low velocities are expected for this very soft organic silt and tend to linear increase with depth as the in-situ stresses increase (i.e., essentially constant cone bearing profile which has been corrected for overburden stresses). The higher velocity values at 12.0 metres are indicative of the variable (in depth) sand unit at approximately 15.0 metres. The velocities obtained from the UBC #8 cone are given in Table B.4.3 and plotted in Figure B.4.4 along with the cone bearing profile. A special note must be made with respect to the cone bearing profiles shown in Figures B.4.3 and B.4.4. These two profiles are the same and are from a different investigation (i.e., different CPT locations) than the velocities shown in Figures B.4.3 and B.4.4. Thus, the profiles are only a rough guide for the change in soil profile with depth (i.e., one should expect some variability with different CPT locations). The velocities shown for the Annacis Pile Research Site are very comparable in each set of data and give greater confidence in the results.

Table B.4.2

Calculated Velocity Profiles for Annacis Pile Site, where Velocities Obtained from Striking each Side of the Hydraulic Pads of the Hammer Shear Source are Compared. The Data was Acquired with an Accelerometer (Unfiltered).

| Depth (m) | January 8, 1988 Pressuremeter Right Side Vs (m/sec) | January 8, 1988 Pressuremeter Left Side Vs (m/sec) | % Difference (Reference-Right Side) |
|---|---|---|---|
| 1.97-2.97 | 55 | 58 | +5 |
| 2.97-3.97 | 41 | 39 | -5 |
| 3.97-4.97 | 50 | 52 | +4 |
| 4.97-5.97 | 63 | 64 | +2 |
| 5.97-6.97 | 84 | 105 | +25 |
| 7.97-8.97 | 90 | 100 | +11 |
| 8.97-9.97 | 64 | 54 | -16 |
| 9.97-10.97 | 58 | 56 | -3 |
| 10.97-11.97 | 152 | 138 | -14 |

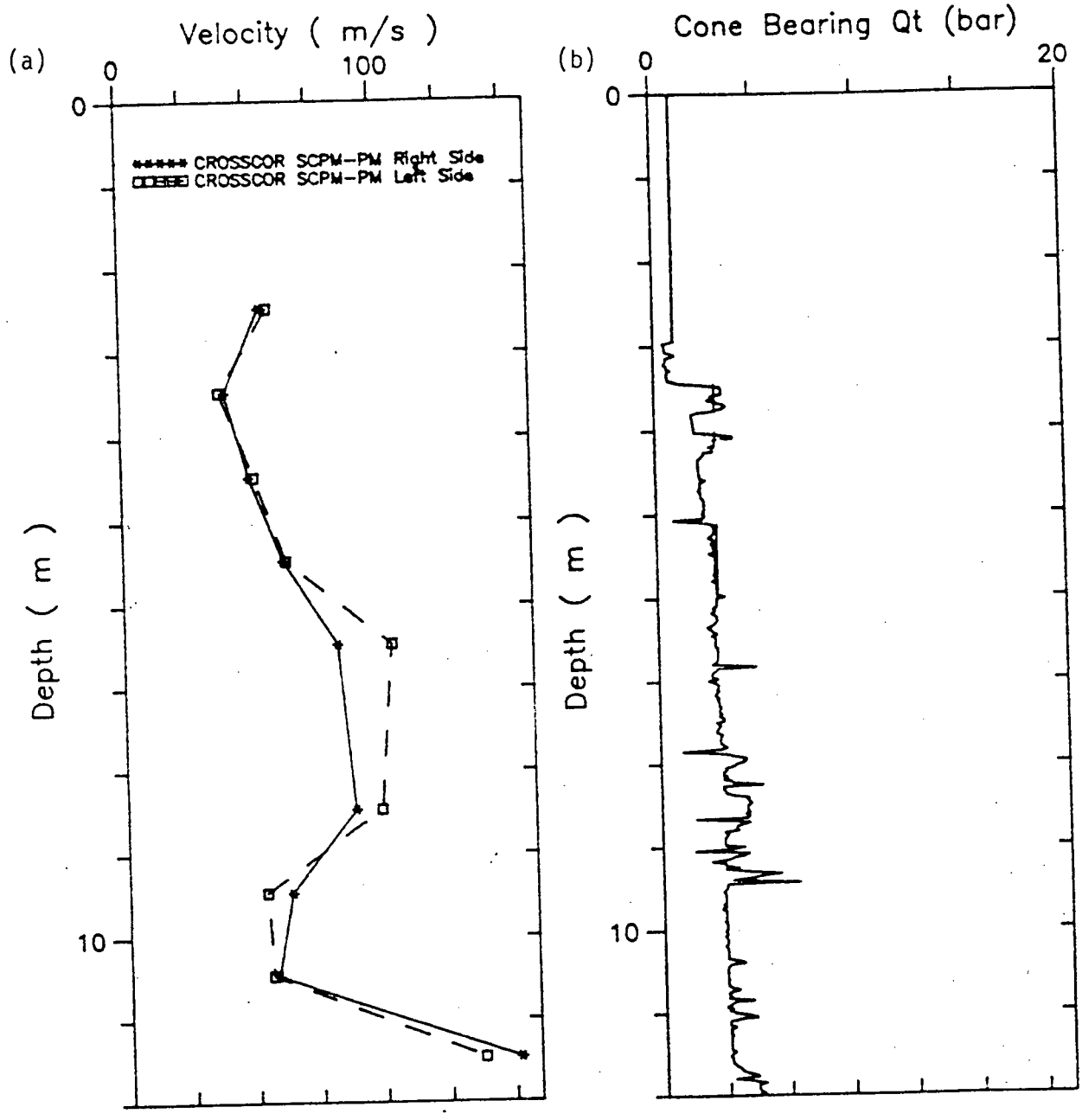


Figure B.4.3. (a) Calculated Velocity Profiles from the Annacis Pile Research Site, where Velocities Obtained from both Sides of the Hydraulic Pads of the Hammer Shear Source are Compared. The Data was Acquired with an Accelerometer (Unfiltered). (b) Cone Bearing Profile of the Annacis Bridge Pile Research Site

Table B.4.3

Calculated Velocity Profiles for Annacis Pile Site, where Velocities Obtained from Striking each Side of the Hydraulic Pads of the Hammer Shear Source are Compared. The Data was Acquired with an Accelerometer (Unfiltered).

| Depth (m) | CROSSCOR January 8, 1988 Cone #8 Right Scale Vs (m/sec) | CROSSCOR January 8, 1988 Cone #8 Left Scale Vs (m/sec) | % Difference (Reference-Right Side) |
|---|---|---|---|
| 1.84-2.84 | 19 | 24 | +25 |
| 2.84-3.84 | 41 | 41 | 0 |
| 3.84-4.84 | 22 | 21 | -4 |
| 4.84-5.84 | 75 | 85 | +13 |
| 5.84-6.84 | 82 | 82 | 0 |
| 6.84-7.84 | 91 | 87 | -4 |
| 7.84-8.84 | 114 | 122 | +7 |
| 8.84-9.84 | 94 | 97 | +3 |
| 9.84-10.84 | 123 | 128 | +4 |
| 10.84-11.84 | 137 | 152 | +11 |

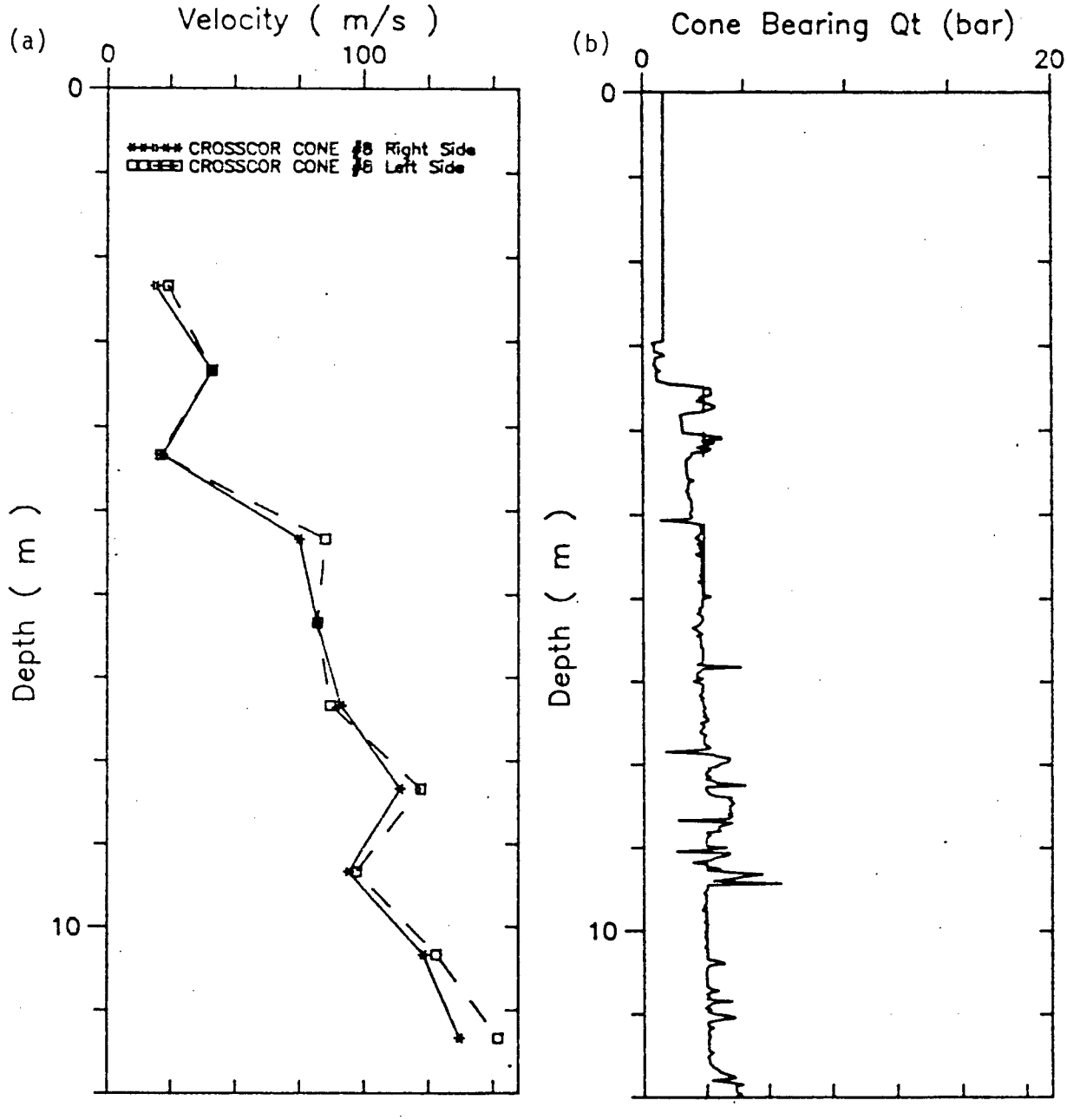


Figure B.4.4. (a) Calculated Velocity Profiles from the Annacis Pile Research Site, where Velocities Obtained from both Sides of the Hydraulic Pads of the Hammer Shear Source are Compared. The Data was Acquired with an Accelerometer (Unfiltered). (b) Cone Bearing Profile of the Annacis Bridge Pile Research Site

## B.5 CROSSCOR in Obtaining Compression Wave Velocities

In this section the application of CROSSCOR to obtaining compression wave velocities is addressed. As was discussed previously, the seismic traces obtained from unfiltered accelerometer data contain information of both shear and compression body waves. The extent of this information largely depends on sources used. A point source such as a Buffalo Gun would give more identifiable shear and compression waves, as opposed to a shear source (i.e., Hammer Shear Source) which gives predominantly shear waves. In order to isolate the individual body wave responses, it is necessary to obtain the frequency spectrum of the seismic traces recorded and bandpass the desired frequencies. In Figure B.5.1 a recorded wavelet is illustrated along with its frequency spectrum. This data was obtained with a P-Plate source at Laing Bridge Site at a depth of 6.8 metres. From the frequency spectrum obtained, one can identify three dominant responses. The first response is the shear wave occurring at 150 Hz, the second response is the compression wave at 900 Hz, and the third response resulted from the resonanting accelerometer at 3000 Hz. In order to isolate the compression wave, a Bandpass (e.g., 800 to 1200 Hz) must be applied which focuses on 900 Hz.

The body wave velocities are largely a function of the in-situ stresses and the composition of the sediments. Figure B.5.2 illustrates a plot of shear and compression wave velocities versus density for all types of sediments and rocks. As is illustrated in this figure, compression waves can vary from 1100 m/sec to 4000 m/sec in sediments. In saturated materials (no gas present) the compression wave velocity must be at least greater than that for water or about 1500 m/sec. Table B.5.1 shows that typical compression wave velocities for clay range from 1100 to 2500 m/sec, and those for loose sand are predominantly 1800 m/sec if saturated.

### Lower Langley 232nd St.

The first set of data discussed is from Lower Langley where a Buffalo Gun source was used. As was illustrated in Figure B.4.1, the seismic traces obtained from Buffalo Gun sources clearly contain identificable S and P waves. The present problem with using this data (as was shown in Section B.4) was that triggering was inconsistent. The compression wave velocities obtained from the Buffalo Gun data are shown in Table B.5.2 where a bandpass of 200 to 1000 Hz was applied. The nonsensical values obtained are most likely a result from triggering problems.

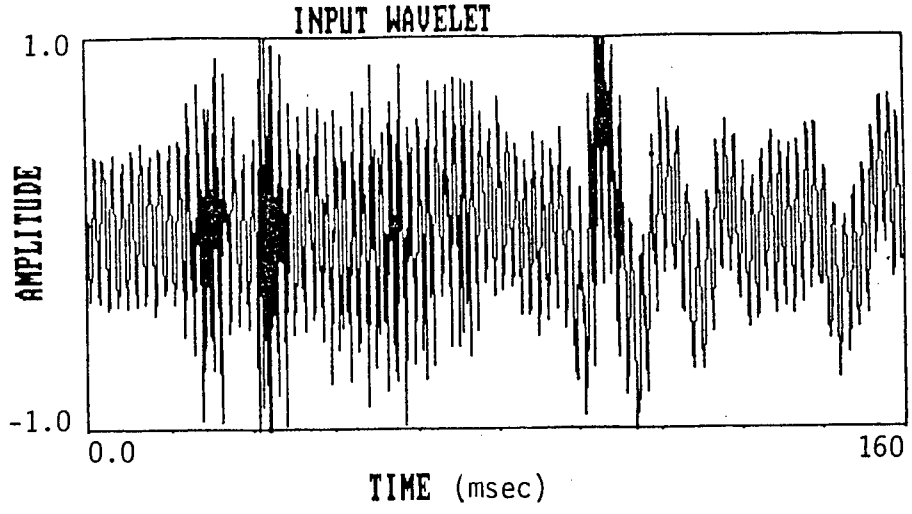


(a) Seismic Trace from Laing Bridge where a P-Plate Source was Used and an Accelerometer (Unfiltered) Recorded the Data at 6.8 Metres.

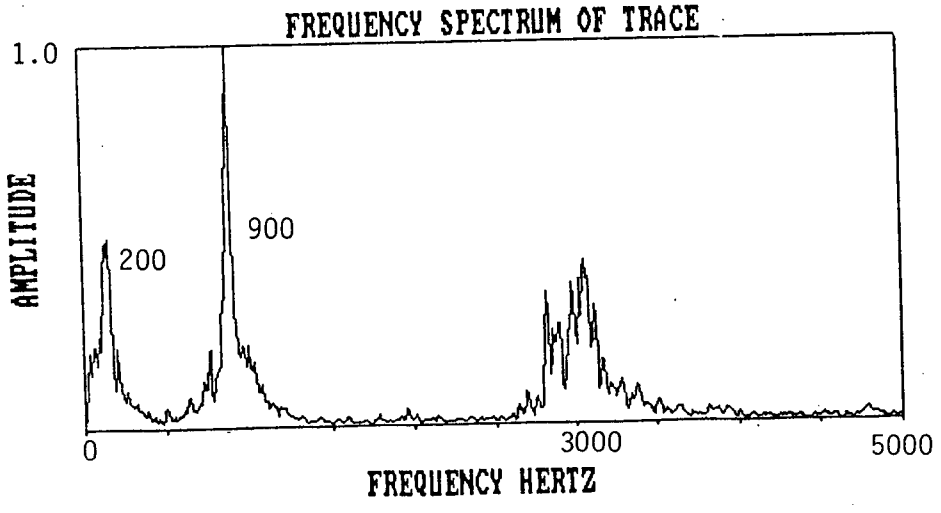


(b) Corresponding Frequency Spectrum of Seismic Trace Illustrating the Three Dominant Responses: Shear Wave at 150 Hz, Compression Wave at 900 Hz, and Resonanting Accelerometer at 3000 Hz.

Figure B.5.1. Seismic Trace from Laing Bridge

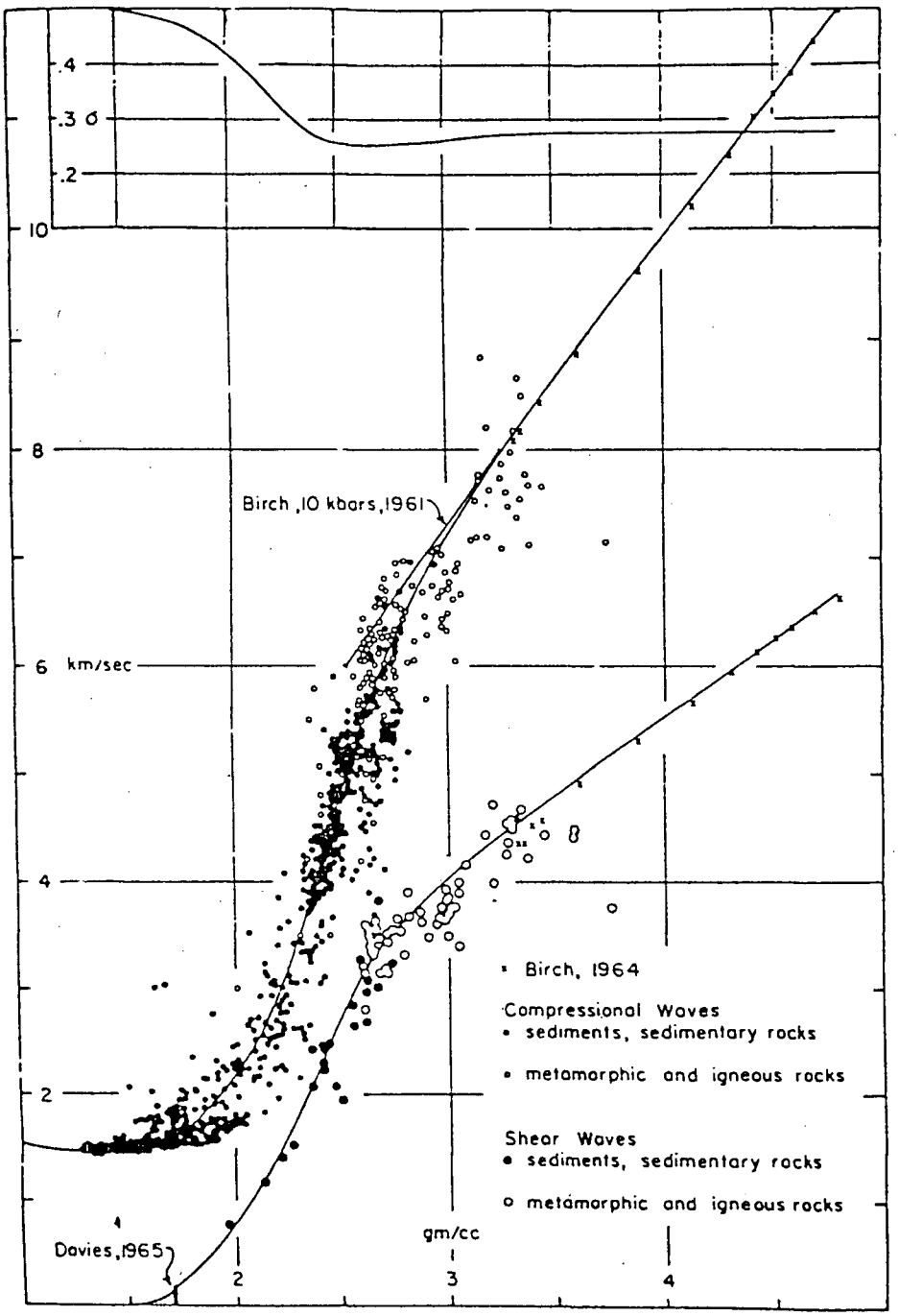


Figure B.5.2. Velocity Versus Density for Compressional and Shear Waves in all Types of Sediments and Rocks. Poisson's Ratio Versus Density at Top of Figure. (Milton B. Dobrin, 1976).

Table B.5.1

## Compressional and Shear Velocities in Sediments and Rocks (Milton B. Dobrin, 1976)

| Material and Source | Compressional velocity | | Shear velocity | |
|---|---|---|---|---|
| | m/s | ft/s | m/s | ft/s |
| Granite: | | | | |
| Barriefield, Ontario | 5640 | 18,600 | 2870 | 9470 |
| Quincy, Mass. | 5880 | 19,400 | 2940 | 9700 |
| Bear Mt., Tex. | 5520 | 17,200 | 3040 | 10,000 |
| Granodiorite, Weston, Mass. | 4780 | 15,800 | 3100 | 10,200 |
| Diorite, Salem, Mass. | 5780 | 19,100 | 3060 | 10,100 |
| Gabbro, Duluth, Minn. | 6450 | 21,300 | 3420 | 11,200 |
| Basalt, Germany | 6400 | 21,100 | 3200 | 10,500 |
| Dunite: | | | | |
| Jackson City, N.C. | 7400 | 24,400 | 3790 | 12,500 |
| Twin Sisters, Wash. | 8600 | 28,400 | 4370 | 14,400 |
| Sandstone | 1400–4300 | 4620–14,200 | | |
| Sandstone conglomerate, Australia | 2400 | 7920 | | |
| Limestone: | | | | |
| Soft | 1700–4200 | 5610–13,900 | | |
| Solenhofen, Bavaria | 5970 | 19,700 | 2880 | 9500 |
| Argillaceous, Tex. | 6030 | 19,900 | 3030 | 10,000 |
| Rundle, Alberta | 6060 | 20,000 | | |
| Anhydrite, U.S. Midcontinent, Gulf Coast | 4100 | 13,530 | | |
| Clay Saturated | 1100–2500 | 3630–8250 | | |
| Loose sand Saturated | 1800 | 5940 | 500 | 1,650 |

SOURCE: Sydney P. Clark, Jr. (ed.), "Handbook of Physical Constants," rev. ed., *Geol. Soc. Am. Mem.* 97, 1966.

Table B.5.2

Calculated Velocity Profile from Lower Langley, where an Accelerometer was Used for Data Acquisition. The Compression Wave Velocities were Obtained from the Buffalo Gun Source and by Applying a Bandpass of 200 to 1000 Hz.

| Depth (m) | CROSSCOR Buffalo Gun Filter Off Vp (m/sec) |
|---|---|
| 1.7-2.7 | 243 |
| 2.7-3.7 | 1200 |
| 3.7-4.7 | 1443 |
| 4.7-5.7 | 330 |
| 5.7-6.7 | 353 |
| 10.7-11.7 | 330 |
| 11.7-12.7 | 332 |
| 12.7-13.7 | * |
| 13.7-14.7 | * |
| 14.7-15.7 | 760 |
| 15.7-16.7 | 3051 |
| 16.7-17.7 | 3060 |
| 17.7-18.7 | 383 |

* => nonsensical compression wave velocities due to poor and/or uncorrelated responses.

Illustrated in Figure B.5.3. are traces obtained from the Buffalo Gun data along with the isolated compression wave responses. This figure illustrates that the compression wave responses are clearly identifiable and correlated (i.e., similar). Thus, one can conclude that if triggering was repeatable, accurate compression wave velocities could be obtained.

The next set of data was from Lower Langley where the Hammer Shear was used. The compression waves velocities obtained from this set of data (unfiltered accelerometer) are shown in Table B.5.3 and were obtained with a bandpass of 750 to 1000 Hz applied. The nonsensical velocities are most likely due to the fact that clear compression wave responses were not obtained. Figure B.5.4 illustrates that the isolated compression wave responses are very noisy and poorly correlated.

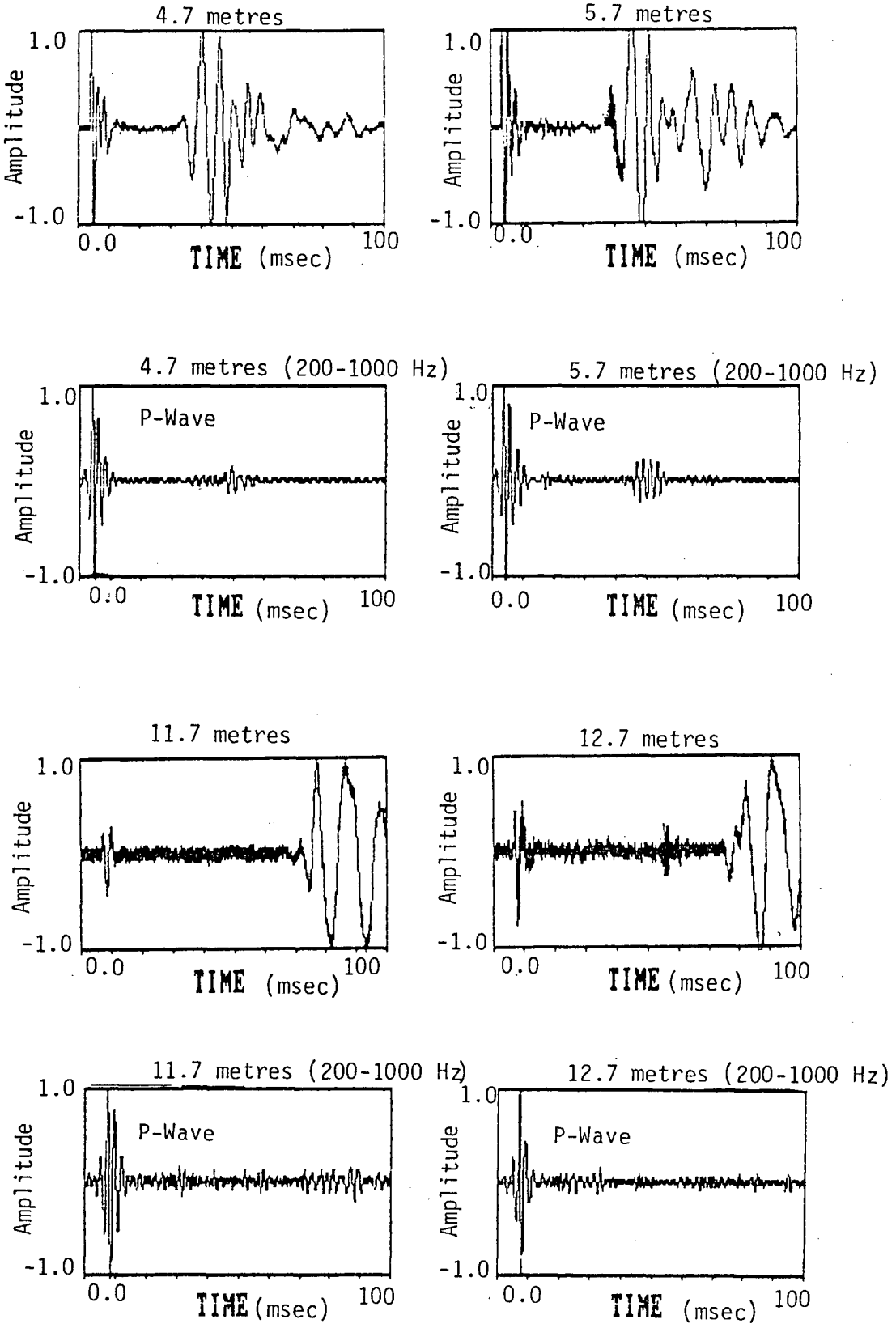


Figure B.5.3. Seismic Traces Obtained at Lower Langley where a Buffalo Gun Source was Used. The Traces were Filtered (200 to 1000 Hz) in order to Extract the Compression Wave Responses. The resulting Compression Wave Responses are Highly Correlated.

Table B.5.3

Calculated Velocity Profiles from Lower Langley, where an Accelerometer was Used for Data Acquisition. The Compression Wave Velocities were Obtained by Applying a Bandpass of 750 to 1500 Hz.

| Depth (m) | CROSSCOR Hammer Source Filter Off Vp (m/sec) |
|---|---|
| 2.7-3.7 | 1042 |
| 3.7-4.7 | 558 |
| 4.7-5.7 | 579 |
| 5.7-6.7 | 676 |
| 6.7-7.7 | 1600 |
| 7.7-8.7 | 692 |
| 8.7-9.7 | 542 |
| 9.7-10.7 | 2448 |
| 10.7-11.7 | * |
| 11.7-12.7 | * |
| 12.7-13.7 | 4937 |
| 13.7-14.7 | * |
| 14.7-15.7 | 1651 |
| 15.7-16.7 | * |
| 16.7-17.7 | * |
| 17.7-18.7 | * |
| 18.7-19.7 | * |
| 19.7-20.7 | * |
| 20.7-21.7 | * |
| 21.7-22.7 | 1244 |
| 22.7-23.7 | * |
| 23.7-24.7 | * |
| 24.7-25.7 | * |
| 25.7-26.7 | 1246 |
| 26.7-27.7 | * |
| 27.7-28.7 | * |

* => nonsensical compression wave velocities are due to poor and/or uncorrelated responses

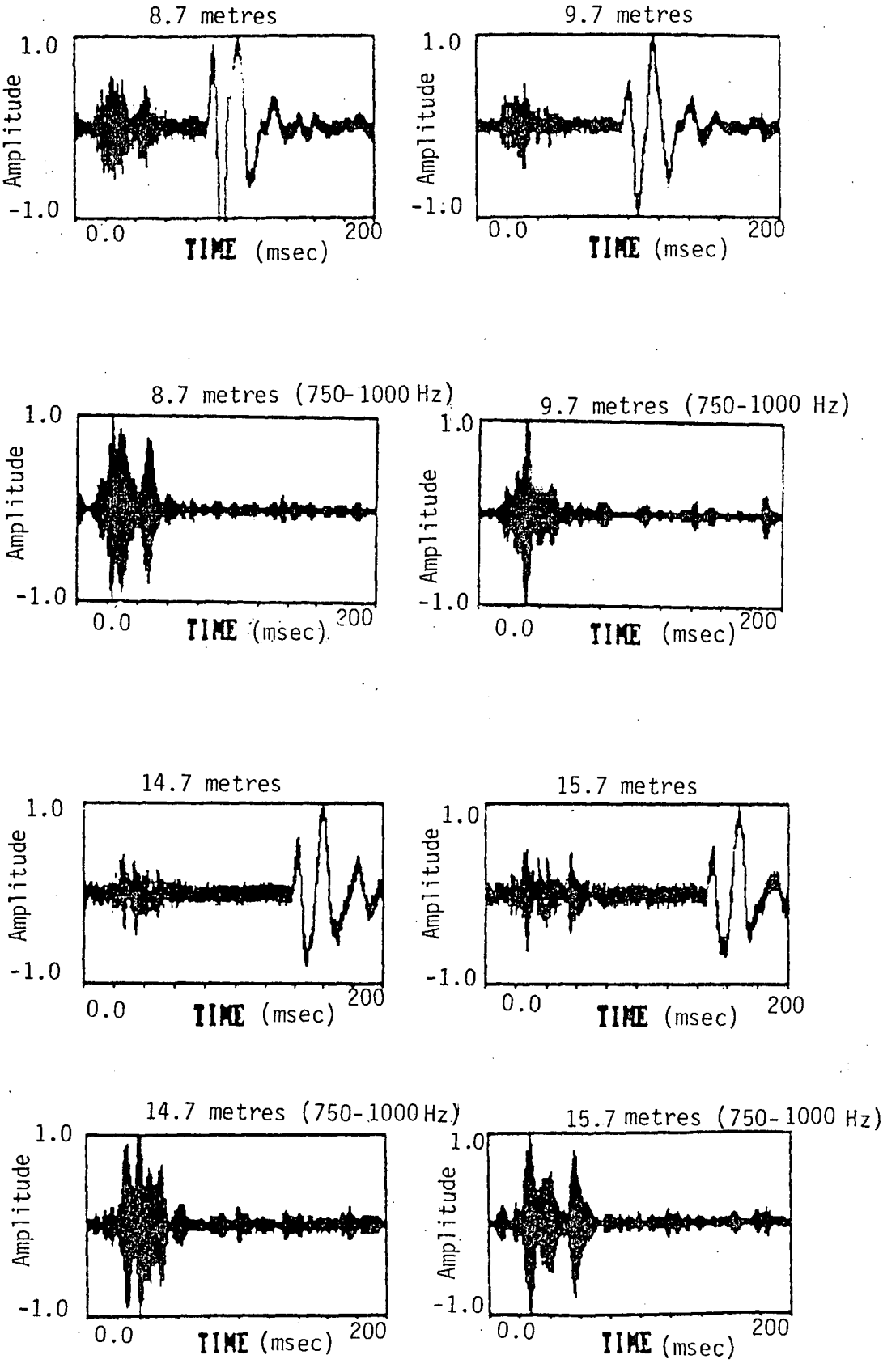


Figure B.5.4. Seismic Traces Obtained at Lower Langley Where a Hammer Shear Source was Used. The Traces were Filtered (1750 to 2000 Hz) in Order to Extract the Compression Wave Responses. The Resulting Compression Waves are Poorly Correlated.

## B.6 Bandwidth Considerations when Applying CROSSCOR

In Section IIIA, it was stated that the crosscorrelation function provides information about the similarity and time difference between two successive wavelets. In this case we are looking for the arrival time difference between the dominant responses of the recorded wavelets. The main idea behind CROSSCOR is to isolate specific body waves in the frequency domain and then crosscorrelate the filtered wavelets in the time domain. The shear and compression body waves are identified by their own band of frequencies where a dominant frequency characterizes the respective wavelet. From the extensive amount of seismic data processed in this research, it was found that in specifying the bandwidth in filtering the most important considerations are to:

(1) Include dominant frequency characterizing wavelet, because the other contributing frequencies do not effect the dominant responses significantly.

(2) The bandwidths specified must be consistent throughout the seismic profile in order that the crosscorrelated dominant responses are similar in transient response specifications (e.g., page 1.4)

In Figure B.6.1 there is a seismic trace (at 2.7 metres) from Lower Langley illustrated along with its' frequency spectrum. From this frequency spectrum the dominant shear wave response is identified at 50 Hz. Figure B.6.2 shows a seismic trace recorded at a depth of 3.7 from the same seismic cone profile. From the frequency spectrum of this seismic wavelet, the dominant shear wave response is also identified at 50 Hz. In Figure B.6.3 the two above wavelets are illustrated along with their filtered responses. The first filtered set of data was bandpassed from 20 to 120 Hz and the second set of filtered data was bandpassed from 30 to 70 Hz. These bandwidths were chosen in order that the filtered wavelets contain the dominant shear wave response of 50 Hz. When crosscorrelated, the two different sets of filtered data gave the same time shift and corresponding velocity of 102 m/sec.

Figure B.6.4 illustrates a seismic trace recorded at a depth of 3.7 metres at the Lower Langley Site. The frequency spectrum illustrated here is slightly more complex than those shown in Figures B.6.1 and B.6.2, because a Buffalo Gun source was used as opposed to the Hammer Shear Source. From Figure B.6.4 the dominant shear wave responses are from 50 to 200 Hz. Figure B.6.5 illustrates

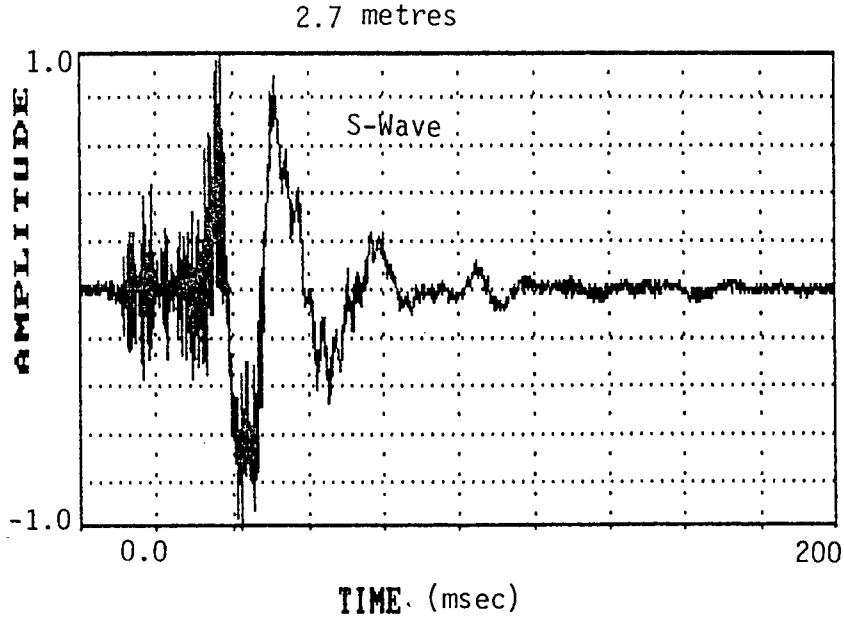


(a) Seismic Trace at 2.7 Metres Acquired with an Unfiltered Accelerometer.

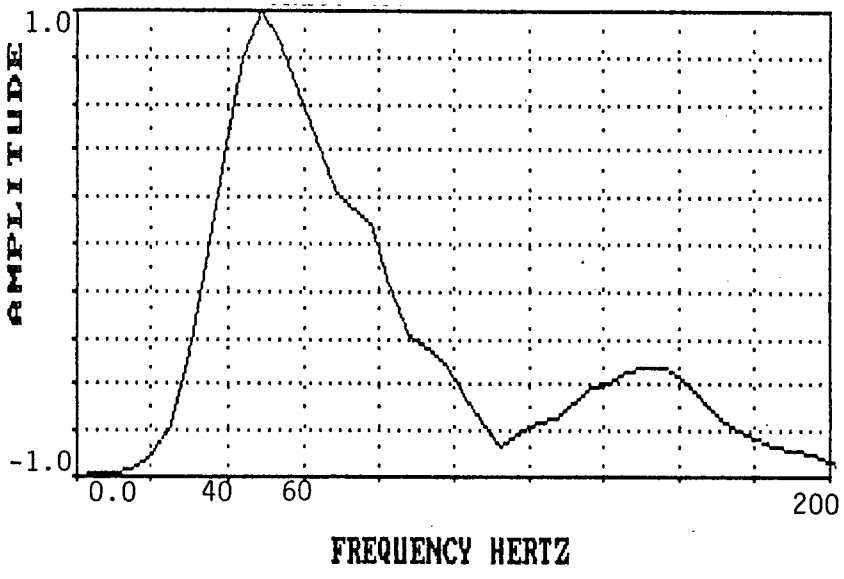


(b) Frequency Spectrum Illustrating Dominant Shear Wave Response at 50 Hz.

Figure B.6.1. Seismic Trace from Lower Langley Where a Hammer Shear Source Was Used.

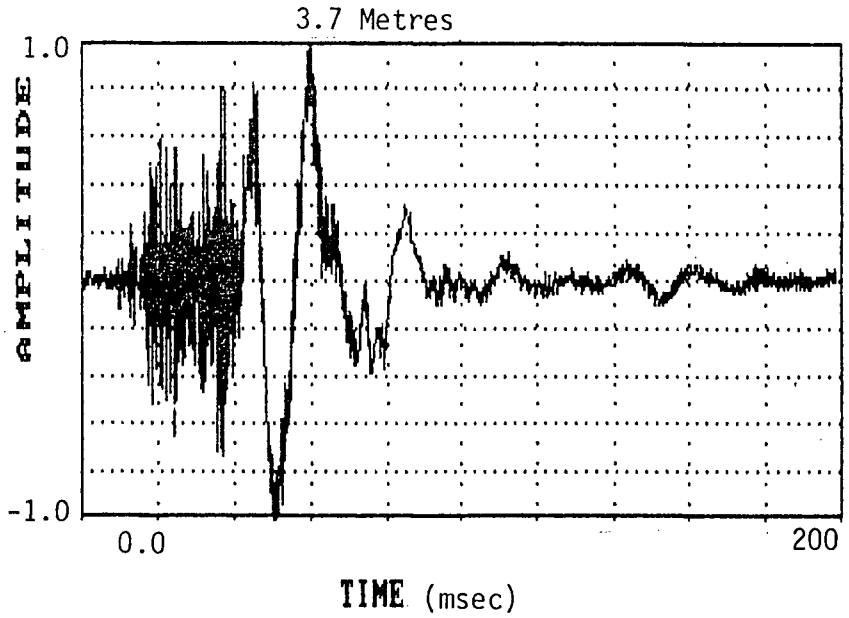


(a) Seismic Trace at 3.7 Metres Acquired with An Unfiltered Accelerometer.

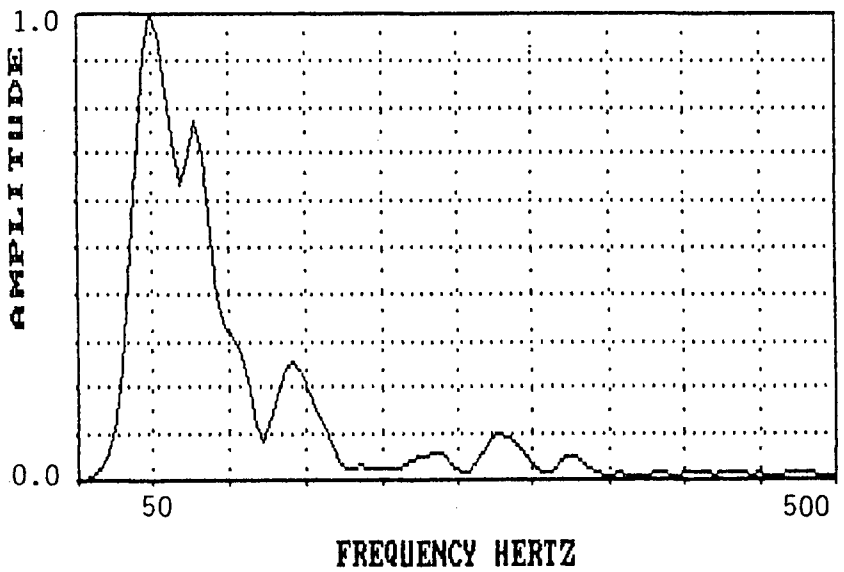


(b) Frequency Spectrum Illustrating Dominant Shear Wave Response at 50 Hz.

Figure B.6.2. Seismic Trace Recorded at Lower Langley Where a Hammer Shear Source was Used.

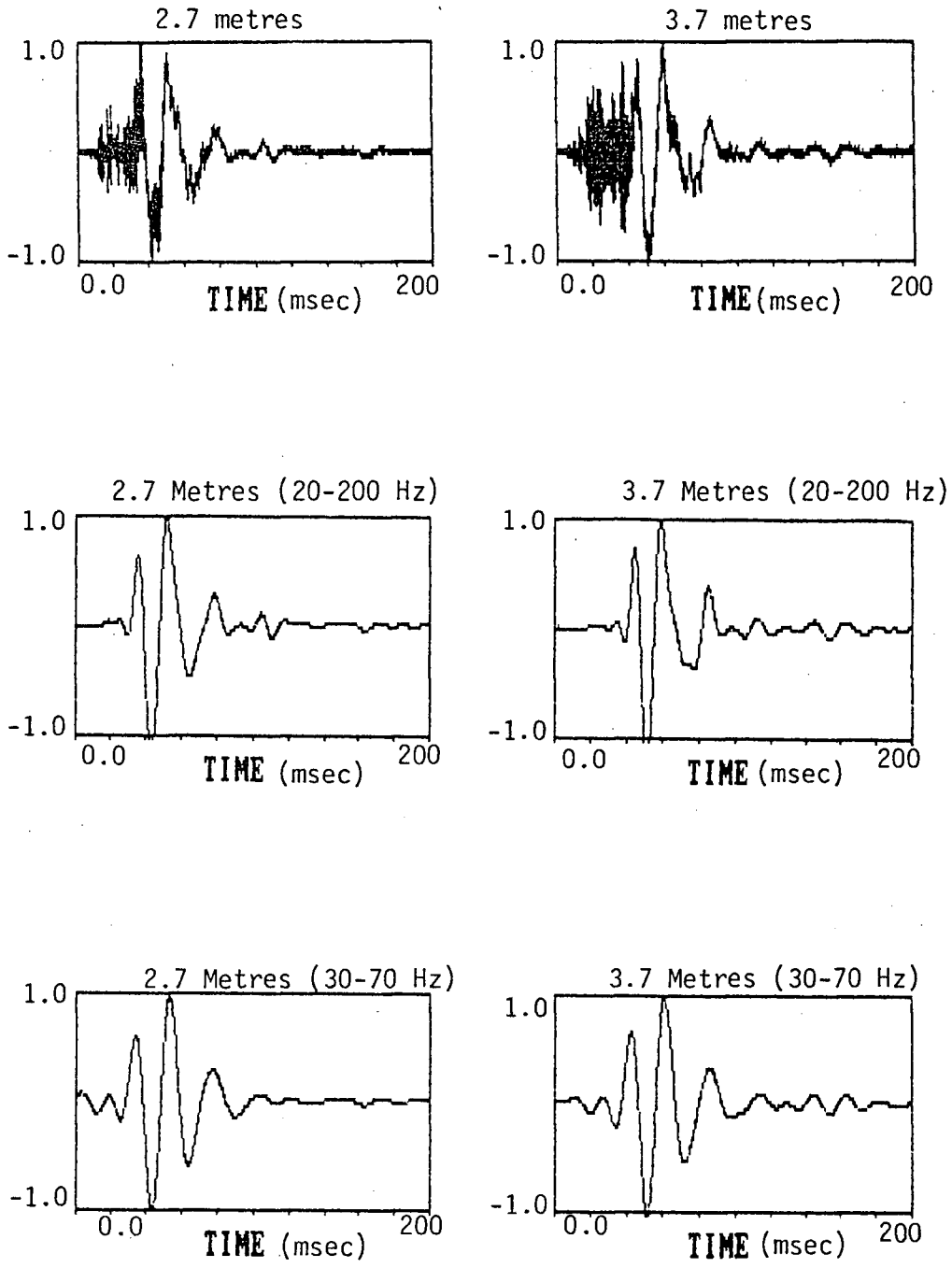


Figure B.6.3. (a) Seismic Traces Recorded at Depths of 2.7 and 3.7 Metres. (b) Trace in (a) Filtered Between 20 to 200 Hz Resulting in a Velocity of 102
Filtered Between 30 to 70 Hz Resulting in a Velocity of 102 m/sec.

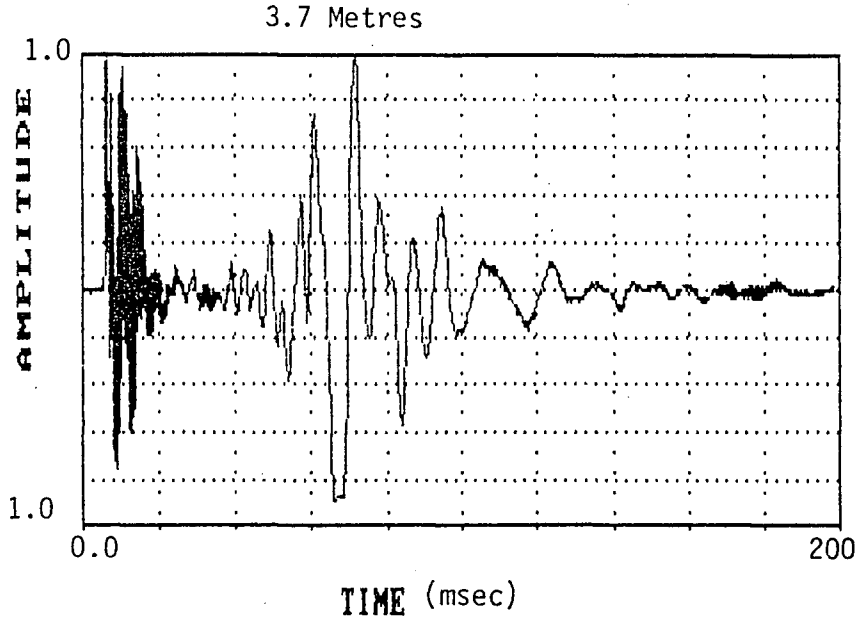


(a) Seismic Trace at 3.7 Metres Acquired with an Unfiltered Accelerometer.

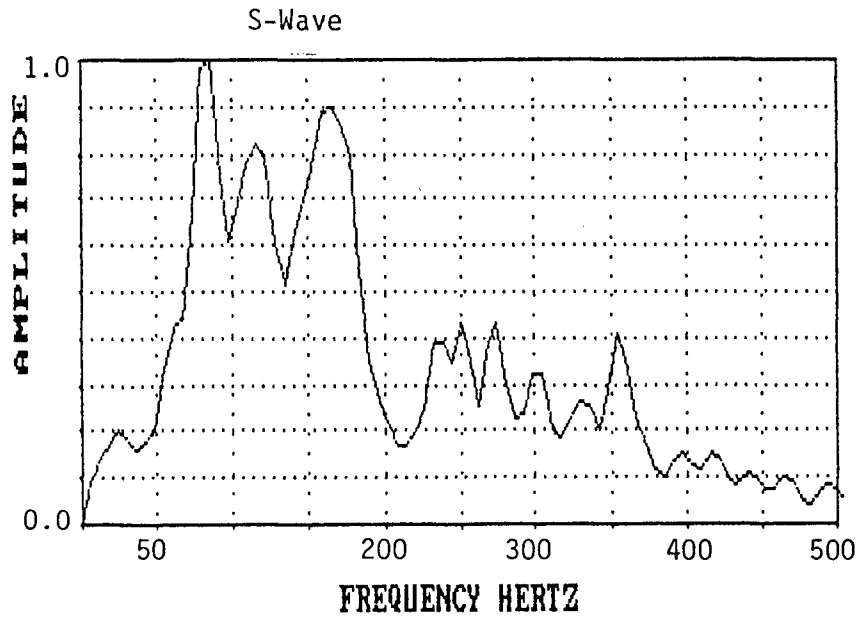


(b) Frequency Spectrum of (a), Illustrating Dominant Shear Wave Responses Situated Between 50 to 200 Hz.

Figure B.6.4. Seismic Trace Recorded at Lower Langley Where a Buffalo Gun Source was Used

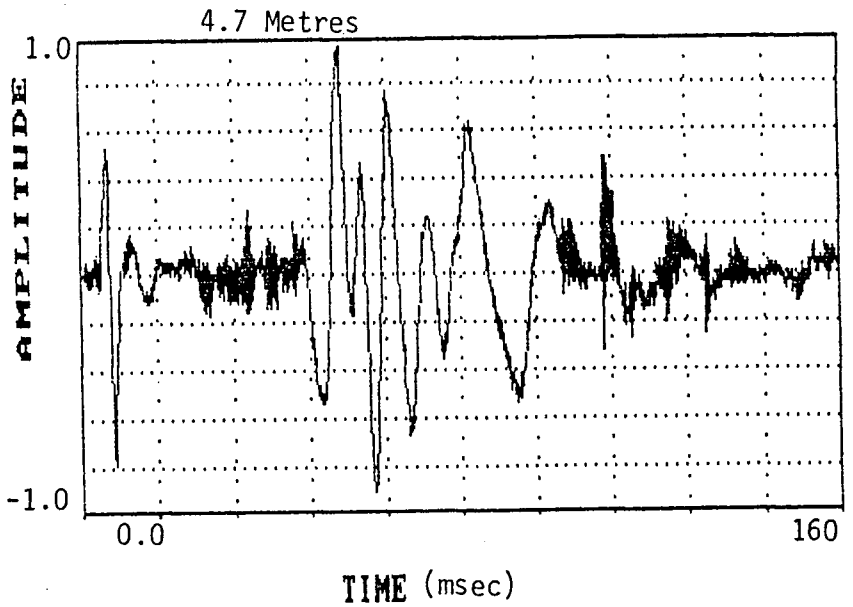


(a) Seismic Trace at 4.7 Metres Acquired with an Unfiltered Accelerometer.

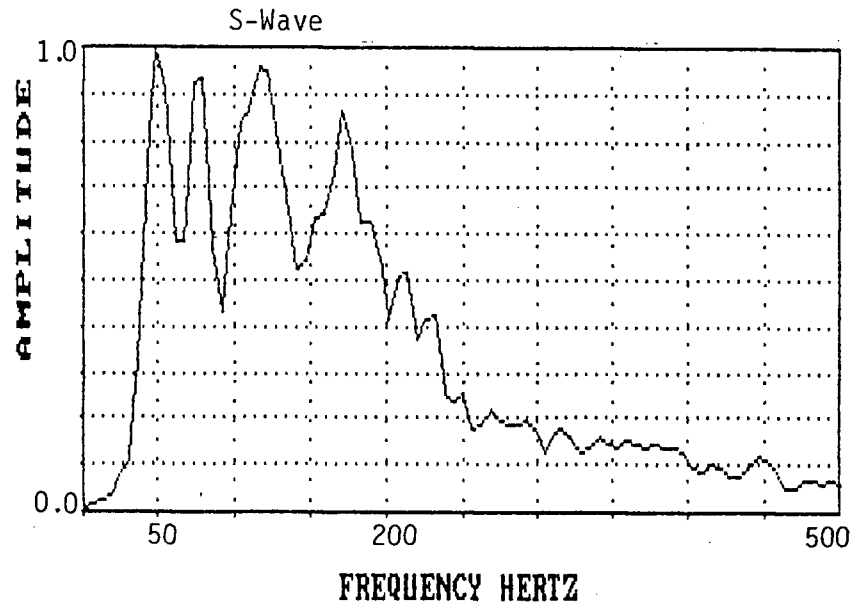


(b) Frequency Spectrum Illustrating Dominant Shear Wave Response Situated Between 50 to 200 Hz.

Figure B.6.5. Seismic Trace Recorded at Lower Langley where a Buffalo Gun Source was Used

another seismic trace at a depth of 4.7 metres from the same seismic cone profile as the trace in Figure B.6.4. From the frequency spectrum illustrated in Figure B.6.5, the dominant shear wave responses are situated from 50 to 200 Hz. Figure B.6.6 illustrates the above two Buffalo Gun traces along with their filtered responses. The first set of filtered data was bandpassed from 20 to 200 Hz, and the second set of filtered data was bandpassed from 60 to 180 Hz. Cross-correlating these two different sets of filtered data resulted in the same time shift and velocity of 94 m/sec. Figure B.6.7 shows the same Buffalo Gun Traces bandpassed between 100 to 200 Hz. The resulting velocity (93 m/sec) obtained from this set of data was negligibly different from those previously obtained.

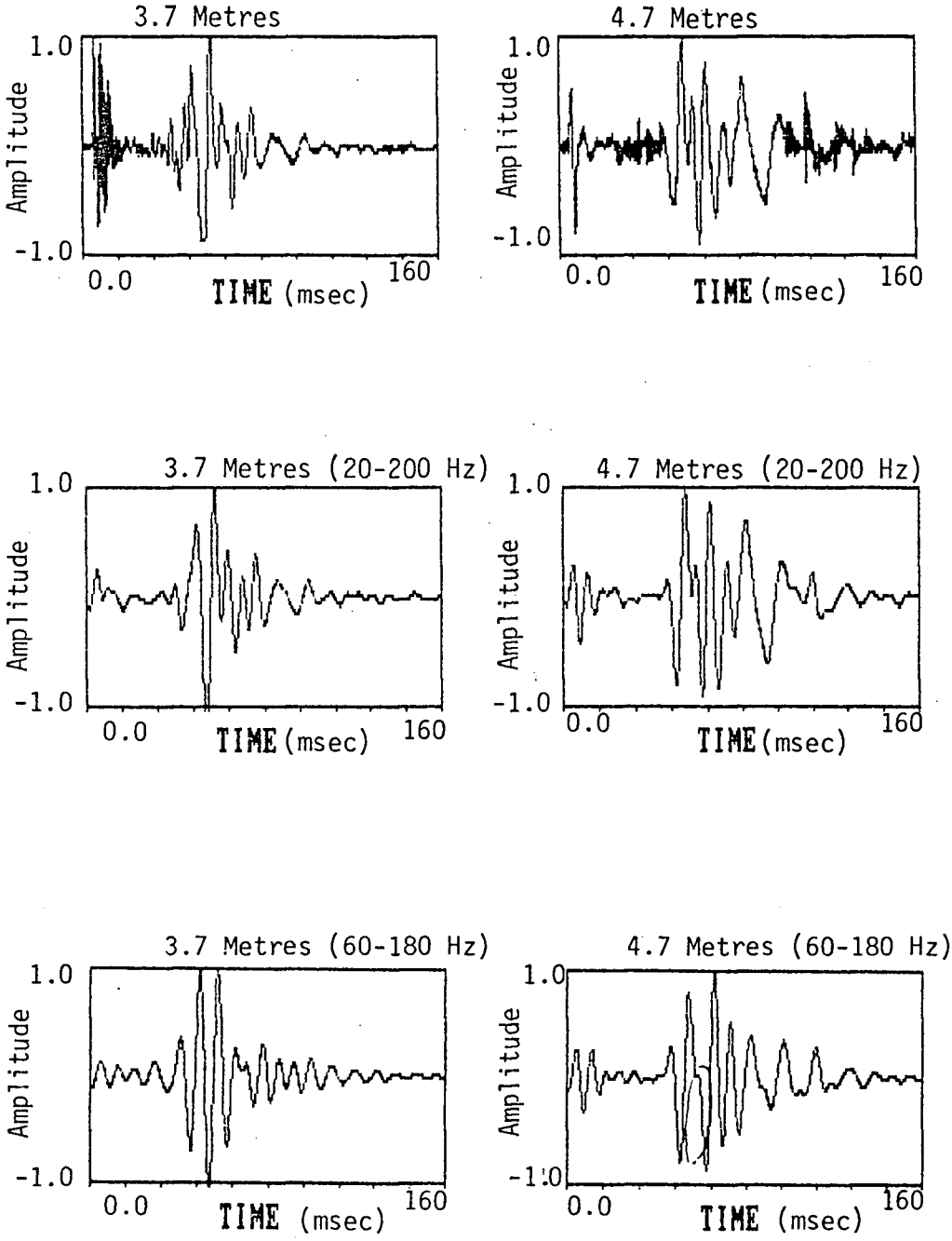


Figure B.6.6. (a) Seismic Traces Recorded at Depths of 3.7 and 4.7 Metres. (b) Trace in (a) Filtered Between 20 to 200 Hz Resulting in a Velocity of 94 m/sec. (c) Traces in (a) Filtered Between 60 to 180 Hz Resulting in a Velocity of 94 m/sec.

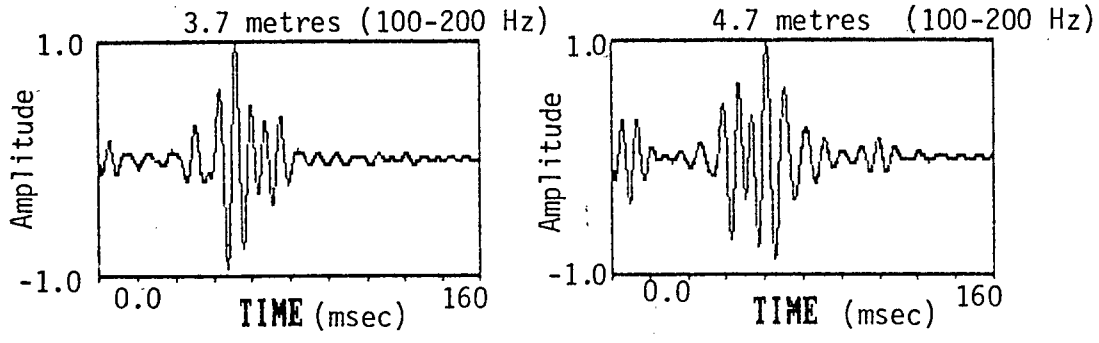


Figure B.6.7. Trace in Figure B.6.6(a) Filtered Between 100 to 200 Hz Resulting in a Velocity of 93 m/sec.

## B.7 CONCLUSIONS

The results from the previous discussions suggest that CROSSCOR is a very beneficial tool to obtain seismic wave velocities. In these investigations, CROSSCOR was also found to be very useful to reduce the noisy accelerometer data where picking cross-overs was difficult or impossible. The program allows one to separate out different seismic events and use all the information contained in the wavelets in obtaining shear and compression wave velocities. When conducting the data reductions, it was found that the different wavelet signatures were consistent throughout a cone profile. Thus, separating out the shear and compression wave instrument responses was routine and CROSSCOR proved to be user friendly. In addition, since CROSSCOR is a digital filter it removes most human bias in determining arrival times, the program allows one to compare velocities from signals obtained on opposite sides of the source, and one may also have the flexibility in using different sources in obtaining seismic wave velocities.

In applying CROSSCOR to Buffalo Gun Source data it was found that compression and shear waves could be identified and isolated. The problem with processing Buffalo Gun data was that triggering was not consistent thorough out a seismic profile resulting in erroneous velocity calculations. It was suggested that the triggering problem could be resolved by using an accelerometer (having a fast response time) instead of the geophone as well as gounding the Buffalo Gun firing pin to create a contact closure (similar to the shear plate).

The performance of CROSSCOR is summarized in the following list of advantages/disadvantages with comparisons made to the reverse polarity method in the list of advantages and comparisons made to the following Kalman Filter formulation in the list of disadvantages.

Advantages

(1) CROSSCOR is able to work with noisy accelerometer data extracting shear and compression waves.

(2) The crosscorrelation function in CROSSCOR makes use of all the information in the signals (averaging out irregularities and putting significance or dominant responses) as opposed to the reverse polarity method which relies only on one cross-over point to determine interval times.

(3) CROSSCOR works as well as the reverse polarity method when reducing clean signals, and CROSSCOR works better than the reverse polarity method with signals containing many dominant low frequencies (e.g., Figures 2.8 and B.2.1).

(4) CROSSCOR can obtain velocity estimates from nonpolarized sources (e.g., the Buffalo Gun Source and comparing one side of the Hammer Shear Source to the other). Thus, CROSSCOR has greater flexibility than the reverse polarity method in working with different types of sources and giving more velocity estimates for a downhole seismic profile as opposed to the reverse polarity method.

(5) CROSSCOR can extract compression wave events from seismic traces and give corresponding compression wave velocities.

(6) CROSSCOR is a user friendly program which has flexibility in specifying the cutoff frequencies if there is a repeatable trigger of fast response and sufficient accuracy and resolution.

Disadvantages

(1) CROSSCOR cannot give soil damping properties.

(2) CROSSCOR cannot give any indication of the shape of the wavelets being recorded (which is a very important parameter in earthquake engineering).

## IV. KALMAN FILTER FOR ESTIMATING AMPLITUDES & ARRIVAL TIMES IN P AND S WAVE ANALYSIS - A PRELIMINARY ASSESSMENT

This section gives a brief description of the Kalman Filter, KF, and presents the equations for using the KF to estimate P-wave and S-wave amplitudes and arrival times. More details of the KF equations, with examples and applications to geophysical problems, can be found in Reference 24.

The KF should be investigated for its possible application to obtaining accurate estimates of the P-wave and S-wave amplitudes and arrival times, for the particular problem we are considering, due to both the flexibility of the KF approach and to limitations of the frequency domain approaches that were discussed in Section III.

The Kalman Filter is an optimal (in a least squares sense) filter which is based on state-space, time-domain formulations of physical problems. Application of this filter requires that the physical problem be modelled by a set of first order differential or difference equations which, with initial conditions, uniquely define the system behaviour. The filter utilizes knowledge of system and measurement dynamics, assumed statistics of system noises and measurement errors, and statistical information about the initial conditions. Figure 4.1 illustrates the basic relation between the system, the measurements, and the Kalman Filter, for application to physical problems.

The Kalman Filter takes into account the statistics of the measurement and state errors, and the apriori model information provides for optimal use of any number, combination, and sequence of external measurements. The Kalman Filter can be applied to problems with linear time-varying systems, and with non-stationary system and measurement statistics. Problems with nonlinearities can sometimes be handled by linearizing the system and measurement equations. Furthermore, the Kalman Filter is readily applied to estimation, smoothing, and prediction.

One of the most important aspects that is realized when applying the KF to solving a specific problem, is that a considerable effort is required to model the physical problem to fit into the framework of the KF. The physical problem must be modelled/approximated by a set of first order differential or difference equations. In addition, the statistical properties of the system

and measurements need to be modelled by first and second order statistics (expected values and covariances). It should also be noted that satisfactory results are not always obtained by a specific formulation of a problem. It may be necessary to try different approaches before satisfactory results are obtained. For example, different smoothing techniques may need to be considered to improve the estimates.

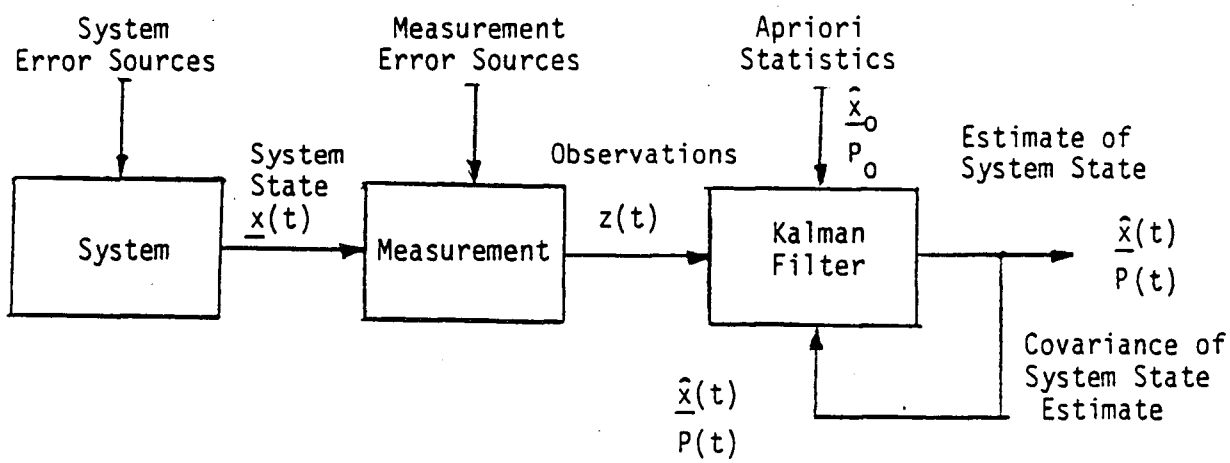


Figure 4.1. Block Diagram of System, Measurements, and Kalman Filter

For the sake of completeness, a summary of the continuous and discrete KF are given in Sections B and C, respectively. Since the modelling of the physical system is an important aspect of the KF approach, Section D gives a fairly detailed discussion of the derivation of differential equations for a typical acceleration measuring device. Sections E and F discuss the specific KF equations for the estimation of P-wave and S-wave amplitudes and arrival times.

A. Kalman Filter Results

As stated earlier, when applying the KF it is important to model the physical problem to fit into the framework of the KF. The KF filter proposed would attempt to model a seismic receiver as a second order system with it's characteristic natural frequency and damping. The modelling of a seismic receiver results in the necessity of thorough calibration and performance indexing. Guigné (1986) also illustrates the importance of instrument calibration when applying his Acoustic Sub-Seabed interrogator, he states, "The spectral response of the transmitter and receiver is also being pursued to refine their overall sensitivity. Providing these parameters are calibrated, it is believed that dynamic modelling of the truncated parametric array can be used as a reliable approach for rapid measurements of attentuation in marine sediments."

The seismic receiver acts as a transform function in respect to the input of noise and body waves propagating through the earth. This interaction is illustrated in Figure 4.2 when we have noise, state x(5), and signal (amplitude $\sim$x(1) and arrival time $\sim$x(2)) interacting with the instrument which is represented by the second order system F(s) with natural frequency $\omega_0$, and damping $\zeta$. The output is a superposition of the noise, x(5), passing through the instrument and giving us the second order responses x(6) and x(7). The body waves (S and P-waves) represented by states x(1) to x(4) result in the second order responses x(8) and x(9). Therefore, knowing the output, transform function (instrument), it is desired to determine the characteristics of the input signal (i.e., maximum amplitude x(1) and arrival time x(2)).

The modelling of a geophone was accomplished by applying the program KALDAT which is given in Appendix C. The noise, state x(5), was modelled by passing white noise through the earth which acts as a low pass filter. The filtering effect of the earth is due to its damping characteristics, which is typically modelled as a first order system (i.e., exponential decay). The extent of the decay is represented by the time constant Tc, where an increasing time constant applies greater attenuation. Figure 4.3 illustrates the effect an increasing time constant has on a white noise input. As shown, an increase in Tc tends to smooth the signal indicating a removal of the higher frequencies. Figure 4.4 illustrates how the second order system responds to varying input noise. Figure 4.4 indicates that as the time constant decreases, the instrument gives a higher frequency response.

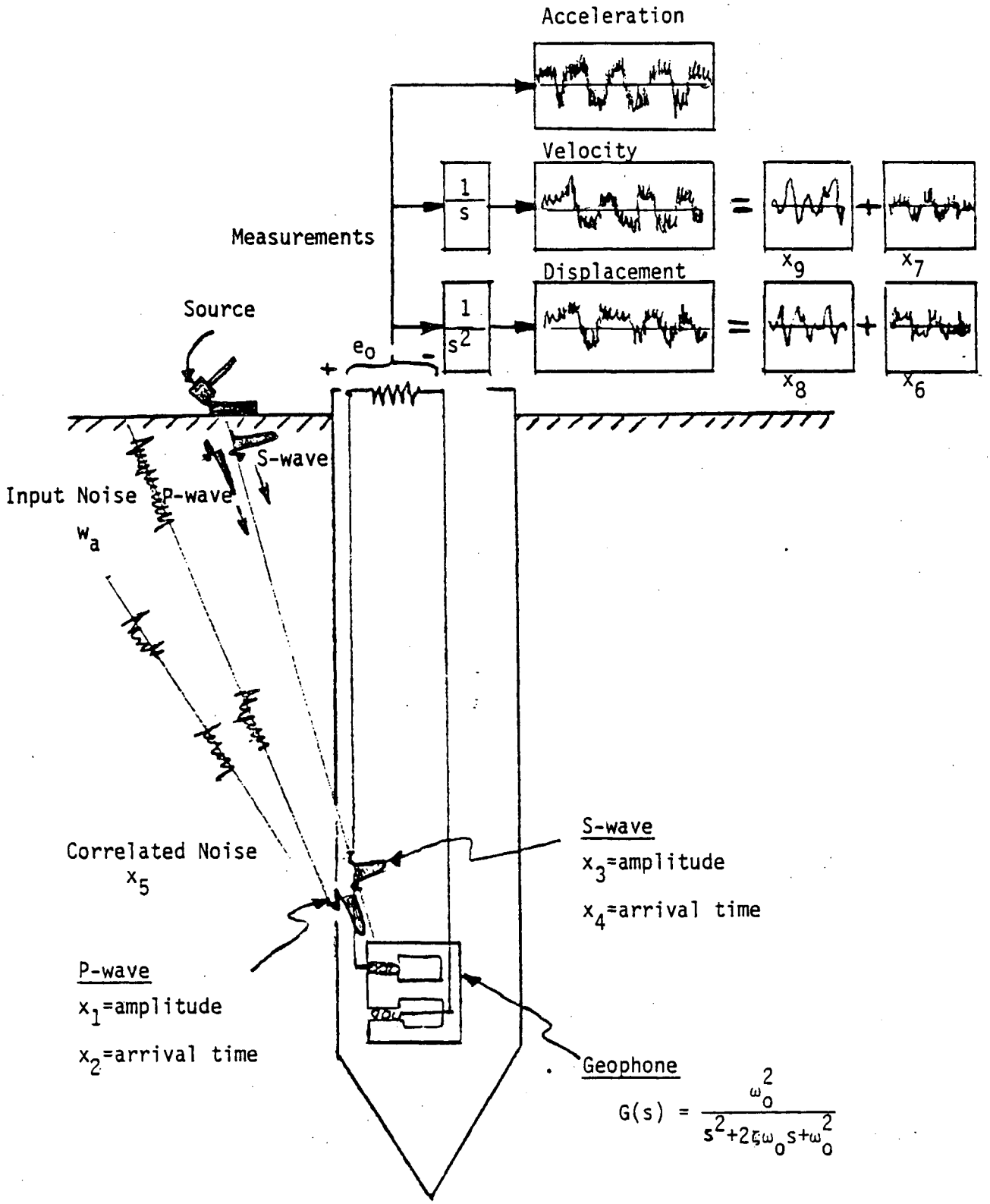


Figure 4.2. Schematic Illustration of the States, $x_i$ for the KF Formulation

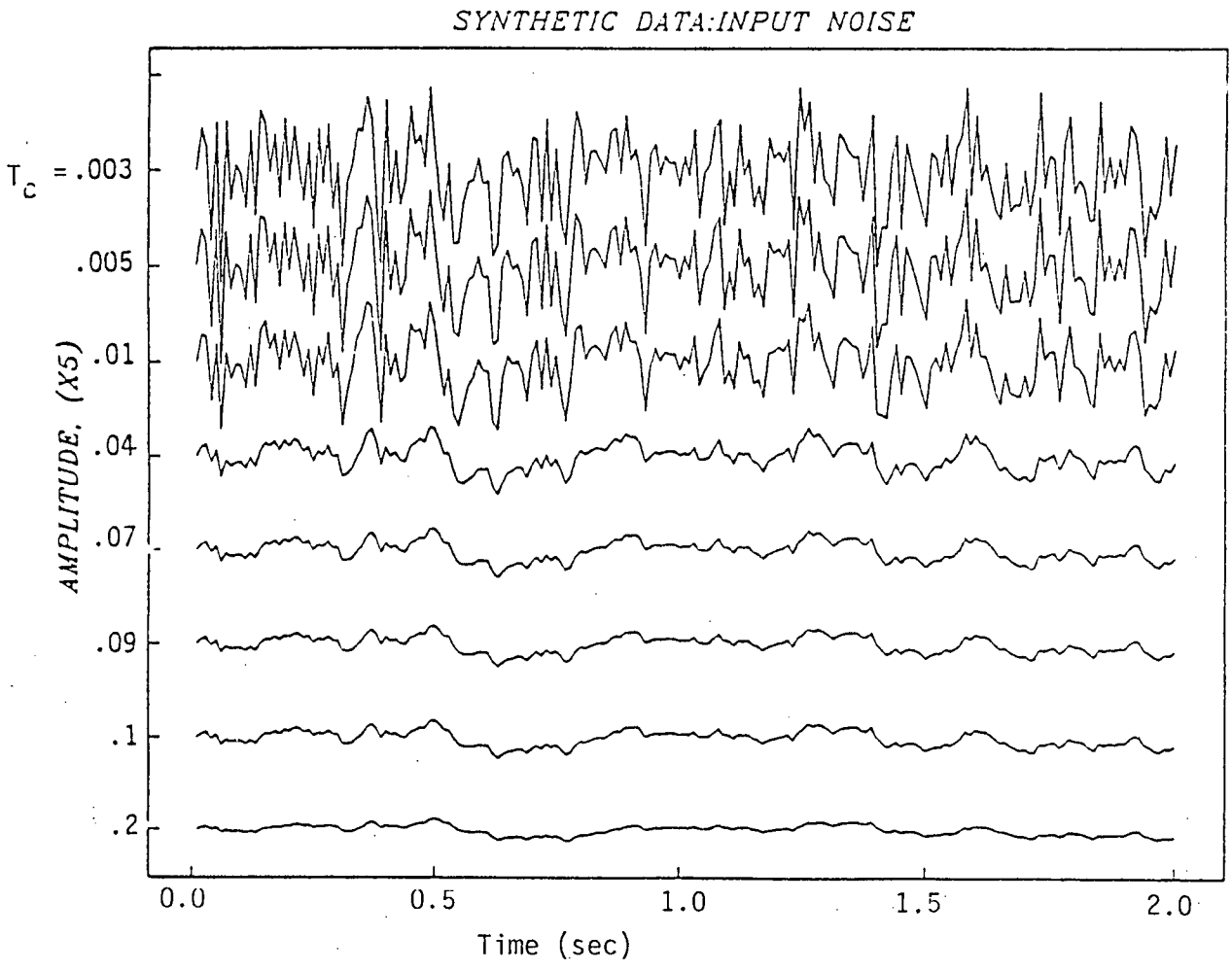


Figure 4.3. The Effect An Increasing Time Constant Has On White Noise (Note: $T_c$ = .003, 005, .01, .04, .07, .09, .1, .2)

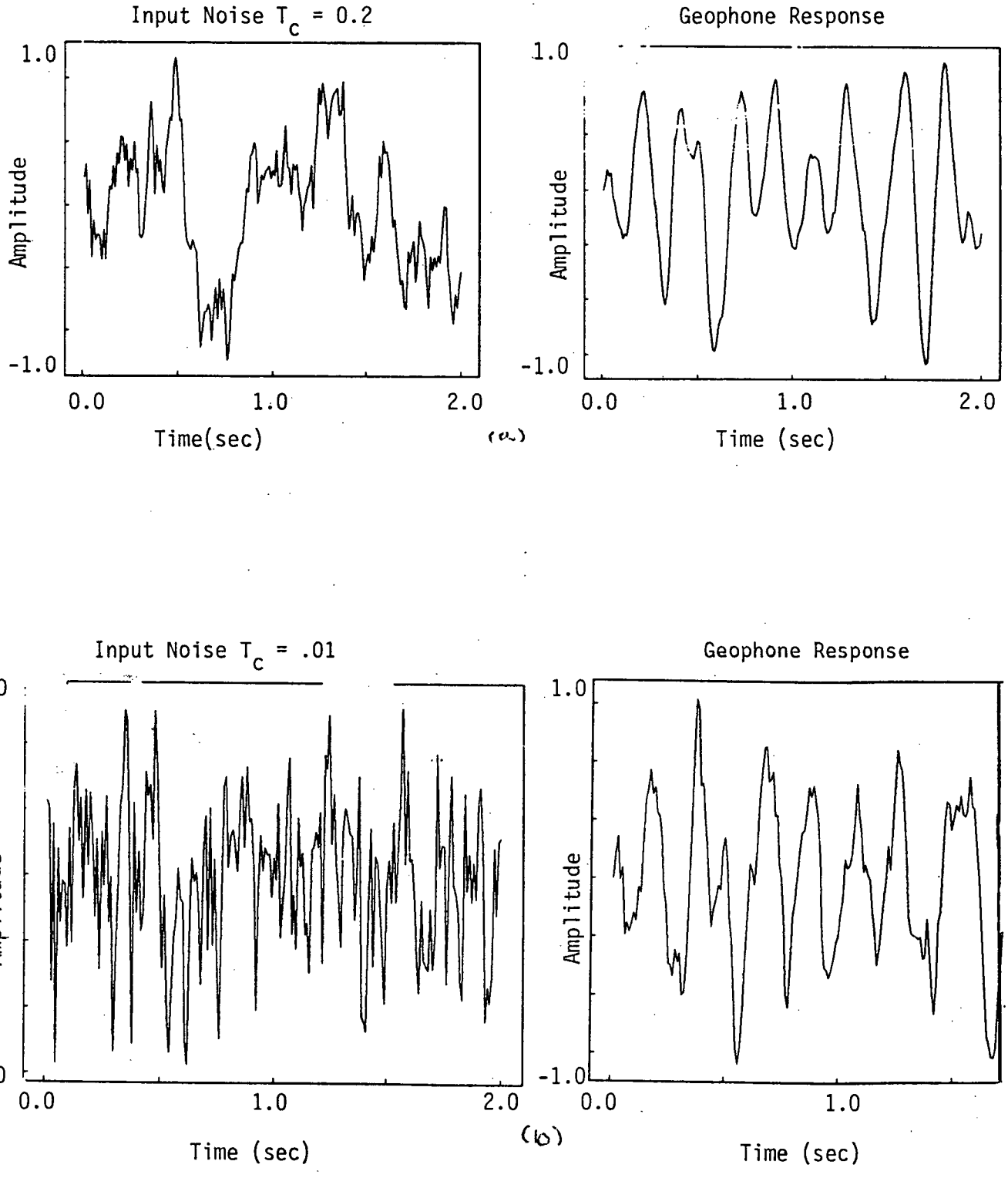


Figure 4.4. Low-Pass Noise with Corresponding Geophone Response as the Constant Increases

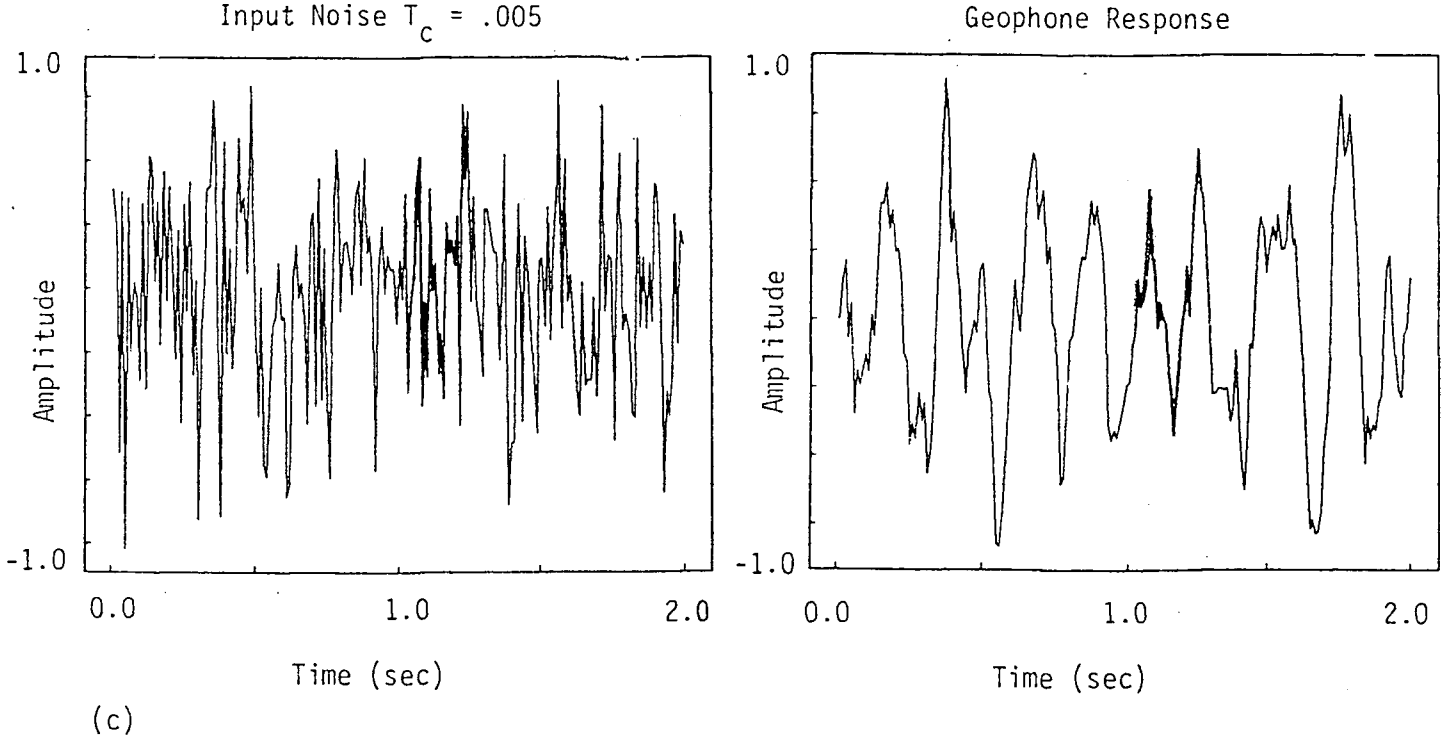


Figure 4.4. Low-Pass Noise with Corresponding Geophone Response as the Time Constant Increases (Cont'd)

Figure 4.5 illustrates the geophones response from the input of the P and S-wave impulses and noise with increasing variance. As is illustrated, the impulses result in an initial displacement than decay which is a function of the damping and natural frequency of the instrument. Also shown is that as the variance of the noise increases, we have a greater geophone response due to noise (i.e., Figure 4.5(a) - (c)).

The performance of the Kalman Filter was analyzed by generating a source wavelet and passing it through the second order instrumentation. The input wavelet and corresponding geophone response is illustrated in Figure 4.6. The impulse was generated by the following coding:

```
      REAL X1(4000),X3(4000),F1,Q,PIE
      PIE=3. 1459265
      DO a I=1,200
      X1(I)=0.0

    1 CONTINUE
      DO 3 I=66, 76
      Q=.01*(I-66)
      X1(i)=2500.*COS(F1*Q)*EXP(-Q)
    3 CONTINUE
      DO 2 I=1,200

      WRITE(1,*) X1(I)
    2 CONTINUE
      STOP
      END
```

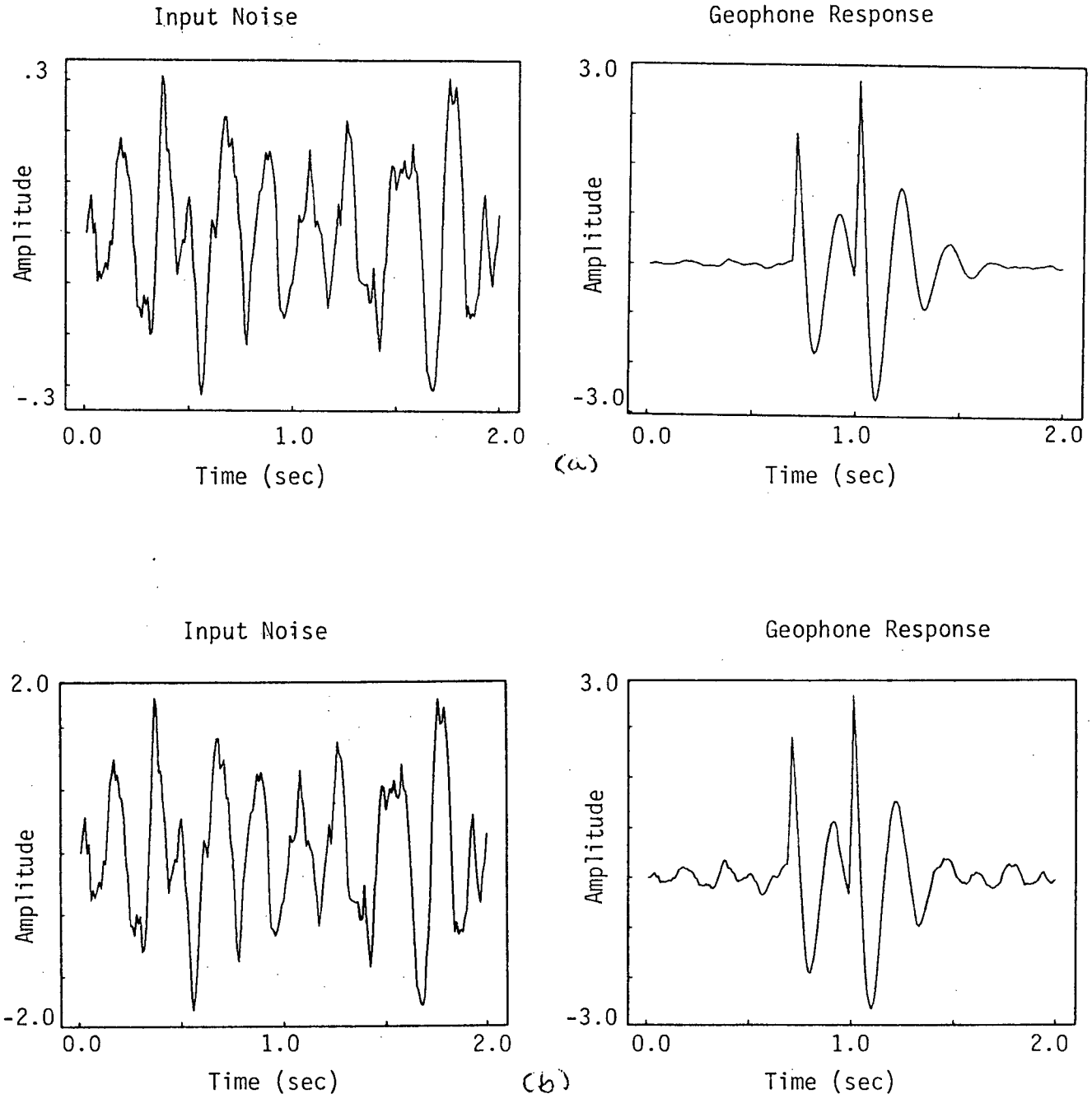


Figure 4.5. Geophone Response Due to P and S-Wave Impulses and Noise with Increasing Variance

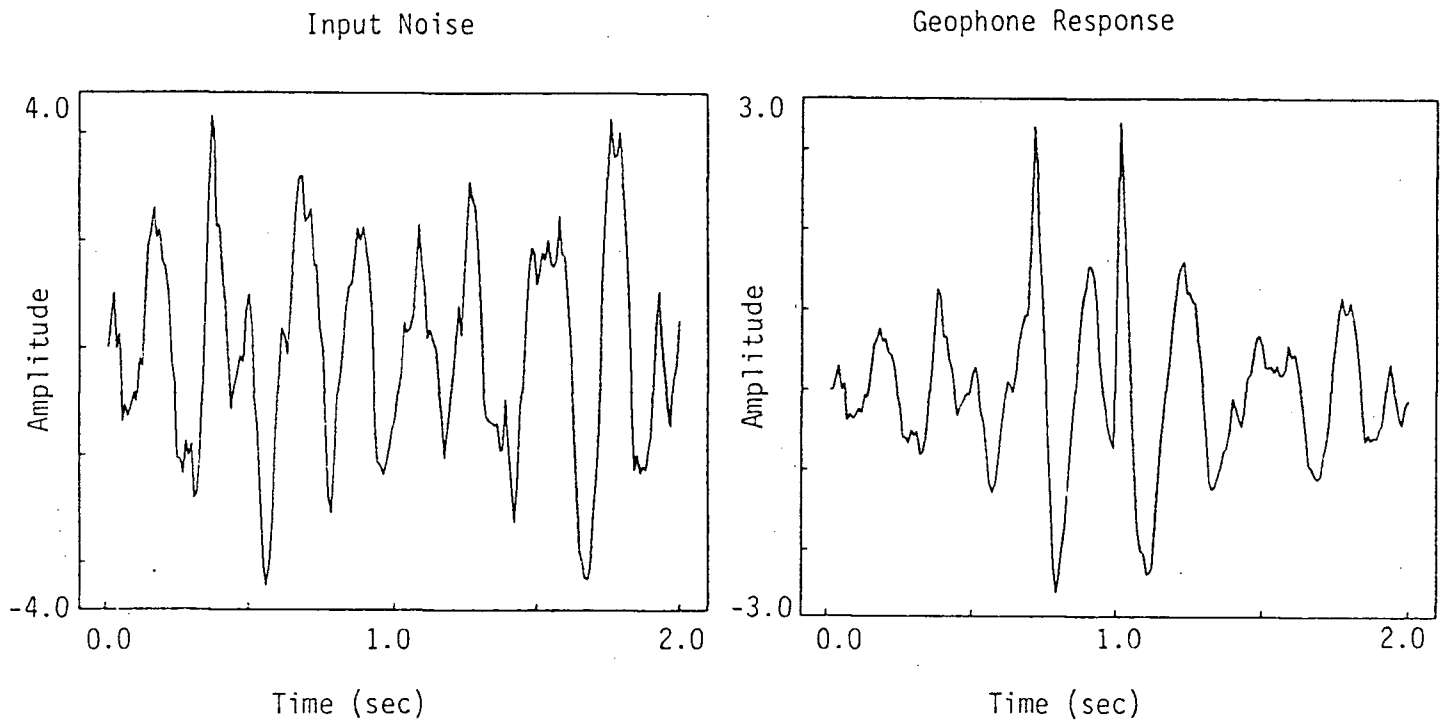


(c)

Figure 4.5. Geophone Response Due to P and S-Wave Impulses and Noise with Increasing Variance (Cont'd)

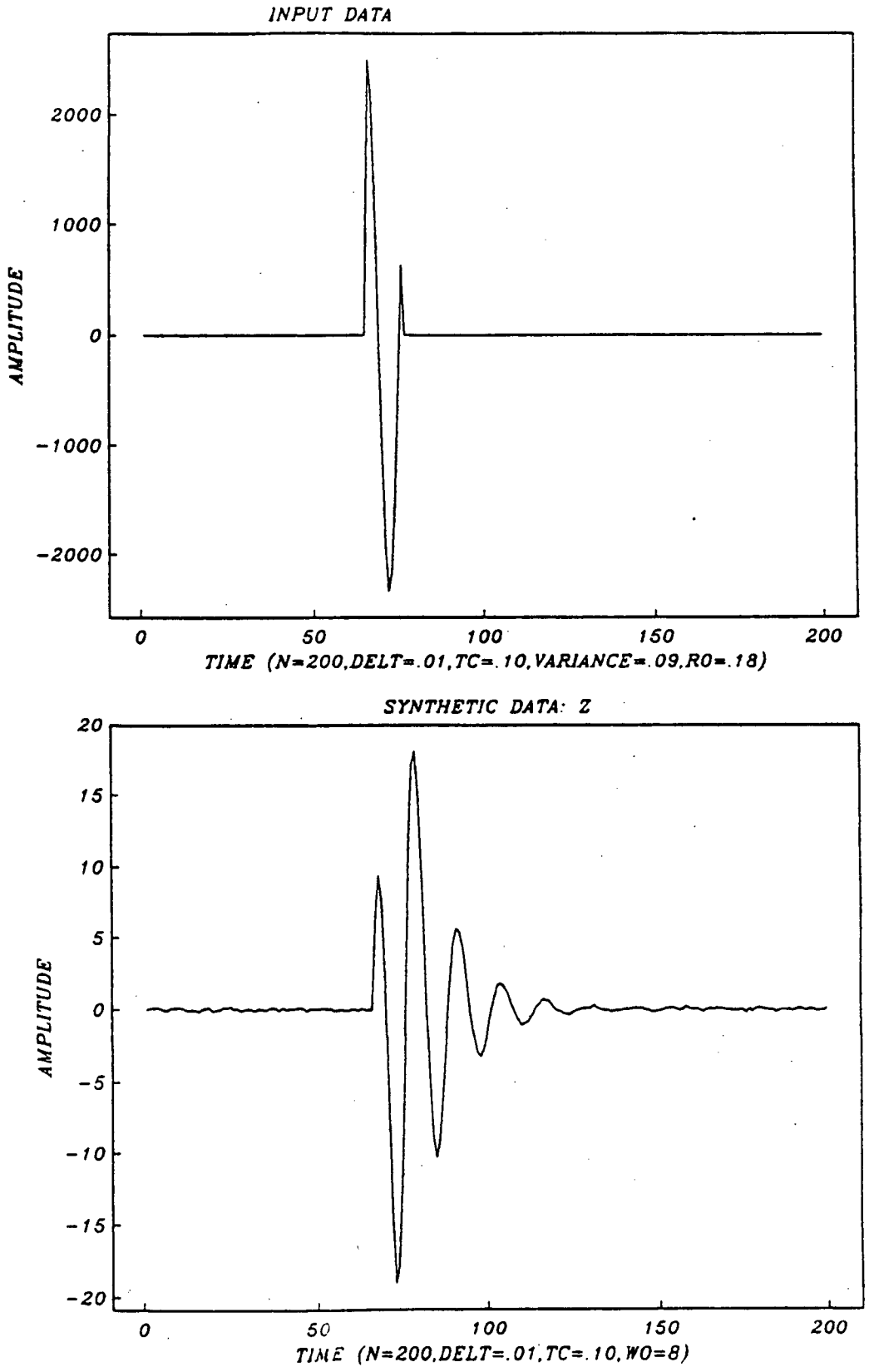


Figure 4.6. Illustrating the Synthetic (a) Input and (b) Geophone Response

The signal is defined by a 50 Hertz cosine wavelet exponentially decaying at .01 and having a maximum amplitude of 2500. The signal is initiated at 66 time units and ends at 76 time units with the total trace lasting for 200 time units.

The second order response is then fed into the Kalman Filter with the output shown in Figures 4.6 and 4.7. The desired parameters in this run are x(1), the signal amplitude, and x(2), the signal arrival time. In the KF it is necessary to give apriori estimates of the above two states, these initial estimates were x(1)=2500 and x(2)=75 time units. Therefore, we put the exact amplitude of the input signal and deviated from the arrival time by 9 time units (i.e., the actual arrival time was 66 time units). In Figure 4.7 we have eight iterations or passes made through the filter, with each subsequent iteration having its initial state value given by the last iteration where the mean square error, Figure 4.8, was minimum. The results show that the arrival time, state x(2), approached the actual value (66 time units) and reached it after seven iterations. The amplitude doesn't change significantly because it was already defined to be the correct value.

The above results are significant, because if this filter can be finely tuned, it would be possible to obtain arrival times and amplitudes on line resulting in velocities and damping characteristics, respectively. In addition, it would also be possible to model and calibrate the sensors used in data acquisition, which is necessary in any type of digital processing.

Additional effort needs to be made to verify the numerical results and models. In addition, it will be necessary to investigate smoothing techniques to obtain reasonable estimates of the P-wave and S-wave parametres x(1) to x(4).

Since the effects of the P-wave and S-wave wavelets pass through measurement interval is a relatively short time, recognition of this fact to derive a suitable smoothing version of the KF needs to be made. In addition, further investigation needs to be made to optimize the method of working multiple passes of the data through the KF.

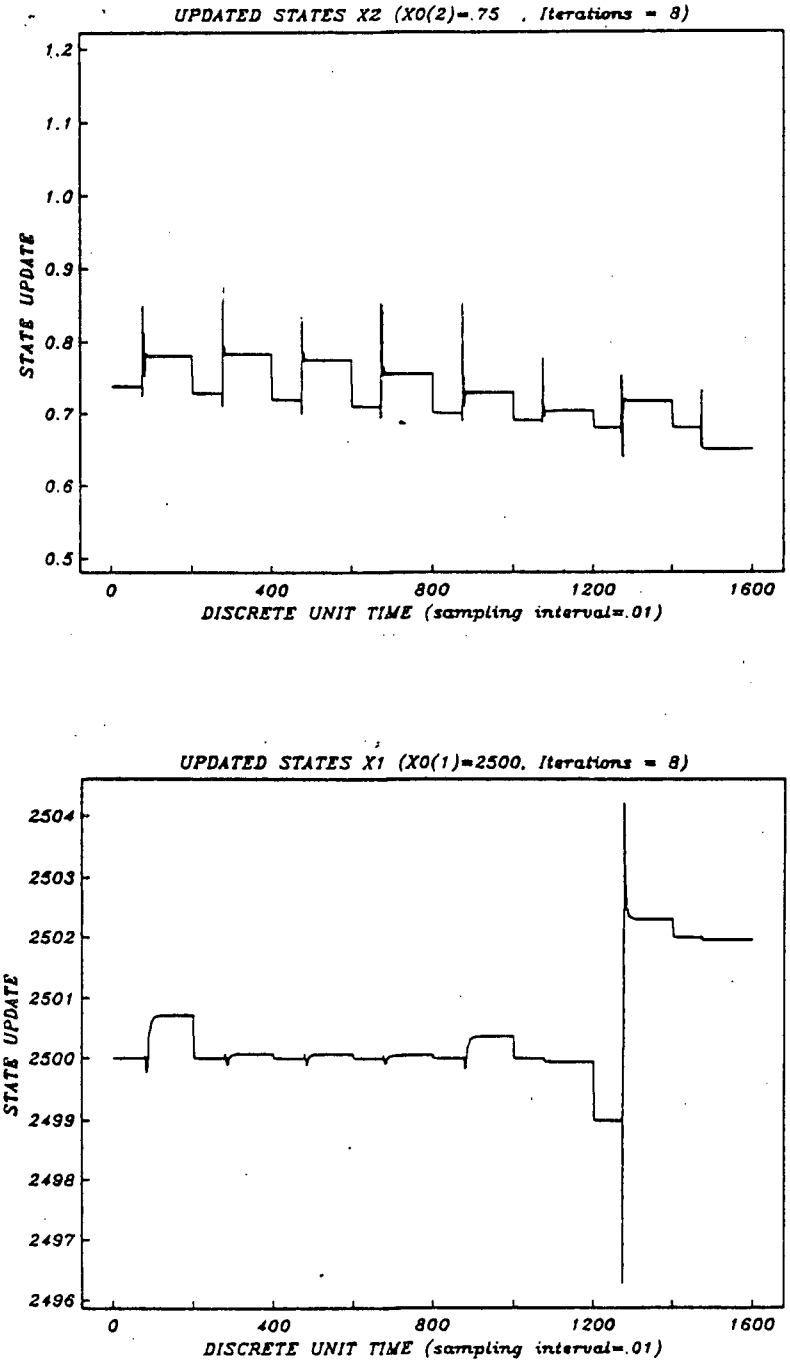


Figure 4.7. Updating the States (a) x(2) (Arrival Time) and (b) x(1) (Amplitude)

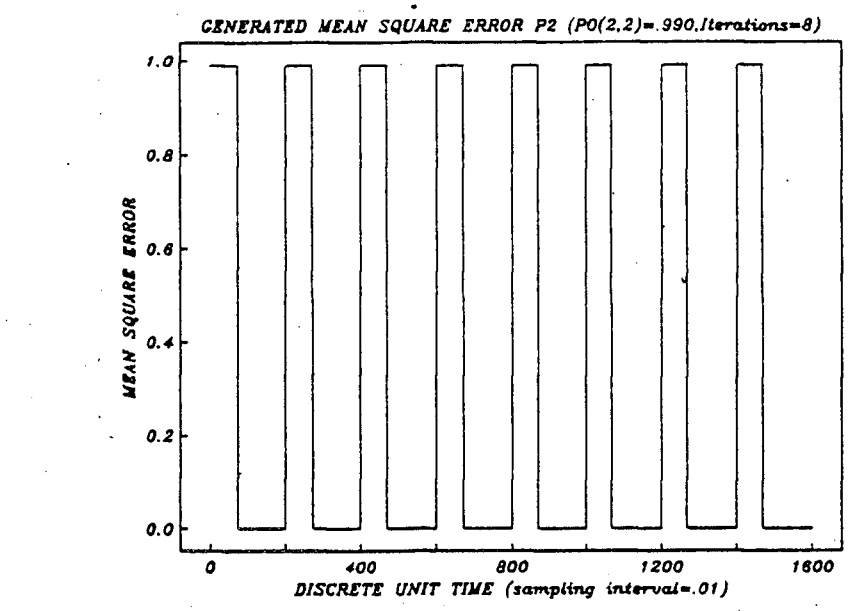


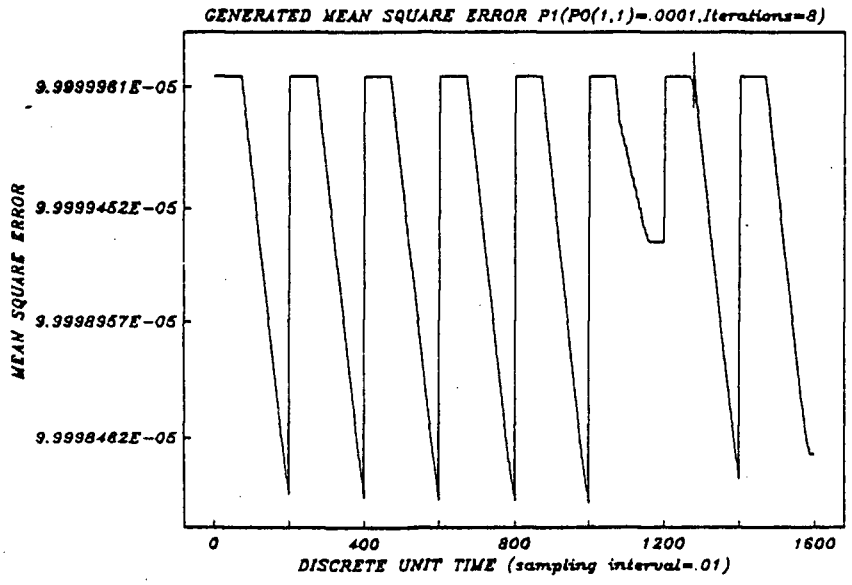


Figure 4.8. Mean Square Error for (a) State x(2) and (b) State x(1)

## B. Description of the Continuous Version of the Kalman Filter

The Kalman Filter, KF, is a method for estimating a state vector $\underline{x}$ from measured data $\underline{z}$. The state vector may be corrupted by a noise vector $\underline{w}$ and the measurement vector is corrupted by a noise vector $\underline{v}$. The KF filter is applicable for systems that can be described by a first order differential equation in $\underline{x}$ and a linear (matrix) equation in $\underline{z}$. The state and measurement equations assumed to be in the following canonical form:

$$\dot{\underline{x}}(t) = F(t)\underline{x}(t) + G(t)\underline{w}(t) \tag{4.1}$$

$$z(t) = H(t)\underline{x}(t) + \underline{v}(t) \tag{4.2}$$

where $\underline{x}$ is an n-vector, $\underline{w}$ is a p-vector, $\underline{z}$ and $\underline{v}$ are m-vectors, and F, G and H are known matrices.

The random (vector) processes $\underline{w}$ and $\underline{v}$ are assumed to be zero mean, white noise processes, so that

$$E(\underline{w}(t))=\underline{0} \text{ and } E(\underline{v}(t))=\underline{0} \tag{4.3a}$$

$$E(\underline{w}(t)\underline{w}(\tau)^T) = Q(t)\delta(t-\tau) \tag{4.3b}$$

$$E(\underline{v}(t)\underline{v}(\tau)^T) = R(t)\delta(t-\tau) \tag{4.3c}$$

It is further assumed that $\underline{w}$ and $\underline{v}$ are statistically independent of each other, so that

$$E(\underline{w}(t)\underline{v}(\tau)^T) = 0 \tag{4.3d}$$

In the above equations the superscript T denotes the vector transpose, the E denotes the expected value operation, and $\delta(t-\tau)$ denotes the Dirac delta function.

Note: The KF can be modified to treat the case when equations (4.3c) and (4.3d) are not true; however, the notation is simplified considerably when these assumptions are made.

It is further assumed that the initial state, $\underline{x}(t_0)\equiv\underline{x}_0$, is a zero mean, Gaussian random process and that the covariance of $\underline{x}_0$ is specified as a positive semi-definite nxn matrix Po. Thus we have

$$E(\underline{x}(t_0))=\underline{0} \text{ and } E(\underline{x}(t_0)\underline{x}(t_0)^T) \equiv P_0 \tag{4.4}$$

We use the notation $\hat{\underline{x}}(t'|t)$ to denote an estimate of the state at a time t', $t'\geq t_0$, based on measurements $\underline{z}(\tau)$ on the interval $t_0\leq\tau\leq t$. It is convenient to make the following definitions:

Definition:
1. If $t'>t$, $\hat{\underline{x}}(t'|t)$ is a predicted estimate.
2. If $t'=t$, $\hat{\underline{x}}(t'|t)$ is a filtered estimate.
3. If $t'<t$, $\hat{\underline{x}}(t'|t)$ is a smoothed estimate.

The estimation error is defined as

$$\tilde{\underline{x}}(t'|t) \equiv \underline{x}(t')-\hat{\underline{x}}(t'|t) \tag{4.5a}$$

and the performance index of the estimation is given by

$$I(\hat{\underline{x}}(t'|t)) \equiv E(\varepsilon(\hat{\underline{x}}(t'|t))) \tag{4.5b}$$

where $\varepsilon(.)$ is an error function of the estimation error.

Although more general error functions can be assumed, we shall assume the $\varepsilon$ is the square of $\tilde{\underline{x}}(t'|t)$; i.e.,

$$I(\tilde{\underline{x}}(t'|t)) = E(\tilde{\underline{x}}(t'|t)\tilde{\underline{x}}(t'|t)^T) \tag{4.5c}$$

The estimation problem can now be stated as follows:

Estimation Problem: Given the system defined by Equations 4.1 and 4.2 with statistics defined by Equation 4.3, and measurements $\underline{z}(\tau)$ over the interval $t_0\leq\tau\leq t$, determine an estimate of $\hat{\underline{x}}(t'|t)$ such that $I(\tilde{\underline{x}}(t'|t))$ is minimized.

The solution to this problem was given by R. E. Kalman (Reference 11) in 1960. This solution is specified by the following equations for the filtered estimate:

State Estimation equation

$$\dot{\underline{\hat{x}}}(t) = F(t)\,\underline{\hat{x}}(t) + K(t)(\underline{z}(t)-H(t)\underline{\hat{x}}(t)).$$

with (4.6)

$$\underline{\hat{x}}(t_0) = \underline{\hat{x}}_0 \text{ given}$$

Kalman Gain matrix

$$K(t) = P(t)H(t)^T R(t)^{-1} \tag{4.7}$$

Estimation Error Covariance (Matrix Ricatti) equation

$$\dot{P}(t) = F(t)P(t) + P(t)F(t)^T + G(t)Q(t)G(t)^T - K(t)R(t)K(t)^T \tag{4.8}$$

with

$$P(t_0) = P_0, \text{ given}$$

Note: The equations for the predicted and smoothed estimates are not given at this time; however, it appears that smoothed estimates should be used to obtain satisfactory results the our particular problem.

A block diagram of the system, measurement, and filtered estimates is shown in Figure 4.9.

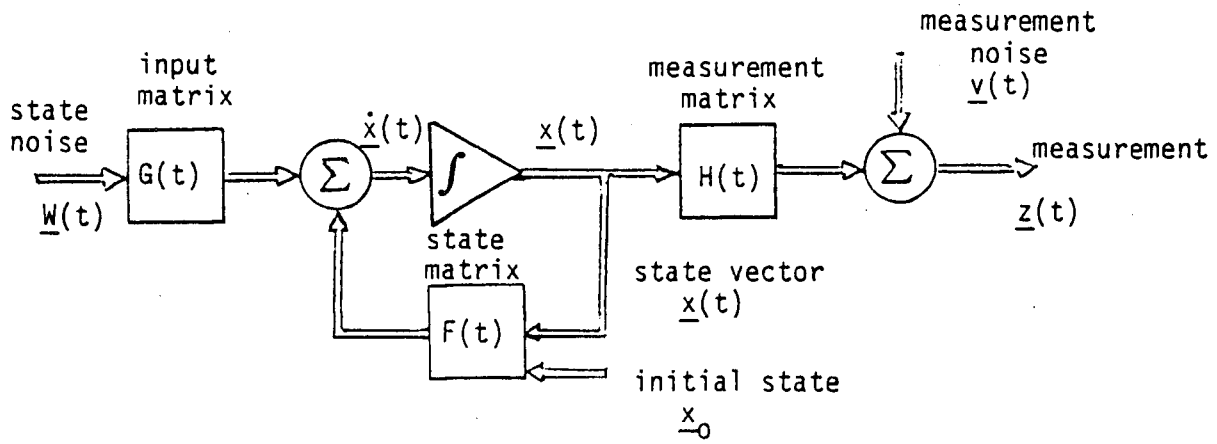


Figure 4.9a. Block Diagram of State and Measurement Equations (4.1 ) and (4.2 ). The Solid Lines Indicate Vector Quantities

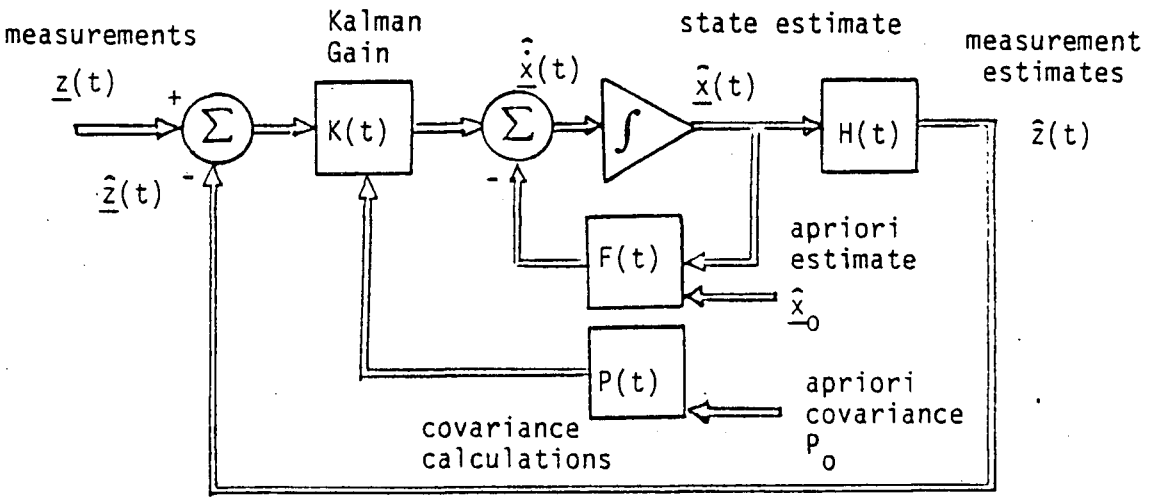


Figure 4.9b. Block Diagram of Continuous Kalman Filter, Equations (4.6 ) and (4.7 )

## C. Description of Discrete Version of the Kalman Filter

In most cases it is more practical to formulate the KF in discrete form; this is especially true for computational purposes. Sometimes the system and measurement equations are naturally in discrete form; at other times it may be necessary to transform the continuous equations into discrete form. It is assumed that the discrete state and measurement equations can be written as

$$\underline{x}_{k+1} = \phi(k+1,k)\underline{x}_k + \Gamma(k+1,k)\underline{w}_k \tag{4.11}$$

$$\underline{z}_{k+1} = H(k+1)\underline{x}_{k+1} + \underline{v}_{k+1} \tag{4.12}$$

where $\underline{x}_{k+1}$ is an n-vector, $\underline{w}_k$ is a p-vector, and $\underline{z}_{k+1}$ and $\underline{v}_{k+1}$ are m-vectors. The nxn matrix $\phi(k+1,k)$ is the state transition matrix; this matrix can be obtained from the continuous case (Equation 4.1) as the solution to the homogeneous (zero input) solution to $\dot{\underline{x}} = F\,\underline{x}$. The nxp matrix $\Gamma(k+1,k)$ is the input transition matrix. The subscript k refers to the discrete time $t=t_k$, k=0, 1,....

The random (vector) processes $\underline{w}_k$ and $\underline{v}_{k+1}$ are assumed to be zero mean, white noise sequences, so that

$$E(\underline{w}_k) = \underline{0} \text{ and } E(\underline{v}_{k+1}) = \underline{0} \tag{4.13a}$$

$$E(\underline{w}_j \underline{w}_k^T) = Q_k\,\delta_{jk} \tag{4.13b}$$

$$E(\underline{v}_{j+1}\,\underline{v}_{k+1}^T) = R_{k+1}\,\delta_{jk} \tag{4.13c}$$

It also assumed that $\underline{w}_k$ and $\underline{v}_k$ are statistically independent of each other, and that the initial state $\underline{x}(t_o)\equiv\underline{x}_o$ is a zero mean, Gaussian random process and that the covariance of $\underline{x}_o$ is specified as a positive semidefinite nxn matrix. Thus we have

$$E(\underline{v}_j \underline{w}_k^T) = 0 \tag{4.13d}$$

$$E(\underline{x}_j) = \underline{0} \text{ and } E(\underline{x}_o \underline{x}_o^T) \equiv P_o \tag{4.14}$$

As in the continuous case, we use the notation $\hat{\underline{x}}(k|j)$ to denote an estimate of the state at time $t_k$, $t_k \geq t_o$, based on measurements $\underline{z}_i$ on the interval $t_o \leq t_i \leq t_j$. As in the continuous case, it is convenient to make the following definitions:

Definition: 1. If $k>j$, $\hat{\underline{x}}(k|j)$ is a predicted estimate.

2. If $k=j$, $\hat{\underline{x}}(j|j)$ is a filtered estimate.

3. If $k<j$, $\hat{\underline{x}}(k|j)$ is a smoothed estimate.

The estimation error is defined as

$$\tilde{\underline{x}}(k|j) \equiv \underline{x}_k - \hat{\underline{x}}(k|j) \tag{4.15a}$$

and the performance index of the estimation is given by

$$I(\hat{\underline{x}}(k|j)) \equiv E(\varepsilon(\tilde{\underline{x}}(k|j))) \tag{4.15b}$$

where $\varepsilon(\cdot)$ is an error function of the estimation errors. We shall choose $\varepsilon$ to be the square of $\tilde{\underline{x}}(k|j)$, i.e.,

$$I(\hat{\underline{x}}(k|j)) = E(\tilde{\underline{x}}(k|j)\tilde{\underline{x}}(k|j)^T) \tag{4.15c}$$

The discrete estimation problem can be stated as follows:

Estimation Problem: Given the discrete system defined by Equations 4.11 and 4.12 with statistics defined by Equations 4.13, and measurements $\underline{z}_i$ over the interval $t_o \leq t_i \leq t_j$, determine an estimate $\hat{\underline{x}}(k|j)$ such that $I(\hat{\underline{x}}(k|j))$ is minimized.

Estimation Equations for the Filtered Estimate, k=j

State Estimation equation

$$\hat{\underline{x}}_{k+1} = \phi(k+1,k)\hat{\underline{x}}_k + K_{k+1}(\underline{z}_{k+1} - H_{k+1}\,\phi(k+1,k)\hat{\underline{x}}_k) \tag{4.16}$$

with

$$\hat{\underline{x}}(t_o) = \hat{\underline{x}}_o \text{ given}$$

Kalman Gain Matrix

$$K_{k+1} = P(k+1|k)H(k+1)^T(H(k+1)P(k+1|k)H(k+1)^T + R(k+1))^{-1} \qquad (4.17)$$

Estimation Error Covariance (Matrix Ricatti) equation

$$P(k+1|k) = \Phi(k+1,k)P(k|k)\Phi(k+1,k)^T + \Gamma(k+1,k)Q\,\Gamma(k+1,k)^T$$

$$P(k+1|k+1) = (I-K_{k+1}H_{k+1})P(k+1|k) \qquad (4.18)$$

with

$$P(0|0) = P_0 \text{ given.}$$

It is noted that $P(k+1|k+1)$ is the covariance of $\tilde{\underline{x}}_{k+1}=\underline{x}_{k+1}-\hat{\underline{x}}_{k+1}$.

Note: The equations for the prediction and smoothed estimates are not given at this time. Application of smoothed estimates to our problem is discussed in Section VI.

The computation sequence for the discrete KF is as follows:

- At $t_0$ specify $\hat{\underline{x}}_0$, $P_0$ and $Q_0$, and compute $\Phi(1,0)$, $H_1$, and $R_1$.
- At $t_1$, compute the projected estimate of the covariance matrix $P(1|0)=\Phi(1,0)P_0\Phi(1,0)^T+Q_0$.
- Compute the gain matrix $K_1=P(1|0)H_1^T(H_1P(1,0)H_1^T+R_1)^{-1}$
- Using the measurement $\underline{z}_1$ at $t=t_1$, the best estimate of the state at $t_1$ is given by

$$\hat{\underline{x}}_1 = \Phi(1,0)\hat{\underline{x}}_0 + K_1(\underline{z}_1-H_1\Phi(1,0)\hat{\underline{x}}_0)$$

- The estimation covariance matrix at $t_1$ is given by

$$P(1|1) = P(1|0) - K_1 H_1 P(1|0)$$

- At $t=t_2$, a new measurement $\underline{z}_2$ is obtained, and the computational cycle is repeated.

D. Derivation of Transfer Function for Geophone

An electromagnatic device whose output is proportional to the input acceleration of its case is shown schematically in Figure 4.10. When the case of the device moves, in the direction of its sensitive axis, the relative motion of the coil and the magnetic field induces a voltage across the coil. The recorder across the coil measures the coil voltage, $e_0$, as a function of time.

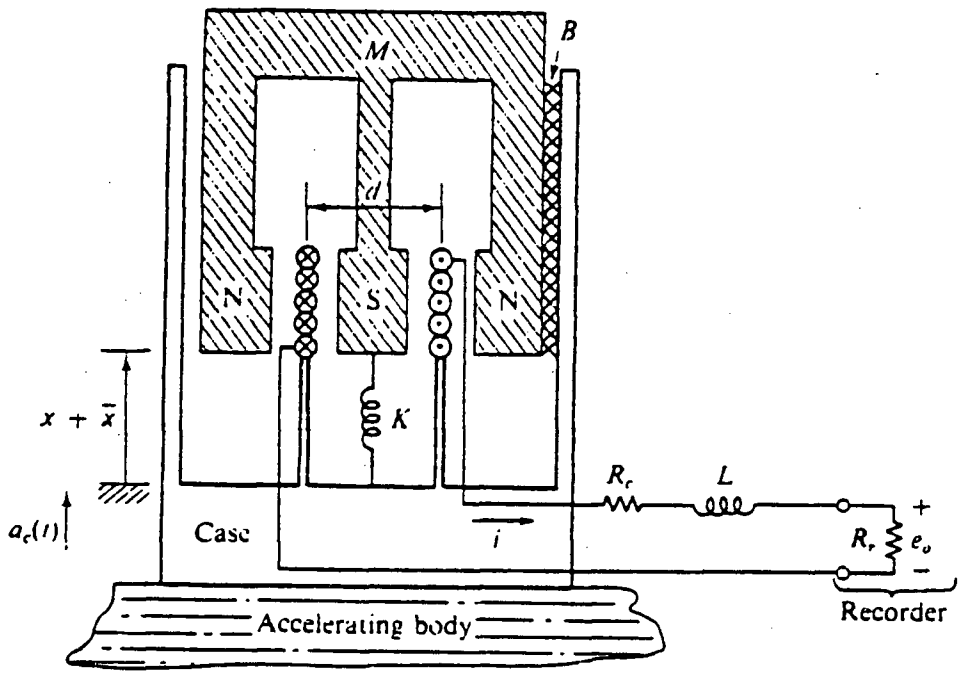


Figure 4.10. Schematic of an Acceleration Measuring Device (Reference 12)

In Figure 4.1, the following parametres are defined:

M - mass of suspended magnet

B - flux density between magnets

K - stiffness of spring which supports the magnet

D - viscous damping between magnet and the case

N - number of turns in coil

$d$ - diameter of coil

$\ell$ - length of coil, $\pi \cdot d \cdot N$

$R_c$ - resistance of coil

$L_c$ - inductance of coil

$R_r$ - resistance of recorder

$a_c(t)$ - acceleration of case relative to a fixed reference

$x_o$ - equilibrium position of M relative to the case

$x$ - dynamic displacement of M relative to the case

The dynamic equations for the device can be derived by summing the voltages induced in the electrical measuring circuit. These two situations are shown schematically in Figure 4.11.

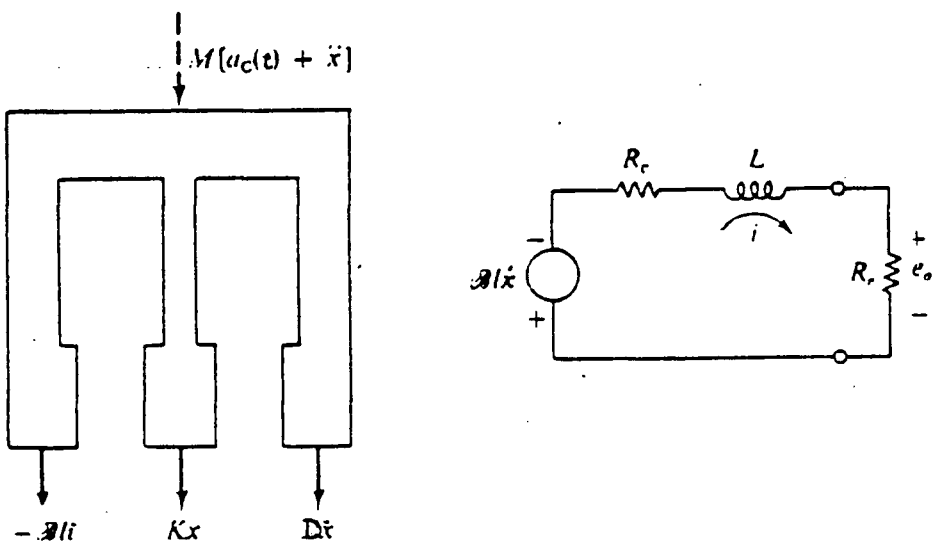


(c) forces on M (b) measuring circuit

Figure 4.11. Schematic of Forces on Magnet and Voltages in Measurement Circuit

In Figure 4.4, the following variables are used:

$\dot{x}$ - velocity of M

$\ddot{x}$ - acceleration of M

$i$ - current in measurement circuit

$B\ell i$ - electrically induced force on the coil

The direction of i is such that a negative voltage is induced in the coil when M moves downward ($\dot{x}>0$). Summing the forces acting on M gives

$$M\ddot{x} + D\dot{x} + Kx = B\ell i - Ma_c \tag{4.21a}$$

and, summing the voltages in the circuit gives

$$L\frac{di}{dt} + R_c i + e_o = -B\ell\dot{x} \quad e_o = R_\gamma i \tag{4.21b}$$

It is noted that if $L\to 0$ in (4.21b), then $iR = -B\ell\dot{x}$, i.e., i is proportional to $\dot{x}$ and $\int i\,dt$ is proportional to x. Also (4.21a) becomes $\ddot{x}+\dot{x}(D+B^2\ell^2/R)/M + Kx/M = -a_c$. Taking the Laplace Transform of these equations gives

$$(Ms^2+Ds+K)X(s) = -B\ell\, I(s) - MA_c(s) \tag{4.22a}$$

$$(Ls+R_c+R_r)I(s) = -B\ell\, sX(s) \tag{4.22b}$$

$$E_o(s) = R_r\, I(s) \tag{4.22c}$$

Since our goal is to obtain the transfer function of the output, $E_o(s)$, over the input, $A_c(s)$, that is

$$T(s) \equiv E_o(s)/A_c(s)$$

it is necessary to eliminate X(s) and I(s) in Equations (4.22). This is accomplished by substituting X(s) from (4.22b) into (4.22a). After some algebraic manipulations we obtain the desired result

$$T(s) = E_o(s)/A_c(s) = R_r\, B\ell Ms/P(s) \tag{4.24a}$$

where

$$P(s) = MLs^3 + (DL+MR)s^2 + (DR+KL+B^2\ell^2)s + KR \tag{4.24b}$$

$$R = R_c + R_r \tag{4.24c}$$

This derivation of the transfer function for a typical accelerometer helps one obtain a better feel for the relationship between the geophone dynamics and the second order model speicifications given in Section II. However, one needs to consider the actual geophone that is used to collect data when one eventually tries to process some of this data with a Kalman Filter.

It is noticed that the current in the coil circuit (or voltage across the load resister $e_o = i*R_r$) is used as the output variable. However, in this case the transfer function that results has an s (Laplace operator) in the numerator -- this is not convenient for applying a second order model.

The integral of this output voltage is more convenient to use (this is analogous to the charge across a capacitor).

Let

$$q_o(t) = \int_o^t e_o(t')dt' \tag{4.25a}$$

Then

$$e_o(t) = \dot{q}_o(t) \text{ and } E_o(s) = sQ_o(s) \tag{4.25b}$$

i.e., it is assumed that the measurement is the integral of the output voltage. In this case the transfer function is

$$\frac{sQ_o(s)}{A_c(s)} = \frac{K_c's}{P(s)} \quad \text{or} \quad \frac{Q_o(s)}{A_c(s)} = \frac{K_c'}{P(s)} \tag{4.26}$$

where

$$K_c' \equiv R_r B\ell M \quad \text{and } P(s) \text{ is as defined above.}$$

Next it is assumed that the coil inductance, L, can be neglected. This approximation is valid for low frequency input accelerations, but not necessarily for high frequency inputs. It might be informative to determine the frequency limits at which this approximation holds when considering P and S waves inputs.

In this case

$$P(s) = MRs^2 + (DR+B^2\ell^2)s + KR \tag{4.27a}$$

so that the transfer functions can be written as

$$\frac{Q_o(s)}{A_c(s)} = \frac{K_c}{s^2+2\zeta\omega_o s+\omega_o^2} \tag{4.27b}$$

where

$$K_c = B\ell R_r/R$$

$$\omega_o^2 = K/M \tag{4.27c}$$

$$\zeta = (D+B^2\ell^2/R)/2M\omega_o$$

In Section II, Table 2.1, the geophone specifications are given as $\omega_o=2\pi*28.0$ and $\zeta=0.18$.

## E. KF Equations for Estimating Amplitudes and Arrival Times

In this Section the KF equation for estimating P-wave and S-wave amplitudes, $A_p$ and $A_s$, and arrival times, $T_p$ and $T_s$, at the geophone location are derived.

In Appendix D the details of the derivation of a discrete model of a second order system with white noise inputs is given. Comparing the transfer function obtained in the previous section (Equation 4.27) with the transfer function in Reference 24 it is seen that they are in the same form, with the following relationship

$$K_c\, a_c(t) = \omega_0^2\, w(t)$$

or

$$w(t) = K_c a_c(t)/\omega_0^2 \qquad (4.28)$$

In other words, with the proper scaling the solution equation for the discrete problem (Equation (D.6.f), Reference 24 can be applied here. A block diagram of the transfer function is shown below.

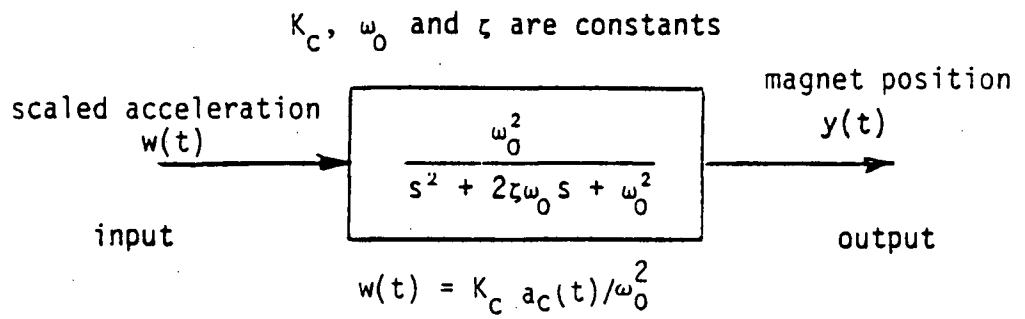


Figure 4.12. Block Diagram of Second Order Geophone Transfer Function

Remember now that $q_o(t)$ is an output of the instrument that is related to the integral of the voltage across a load resistor $R_r$ in the coil circuit. This could be the voltage across some sort of a capacitance circuit -- it depends on how a particular instrument is designed.

One could assume that the measurements (for the KF formulation) are $\ddot{q}(t_k)+v(t_k)$, where $v(t_k)$ is white noise which could be due to computer roundoff, quantization, circuit noise, etc. Actually it might be better to assume that $q(t_k)$ times a scale factor (say h) is observed to be more general in the KF formulation -- h can always set to 1.0 later on.

NOTE: The quantity q(t) will be proportional to what would probably called geophone "position".

If you have a geophone that gives "acceleration", then this will be $\ddot{q}(t)$, or the second component ($\dot{y}_2(t)$) in the state vector formulation which follows.

With the above comments in mind, we define

$$y(t) \equiv q_o(t) \tag{4.29a}$$

then we can write

$$\ddot{y}(t) + 2\zeta\omega_o\dot{y}(t) + \omega_o^2\, y(t) = K_i\, a_c(t) \tag{4.29b}$$

Next define

$$y_1(t) \equiv y(t),\ y_2(t) \equiv \dot{y}(t),\ \underline{y} \equiv (y_1,y_2)^T, \text{ and}$$
$$u(t) \equiv a_c(t) \tag{4.29c}$$

so that the following vector differential equation (d.e.) can be written

$$\dot{\underline{y}} = F\,\underline{y} + \underline{b}\,u \tag{4.29d}$$

Note that y(t) corresponds to the instrument output, which is referred to as the "position".

NOTE: The geophone case acceleration $a_c$ is assumed to consist of background noise and P-wave and S-wave accelerations. Since the geophone transfer function is linear, the noise and signal (P-wave and S-wave) can be treated separately.

For the KF formulation define the following state variables

$$x_1 \equiv a_p$$

$$x_2 \equiv t_p$$

$$x_3 \equiv a_s$$

$$x_4 \equiv t_s$$

$x_5 \equiv$ geophone input due to background noise (first order correlation will be assumed)

$x_6 =$ geophone output due to background noise ($x_5$)

$$x_7 = \dot{x}_6$$

$x_8 =$ geophone output due to P&S waves

$$x_9 = \dot{x}_8$$

NOTE: $x_6$ & $x_7$ and $x_8$ & $x_9$ are represented by the same second order d.e.

If we assume that the input noise and P-wave and S-wave acceleration "impulses" are constant over a sampling interval $\Delta$, then Equation (4.6f) (Reference 4) can be used to obtain the discrete equation. Actually, the P and S waveforms can be more general than "impulses".

$$\begin{bmatrix} x_6(k+1) \\ x_7(k+1) \end{bmatrix} = \begin{bmatrix} a_{11} & a_{12} \\ a_{21} & a_{22} \end{bmatrix} \begin{bmatrix} x_6(k) \\ x_7(k) \end{bmatrix} + \begin{bmatrix} b_{11} \\ b_{21} \end{bmatrix} x_5(k) \qquad (4.30a)$$

where $\Delta \equiv t_{k+1} - t_k$ and $x_5(k)$ is the geophone <u>input</u> noise. The constants $a_{ij}$, $b_{ij}$ are defined by Equation (4.6f) of Reference 4, and will be discussed later.

The variables $x_i$ and $x_9$ are governed by the same discrete equation, except that it is clearer to write the outputs as a function of $t_p$ and $t_s$. Thus (assuming $t_p < t_s$).

If $t_{k+1} < t_p$

$$\begin{bmatrix} x_8(k+1) \\ x_9(k+1) \end{bmatrix} = \begin{bmatrix} 0 \\ 0 \end{bmatrix} \qquad (4.30b)$$

If $t_{k+1} = t_p$

$$\begin{bmatrix} x_8(k+1) \\ x_9(k+1) \end{bmatrix} = \begin{bmatrix} b_{11} \\ b_{12} \end{bmatrix} x_1(k+1)/\Delta \qquad (4.30c)$$

<u>NOTE</u>: $x_2(k+1) = t_p$ and $x_1(k+1) = a_p$. We divide by $\Delta$ to approximate a $\delta$-function for the P-wave. Generalizations are discussed later.

If $t_p < t_{k+1} < t_s$

$$\begin{bmatrix} x_8(k+1) \\ x_9(k+1) \end{bmatrix} = \begin{bmatrix} a_{11} & a_{12} \\ a_{21} & a_{22} \end{bmatrix} \begin{bmatrix} x_8(k) \\ x_9(k) \end{bmatrix} \qquad (4.30d)$$

If $t_{k+1} = t_s$

$$\begin{bmatrix} x_8(k+1) \\ x_9(k+1) \end{bmatrix} = \begin{bmatrix} a_{11} & a_{12} \\ a_{21} & a_{22} \end{bmatrix} \begin{bmatrix} x_8(k) \\ x_9(k) \end{bmatrix} + \begin{bmatrix} b_{11} \\ b_{21} \end{bmatrix} x_3(k)/\Delta \qquad (4.30e)$$

NOTE: $x_4(k+1) = t_s$ and $x_3(k+1) = a_s$

Thus the "nonlinearity" occurs in the times $t_p$ and $t_s$ (i.e., $x_2(k+1)$ and $x_4(k+1)$). However, this nonlinearity is subtle, and will be discussed in more detail in a later section.

It will be assumed that the input noise to the instrument (geophone) is first order correlated, i.e., it is assumed that

$$\dot{x}_5 + \gamma x_5 = \gamma w_a \qquad (4.31a)$$

where $\gamma=1/T_c$, and $T_c$ is the time constant of the input noise to the instrument, and $w_a$ is a white noise process with

$$Exp(w_a) = 0 \text{ and } Cov(w_a) = q_a \qquad (4.31b)$$

This noise model is discussed in more detail in a separate section. If $w_a$ is assumed constant over a sampling interval, $\Delta$, then a discrete model for the input noise can be written as

$$x_5(k+1) = a_w x_5(k) + b_w w_a(k) \qquad (4.31c)$$

where

$$a_w = e^{-\gamma\Delta} \text{ and } b_w = (1-e^{-\gamma\Delta}) \qquad (4.31d)$$

Note: $x_1$ to $x_4$ are assumed to be constants, i.e.,

$$x_i(k+1) = x_i(k) \qquad i = 1,2,3,4$$

One can always assume that they are random constants and associate expected values, variances, etc., to them.

Defining the state vector $\underline{x}$ as

$$\underline{x} \equiv (x_1, x_2, \ldots, x_9)^T \tag{4.32a}$$

One can write the discrete state recurrence equation as

$$\underline{x}_{k+1} = \underline{f}\,(\underline{x}_k, t_k) + \underline{w}_{k+1} \tag{4.32b}$$

where

$$\underline{w}_{k+1} = (0,0,0,0,b_w,0,0,0)w_a(k+1) \tag{4.32c}$$

the uncorrelated input noise to the geophone

The vector $\underline{f}$ needs to be written as a function of $x_2(k+1)$ and $x_4(k+1)$ (i.e., $t_p$ and $t_s$) to see how it is incorporated into the KF.

The measurement equation for this problem is assumed to be (as discussed above) -- i.e., assume we are measuring velocity.

$$z(k+1) = H\,\underline{x}(k+1) + v(k+1) \tag{4.33a}$$

where

$$H \equiv (0\ 0\ 0\ 0\ 0\ 0\ 1\ 0\ 1)m_v \quad (m_v \text{ is a scalar}) \tag{4.33b}$$

$$\text{cov}\,(v(k+1)) = r_m \text{ and } \exp\,(v(k+1)) = 0 \tag{4.33c}$$

i.e., we have a scalar measurement $m_v(x_7+x_9)$ with uncorrelated measurement noise having variance $r_m$.

We write

$$\underline{f}(\underline{x}_k, t_k) = F\,\underline{x}_k \tag{4.34a}$$

where

$$F \equiv \begin{bmatrix} I_c & 0 & 0 \\ \hline 0 & A_n & 0 \\ \hline B_s & 0 & A'_s \end{bmatrix} \tag{4.34b}$$

where

$$I_c = \begin{bmatrix} 1 & 0 & 0 & 0 \\ 0 & 1 & 0 & 0 \\ 0 & 0 & 1 & 0 \\ 0 & 0 & 0 & 1 \end{bmatrix}$$ an identity matrix to represent the 4 constant state variables

$$A_n = \begin{bmatrix} b_{11} & a_{11} & a_{12} \\ b_{21} & a_{21} & a_{22} \end{bmatrix}$$ the $a_{ij}$ and $b_{ij}$ specified above

$$B_s = \begin{bmatrix} b'_{11} & 0 & b''_{11} & 0 \\ b'_{21} & 0 & b''_{21} & 0 \end{bmatrix} \quad \text{and} \quad A'_s = \begin{bmatrix} a_{11} & a_{12} \\ a_{21} & a_{22} \end{bmatrix}$$

It is noted that the coefficients $b'_{ij}$, $b''_{ij}$ depend on the constants $x_2(k+1)$ and $x_4(k+1)$. In the KF implementation one makes estimates of $x_2$ & $x_4$ at t=0, and call them $\hat{x}_2(0)$ & $\hat{x}_4(0)$. The KF will not change these estimates until $t_{k+1} \geq \hat{x}_2(0)$, and $\hat{x}_i(k+1) = x_i(0)$ (i=2,4) for $t_{k+1} < \hat{x}_2(0)$.

Note: One can see the distinction between generating the geophone data with the models, and estimating the parameters with the models. In one case, $x_i(0)$, i=1 to 4 are known, and in the other case, the estimates $\hat{x}_i(0)$ are used to obtain updated estimates $\hat{x}_i(k+1)$, i=1 to 4.

If $\hat{x}_i(T)$ denotes the estimates of $x_i$, i = 1 to 4, at the end of the geophone trace, then one could reprocess the data with the KF using $\hat{x}_i(0) = \hat{x}_i(T)$ for the next pass. Hopefully this process will converge!!

Note: It is convenient to define F in terms of matrices $I_c$, $A_n$, $B_s$, and $A_s$ because when you propagate ahead in the KF you need to make operations like $FPF^T$, and, by partitioning F, one can make simplifications over the intervals $(0,x_2)$, $(x_2,x_4)$, and $(x_4,T)$, where T is the end time of the geophone trace.

The Kalman Filter Equations for Velocity Measurements

We have the state equation, at time $t_{k+1}=(k+1)$ ,

$$\underline{x}_{k+1} = \underline{f}(\underline{x}_k, t_k) + \underline{w}_{k+1} \tag{4.35a}$$

where

$$\underline{w}_{k+1} = (0,0,0,0,b_w,0,0,0,0)^T w_a(k+1) \quad \text{cov}(w_a(k+1)) = q_a$$

and the measurement equation

$$z_{k+1} = H\,\underline{x}_{k+1} + v_m(k+1) \quad \text{cov}(v_m(k+1) = r_m \tag{4.35b}$$

where

$$H = (0\ 0\ 0\ 0\ 0\ 0\ m_v\ 0\ m_v)$$

NOTE: $w_a(k+1)$ and $v_m(k+1)$ are both zero mean, white noise sequences.

Let P denote the 9x9 state estimate covariance matrix

Assume initial estimate of the state and estimation matrix, $\underline{x}_o$ and $P_o$, are available.

Step 1 Compute $\Phi=\partial\underline{f}/\partial\underline{x}$ if $\hat{x}_2(k+1) \leq t_{k+1} \leq \hat{x}_4(k+1) + N_p\Delta$, or if $\hat{x}_4(k+1) \leq t_{k+1} \leq \hat{x}_4(k+1) + N_s\Delta$. Otherwise, $\Phi=F$.

Step 2 Propagate the estimate of the state ahead one step, i.e.,

$$\underline{\hat{x}}'_{k+1} = \underline{f}(\underline{\hat{x}}_k, t_k) \tag{4.36a}$$

Step 3 Propagate Covariance matrix ahead

$$P'_{k+1} = \Phi P_k \Phi^T + Q \tag{4.36b}$$

where all the elements of Q are zeros except $Q(5,5) = b_w^2\, q_a$

Step 4 Compute the updated measurement noise covariance

$$r'_{k+1} = H\, P'_{k+1} H^T + r_m$$
$$= m_v^2 (P'_{77}+P'_{79}+P'_{97}+P'_{99}) + r_m \quad \text{a scalar} \tag{4.36c}$$

The $p'_{ij}$ refer to elements of matrix $P'_{k+1}$

Step 5 Compute the Kalman Gain matrix

$$K_{k+1} = \frac{1}{r'_{k+1}} P'_{k+1} \underline{H}^T$$

$$= \frac{m_v}{r'_{k+1}} \begin{bmatrix} p'_{17} + p'_{19} \\ p'_{26} + p'_{29} \\ \cdots\cdots\cdots \\ p'_{97} + p'_{99} \end{bmatrix} \tag{4.36d}$$

Step 6 Compute measurement residuals

$$\Delta z_{k+1} = z_{k+1} - H\, \underline{\hat{x}}'_{k+1}$$
$$= z_{k+1} - m_v(\hat{x}'_7(k+1) + \hat{x}'_9(k+1)) \tag{4.36e}$$

Step 7 Compute new State Estimate

$$\underline{\hat{x}}_{k+1} = \hat{x}'_{k+1} + K_{k+1}\, \Delta z_{k+1} \tag{4.36f}$$

Step 8 Update State Estimation Error Covariance matrix

$$P_{k+1} = P'_{k+1} - K_{k+1}\, H\, P'_{k+1} \tag{4.36g}$$

Note: Since $H\,P'_{k+1} = m_v(P'_{17} + p'_{19}, \ldots, p'_{97} + p'_{99})$, and

$$K_{k+1}\,H\,P'_{k+1} = \begin{bmatrix} K_{11}(p'_{17} + p'_{19}) & \cdots & K_{11}(p'_{97} + p'_{99}) \\ & \cdots & \\ K_{91}(p'_{17} + p'_{19}) & \cdots & K_{91}(p'_{97} + p'_{99}) \end{bmatrix}$$

A considerable number of the computations are saved by using the fact that $H\,P'_{k+1}$ is a 1x9 vector and $K_{k+1}$ is a 9x1 vector.

## F. Comments on Computing the Estimation Error Covariance Matrix, P

Since a considerable portion of the calculations required to obtain the KF estimates are related to updating the Estimation Error Covariance Matrix, P, it is useful to note possible computational efficiencies which might be readily implemented. The essential computational efficiencies are related to the structure of the state transition matrix, $\Phi$, and to the rather simple structure of the measurement matrix, H. That is, the upper left 4x4 portion of the $\Phi$ matrix is an identity matrix, the upper right 4x5 matrix is a null matrix, and the H matrix is a 9x1 vector with mostly zero elements.

The P matrix is first updated over a sampling interval, $\Delta$, to the P' matrix by the following equation:

$$P'_{k+1} = \Phi P_k \Phi^T + Q \tag{4.37a}$$

where, as previously noted, all elements of the state noise covariance matrix Q are zero, except for the Q(5,5) element. The state transition matrix $\Phi$ is of the following form:

$$\Phi \equiv \begin{bmatrix} I_{44} & 0_{45} \\ B_{54} & A_{55} \end{bmatrix} \tag{4.37b}$$

where

$I_{44}$ denotes a 4x4 identity matrix

$0_{45}$ denotes a 4x5 null matrix

$$A_{55} = \begin{bmatrix} a_w & 0 & 0 & 0 & 0 \\ b_{11} & a_{11} & a_{12} & 0 & 0 \\ b_{21} & a_{21} & a_{22} & 0 & 0 \\ 0 & 0 & 0 & a_{11} & a_{12} \\ 0 & 0 & 0 & a_{21} & a_{22} \end{bmatrix}$$

and

$$B_{54} = \begin{bmatrix} 0 & 0 & 0 & 0 \\ 0 & 0 & 0 & 0 \\ 0 & 0 & 0 & 0 \\ b'_{11} & c_{11} & b''_{11} & c'_{11} \\ b'_{21} & c_{21} & b''_{21} & c'_{21} \end{bmatrix}$$

The elements of the $A_{55}$ and $B_{54}$ matrix have been previously defined. It is noted that if the time $t_{k+1}$ falls into any of the following intervals

$$t_{k+1} < \hat{x}_2(k+1)$$

or

$$\hat{x}_2(k+1) + N_p \cdot \Delta \leq t_{k+1} < \hat{x}_4(k+1) \tag{4.38}$$

or

$$t_{k+1} > \hat{x}_4(k+1) + N_s \cdot \Delta$$

then $B_{54} = O_{54}$, i.e., a 5x4 null matrix.

The updated P matrix for time $t_{k+1}$ is given by the following equation:

$$P_{k+1} = P'_{k+1} - K_{k+1} H P'_{k+1} \tag{4.39}$$

where $K_{k+1}$ is the Kalman Gain matrix given by

$$K_{k+1} = P'_{k+1} H^T / r'_{k+1} \tag{4.40}$$

where

$$r'_{k+1} = H P'_{k+1} H^T + r_m \tag{4.41}$$

To simplify the notation, the time subscripts k and k+1 are dropped for the rest of this section since it is clear that P and K are being updated from time $t_k$ to time $t_{k+1}$. The subscripts on the matrices $A_{55}$ and $B_{54}$ will also be dropped.

Since $H = m_v(0\ 0\ 0\ 0\ 0\ 0\ 1\ 0\ 1)$, for the velocity measurement case, it is evident that

$$P'H^T = m_v \begin{bmatrix} p'_{17} + p'_{17} \\ \cdot\ \cdot\ \cdot \\ p'_{97} + p'_{99} \end{bmatrix} \tag{4.42a}$$

and

$$r' = m_v^2(p'_{77}+p'_{79}+p'_{97}+p'_{99}) + r_m \tag{4.42b}$$

where the $p'_{ij}$ are elements of P'. The gain matrix has the fairly simple form

$$K = \frac{1}{r'} P'H^T = \frac{m_v}{r'} \begin{bmatrix} p'_{17} + p'_{19} \\ \cdots \\ p'_{97} + p'_{99} \end{bmatrix} \tag{4.43}$$

It is next necessary to partition the P and P' matrices into the same structure as the partitioning of the $\Phi$ matrix. Thus we define

$$P \equiv \begin{bmatrix} P_a & P_b \\ P_b^T & P_c \end{bmatrix} \tag{4.44a}$$

where

$P_a$ denotes a 4x4 symmetric matrix

$P_b$ denotes a 4x5 matrix

$P_c$ denotes a 5x5 symmetric matrix

With these definitions it is seen that the following matrix product is obtained

$$\Phi\ P\ \Phi^T = \begin{bmatrix} P_a & P_aB^T+P_bA^T \\ BP_a+AP_b^T & BP_cB^T+BP_bA^T+AP_b^TB^T+AP_cA^T \end{bmatrix} \qquad (4.44b)$$

For convenience of notation, the following matrix products are defined:

$$X = BP_bA^T$$

$$Y = P_aB^T + P_bA^T \qquad (4.44c)$$

and

$$Z = BP_cB^T$$

Since the matrix B has three rows which are all zero (top three), it is readily seen that the only non-zero elements of matrix Z are the bottom right 4 elements. The details of these calculations are given in the "Summary of Equations" section. It is noted that if $t_{k+1}$ falls into one of the intervals defined above, then the computations are reduced considerably since

$$X = 0$$

$$Y = P_b A^T \tag{4.44d}$$

and

$$Z = 0$$

It is also noted that some of the calculation involving products with the B matrix are eliminated by the fact that the top three rows of B are all zeros. With the above definition of X, Y, and Z it is seen that

$$P' = \begin{bmatrix} P_a & Y \\ Y^T & Z+X+X^T+AP_cA^T \end{bmatrix} + Q \tag{4.45}$$

In the final step of updating the P matrix, it is convenient make a different partitioning of P'. This partitioning is based on the structure of the H matrix. In particular, it is readily seen that

$$P = P' - P'' \tag{4.46a}$$

where

$$P'' = \frac{1}{r^T} P'(H^T H)P' \tag{4.46b}$$

Since

$$H^T H = m_v^2 \begin{bmatrix} 0_1 & 0_2 \\ 0_2^T & I_3 \end{bmatrix}$$

where

$0_1$ denotes a 6x6 null matrix

$0_2$ denotes a 6x3 null matrix

and

$$I_3 = \begin{bmatrix} 1 & 0 & 1 \\ 0 & 0 & 0 \\ 1 & 0 & 1 \end{bmatrix}$$

it is convenient to partition P' into the same structure, i.e.,

$$P' = \begin{bmatrix} P_1' & P_2' \\ P_2^T & P_3' \end{bmatrix} \tag{4.46c}$$

where $P_1'$, $P_2'$ and $P_3'$ are dimensioned the same as $0_1$, $0_2$, and $I_3$, respectively.

With this partitioning, it is seen that

$$H^T H P' = \begin{bmatrix} 0_1 & 0_2 \\ P_1'^T & P_3 \end{bmatrix} \tag{4.46d}$$

and

$$P'(H^T H)P' = \begin{bmatrix} P_2' P_2'^T & P_2' P_3' \\ P_3' P_2^T & P_3' P_3' \end{bmatrix} \tag{4.46e}$$

where, it is noted that $P_1'$ and $P_3'$ are symmetric matrices.

The details of these calculations, and the computational efficiencies achieved, are discussed in the "Summary of Equations" Section VI.

G. Evaluation of Partials with Respect to $x_2$ and $x_4$

According to Leibnitz's rule, we have

$$\frac{d}{d\alpha}\int_{\phi_1(\alpha)}^{\phi_2(\alpha)} f(t,\alpha)dt = \int_{\phi_1(\alpha)}^{\phi_2(\alpha)} \frac{\partial f}{\partial \alpha}(t,\alpha)\,dt$$

$$+ f(\phi_1,\alpha)\frac{d\phi_1}{\phi\alpha} - f(\phi_2,\alpha)\frac{d\phi_2}{\phi\alpha} \qquad (4.47)$$

In the present case, $\phi_1(\alpha)=x_2+n\Delta-\Delta$ and $\phi_2(\alpha)=x_2+n\Delta$, n=1 to $N_p$. Thus

$$\frac{d\phi_1}{dx_2} = 1 \text{ and } \frac{d\phi_2}{dx_2} = 1 \qquad (4.48a)$$

Also $f(t,\alpha)$ is not a function of $\alpha$ (i.e., $x_2$) thus

$$\frac{\partial f(t,\alpha)}{\partial \alpha} = 0 \qquad (4.48b)$$

Thus

$$\frac{d}{d\alpha}\int_{x_2+n\Delta-\Delta}^{x_2+n\Delta} f(t)dt = f(x_2+n\Delta-\Delta)-f(x_2+n\Delta) \qquad (4.48c)$$

Since the present problem is time invariant (i.e., the solution for the second order system depends only on the difference $x_2+\Delta-x_2=\Delta$, we need only consider the limits 0 and $\Delta$.

NOTE: One needs to be careful on what the values of $a_p(t)$ (and $a_s(t)$) are over this interval. That is, the limits 0 and $\Delta$ do not change, but the values of $a_p(t)$ do. Thus the limits of integration are

$$\phi_2(\alpha) = x_2 + n\,\Delta$$

$$\phi_1(\alpha) = x_2 + (n-1)\Delta \qquad n=1,2,\ldots,N_p. \qquad (4.48d)$$

However, since the system is time-invariant, one needs only to consider the sampling interval, $\Delta$.

Typically, as previously noted, the input wavelets will have the form shown below (the same arguments are also true for the S-wave).

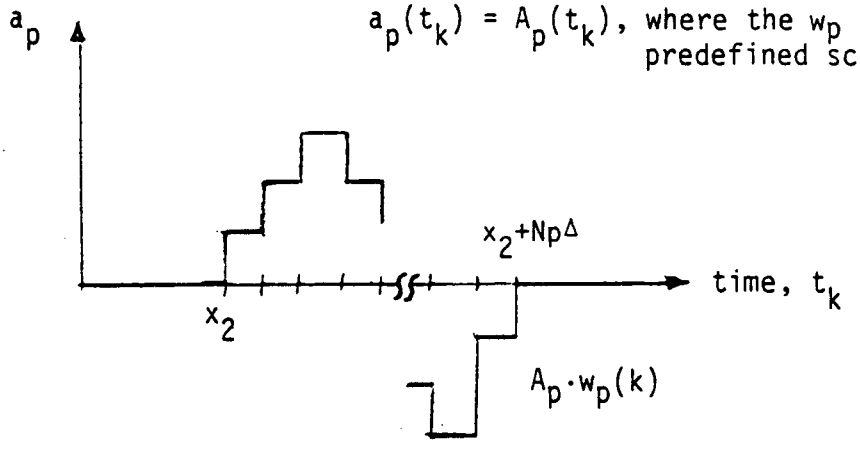


According to Equation (4.6b) of Reference 4, we have

$$\int_0^{\Delta} e^{F\cdot(\Delta-t)} \begin{bmatrix} 0 \\ \omega^2 \end{bmatrix} a_p(t)dt = \frac{\omega^2 e^{-\zeta'\Delta}}{\rho} \int_0^{\Delta} e^{-\zeta' t} \begin{bmatrix} \frac{1}{\omega} \sin \rho'(\Delta-t) \\ -\zeta \sin\rho'(\Delta-t)+\cos\rho'(\Delta-t) \end{bmatrix} dt \cdot a_p(t_k)$$

Define

$$f(t) = e^{-\zeta' t} \begin{bmatrix} \frac{1}{\omega} \sin\rho'(\Delta-t) \\ -\zeta \sin \rho'(\Delta-t)+\rho\cos\rho'(\Delta-t) \end{bmatrix} a_p(t_k) \qquad (4.49a)$$

then

$$f(0) = \begin{bmatrix} \frac{1}{\omega} \sin \rho'' \\ -\zeta \sin \rho''+\rho\cos\rho'' \end{bmatrix} a_p(t_k) \qquad (4.49b)$$

and

$$f(\Delta) = e^{-\zeta''} \begin{bmatrix} 0 \\ \rho \end{bmatrix} a_p(t_{k+1}) \qquad (4.49c)$$

Thus

$$f(0)-f(\Delta) = \begin{bmatrix} \frac{1}{\omega}\sin\rho'' \\ \cos(\rho''+\alpha)-\rho e^{-\zeta''} \end{bmatrix} A_p \cdot (w_p(t_k)-w_p(t_{k+1})) \qquad (4.50a)$$

where

$$\rho'' = \rho'\Delta = \rho\cdot\omega\cdot\Delta$$

$$\zeta'' = \zeta'\Delta = \zeta\cdot\omega\cdot\Delta \qquad (4.50b)$$

$$k = x_2/\Delta \text{ to } x_2/\Delta + N_p$$

Note: $x_2$ and $x_4$ should be selected/estimated so that they are multiples of the sampling time $\Delta$.

Therefore

$$\frac{d}{dx_2}\int_{t^-}^{t^+} f(t)dt = \begin{bmatrix} \frac{\omega e^{-}}{\rho}^{''} \sin\rho'' \cdot ap(t^-) \\ \frac{\omega^2 e^{-\zeta''}}{\rho} \cos(\rho''+\alpha) \cdot ap(t^-) - \rho\omega^2 e^{-2\zeta''} ap(t^+) \end{bmatrix}$$

$$= \frac{\omega^2 e^{-\zeta''}}{\rho} \begin{bmatrix} \frac{1}{\omega}\sin\rho'' \cdot ap(t^-) \\ \cos(\rho''+\alpha) \cdot ap(t^-) - \rho\, e^{-\zeta''} ap(t^+) \end{bmatrix} \qquad (4.51a)$$

where

$$t^- = x_2 + n\,\Delta - \Delta$$

$$t^+ = x_2 + n\,\Delta \qquad (4.51b)$$

$$n = 1 \text{ to } Np$$

Alternatively, if we use Equation (D.6.e) of Appendix D we have

$$y_f(\Delta) = \frac{\omega^2}{\rho} e^{-\zeta''} \begin{bmatrix} \frac{-1}{\omega}\cos\rho'' & \frac{1}{\omega}\sin\rho'' \\ \sin(\rho''+\alpha) & \cos(\rho''+\alpha) \end{bmatrix} \int_0^{\Delta} e^{-\zeta' t} \begin{bmatrix} \sin\rho' t \\ \cos\rho' t \end{bmatrix} dt \cdot w_k$$

where

$$\alpha = \sin^{-1}\zeta$$

Applying similar notation, i.e., letting

$$f'(t) = e^{-\zeta' t} \begin{bmatrix} \sin\rho' t \\ \cos\rho' t \end{bmatrix} \tag{4.52a}$$

we obtain

$$f'(0) = e^{-o} \begin{pmatrix} 0 \\ 1 \end{pmatrix} a_p(t^-) \tag{4.52b}$$

$$f'(\Delta) = e^{-\zeta''} \begin{pmatrix} \sin\rho'' \\ \cos\rho'' \end{pmatrix} a_p(t^+) \tag{4.52c}$$

Thus

$$\frac{d}{dx_2}\int_{t^-}^{t^+} f(t)dt = \frac{\omega^2 e^{-\zeta''}}{\rho} \begin{bmatrix} \frac{1}{\omega}\sin\rho''\cdot a_p(t^-) - e^{-\zeta''}(\overbrace{-\cos\rho''\sin\rho''+\sin\rho''\cos\rho''}^{0})a_p(t^+) \\ \cos(\rho''+\alpha)\cdot a_p(t^-) - e^{-\zeta''}(\underbrace{\sin\rho''+\alpha)\sin\rho''+\cos(\rho''+\alpha)\cos\rho''}_{\rho})a_p(t^+) \end{bmatrix}$$

$$= \frac{\omega^2 e^{-\zeta''}}{\rho} \begin{bmatrix} \frac{1}{\omega}\sin\rho''\cdot a_p(t^-) \\ \cos(\rho''+\alpha)\cdot a_p(t^-) - \rho e^{-\zeta''} a_p(t^+) \end{bmatrix} \tag{4.53a}$$

which is the same result as above. Since this result holds for both the P-wave and the S-wave, we can write, for i=2 and 4,

$$\frac{d}{dx_i}\int_{x_i+n\Delta-\Delta}^{x_i+n\Delta} f(t)dt = \frac{\omega^2 e^{-\zeta''}}{\rho}\begin{bmatrix}\frac{1}{\omega_o}\sin\rho''\cdot w_{i-1}(t^-)\\ \cos(\rho''+\alpha)\cdot w_{i-1}(t^-)-\rho e^{-\zeta''}w_{i-1}(t^+)\end{bmatrix} \qquad (4.53b)$$

where

$$w_1(t^-) = x_1(t^-)\cdot w_p(t^-) \quad t^- = x_2+n\cdot\Delta-\Delta,\ n=1 \text{ to } N_p$$
$$w_3(t^-) = x_3(t^-)\cdot w_s(t^-) \quad t^- = x_4+n\Delta-\Delta,\ n=1 \text{ to } N_s \qquad (4.53b)$$

Note: When the $w_i$ are both zero, these partials are zero and there is no need to evaluate them in the computational algorithms. Furthermore, since these partials are required before updated estimates can be obtained, the estimates from the previous sampling interval, i.e.,

$$\hat{x}_1(t^-\Delta),\ \hat{x}_2(t^-\Delta),\ \hat{x}_3(t^-\Delta),\ \text{and}\ \hat{x}_4(t^-\Delta) \qquad (4.53c)$$

are used.

If the state vector is defined by

$$\underline{x}_{k+1} = F\,\underline{x}_k + G\,w_k,$$

then F is used for updating $\underline{x}_k$, and $\Phi = \frac{\partial F}{\partial \underline{x}}$ is used for updating the estimation error covariance matrix $P_k$. It is noted that

$$\Phi = F \quad \text{for} \quad t_k<\hat{x}_2 \quad \text{and} \quad t_k>\hat{x}_4+N_s\cdot\Delta$$

and $\Phi=F$ for $x_2\leq t_k\leq x_4+N\Delta_s$ except for the following elements:

$$\partial F_{82}/\partial x_2,\ \partial F_{92}/\partial x_2,\ \partial F_{84}/\partial x_4,\ \text{and}\ \partial F_{94}/\partial x_2$$

In summary, these elements can be written for i=2 and 4, as

$$\begin{bmatrix}\Phi_{8i}\\ \Phi_{9i}\end{bmatrix} = c_1\begin{bmatrix}c_2\cdot w_{i-1}(t^-)\\ c_3\cdot w_{i-1}(t^-) - c_4\cdot w_{i-1}(t^+)\end{bmatrix}\hat{x}_{i-1}(t^-) \qquad (4.54a)$$

where

$$c_1 = \omega^2 e^{-\zeta''}\rho \qquad \zeta'' = \zeta\omega\Delta$$

$$c_2 = \frac{1}{\omega}\sin\rho'' \qquad \rho'' = \rho\omega\Delta \tag{4.5b}$$

$$c_3 = \cos(\rho''+\alpha) \qquad \alpha = \sin^{-1}\zeta$$

$$c_4 = \rho e^{-\zeta''}$$

$\hat{x}_{i-1}(t^-)$ = best estimates of $x_{i-1}$ at $t^-$, i = 2 and 4

$$w_1(t^-) = w_p(\hat{x}_2+n\Delta-\Delta) \quad n = 1 \text{ to } N_p$$

$$w_1(t^+) = w_1(t^-+\Delta) \tag{4.54c}$$

$$w_3(t^-) = w_p(\hat{x}_4+n\Delta-\Delta) \quad n = 1 \text{ to } N_s$$

$$w_3(t^+) = w_3(t^-+\Delta)$$

Note: The parametres $c_i$, i=1 to 4, are constants and can be precomputed. The weighting factors $w_p$ and $w_s$ are known functions of time.

# V. SUMMARY & CONCLUSIONS

In this research a new approach of digital filtering in determine shear wave and compression wave velocities is introduced with great success. The technique currently being used at U.B.C. (Campanella and Robertson, 1986) relies upon the polarity of shear waves to determine arrival times of shear waves at specific depth intervals to calculate shear wave velocities over each depth interval.

The reverse polarity method requires the shear waves to be polarized 180 out of phase. These waves are obtained by generating shear waves on opposite sides of the seismic source. Thus, it is necessary to use two seismic waves to determine one reference arrival time as opposed to digital filtering methods where only one seismic wave is necessary. Once the waves are recorded, it is necessary to visually pick a cross-over or reference arrival time from the oppositely polarized waves. The determination of the cross-over can be difficult when low or high frequency noise or signal is present. Therefore, analogue filtering is often applied in order to assist in the understanding and reduction of the time series recorded. Stokoe and Hoar (1978) suggest that filtering should be minimized because it may significantly distort the signal and erroneously alter arrival times. An additional consideration is that the reverse polarity method demands that in picking a cross-over, a consistent method must be used. For instance, one may decide that the second cross-over will be used throughout the seismic investigation. But it has been found that a single criterion may not be appropriate throughout the seismic profile due to varying instrument responses and frequencies changing slightly with soil layering.

The two filtering methods considered in this thesis are the one based on frequency domain filtering, where Fast Fourier, Butterworth, and crosscorrelation algorithms are implemented, and one based on time domain techniques, where a Kalman Filter is designed to model the instrument and the physical environment. The crosscorrelation method relies upon filtering response data such that a specific wave is analyzed (e.g., SH-wave) when applying the crosscorrelation function. The crosscorrelation function is applied to two successive waves (corresponding to the successive depths) where the maximum value of the cross-correlation function is directly related to the difference in travel times

between the waves. With this arrival time difference, a velocity can be calculated. The method is very advantageous because it allows one to focus on a specific wavelet and use all the information of the wavelets present averaging out any noises or irregularities and relying upon dominant responses as opposed to the reverse polarity method where there is dependence on one point (i.e., the cross-over) to define arrival time differences. Some important aspects of digital filtering to consider when implementing the cross-correlation function are: sampling rate, Gibbs' phenomenon, alaising, the Butterworth filter, and d.c. shifts.

The crosscorrelation filter was coded in Fortran language, and the program is referred to as CROSSCOR. CROSSCOR is a graphics interactive program which displays the frequency spectra, unfiltered and filtered times series and cross-correlations on a mainframe graphics terminal which has been adapted to run on the IBM P.C. CROSSCOR was tested by superpositioning several sinusoidal waves and filtering out the desired frequencies. CROSSCOR was applied to real data to assess its performance and reliability. Results from five research sites are given, and the velocity profiles from different methods of data acquisition and reduction are presented and compared along with the respective cone profiles.

The first research site analyzes data acquired at the McDonald Farm Site in Richmond, B.C. In this case study five sets of data were compiled and two different sensors were used. The first sensor was the Hogentogler Super Cone Velocity transducer and the second sensor was the UBC Seismic Cone Pressuremeter, which had two accelerometers installed. The seismic data was reduced by the reverse polarity method and CROSSCOR, and compared with cone bearing profiles. The second site was located at the Grant McConachie Way in Richmond, B.C., where UBC #7 seismic cone was used with an accelerometer sensor installed. Two different types of sources were compared in this investigation, i.e, the shear and compression waves sources. The third research site analyzes data acquired at the Tilbury National Gas Plant Site on Tilbury Island where the UBC seismic cone pressuremeter was used for data acquisition. The fourth site was the Annacis Bridge Pile Research Site where the UBC Seismic Cone Pressuremeter and UBC #8 Seismic Cone were used for data acquisition. In this investigation shear velocities were obtained using shear sources. Since both sides of the source were used, it was possible to obtain two velocity estimates for one depth increment using CROSSCOR as opposed to the reverse polarity method which allows for only one velocity estimate. The last research site was the Lower

was the Lower Langley 232nd St. Site. In this investigation filtered (analogue) and unfiltered reverse polarized Hammer Shear Source data was obtained. In addition, point source Buffalo Gun data was reduced with CROSSCOR which resulted in separating and measuring both shear and compression wave velocities.

The results from the synthetic data and research sites indicate that CROSSCOR is a very beneficial tool to obtain seismic wave velocities. The program allows one to separate out different seismic events and use all the information contained in the wavelets in obtaining shear and compression wave velocities. The procedure in extracting the desired instrument responses proved to be routine and user friendly due to the different responses being consistent throughout a cone profile. In addition, since CROSSCOR is a digital filter it removes most human bias (e.g., determining cross-overs in the reverse polarity method) in determining arrival times, the program allows one to compare velocities from signals obtained on opposite sides of the source, and one may also have the flexibility in using different sources in obtaining seismic wave velocities. The problem with triggering when applying the Buffalo Gun Source may be resolved by using an accelerometer (having a fast response time) as the trigger as well as grounding the Buffalo Gun firing pin to create a contact closure (similar to the Hammer Shear Source).

The Kalman Filter was applied in the manner in which it modelled the sensors used and the physical environment of the body waves and noise generation. The KF was investigated for its possible application to obtaining accurate estimates on the P-wave and S-wave amplitudes and arrival times. The KF is a very flexible tool which allows one to model the problem considered accurately. In addition, the KF works in the time domain which removes many of the limitations of the frequency domain techniques.

The Kalman Filter is an optimal (in a least squares sense) filter which is based on state-space, time-domain formulations of physical problems. Application of this filter requires that the physical problem be modelled by a set of first order differential or difference equations which, with initial conditions, uniquely define the system behaviour. The filter proposed attempts to model a seismic receiver as a second order system with it's characteristic natural frequency and damping. The instrument acts as a transform function in respect to the input of noise and body waves propagating through the earth.

The performance of the Kalman Filter was analyzed by generating a source wavelet and passing it through the second order instrumentation. The second order response is than fed into the Kalman Filter with the arrival time and maximum amplitude being determined. The filter was found to perform well and it has much promise in respect that if it is finely tuned, it would be possible to obtain arrival times and amplitudes on line resulting in velocities and damping characteristics, respectively. There are many other forms of the filter which could be implemented such as smoothing. Smoothing would allow one to use all the information in the seismic trace to determine the location and shape of the wavelets being recorded (which is a very important parameter in earthquake engineering). The damping obtained from the KF would be a definite advantage over conventional techniques which rely on power spectrum measurements to determine the damping characteristics of a soil profile with depth. Since the power spectrum depends on more variables (e.g., initial energy of source, frequency content of body waves, and coherency between successive traces), there is greater chance of error than the Kalman Filter formulation.

# VI. SUGGESTIONS FOR FUTURE RESEARCH

The research in this thesis indicates that digital filters are extremely beneficial in in-situ testing. As was outlined, there are many different types of filters one can implement; therefore, it is important to become fluent in all the different filtering techniques and apply the ones which best suit the problem considered. The frequency domain approach is a well established method of manipulating the data to obtain desired frequencies, while the state space approach is the "state-of-the-art" technique in time series analysis.

Future research at UBC should concentrate having the in-situ group becoming more fluent on the above techniques in digital filtering in order to expand the possible goetechnical parametres that can be obtained in in-situ testing. One of these parametres is damping of the soil. Soil damping and the shape of the seismic wavelets are very important parametres in earthquake engineering. Another area of interest in geotechnical engineering is seismic tomography. Seismic Tomography combines the data from a large number of waves in a given soil profile to construct a three dimentional image of the medium (e.g., velocity and damping) that the waves have travelled through. Therefore, if one establishes accurate methods for determining P and S-wave velocities and attenuation, the next step would be to apply tomographic concepts.

Further research at UBC should also concentrate on making newly developed programs user friendly. The programs should be tested extensively in the field with industry and effort made into developing the best, most reliable, and efficient techniques and programs for seismic data reduction.

LIST OF REFERENCES


1. Richart, F. E., Jr., Hall, J. R., Jr., and Woods, R. D., (1970), "Vibrations of Soils and Foundations," Prentice-Hall, Inc., Englewood Cliffs, New Jersey, 414 pp.

2. Mooney, H. M. (1974), "Seismic Shear Waves in Engineering," Journal of the Geotechnical Engineering Division, ASCE, Vol. 100, No. GT8, Aug. Proc, Paper 10745, pp. 905-923.

3. Borm, G. W., (1977), "Methods from Exploration Seismology: Reflection, Refraction, and Borehole Prospecting," Proceedings of DMSR 77, Karlsruhe, 5-16 Sept. 1977, Vol. 3, pp. 87-114.

4. Rice, A., 1984, "The Seismic Cone Penetrometer," M.A.Sc. Thesis, Dept. of Civil Engineering, University of British Columbia, Vancouver, B.C.

5. Laing, N. L., 1985, "Sources and Receivers with the Seismic Cone Test," M.A.Sc. Thesis, Dept. of Civil Engineering, University of British Columbia, Vancouver, B.C.

6. Close & Fredrick, Modelling and Analysis Dynamic Systems, Houghton Miflin Co., 1978.

7. Ogata, J., Discrete Process Control, Cambridge University Press, 1987.

8. Ewing, Jardetz, and Press, Elastic Waves in Layered Media, McGraw-Hill Series in the Geological Sciences, 1957.

9. K. H. Stokoe and R. S. Hoar, "Variables Affecting In-Situ Seismic Measurements," Proceeding of Conference on Earthquake Engineering and Soil Dynamics, ASCE Goetechnical Engineering Division Specialty Conference, Pasadena, CA, Vol. II, pp. 919-939, 1978.

10. Lancaster, Active Filter Cookbook, Howard W. Sands and Company, 1982.

11. R. E. Sheriff and L. P. Geldart, Exploration Seismology, Volume 2, Data Processing and Interpretation, Cambridge University Press, 1983.

12. George W. Stinson, Introduction to Airborne Radar, Hughes Aircraft Co., 1983.

13. E. R. Kanasevich, Time Sequence Analysis in Geophysics, Third Edition, the University of Alberta Press, 1981.

14. R. E. Thomson and K. Y. Chow, "Butterworth and Lanczos-Window Cosine Digital Filters: with Application to Data Processing on the UNIVAC 1106 Computer," Pacific Marine Science Report 80-9, Institute of Ocean Sciences, Sidney, B.C.

15. E. A. Robinson, "Collection of Fortran II Programs for Filtering and Spectral Analysis of Signal Channel Time Series," Chapter 22 of textbook by Unknown.

16. U.B.C. Plotting Programs, Unpublished Notes.

17. Campanella, R. G., Robertson, P. K., and Gillespies, D., 1982, "Cone Penetration Testing in Deltaic Soils," Canadian Geotechnical Journal, Vol. 20, February.

18. Howie, J. A., 1989, Ph.D. Thesis (in preparation), University of British Columbia, Vancouver, B.C.

19. Davies, M., 1987, "Predicting Axially and Laterally and Pile Behaviour Using In-Situ Testing Methods," M.A.Sc. Thesis, Department of Civil Engineering, University of British Columbia, Vancouver, B.C.

20. Greig, J., 1985, "Estimating Undrained Shear Strength of Clay from Cone Penetration Tests," M.A.Sc, Thesis, Department of Civil Engineering, University of British Columbia, Vancouver, B.C.

21. Dobrin, M. B., 1975, "Introduction to Geophysical Prospecting, McGraw-Hill Company.

22. Guigne', J.Y., "Acoustic Sub-Seabed Interrogator," Ph.D., University of Bath-England, 1986.

23. Asten, M. W., "Theory and Practice of Geophone Calibration In-Situ Using Modified Step Method," IEEE Trans. Geosc., Vol. GE-15, No. 4, pp. 208-214, October, 1977.

24. Baziw, E. J., "Concepts of Kalman Filtering and the Application to Seismic Time Series Analysis," Bachelors of Applied Science Thesis, University of British Columbia, April 1986.

25. Kalman, R. E., "A New Approach to Linear Filtering and Prediction Problems," J. Basic Energy, Series D, Vol. 45, pp. 25-36, March 1960.

# APPENDIX A

## Program listing of CROSSCOR

Listing of CROSSCOR at 16:44:17 on JUL 27, 1988 for CCid=SEIS on G

```
      1            REAL       CI1(2048),CI2(2048),X(2048),Y(2048),W(2048)
      2            REAL       XX(2048),YY(2048),FC1,FC2,FC3,FC4,D1(8),G1
      3            REAL       AVRGX,AVRGY,XZ(2048),YZ(2048),D2(8),G2,DELT
      4            REAL       DLT,G(5000),GA(10000),CMAX,EX(10000)
      5            INTEGER    LG,LA,LMAX,HMAX
      6            REAL       X1(2048),Y1(2048),FN
      7      C
      8            READ(3,*) N1,DELT
      9            DLT=1000.0*DELT
     10            FN=0.5/DELT
     11            DO 100 I=1,N1
     12            READ(1,*) X(I)
     13            READ(2,*) Y(I)
     14        100 CONTINUE
     15      C
     16      C
     17            CALL NORME(N1,X)
     18            CALL NORME(N1,Y)
     19            CALL REMAV(N1,X,AVRGX)
     20            CALL REMAV(N1,Y,AVRGY)
     21            CALL POW2(N1,X,Y,N)
     22      C
     23            DO 102 I=1,N1
     24            XX(I)=X(I)
     25            YY(I)=Y(I)
     26        102 CONTINUE
     27      C
     28            CALL FASTF(X,Y,N)
     29            CALL FXFFT(X1,Y1,X,Y,N)
     30            CALL SMOOTH(X1,N)
     31            CALL SMOOTH(Y1,N)
     32            CALL RAD(W,N,DELT)
     33            CALL NORME(N,X1)
     34            CALL NORME(N,Y1)
     35            NN=N/2
     36            DO 101 I=1,NN
     37            WRITE(7,*) W(I),X1(I)
     38            WRITE(8,*) W(I),Y1(I)
     39        101 CONTINUE
     40      C
     41            CALL PL(X1,W,NN)
     42      C
     43             WRITE(6,4)
     44          4 FORMAT('What frequencies do you want filtered?')
     45            READ(5,*)FC1,FC2
     46      C
     47      C
     48            CALL PL(Y1,W,NN)
     49      C
     50            WRITE(6,4)
     51            READ(5,*)FC3,FC4
     52      C
     53      C
     54            CALL BNDPAS(FC1,FC2,DLT,D1,G1)
     55            CALL FILTER(XX,N1,D1,G1,IG1)
     56            CALL BNDPAS(FC3,FC4,DLT,D2,G2)
     57            CALL FILTER(YY,N1,D2,G2,IG2)
     58            CALL NORME(N1,XX)
```

Listing of CROSSCOR at 16:44:17 on JUL 27, 1988 for CCid=SEIS on G

```
      CALL NORME(N1,YY)
C
      DO 201 I=1,N1
      WRITE(9,*) XX(I)
      WRITE(10,*) YY(I)
201   CONTINUE
C
      LG=2*N1-1
C
      CALL CROSS(N1,XX,N1,YY,LG,G)
C
      LA=2*LG
      DO 30 J=1,LG
      IJ=J-1
      GA(J+LG)=G(J)
30    CONTINUE
C
      CALL CROSS(N1,YY,N1,XX,LG,G)
      LH=LG+1
      DO 40 II=1,LG
      GA(II)=G(LH-II)
40    CONTINUE
C
C
      DO 50 I=1,LG
      EX(I)=I-LG
50    CONTINUE
C
      LGG=LG+1
C
      DO 53 I=LGG,LA
      EX(I)=I-LG
53    CONTINUE
C
      DO 109 I=1,LA
      WRITE(11,*) EX(I),GA(I)
109   CONTINUE
C
      CALL MAXSN(LA,GA,CMAX,LMAX)
C
       HMAX=LMAX-LG-1
C
      CALL PLA(GA,EX,LA)
C
      WRITE(6,300) HMAX
300   FORMAT ('The Maximum Time Shift is :     ',I7)
C
      WRITE(6,303) FN
303   FORMAT('CORRECT IF NOT FILTERED PAST NYQUIST Fn = ',F9.1,' HZ ')
C
      STOP
      END
C
      SUBROUTINE FASTF(FR,FI,N)
C
C     N is the number of data points=2**M
C     FR is the real data set
C     FI is the imaginary part of data set(=0.0 if only real)
```

Listing of CROSSCOR at 16:44:17 on JUL 27, 1988 for CCid=SEIS on G

```
      C     First compute M
      C
            REAL FR(N),FI(N),GR,GI,ER,EI,EU,EZ
            M=0
            KD=N
          1 KD=KD/2
            M=M+1
            IF(KD.GE.2) GO TO 1
            ND2 = N/2
            NM1 = N-1
            L=1
      C
      C     Shuffle input data in binary digit reverse order
      C
            DO 4 K=1,NM1
            IF (K.GE.L) GO TO 2
            GR = FR(L)
            GI = FI(L)
            FR(L) = FR(K)
            FI(L) = FI(K)
            FR(K) = GR
            FI(K) = GI
        2   NND2 = ND2
        3   IF (NND2.GE.L) GO TO 4
            L = L-NND2
            NND2 = NND2/2
            GO TO 3
        4   L = L + NND2
            PI = 3.14159265
      C
      C     First arrange accounting of M stage
      C
            DO 6 J=1,M
            NJ = 2**J
            NJD2 = NJ/2
            EU = 1.0
            EZ = 0.0
            ER = COS(-PI/NJD2)
            EI = SIN(-PI/NJD2)
      C
      C     Compute Fourier transform in each M stage
      C
            DO 6 IT=1,NJD2
            DO 5 IW=IT,N,NJ
            IWJ = IW + NJD2
            GR = FR(IWJ)*EU - FI(IWJ)*EZ
            GI = FI(IWJ)*EU + FR(IWJ)*EZ
            FR(IWJ) = FR(IW) - GR
            FI(IWJ) = FI(IW) - GI
            FR(IW) = FR(IW) + GR
          5 FI(IW) = FI(IW) + GI
            SEU = EU
            EU = SEU*ER-EZ*EI
          6 EZ = EZ*ER + SEU*EI
            RETURN
            END
      C
      C  FXFFT corrects the amplitudes of FASTF, as outlined by Kanasewich
```

Listing of CROSSCOR at 16:44:17 on JUL 27, 1988 for CCid=SEIS on G

```
      C
            SUBROUTINE FXFFT(X1,Y1,X,Y,N)
            REAL  X(N),Y(N),X1(N),Y1(N),A(3000),B(3000),C(3000)
            REAL  D(3000),E(3000),F(3000),G(3000),H(3000)
            DO 10 I=1,N
            A(I)=.5*(X(I)+X(N+2-I))
            B(I)=.5*(Y(I)-Y(N+2-I))
            C(I)=A(I)*A(I)
            D(I)=B(I)*B(I)
            X1(I)=SQRT(C(I)+D(I))
            E(I)=.5*(X(I)-X(N+2-I))
            F(I)=.5*(Y(I)+Y(N+2-I))
            G(I)=E(I)*E(I)
            H(I)=F(I)*F(I)
            Y1(I)=SQRT(G(I)+H(I))
         10 CONTINUE
            RETURN
            END
      C
      C  POW2 determines M in N=2**M for a specific trace length(i.e,L),
      C  and then pads the rest of the trace, L to N, with zeros.
      C
            SUBROUTINE POW2(L,X,Y,N)
            DIMENSION X(L),Y(L)
            REAL      TT,ST,SS,S
            SS=0.30103
            TT=FLOAT(L)
            ST=LOG10(TT)
            S=ST/SS+1.0
            Q=IFIX(S)
            N=1
            DO 20 I=1,Q
            N=2*N
         20 CONTINUE
            DO 10 I=L,N
            X(I)=0.0
            Y(I)=0.0
         10 CONTINUE
            RETURN
            END
      C
      C  NORME is normilization of an array by it's RMS energy.
      C
            SUBROUTINE NORME(LL,F)
            REAL     F(4000),FS,Z
            INTEGER  FF
      C     IF(LL) 30,30,10
            CALL MAXSN(LL,F,FS,FF)
            WRITE(6,*) FS
            Z=FS
            DO 20 I=1,LL
         20 F(I)=F(I)/Z
            RETURN
            END
      C
      C DOT IS DOT PRODUCT
            SUBROUTINE DOT (L,X,Y,ANS)
            IMPLICIT REAL*8 (A-H,O-Z)
```

Listing of CROSSCOR at 16:44:17 on JUL 27, 1988 for CCid=SEIS on G

```
      233            REAL*8 X(2),Y(2),ANS
      234            ANS=0.0
      235            IF(L) 30,30,10
      236       10   DO 20 I=1,L
      237       20   ANS=ANS+X(I)*Y(I)
      238       30   RETURN
      239            END
      240       C
      241       C  REMAV removes the arithmetic average inorder DC shifts are removed
      242       C
      243            SUBROUTINE REMAV(LY,Y,AVERG)
      244            DIMENSION Y(2)
      245            S=0.
      246            DO 10 I=1,LY
      247         10 S=S+Y(I)
      248            AVERG=S/FLOAT(LY)
      249            DO 20 I=1,LY
      250         20 Y(I)=Y(I)-AVERG
      251            RETURN
      252            END
      253       C
      254            SUBROUTINE RAD(W,N,DELT)
      255            DIMENSION W(N)
      256            REAL      SS,ST
      257       C
      258            DO 10 I=1,N
      259            SS=FLOAT(I)
      260            ST=FLOAT(N)
      261            W(I)=SS/(ST*DELT)
      262         10 CONTINUE
      263            RETURN
      264            END
      265       C
      266       C  Smooth computes smoothed spectrum from the cosine transform
      267       C  using Turkey+Hamming formula. The subroutine inputs are
      268       C     SPECT=unsmoothed spectrum
      269       C     LS=its lenght
      270       C  The subroutine output is
      271       C     SPECT=smoothed spectrum
      272       C
      273            SUBROUTINE SMOOTH(SPECT,LS)
      274       C
      275            DIMENSION SPECT(LS)
      276            MM=LS-1
      277            A=.54*SPECT(1)+.46*SPECT(2)
      278            B=.54*SPECT(LS)+.46*SPECT(MM)
      279            SJ=SPECT(1)
      280            SK=SPECT(2)
      281            DO 10 J=2,MM
      282            SI=SJ
      283            SJ=SK
      284            SK=SPECT(J+1)
      285            SPECT(J)=.54*SJ+.23*(SI+SK)
      286         10 CONTINUE
      287            SPECT(1)=A
      288            SPECT(LS)=B
      289            RETURN
      290            END
```

Listing of CROSSCOR at 16:44:17 on JUL 27, 1988 for CCid=SEIS on G

```
      C
            SUBROUTINE PL(AMP,Z,L)
            REAL    AMP(3000),Z(3000),SS(3000),TT(3000)
            INTEGER   L,FSMPL
          1 N=0
            DO 100 I=1,L
            SS(I)=Z(I)
            TT(I)=AMP(I)
            IF(I.EQ.L) GO TO 200
        100 N=I
      C
      C
      C IF EQUAL TO ZERO TERMINATE PROGRAM
      C
        200 IF(N.EQ.0) GO TO 300
      C     CALL SUBROUTINE TO DO THE PLOTTING
            CALL SUMFUN(SS,TT,L)
      C     AND RETURN FOR MORE DATA
      C     PROGRAM COMES HERE WHEN FINISHED.
        300 CONTINUE
      C TERMINATING PLOTTING THEN STOP
            CALL PLOTND
            RETURN
            END
      C
            SUBROUTINE SUMFUN(X,Y,N)
      C SUBROUTINE DRAWS A LINE THROUGH N POINTS
            REAL    X(N),Y(N)
      C     REAL AMPS(3000),ZS(3000)
      C
      C
      C     AMPMIN=AMP(1)
      C
      C     DO 10 I=1,N
      C     AMPS(I)=SNGL(AMP(I))
      C     ZS(I)=SNGL(Z(I))
      C     AMPMIN=AMIN1(AMPMIN,AMPS(I))
      C  10 CONTINUE
      C FIRST SCALE THE POINTS
            CALL SCALE(X,N,10.0,XMIN,DX,1)
            CALL SCALE(Y,N,10.0,YMIN,DY,1)
            CALL AXIS(0.,0.,'FREQUENCY',-9,10.0,0.,XMIN,DX)
            CALL AXIS(0.,0.,'AMPLITUDE',9,10.0,90.,YMIN,DY)
      C FINALLC PLOT THE LINES
            CALL LINE(X,Y,N,1)
      C MOVE THE ORIGIN AND RETURN
            RETURN
            END
      C
            SUBROUTINE PLA(AMP,Z,L)
            REAL    AMP(3000),Z(3000),SS(3000),TT(3000)
            INTEGER   L,FSMPL
          1 N=0
            DO 100 I=1,L
            SS(I)=Z(I)
            TT(I)=AMP(I)
            IF(I.EQ.L) GO TO 200
        100 N=I
```

Listing of CROSSCOR at 16:44:17 on JUL 27, 1988 for CCid=SEIS on G

```
      C
      C
      C IF EQUAL TO ZERO TERMINATE PROGRAM
      C
        200 IF(N.EQ.0) GO TO 300
      C     CALL SUBROUTINE TO DO THE PLOTTING
            CALL SUMFN1(SS,TT,L)
      C     AND RETURN FOR MORE DATA
      C     PROGRAM COMES HERE WHEN FINISHED.
        300 CONTINUE
      C TERMINATING PLOTTING THEN STOP
            CALL PLOTND
            RETURN
            END
      C
            SUBROUTINE SUMFN1(X,Y,N)
      C SUBROUTINE DRAWS A LINE THROUGH N POINTS
            REAL    X(N),Y(N)
      C     REAL AMPS(3000),ZS(3000)

      C
      C     AMPMIN=AMP(1)

      C     DO 10 I=1,N
      C     AMPS(I)=SNGL(AMP(I))
      C     ZS(I)=SNGL(Z(I))
      C     AMPMIN=AMIN1(AMPMIN,AMPS(I))
      C  10 CONTINUE
      C FIRST SCALE THE POINTS
            CALL SCALE(X,N,10.0,XMIN,DX,1)
            CALL SCALE(Y,N,10.0,YMIN,DY,1)
            CALL AXIS(0.,0.,'TIME SHIFT',-9,10.0,0.,XMIN,DX)
            CALL AXIS(0.,0.,'CROSS CORRELATION VALUE',9,10.0,90.,YMIN,DY)
      C FINALLC PLOT THE LINES
            CALL LINE(X,Y,N,1)
      C MOVE THE ORIGIN AND RETURN
            RETURN
            END
      C
            SUBROUTINE BNDPAS(F1,F2,DELT,D,G)
      C
      C     Subroutine by Dave Ganley on March 5, 1977.
      C
      C     The purpose of this subroutine is to design and apply a
      C     recursive Butterworth band pass filter. In order to design
      C     the filter a call must be made to BNDPAS and then the
      C     filter may be applied by calls to filter. The filter
      C     will have 8 poles in the s plane and is in forward and
      C     reverse directions so as to have zero phase cutoff
      C     frequencies. The attenuation will be -6DB and the rolloff
      C     will be about 96 DB per Octave. A Billinear Z transform is
      C     used in designing the filter to prevent aliasing problems.
      C
            COMPLEX P(4),S(8),Z1,Z2
            DIMENSION D(8),X(2048),XC(3),XD(3),XE(3)
            DATA ISW/0/,TWOPI/6.2831853/
      C
      C     This section calculates the filter and must be called
```

Listing of CROSSCOR at 16:44:17 on JUL 27, 1988 for CCid=SEIS on G

```
      C     before filter is called.
      C
      C     F1 = Low frequency cutoff (6 DB Down)
      C     F2 = High frequency cutoff (6 DB down)
      C     DELT = Sample interval in milliseconds
      C     D = Will contain 8 Z domain coefficients of recursive filter
      C     G = Will contain the gain of the filter
      C
            WRITE(6,1) F1,F2,DELT
          1 FORMAT('BANDPASS FILTER DESIGN FOR A BAND FROM',F8.3,'TO',F8
           1.3,'HERTZ.',//'SAMPLE INTERVAL IS',F5.2,'MILLISECONDS.')
            DT = DELT/1000.0
            TDT = 2.0/DT
            FDT = 4.0/DT
            ISW = 1
            P(1) = CMPLX(-.3826834,.9238795)
            P(2) = CMPLX(-.3826834,-.9238795)
            P(3) = CMPLX(-.92388795,.3826834)
            P(4) = CMPLX(-.99238795,-.382684)
            W1 = TWOPI*F1
            W2 = TWOPI*F2
            W1 = TDT*TAN(W1/TDT)
            W2 = TDT*TAN(W2/TDT)
            HWID = (W2-W1)/2.0
            WW = W1*W2
            DO 19 I=1,4
            Z1 = P(I)*HWID
            Z2 = Z1*Z1-WW
            Z2 = CSQRT(Z2)
            S(I)= Z1+Z2
         19 S(I+4) = Z1-Z2
      C     WRITE(6,2) S
      C    2 FORMAT('-S PLANE POLES ARE AT: ',/'',8(/'',E12.6,'+I',E12.6))
            G = .5/HWID
            G = G*G
            G = G*G
            DO 29 I=1,7,2
            B = -2.0*REAL(S(I))
            Z1 = S(I)*S(I+1)
            C = REAL(Z1)
            A = TDT+B+C/TDT
            G = G*A
            D(I) = (C*DT-FDT)/A
         29 D(I+1) = (A-2.0*B)/A
            G = G*G
      C     WRITE(6,3)
      C    3 FORMAT('-FILTER IS (1-Z**2)**4/B1*B2*B3*B4')
      C     WRITE(6,4) D
      C    4 FORMAT(4(/'B(I)=1+',E12.6,'Z+',E12.6,'Z**2'))
      C     WRITE(6,5) G
      C    5 FORMAT('-FILTER GAIN IS',E12.6)
            RETURN
      C
      C
            ENTRY FILTER(X,N,D,G,IG)
      C
      C     X = Data vector of length N containing data to be filtered
      C     D = Filter coefficients calculated by BNDPAS
```

Listing of CROSSCOR at 16:44:17 on JUL 27, 1988 for CCid=SEIS on G

```
C      G = Filter Gain
C      IG = 1 Means to remove the filter gain so that the gain
C           is unity.
C
       IF(ISW.EQ.1) GO TO 31
       WRITE(6,6)
     6 FORMAT('1BNDPAS MUST BE CALLED BEFORE FILTER')
       CALL EXIT
C
       WRITE(6,*) X(1)
C      Apply filter in forward direction
C
    31 XM2=X(1)
       XM1=X(2)
       XM=X(3)
       XC(1)=XM2
       XC(2)=XM1-D(1)*XC(1)
       XC(3)=XM-XM2-D(1)*XC(2)-D(2)*XC(1)
       XD(1)=XC(1)
       XD(2)=XC(2)-D(3)*XD(1)
       XD(3)=XC(3)-XC(1)-D(3)*XD(2)-D(4)*XD(1)
       XE(1)=XD(1)
       XE(2)=XD(2)-D(5)*XE(1)
       XE(3)=XD(3)-XD(1)-D(5)*XE(2)-D(6)*XE(1)
       X(1)=XE(1)
       X(2)=XE(2)-D(7)*X(1)
       X(3)=XE(3)-XE(1)-D(7)*X(2)-D(8)*X(1)
       DO 39 I=4,N
       XM2=XM1
       XM1=XM
       XM=X(I)
       K=I-((I-1)/3)*3
       GO TO (34,35,36),K
    34 M=1
       M1=3
       M2=2
       GO TO 37
    35 M=2
       M1=1
       M2=3
       GO TO 37
    36 M=3
       M1=2
       M2=1
    37 XC(M)=XM-XM2-D(1)*XC(M1)-D(2)*XC(M2)
       XD(M)=XC(M)-XC(M2)-D(3)*XD(M1)-D(4)*XD(M2)
       XE(M)=XD(M)-XD(M2)-D(5)*XE(M1)-D(6)*XE(M2)
    39 X(I)=XE(M)-XE(M2)-D(7)*X(I-1)-D(8)*X(I-2)
C
C      Filter in reverse direction
C
       XM2=X(N)
       XM1=X(N-1)
       XM=X(N-2)
       XC(1)=XM2
       XC(2)=XN1-D(1)*XC(1)
       XC(3)=XM-XM2-D(1)*XC(2)-D(2)*XC(1)
       XD(1)=XC(1)
```

Listing of CROSSCOR at 16:44:17 on JUL 27, 1988 for CCid=SEIS on G

```
      XD(2)=XC(2)-D(3)*XD(1)
      XD(3)=XC(3)-XC(1)-D(3)*XD(2)-D(4)*XD(1)
      XE(1)=XD(1)
      XE(2)=XD(2)-D(5)*XE(1)
      XE(3)=XD(3)-XD(1)-D(5)*XE(2)-D(6)*XE(1)
      X(N)=XE(1)
      X(N-1)=XE(2)-D(7)*X(1)
      X(N-2)=XE(3)-XE(1)-D(7)*X(2)-D(8)*X(1)
      DO 49 I=4,N
      XM2=XM1
      XM1=XM
      J=N-I+1
      XM=X(J)
      K=I-((I-1)/3)*3
      GO TO (44,45,46),K
   44 M=1
      M1=3
      M2=2
      GO TO 47
   45 M=2
      M1=1
      M2=3
      GO TO 47
   46 M=3
      M1=2
      M2=1
   47 XC(M)=XM-XM2-D(1)*XC(M1)-D(2)*XC(M2)
      XD(M)=XC(M)-XC(M2)-D(3)*XD(M1)-D(4)*XD(M2)
      XE(M)=XD(M)-XD(M2)-D(5)*XE(M1)-D(6)*XE(M2)
   49 X(J)=XE(M)-XE(M2)-D(7)*X(J+1)-D(8)*X(J+2)
      IF(IG.NE.1) RETURN
      DO 59 I=1,N
   59 X(I)=X(I)/G
      WRITE(6,*) (X(I), I=1,N)
      RETURN
      END
C
C  Subroutine DOT finds the dot product of two arrays.
C
      SUBROUTINE DOT(L,X,Y,ANS)
C
      IMPLICIT REAL (A-H,O-Z)
      REAL    X(2),Y(2),ANS
      ANS=0.0
      IF(L) 30,30,10
   10 DO 20 I=1,L
   20 ANS=ANS+X(I)*Y(I)
   30 RETURN
      END
C
C  Subroutine CROSS finds the cross product of two arrays
C
      SUBROUTINE CROSS(LX,X,LY,Y,LD,D)
C
      IMPLICIT REAL (A-H,O-Z)
      REAL    X(2),Y(2),D(2)
      DO 10 I=1,LD
   10 CALL DOT(MINO(LY+I-1,LX)-I+1,X(I),Y,D(I))
```

Listing of CROSSCOR at 16:44:17 on JUL 27, 1988 for CCid=SEIS on G

```
      RETURN
      END
C
C  Subroutine MAXSN finds the maximum value of an array,
C  taking into account the algerbraic signs of the elements.
C
      SUBROUTINE MAXSN(LX,X,XMAX,INDEX)
C
      REAL  X(2),XMAX
      XMAX=X(1)
      DO 10 I=1,LX
   10 XMAX=AMAX1(XMAX,X(I))
      DO 20 J=1,LX
      INDEX=J
      IF(X(J)-XMAX) 20,30,20
   20 CONTINUE
   30 RETURN
      END
```

# APPENDIX $\beta$

Program listing of KALDAT, the discrete model of the second order system.

Listing of KALDAT at 18:25:29 on DEC 12, 1987 for CCid=SEIS

```
     1      C This program generates synthetic geophone  data inorder
     2      C to determine the performance of the Kalman filter. The input
     3      C noise, wk, is white, and has a gaussian distribution with
     4      C mean=0.0 and standard deviation=SIGMA
     5      C
     6      C
     7            REAL       A11,A12,A21,A22,B11,B21,WO,RO,PO,RO1,PO1
     8            REAL       TC,GAMA,HO,H1,H2,KI,WSIGMA,WMEAN,WS,ALPH,DELT
     9            REAL       D11,D12,VS,AW,BW,QA,SSS,SA,SS,BB11,BB1,ST,SH,SP
    10            REAL       X1(4000),X2(4000),X3(4000),X4(4000),X5(4000)
    11            REAL       X6(4000),X7(4000),X8(4000),X9(4000),Z(4000)
    12            REAL       X81(4000),X82(4000),X91(4000),X92(4000),V(4000)
    13            INTEGER    T
    14      C
    15      C
    16            PIE=3.1415927
    17      C
    18      C     length of desired time series
    19            T=200
    20      C
    21      C    sampling interval,delta
    22            DELT=.01
    23      C
    24      C     standard deviation of noise present
    25            WSIGMA=.09
    26            VSIGMA=.009
    27      C
    28      C     natural frequency of insrument
    29            WO=8*2*PIE
    30      C
    31      C    damping of instrument
    32            RO=.18
    33      C
    34      C     KI factor.
    35            KI=1.0
    36      C
    37      C    gain on measurement H
    38            HO=.29
    39      C
    40      C    time constant
    41            TC=.10
    42      C
    43            DO 100 I=1,T
    44            READ(15,*) X1(I),X3(I)
    45          100 CONTINUE
    46      C
    47            WMEAN=0.0
    48            GAMA=1/TC
    49            ALPH=ASIN(RO)
    50            RO1=RO*WO*DELT
    51            PO=SQRT(1-RO*RO)
    52            PO1=PO*WO*DELT
    53            AA=EXP(-RO1)/PO
    54            A11=AA*(COS(PO1-ALPH))
    55            A12=(AA*SIN(PO1))/WO
    56            A21=-AA*(WO*SIN(PO1))
    57            A22=AA*(COS(PO1+ALPH))
  59.5            B11=(1.0-A11)*KI/(WO*WO)
```

```
 59.7          B12=-A21*KI/(WO*WO)
 60            H1=-WO*WO
 61            H2=-2*RO*WO
 62            QA=GAMA*DELT
 63            AW=EXP(-QA)
 64            BW=1.0 -AW
 65            X5(1)=0.0
 66            X6(1)=0.0
 67            X7(1)=0.0
 68            X8(1)=0.0
 70            X9(1)=0.0
 72             Z(1)=0.0
 73            WRITE(6,*) AW,BW
 74      C
 75            DO 1 I=1,T
 76      C
 77      C At this point it is necessary to generate the Gaussian noise
 78      C as input input our first order transform function(which represents
 79      C a low pass filter) which has X5 as our output. X5 is then feed
 80      C into our second order model.
 81      C
 82            TK=I
 83            ST=1.0*I
 84            SH=2.0*I
 85            SS=SQRT(DELT)
 85.5          SP=GAMA/2.0
 86      C
 87            CALL RNGAUS(WS,WMEAN,WSIGMA,TK,ST)
 88
 89            NN=I+1
 90      C
 91            X5(NN)=X5(I)*AW+BW*WS
 92      C
 93      C
 94            X6(NN)=B11*X5(I)+A11*X6(I)+A12*X7(I)
 95      C
 96      C
 97            X7(NN)=B12*X5(I)+A21*X6(I)+A22*X7(I)
 98      C
 99            BB11=B11*X1(I)
100            BB1=B11*X3(I)
101      C
102            X8(NN)=A11*X8(I)+A12*X9(I)+BB11+BB1
105
106      C
107      C
108            X9(NN)=A21*X8(I)+A22*X9(I)+B12*X1(I)+B12*X3(I)
111      C
112      C
113            CALL RNGAUS(VS,WMEAN,VSIGMA,TK,SH)
114      C
115            Z(NN)=HO*(X7(NN)+X9(NN))+VS/SS
116      C
117            WRITE(2,*) X5(I)
118      C
119         1 CONTINUE
120      C
121            DO 2 J=1,T
```

```
122             WRITE(1,*) Z(J)
123           2 CONTINUE
124       C
125       C
126       C     DO 2 J=1,T
127       C     WRITE(2,*) X5(J)+1.4
128       C   2 CONTINUE
129       C
130             STOP
131             END
132       C
133             SUBROUTINE RNGAUS(W,WMEAN,WSIGMA,TK,SS)
134       C
135             REAL     RNSED,WMEAN,C1,C2,C3,WSIGMA,W,SS
136             INTEGER TK
137             DATA     IRNSED/1/
138             DATA     TWOPI/6.283185307/
139       C
140       C     IF (TK.LT.10.0) THEN
141       C         SS=TK*1000.0+1.0
142       C     ELSE
143       C         SS=TK*100.0+1
144       C     END IF
145       C
146       C
147             GO TO (10,20,30) IRNSED
148       C
149          10 RNSED=ABS(RNSED)
150             C1=RAND(RNSED)
151       C
152       C First call for a random number.
153       C
154          20     C1=SQRT(-2.*ALOG(RAND(0.)))
155             C2=TWOPI*RAND(0.)
156             C3=C1*COS(C2)
157             IRNSED=3
158             GO TO 40
159       C
160       C Second call for random number.
161       C
162          30        C3=C1*SIN(C2)
163             IRNSED=2
164       C
165          40 W=WMEAN+WSIGMA*C3
166       C
167             RETURN
168              END
```

# APPENDIX C

Program listing of the Kalman Filter, KALMAN 4

```
Listing . KALMAN4 at 10:07:47 on DEC 13, 1987 for CCid=SEIS

      C
      C
      C*****************************************************************
      C*                                                               *
      C*                        MAIN PROGRAM                           *
      C*                                                               *
      C*                                                               *
      C*                                                               *
      C*                                                               *
      C*                                                               *
      C*                                                               *
      C*****************************************************************
      C
      C
      C
            INTEGER SNP,SN,ST,SI,SP,NT,FT,KT,QT,T,IDEX4,IDEX2
      16.5  INTEGER TE(4)
      16.7  REAL X2,X22,X4,X44
      C
            REAL WO,RO,KI,BB,LL,RR,R,DELT,A11,A21,A12,A22
            REAL AA,ALPH,ESP,B11,B12,QR,GAMA,C1,C2,C3,C4,FO1,RO1
            REAL PIE,AN,RW,HH,TC,AW,QW,RA,PW,MV,HV(9)
            REAL XMIN1,XMIN2,XMIN3,XMIN4,XMAX4,XMAX2,SNN,SPP
            REAL PH1(500),PH2(500),PH3(500),PH4(500),XH1(500),XH2(500)
            REAL XH3(500),XH4(500),KK,QD,N1,NPP,NSS,SD,N3
            INTEGER INDEX1,INDEX2,INDEX3,INDEX4,N2,N4,NP(6),NS(6)
      C
            REAL Z(2000),WP(200),WS(200),BB11,BB21,BB1,BB2
            REAL KS(9),KH(9,9),BETA(10),QN(2,2),PSO(9,9)
            REAL PS(9,9),PS1(4,4),PS2(4,5),PS2T(5,4),PS3(5,5)
            REAL PU(9,9),PU1(4,4),PU2(4,5),PU2T(5,4),PU3(5,5)
            REAL FS(9,9),FS1(5,4),FS2(5,5),XU(9),XE(9),XO(9)
            REAL FL(9,9),FL1(5,4),FL2(5,5),H11(200),H12(200)
      C
      C
      C  Defining parameters:
      C
      C  WO=natural frequency of instrument  RO=damping of instrument
      C  KI=coefficient which takes into account instrument inductance,
      C     resistance and magnetic field.
      C  DELT=sampling interval  AN=white noise input into second order
      C                                system.
      C  ER=covariance on measurement noise QR=covariance on state noise
      C
      C initial estimates of the states
      C
            READ(11,*)XO(1),XO(2),XO(3),XO(4),XO(5),XO(6),XO(7),XO(8)
           1,XO(9),FT
      C
      C
            DO 76 I=1,9
             DO 77 J=1,9
              PSO(I,J)=0.0
         77 CONTINUE
         76 CONTINUE
      C
            READ(11,*)PSO(1,1),PSO(2,2),PSO(3,3),PSO(4,4),PSO(5,5),
           1PSO(6,6),PSO(7,7),PSO(8,8),PSO(9,9),PSO(6,7),PSO(8,9),
```

```
     1PSO(1,8),PSO(1,9),PSO(2,8),PSO(2,9),
     1PSO(3,8),PSO(3,9),PSO(4,8),PSO(4,9)
C
C
      PSO(8,1)=PSO(1,8)
      PSO(9,1)=PSO(1,9)
      PSO(8,3)=PSO(3,8)
      PSO(9,3)=PSO(3,9)
      PSO(8,4)=PSO(4,8)
      PSO(9,4)=PSO(4,9)
      PSO(8,2)=PSO(2,8)
      PSO(9,2)=PSO(2,9)
      PSO(7,6)=PSO(6,7)
      PSO(9,8)=PSO(8,9)
C
      DELT=.01
C
      KI=1.0
C
      T=200
C
      PIE=3.1415927
C
      WO=8*2*PIE
C
      RO=.18
C
C NP: length of input P-wave
      NS(1)=1
C     NP(2)=2
C     NP(3)=3
      NSS=1
C
C NS: length of input S-wave
      DO 232 I=1,10
      NP(I)=I
C     NS(3)=3
  232 CONTINUE
      NPP=9
C
C WP: coefficients defining P-wave
      WS(1)=0.0
C     WP(2)=1.0
C     WP(3)=0.0
C     WP(4)=0.0
C     WP(5)=.6
C     WP(6)=.8
C
C WS: coefficients defining S-wave
      DO 323 I=1,10
      F1=50.0
      QAS=.01*(I)
      WP(I)=COS(F1*QAS)*EXP(-QAS)
  323 CONTINUE
C     WS(2)=1.0
C     WS(3)=0.0
C     WS(4)=0.0
C     WS(5)=.6
```

```
115       C      WS(6)=.8
116       C
117       C
118       C MV: gain or amplification on recorder
119             MV=.29
120       C
121       C FT: number of iterations desired
122       C      FT=4
123       C
124             DO 78 I=1,T
125              READ(8,*) Z(I)
126          78 CONTINUE
127       C
128       C TC: time constant
129             TC=.10
130       C
131       C
132             ESP=1/TC
133             H1=-WO*WO*1.0
134             KI=1.0
135             H2=-2*RO*WO*1.0
136             PO=SQRT(1-RO*RO)
137             RO1=RO*WO*DELT
138             PO1=PO*WO*DELT
139             GAMA=ATAN(RO/PO)
140             ALPH=ASIN(RO)
141             AA=EXP(-RO1)/PO
142             A12=(AA*SIN(PO1))/WO
143             A21=-AA*(WO*SIN(PO1))
144             A22=AA*(COS(PO1+ALPH))
145             A11=AA*(COS(PO1-ALPH))
146             B11=(1-A11)*KI/(WO*WO)
147             B12=-A21*KI/(WO*WO)
148             C1=((WO*WO)*EXP(-RO1))/PO
149             C2=SIN(PO1)/WO
150             C3=COS(PO1+ALPH)
151             C4=PO*EXP(-RO1)
152             AW=EXP(-ESP*DELT)
153             BW=1.0-AW
154             QR=.09
155             QW=BW*BW*QR
156             RW=.009
157       C
158             DO 9 I=1,9
159              XE(I)=XO(I)
160          9 CONTINUE
161       C
162             DO 1 III=1,FT
163       C
163.5           TE(1)=IFIX(XE(1))
163.7           TE(3)=IFIX(XE(3))
163.75          XE(1)=FLOAT(TE(1))
163.77          XE(3)=FLOAT(TE(3))
163.8     C
163.9     C
164             X2=XE(2)/DELT
165             TE(2)=IFIX(X2)
166             X22=TE(2)*DELT
```

```
167             XE(2)=X22
167.5   C
168             X4=XE(4)/DELT
169             TE(4)=IFIX(X4)
170             X44=TE(4)*DELT
171             XE(4)=X44
171.5   C
171.6   C       WRITE(6,*) XE(1),XE(2),XE(3),XE(4)
171.7   C
172             XE(5)=XO(5)
173             XE(6)=XO(6)
174             XE(7)=XO(7)
175             XE(8)=XO(8)
176             XE(9)=XO(9)
177     C
178             DO 70 I=1,9
179              DO 80 J=1,9
180              PS(I,J)=PSO(I,J)
181          80 CONTINUE
182          70 CONTINUE
183     C
184             DO 30 I=1,4
185              DO 31 J=1,4
186              PS1(I,J)=PS(I,J)
187          31 CONTINUE
188          30 CONTINUE
189     C
190             DO 32 I=5,9
191              DO 33 J=5,9
192              D=J-4
193              DD=I-4
194              PS3(DD,D)=PS(I,J)
195          33 CONTINUE
196          32 CONTINUE
197     C
198             DO 34 I=1,4
199              DO 35 J=5,9
200              D=J-4
201              PS2(I,D)=PS(I,J)
202          35 CONTINUE
203          34 CONTINUE
204     C
205     C
206             DO 17 I=1,9
207              DO 18 J=1,9
208                 FS(I,J)=0.0
209                 FL(I,J)=0.0
210          18 CONTINUE
211          17 CONTINUE
212     C
213     C
214             FS(5,5)=AW
215             FS(6,5)=B11
216             FS(6,6)=A11
217             FS(6,7)=A12
218             FS(7,5)=B12
219             FS(7,6)=A21
220             FS(7,7)=A22
```

```
      FS(8,8)=A11
      FS(8,9)=A12
      FS(9,8)=A21
      FS(9,9)=A22
C
      DO 21 I=1,5
       DO 22 J=1,5
         FL(I,J)=FS(I,J)
   22 CONTINUE
   21 CONTINUE
C
      DO 23 I=1,4
         FS(I,I)=1.0
         FL(I,I)=1.0
   23 CONTINUE
C
      SI = 0
      SP = 0
C
C
C
      DO 2 II=1,T
C
      KT=II
C
C
C Lines 328-356  define the error transition matrix, BS, which
C has nonnull components defined by the discrete second order
C system equations(i.e, B11,B12). This matrix is also a component
C of the state transition matrix, F, and is a function of the P and
C S-wave time of arrivals(tp-X2,ts-X4).
C
C
C
      N1=NPP*DELT
C
      QD=XE(2)+N1
      KK=KT*DELT
      IF (KK.GE.XE(2).OR.KK.GE.XE(4)) THEN
      FS(8,8)=A11
      FL(8,8)=A11
      FS(8,9)=A12
      FL(8,9)=A12
      FS(9,8)=A21
      FL(9,8)=A21
      FS(9,9)=A22
      FL(9,9)=A22
C
C
      ELSE
      GOTO 109
C
      END IF
C
  109 IF (KK.LT.XE(2).OR.KK.GT.QD) THEN
C
      BB11=0.0
      BB21=0.0
```

Listing of KALMAN4 at 10:07:47 on DEC 13, 1987 for CCid=SEIS

```
279             GOTO 173
280       C
281             ELSE
282       C
283                  SI=SI+1
284       C
285             IF (SI.GT.NPP+1) THEN
286             GOTO 173
287             ELSE
288             GOTO 174
289             END IF
290          174      N2=NP(SI)
291                   BB11=B11*WP(N2)
292                   BB21=B12*WP(N2)
293       C
294          173 END IF
295       C
296       C
297             N3=NSS*DELT
298             SD=XE(4)+N3
299       C
300             IF (KK.LT.XE(4).OR.KK.GT.SD) THEN
301       C
302             BB1=0.0
303             BB2=0.0
304       C
305             ELSE
306                  SP=SP+1
307             IF (SP.GT.NSS+1) THEN
308             GOTO 171
309             ELSE
310             GOTO 172
311             END IF
312          172      N4=NS(SP)
313                   BB1=B11*WS(N4)
314                   BB2=B12*WS(N4)
315
316       C      WRITE(6,*) KK,XE(4),SD,WS(N4)
317       C
318          171 END IF
319       C
320       C      WRITE(6,*)BB11,BB21,BB1,BB2
321       C
322                 FS(8,1)=BB11
323                 FS(9,1)=BB21
324                 FS(8,3)=BB1
325                 FS(9,3)=BB2
326                 FL(8,1)=BB11
327                 FL(9,1)=BB21
328                 FL(8,3)=BB1
329                 FL(9,3)=BB2
330       C
331       C      WRITE(6,*) FS(8,1),FS(9,1),FS(8,3),FS(9,3),KK
332       C
333             DO 303 I=1,9
334              HV(I)=0.0
335           303 CONTINUE
336       C
```

```
      337            HV(7)=MV
      338            HV(9)=MV
      339      C
      340            CALL XUPDAT(XU,XE,FS)
      341      C
      342      C
      343            CALL EXTEND(FL,C1,C2,C3,C4,XU,KK,N1,N2,WS,WP,DELT,N3,N4,FT)
      344      C
      345      C
      346      C
      347            CALL EXTRAP(PU,PS,FL)
      348      C
      349      C
      350            PU(5,5)=PU(5,5)+QW
      351      C
      352            CALL GAIN(HV,PU,RW,KS)
      353      C
      354            CALL NWSTAT(XE,KS,XU,MV,KT,Z)
      355      C
      356            CALL PUPDAT(HV,KS,PU,PS)
      357      C
      358      C
      359            PH1(KT)=PS(1,1)
      360            PH2(KT)=PS(2,2)
      361            PH3(KT)=PS(3,3)
      362            PH4(KT)=PS(4,4)
      363            XH1(KT)=XE(1)
      364            XH2(KT)=XE(2)
      365            XH3(KT)=XE(3)
      366            XH4(KT)=XE(4)
      367      C
      368            WRITE(1,*) PH1(KT)
      369            WRITE(2,*) PH2(KT)
      370            WRITE(3,*) PH3(KT)
      371            WRITE(4,*) PH4(KT)
      372            WRITE(5,*) XE(1)
      373            WRITE(7,*) XE(2)
      374            WRITE(10,*) XE(3)
      375            WRITE(9,*) XE(4)
      376      C
      377          2 CONTINUE
      378      C
      379      C
      380      C
      381            CALL MINSN(T,PH1,XMIN1,INDEX1)
      382      C     WRITE(6,*) XMIN1,XH1(INDEX1),INDEX1
      383      C
      384            XE(1)=XH1(INDEX1)
      385      C
      386            CALL MINSN(T,PH2,XMIN2,INDEX2)
      387            XE(2)=XH2(INDEX2)
      388      C
      389            CALL MINSN(T,PH3,XMIN3,INDEX3)
      390      C     WRITE(6,*) XMIN3,XH3(INDEX3),INDEX3
      391      C
      392            XE(3)=XH3(INDEX3)
      393      C
      394            CALL MINSN(T,PH4,XMIN4,INDEX4)
```

```
      XE(4)=XH4(INDEX4)
C     WRITE(6,*) XMIN4,XE(4),INDEX4
C
      CALL MAXSN(T,PH2,XMAX2,IDEX2)
C     WRITE(6,*) XMAX2,XH2(IDEX2+2),IDEX2
C
C
      CALL MAXSN(T,PH4,XMAX4,IDEX4)
C     WRITE(6,*) XMAX4,XH4(IDEX4),IDEX4
C
C     IF (INDEX2.EQ.1) THEN
C
C     XE(2)=XH2(IDEX2)
C
C     ELSE
C
C     XE(2)=(XH2(INDEX2+2)+XH2(INDEX2)+XH2(INDEX2+1))/3
C
C     END IF
C
C
C
C     IF (INDEX4.EQ.1) THEN
C
C     XE(4)=(XH4(IDEX4+2)+XH4(IDEX4)+XH4(IDEX4+1))/3
C     XE(4)=XH4(IDEX4)
C     ELSE
C
C     XE(4)=(XH4(INDEX4+2)+XH4(INDEX4)+XH4(INDEX4+1))/3
C
C     END IF
C
C
C     SNN=XE(2)/DELT
C     SN=IFIX(SNN)
C     XE(2)=SN*DELT
C     WRITE(6,*) XE(2)
C
C     SPP=XE(4)/DELT
C     SNP=IFIX(SPP)
C     XE(4)=SNP*DELT
C     WRITE(6,*) XE(4)
C
      WRITE(6,*) XMIN2,XE(2),INDEX2
C
      WRITE(6,*) XMIN1,XE(1),INDEX1
C
    1 CONTINUE
C
      STOP
      END
C
C
C  This subroutine extrapolates the state matrix X(I).
C
      SUBROUTINE XUPDAT(XU,XE,FS)
C
      REAL      XU(9),XE(9),FS(9,9)
```

```
      INTEGER   OR
C
      OR = 9
C
      CALL GMATV(FS,XE,XU,OR,OR,OR)
C
      RETURN
      END
C
C
C This subroutine propagates and updates the Kalman gain matrix K,
C which is a function of P and S-wave arrivals.
C
      SUBROUTINE GAIN(HV,PU,RW,KS)
C
      REAL        RW,PU(9,9),KS(9),HV(9),TMP1(9)
      REAL        DOT,TMP2(9)
      INTEGER     OR
C
      OR = 9
C
      CALL GVMAT(HV,PU,TMP1,OR,OR,OR)
C
      DOT = GVV(TMP1,HV,OR) + RW
C     WRITE(6,*) DOT
C
      CALL GMATV(PU,HV,TMP2,OR,OR,OR)
C
      DO 1 I=1,9
      KS(I)=TMP2(I)/DOT
    1 CONTINUE
C
      RETURN
      END
C
C
C  This subroutine gives us state estimate updates.
C
      SUBROUTINE NWSTAT(XE,KS,XU,MV,KT,Z)
C
      REAL       DELTZ,Z(2000),XU(9),XE(9)
      REAL       KS(9),MV
      INTEGER    KT

C     DELTZ(KT)=Z(KT)-H(1)*X1(KT)-H(2)*XE(2)-H(3)*X3(KT)-H(4)*XE(4)
C    1-H(5)*X5(KT)-H(6)*X6(KT)-H(7)*X7(KT)-H(8)*X8(KT)-H(9)*X9(KT)
C
      DELTZ=Z(KT)-MV*(XU(7)+XU(9))
C
C     WRITE(6,*) KS(1),KS(2),KS(3),KS(4),KT
C
      XE(1)=XU(1)+KS(1)*DELTZ
      XE(2)=XU(2)+KS(2)*DELTZ
      XE(3)=XU(3)+KS(3)*DELTZ
      XE(4)=XU(4)+KS(4)*DELTZ
      XE(5)=XU(5)+KS(5)*DELTZ
      XE(6)=XU(6)+KS(6)*DELTZ
      XE(7)=XU(7)+KS(7)*DELTZ
```

```
      XE(8)=XU(8)+KS(8)*DELTZ
      XE(9)=XU(9)+KS(9)*DELTZ
C
      RETURN
      END
C
C  Since the transition matrix, F, is nonlinear with respect to
C  the state parameters X2 and X4, it is necessary to linearize
C  it. This is accomplished in the following subroutine, by
C  applying Leibnitz's rule and the extended Kalman filter
C  equations.
C
      SUBROUTINE EXTEND(FL,C1,C2,C3,C4,XU,KK,N1,N2,WS,WP,DELT,N3,N4,FT
     1)
C
      INTEGER   MS,SL,SH,N2,N4,FT
      REAL      MM,NN,C1,C2,C3,C4,DELT,N1,N3,KK
      REAL      XU(9),WP(200),WS(200),FL(9,9)
C
C
      MM=XU(2)+N1
C     WRITE(6,*)KK,XU(2),MM
      IF (KK.LT.XU(2).OR.KK.GT.MM) THEN
C
      FL(8,2)=0.0
      FL(9,2)=0.0
C
      ELSE
C
      SH=N2+1
C
      FL(9,2)=C1*(C3*WP(N2)-C4*WP(SH))*XU(1)
      FL(8,2)=C1*C2*WP(N2)*XU(1)
C     WRITE(6,*)FL(9,2),FL(8,2),C1,C2,C3,WP(N2),XU(1)
C
C
      END IF
C
C
      NN=XU(4)+N3
C
      IF (KK.LT.XU(4).OR.KK.GT.NN) THEN
C
      FL(8,4)=0.0
      FL(9,4)=0.0
C
      ELSE
C
      SL=N4+1
C
      FL(8,4)=C1*C2*WS(N4)*XU(3)
      FL(9,4)=C1*(C3*WS(N4)-C4*WS(SL))*XU(3)
C
      WRITE(6,*) FL(8,4),FL(9,4)
  104 END IF
C
      RETURN
```

```
      END
C
C  This subroutine extrapolates the error covariance matrix P.
C
      SUBROUTINE EXTRAP(PU,PS,FL)
      REAL       PS(9,9),PU(9,9),FL(9,9),FLT(9,9)
      REAL       TMP1(9,9),TMP2(9,9)
      INTEGER    OR
C
C
      OR = 9
      CALL GTRAN(FL,FLT,OR,OR,OR,OR)
C
      CALL GMULT(FL,PS,TMP1,OR,OR,OR,OR,OR,OR)
C
      CALL GMULT(TMP1,FLT,PU,OR,OR,OR,OR,OR,OR)
C


C
      RETURN
      END
C  This subroutine updates the error covariance matrix P.
C
      SUBROUTINE PUPDAT(HV,KS,PU,PS)
      REAL       KS(9),PU(9,9),HV(9),ID(9,9),TMP1(9,9)
      REAL       TMP2(9,9),PS(9,9)
      INTEGER    OR
C
      OR = 9
C
      CALL UNIT(ID,OR,OR)
C
      DO 1 I=1,9
       DO 2 J=1,9
         TMP1(I,J)=KS(I)*HV(J)
    2 CONTINUE
    1 CONTINUE
C
      CALL GSUB(ID,TMP1,TMP2,OR,OR,OR,OR,OR)
C
      CALL GMULT(TMP2,PU,PS,OR,OR,OR,OR,OR,OR)
C
      RETURN
      END
C
      SUBROUTINE MINSN(LX,X,XMIN,INDEX)
C
      REAL X(2)
      XMIN=X(1)
      DO 10 I=1,LX
   10 XMIN=AMIN1(XMIN,X(I))
      DO 20 J=1,LX
      INDEX=J
      IF(X(J)-XMIN) 20,30,20
   20 CONTINUE
   30 RETURN
      END
C
```

Listing of KALMAN4 at 10:07:47 on DEC 13, 1987 for CCId=SEIS

```
      SUBROUTINE MAXSN(LX,X,XMAX,INDEX)
C
      REAL X(2)
      XMAX=X(1)
      DO 10 I=1,LX
   10 XMAX=AMAX1(XMAX,X(I))
      DO 20 J=1,LX
      INDEX=J
      IF(X(J)-XMAX) 20,30,20
   20 CONTINUE
   30 RETURN
      END
```